frontiers | Research Topics

Progress in neuroacanthocytosis syndromes and related diseases including other bulk lipid transfer disorders

Edited by
Lars Kaestner, Manuel J. Rodriguez, Andreas Hermann, Kevin Peikert, Ruth Walker, Merce Masana and Adrian Danek

Published in
Frontiers in Neuroscience
Frontiers in Neurology

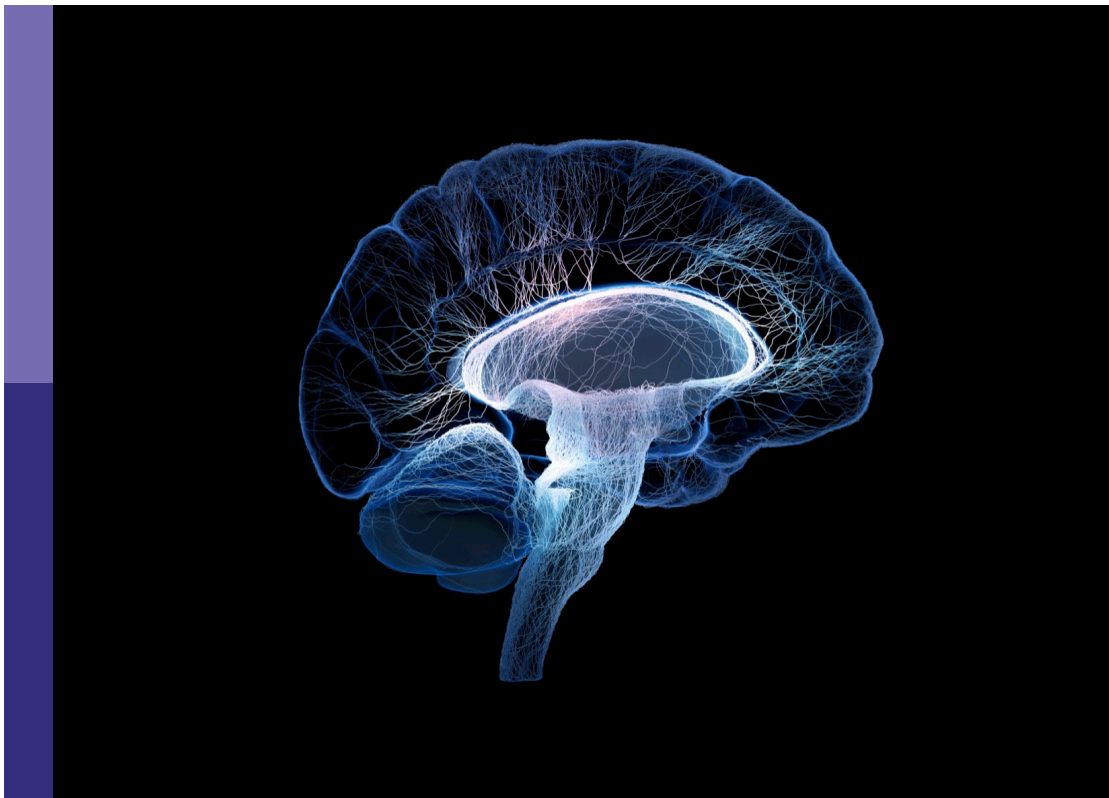

ISSN 1664-8714
ISBN 978-2-8325-6605-3
DOI 10.3389/978-2-8325-6605-3

Generative AI statement
Any alternative text (Alt text) provided alongside figures in the articles in this ebook has been generated by Frontiers with the support of artificial intelligence and reasonable efforts have been made to ensure accuracy, including review by the authors wherever possible. If you identify any issues, please contact us.

About Frontiers

Frontiers is more than just an open access publisher of scholarly articles: it is a pioneering approach to the world of academia, radically improving the way scholarly research is managed. The grand vision of Frontiers is a world where all people have an equal opportunity to seek, share and generate knowledge. Frontiers provides immediate and permanent online open access to all its publications, but this alone is not enough to realize our grand goals.

Frontiers journal series

The Frontiers journal series is a multi-tier and interdisciplinary set of open-access, online journals, promising a paradigm shift from the current review, selection and dissemination processes in academic publishing. All Frontiers journals are driven by researchers for researchers; therefore, they constitute a service to the scholarly community. At the same time, the *Frontiers journal series* operates on a revolutionary invention, the tiered publishing system, initially addressing specific communities of scholars, and gradually climbing up to broader public understanding, thus serving the interests of the lay society, too.

Dedication to quality

Each Frontiers article is a landmark of the highest quality, thanks to genuinely collaborative interactions between authors and review editors, who include some of the world's best academicians. Research must be certified by peers before entering a stream of knowledge that may eventually reach the public - and shape society; therefore, Frontiers only applies the most rigorous and unbiased reviews. Frontiers revolutionizes research publishing by freely delivering the most outstanding research, evaluated with no bias from both the academic and social point of view. By applying the most advanced information technologies, Frontiers is catapulting scholarly publishing into a new generation.

What are Frontiers Research Topics?

Frontiers Research Topics are very popular trademarks of the *Frontiers journals series*: they are collections of at least ten articles, all centered on a particular subject. With their unique mix of varied contributions from Original Research to Review Articles, Frontiers Research Topics unify the most influential researchers, the latest key findings and historical advances in a hot research area.

Find out more on how to host your own Frontiers Research Topic or contribute to one as an author by contacting the Frontiers editorial office: frontiersin.org/about/contact

Progress in neuroacanthocytosis syndromes and related diseases including other bulk lipid transfer disorders

Topic editors

Lars Kaestner — Saarland University, Germany
Manuel J. Rodriguez — University of Barcelona, Spain
Andreas Hermann — University Hospital Rostock, Germany
Kevin Peikert — University Hospital Rostock, Germany
Ruth Walker — James J. Peters VA Medical Center, United States Department of Veterans Affairs, United States
Merce Masana — University of Barcelona, Spain
Adrian Danek — Ludwig Maximilian University of Munich, Germany

Citation

Kaestner, L., Rodriguez, M. J., Hermann, A., Peikert, K., Walker, R., Masana, M., Danek, A., eds. (2025). *Progress in neuroacanthocytosis syndromes and related diseases including other bulk lipid transfer disorders*. Lausanne: Frontiers Media SA. doi: 10.3389/978-2-8325-6605-3

Table of contents

frontiers | Frontiers in Neuroscience

TYPE Editorial
PUBLISHED 30 June 2025
DOI 10.3389/fnins.2025.1635008

OPEN ACCESS

EDITED AND REVIEWED BY
Einar M. Sigurdsson,
New York University, United States

*CORRESPONDENCE
Lars Kaestner
lars_kaestner@me.com

RECEIVED 25 May 2025
ACCEPTED 28 May 2025
PUBLISHED 30 June 2025

CITATION
Danek A, Hermann A, Kaestner L, Masana M, Peikert K, Rodriguez MJ and Walker RH (2025) Editorial: Progress in neuroacanthocytosis syndromes and related diseases including other bulk lipid transfer disorders.
Front. Neurosci. 19:1635008.
doi: 10.3389/fnins.2025.1635008

Editorial: Progress in neuroacanthocytosis syndromes and related diseases including other bulk lipid transfer disorders

Adrian Danek[1], Andreas Hermann[2,3,4], Lars Kaestner[5,6]*, Mercè Masana[7,8,9], Kevin Peikert[2,3,4], Manuel J. Rodriguez[7,8,9] and Ruth H. Walker[10,11]

[1]Neurologische Klinik und Poliklinik, LMU Klinikum, LMU Munich, Munich, Germany, [2]Translational Neurodegeneration Section "Albrecht Kossel", Department of Neurology, University Medical Center Rostock, University of Rostock, Rostock, Germany, [3]Center for Transdisciplinary Neurosciences Rostock (CTNR), University Medical Center Rostock, Rostock, Germany, [4]United Neuroscience Campus Lund-Rostock (UNC), Rostock, Germany, [5]Theoretical Medicine and Biosciences, Medical Faculty, Saarland University, Homburg, Germany, [6]Dynamics of Fluids, Experimental Physics, Faculty of Natural Science and Technology, Saarland University, Saarbrücken, Germany, [7]Department of Biomedical Sciences, School of Medicine and Health Sciences, Institute of Neurosciences, Universitat de Barcelona, Barcelona, Spain, [8]August Pi i Sunyer Biomedical Research Institute (IDIBAPS), Barcelona, Spain, [9]Networked Biomedical Research Centre for Neurodegenerative Disorders (CIBERNED), Madrid, Spain, [10]Department of Neurology, James J. Peters Veterans Affairs Medical Center, Bronx, NY, United States, [11]Department of Neurology, Icahn School of Medicine at Mount Sinai, New York City, NY, United States

KEYWORDS

BLTP, VPS13, XK, neurodegeneration, neurodevelopment, neuroacanthocytosis

Editorial on the Research Topic
Progress in neuroacanthocytosis syndromes and related diseases including other bulk lipid transfer disorders

The rare conditions XK disease (McLeod syndrome) and VPS13A disease (chorea-acanthocytosis) have historically been termed "neuroacanthocytosis" due to the association of neurodegeneration, particularly of the basal ganglia, with spiky deformed red blood cells (acanthocytes). Even more obsolete is the 1960s' designation "Levine-Critchley syndrome": genetic analyses of the reported families have determined that Levine's patients were affected by mutations of *XK* and those of Critchley by *VPS13A* variants. Two multi-author books summarize early developments (Danek, 2004; Walker et al., 2008).

Clinical updates regarding VPS13A disease and XK disease are regularly provided in open access resources (Peikert et al., 2023; Jung et al., 2021). Typical presentations are in young adults of any sex, often siblings (due to autosomal-recessive *VPS13A* mutations), or in middle-aged men, often maternal uncles and nephews (due to X-linked *XK* mutations). In addition to disorders of movement, cognition, and behavior ("huntingtonism"), there may be seizures, neuropathy, and myopathy. Impairment of activities of daily life and a reduced life span are typical, however clinical features can vary considerably. The presence of acanthocytosis is unreliable as a biomarker and, unfortunately, erythrocyte sedimentation rate prolongation as well as creatine kinase elevation, typical in both conditions, are non-specific and easily overlooked. The two conditions' close resemblance is likely explained by the recent observations that the XK and VPS13A proteins interact

to enable bulk lipid transport at contact sites between various cell organelles as well as the cell membrane.

Testing at the DNA or protein level (genes: *VPS13A* and *XK*; proteins: VPS13A/chorein and Kell complex red cell antigen Kx) clearly distinguishes the two conditions, however, diagnostic delay continues to be a significant issue due to a variety of factors, including access to molecular testing. It is critical to use the genetic nomenclature rather than the historical term "neuroacanthocytosis" to ensure that patients receiving these diagnoses have been confirmed to carry causative variants of the responsible genes. As we enter the era of molecular treatments, this research topic becomes even more critical.

The VPS13 family comprises additional proteins involved in neurodegeneration (VPS13C, VPS13D) and neurodevelopment (VPS13B, associated with Cohen syndrome) and belongs to the newly recognized superfamily of bridge-like lipid transfer proteins (BLTPs; within this nomenclature, the VPS13 proteins are known as BLTP5A-BLTP5D). This family also includes "Tweek" (BLTP1, involved in a neurodevelopmental disorder) and "Hobbit" (BLTP2). Research in this field has rapidly taken off and flourishes (Levine and Conibear, 2024; Hanna et al., 2023; Reinisch et al., 2025).

Below we summarize the contributions to the Research Topic "Progress in Neuroacanthocytosis Syndromes and Related Diseases Including other Bulk Lipid Transfer Disorders" that grew out of the 11th International Neuroacanthocytosis Symposium (Kaestner, 2023). Further contributions resulted from the "VPS13 forum," a teleconferencing discussion format that developed with the COVID-19 pandemic (Peikert and Danek, 2023).

Swan exhaustively reviews the BLTP family as well as its members' respective proteins and asks essential questions about their transport function; whether it is just unidirectional or works both ways, how selective for lipid type it is, what drives it, and how it may be regulated. Neiman elaborates this perspective: molecular dysfunction might be treated with transport-enhancing molecules or with bypassing agents. Naturally existing bypasses or duplicate pathways in some of the congenital BLTP diseases offer excellent explanations for delays of their onset into early (VPS13A) and even late (XK) adulthood, while non-viability with complete *VPS13D* knockdown (Seong et al., 2018) marks certain lipid transport pathways as essential for survival: their loss cannot be compensated for.

Osmotic gradient ektacytometry of erythrocytes for diagnostic screening was comprehensively explored by Hernández et al.. Along with microfluidic assays the approach is promising, however sensitivity, specificity, and availability of these novel screening test candidates need further elaboration. Ektacytometry in a complex single case of VPS13A disease who also harbored a *CANVAS* mutation confirmed its usefulness as well as in another VPS13A case and a patient with XK disease, but, as reported by Paucar et al., was normal in acanthocytosis associated with liver disease. Based on their single case observation, Xu et al. review the status of treating VPS13A disease symptomatically with deep brain stimulation.

The presentations of XK and VPS13A diseases with a clinical phenotype similar to Huntington's disease (HD) invite a comparison between these disorders, which share the feature of caudate nucleus vulnerability. García-García et al. undertook one such study and in both, HD transgenic mouse and HD human brain, found VPS13A distribution and expression essentially unaltered.

Turning to XK disease presentation, Walker et al. report four new cases with proven mutations and typical Kell blood group findings, and provide follow-up on members from two known families. Dambietz et al. report on the protracted diagnostic process in one patient with cerebrospinal fluid T-cell abnormalities. If confirmed in absence of COVID-19, this novel finding suggests as yet unexplored functions of XK (see also Tanti et al., 2024).

Complementing the neurological, psychiatric, cardiologic, and hematologic perspectives of BLTP diseases, Schottmann et al. focus on the pediatric and ophthalmological condition of Cohen syndrome and on intricacies of its genetic testing and prediction. In their family with two clinically affected members four rare *VPS13B* variants were detected. Of one in particular, the disease-causing property was unclear until it underwent functional testing. Vacca et al. review the molecular mechanisms possibly underlying VPS13B disease, focusing on studies in mice and the naturally occurring VPS13B disease model of Border Collies ("trapped neutrophil syndrome").

The articles collected here represent a number of recent advances in this rapidly-evolving field. The ultimate goal is to develop and validate therapies for these devastating neurological and multi-organ disorders, and additionally to add to understanding of cellular processes which may benefit other fields.

Author contributions

AD: Writing – original draft. AH: Writing – review & editing. LK: Writing – original draft. MM: Writing – review & editing. KP: Writing – review & editing. MJR: Writing – review & editing. RHW: Writing – original draft.

Acknowledgments

We are grateful to the ongoing support of Advocacy for Neuroacanthocytosis Patients (https://naadvocacy.org/) and NA Advocacy USA (https://www.naadvocacyusa.org/), and for the critical participation of patients and carers in our multi-disciplinary research. The 12th symposium will take place in Lausanne, Switzerland, this September (International Conference on Neuroacanthocytosis, Cohen Syndrome, and other VPS13-related disorders: https://events.ophtalmique.ch/evenement/vps13-meeting/). As with all previous meetings, we invite the participation of both clinicians and basic scientists, and welcome investigators in adjoining fields such as veterinary medicine (e.g., trapped neutrophil syndrome) and microbiology (role of bulk lipid transfer for e.g., bacterial integrity).

Conflict of interest

The authors declare that the research was conducted in the absence of any commercial or financial relationships that could be construed as a potential conflict of interest.

The author(s) declared that they were an editorial board member of Frontiers, at the time of submission. This had no impact on the peer review process and the final decision.

Generative AI statement

The authors declare that no Gen AI was used in the creation of this manuscript.

Publisher's note

References

Danek, A. (2004). *Neuroacanthocytosis Syndromes*. Dordrecht, The Netherlands: Springer. doi: 10.1007/1-4020-2898-9

Hanna, M., Guillén-Samander, A., and De Camilli, P. (2023). RBG motif bridge-like lipid transport proteins: structure, functions, and open questions. *Annu. Rev. Cell Dev. Biol.* 39, 409–434. doi: 10.1146/annurev-cellbio-120420-014634

Jung, H. H., Danek, A., Walker, R. H., Frey, B. M., and Peikert, K. (2021). "McLeod neuroacanthocytosis syndrome," in *GeneReviews®* (Seattle, WA: University of Washington, Seattle). Available online at: http://www.ncbi.nlm.nih.gov/books/NBK1354/

Kaestner, L. (2023). Proceedings of the eleventh international meeting on neuroacanthocytosis syndromes. *Tremor Other Hyperkinet Mov* 13:41. doi: 10.5334/tohm.826

Levine, T. P., and Conibear, L. (2024). Editorial on special collection in contact: VPS13 and bridge-like lipid transfer proteins: a new mode of intracellular continuity. *CONTACT* 7:25152564241238538. doi: 10.1177/25152564241238538

Peikert, K., and Danek, A. (2023). VPS13 forum proceedings: XK, XK-related and VPS13 proteins in membrane lipid dynamics. *Contact* 6:25152564231156994. doi: 10.1177/25152564231156994

Peikert, K., Dobson-Stone, C., Rampoldi, L., Miltenberger-Miltenyi, G., Neiman, A., De Camilli, P., et al. (2023). "VPS13A Disease," in *GeneReviews®*, (Seattle, WA: University of Washington, Seattle). Available online at: http://www.ncbi.nlm.nih.gov/books/NBK1387/

Reinisch, K. M., De Camilli, P., and Melia, T. J. (2025). Lipid dynamics at membrane contact sites. *Annu. Rev. Biochem.* doi: 10.1146/annurev-biochem-083024-122821. [Epub ahead of print].

Seong, E., Insolera, R., Dulovic, M., Kamsteeg, E.-J., Trinh, J., Brüggemann, N., et al. (2018). Mutations in *VPS13D* lead to a new recessive ataxia with spasticity and mitochondrial defects. *Ann. Neurol.* 83, 1075–1088. doi: 10.1002/ana.25220

Tanti, G. K., Brill, M. L., Kalluri, S., Srivastava, R., Lepennetier, G., Öllinger, R., et al. (2024). "Xk is a novel oligodendrocyte protein with a potential role in de/remyelination," in *Program No. PSTR325.01. 2024 Neuroscience Meeting Planner*. Chicago, IL: Society for Neuroscience. Available online at: https://www.abstractsonline.com/pp8/#!/20433/presentation/19115

Walker, R. H., Saiki, S., and Danek, A. (2008). *Neuroacanthocytosis Syndromes II*. Berlin Heidelberg, Germany: Springer. doi: 10.1007/978-3-540-71693-8

frontiers | Frontiers in Neuroscience

TYPE Perspective
PUBLISHED 14 December 2023
DOI 10.3389/fnins.2023.1321250

OPEN ACCESS

EDITED BY
Merce Masana,
University of Barcelona, Spain

REVIEWED BY
Fabrizio Vacca,
Hôpital Ophtalmique Jules-Gonin, Switzerland
Joanna Kamińska,
Institute of Biochemistry and Biophysics (PAS), Poland

*CORRESPONDENCE
Aaron M. Neiman
✉ aaron.neiman@stonybrook.edu

RECEIVED 13 October 2023
ACCEPTED 29 November 2023
PUBLISHED 14 December 2023

CITATION
Neiman AM (2023) Pharmacological interventions for lipid transport disorders. *Front. Neurosci.* 17:1321250. doi: 10.3389/fnins.2023.1321250

Pharmacological interventions for lipid transport disorders

Aaron M. Neiman*

Department of Biochemistry and Cell Biology, Stony Brook University, Stony Brook, NY, United States

The recent discovery that defects in inter-organelle lipid transport are at the heart of several neurological and neurodegenerative disorders raises the challenge of identifying therapeutic strategies to correct lipid transport defects. This perspective highlights two potential strategies suggested by the study of lipid transport in budding yeast. In the first approach, small molecules are proposed that enhance the lipid transfer activity of *VPS13* proteins and thereby compensate for reduced transport. In the second approach, molecules that act as inter-organelle tethers could be used to create artificial contact sites and bypass the loss of endogenous contacts.

KEYWORDS

membrane contact site (MCS), *VPS13* genes, lipid transport, proteolysis-targeting chimeric (PROTAC) molecule, neuroacanthocytosis, Parkinson's disease

Introduction

Mutations in the *VPS13* gene family in humans (*VPS13A*, *B*, *C* or *D*) are associated with VPS13A disease, Cohen Syndrome, Parkinson's disease or cerebellar ataxia, respectively (Holmes et al., 2001; Rampoldi et al., 2001; Kolehmainen et al., 2003; Hayflick et al., 2013; Lesage et al., 2016; Gauthier et al., 2018; Seong et al., 2018). Recently it was discovered that *VPS13* genes encode proteins that bind the membranes of different organelles and mediate transfer of lipids between those membranes through a hydrophobic channel within the VPS13 protein (Figure 1A). These findings suggest that a failure in lipid transport is the basis of the different VPS13 family diseases and that the proper lipid composition of different organelles is critical to prevent these disorders.

The recognition of the molecular function of the VPS13 family raises an important general question in the potential treatment of this class of diseases – how can pharmacological intervention be used to reverse the cellular effects of a lipid transport defect? The purpose of this perspective is to consider potential strategies for the development of pharmaceuticals that can directly restore lipid transport and thereby address the root cause of the disease. I highlight results from studies using the yeast model system that suggest two possible avenues for the development of such drugs.

Strategy 1: lipid transport enhancers: improving the function of mutant VPS13 proteins

In yeast there is a single *VPS13* gene that is required for multiple, independent processes, including spore formation, vacuolar sorting, mitochondrial integrity and endoplasmic reticulum (ER)-phagy (Bankaitis et al., 1986; Park and Neiman, 2012; Park et al., 2016; Chen et al., 2020). For example, the Vps13 protein acts in parallel with a different lipid transfer protein complex, termed ERMES, to mediate lipid transport between mitochondria and other organelles (Lang

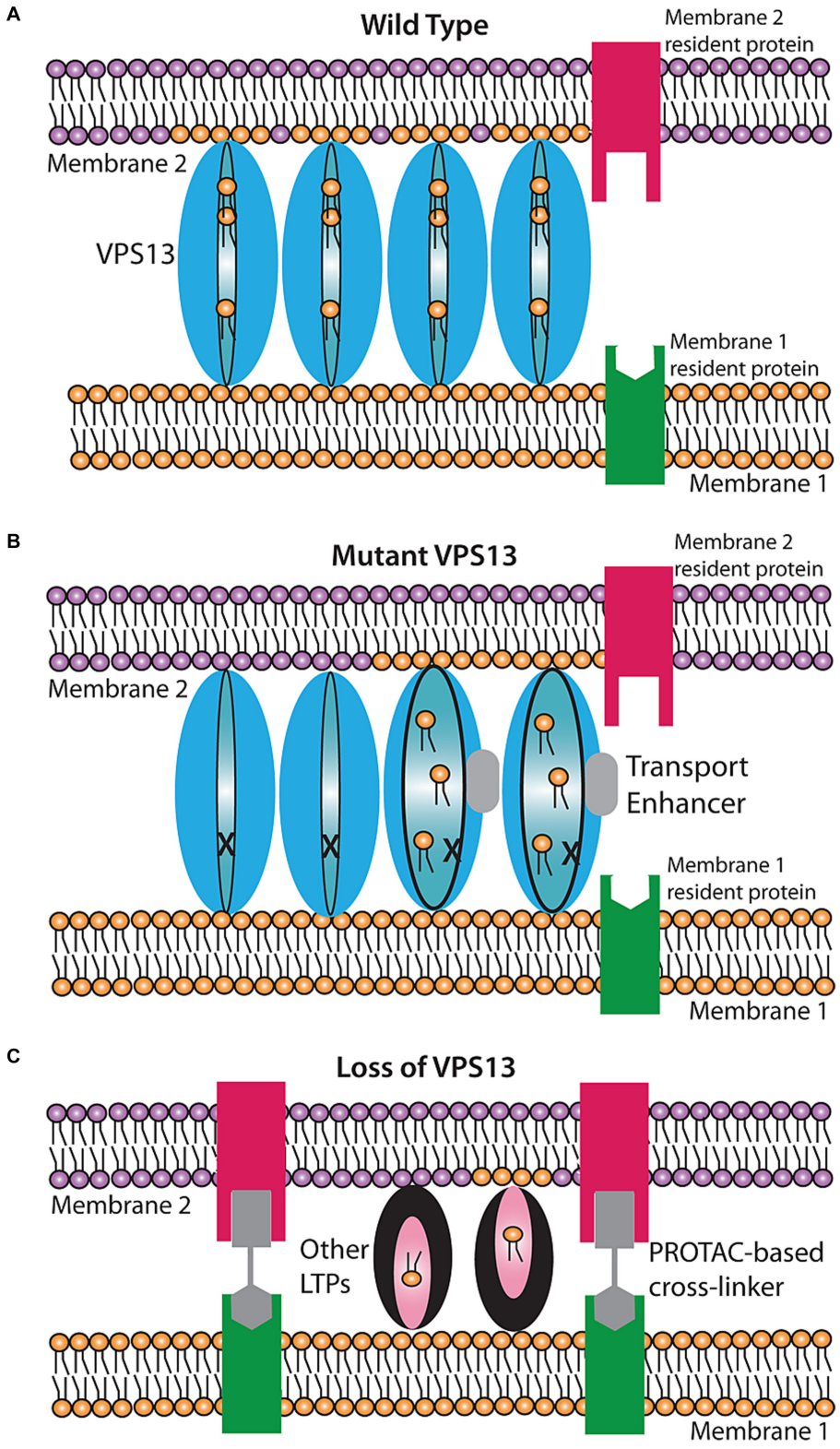

FIGURE 1
Proposed models for rescue of lipid transport in VPS13 mutant cells. **(A)** Wild-type transport at a VPS13-mediated contact site. VPS13 protein (blue oval) can transfer lipids between membranes through a hydrophobic channel in the protein. **(B)** Rescue by a transport enhancer. In the presence of a defective VPS13 (indicated by the 'X'), transport is stopped. A transport enhancer (gray box) triggers a conformational change in the VPS13 protein restoring transport function. **(C)** Rescue by a bypass agent. In cells entirely lacking VPS13, new contact sites can be created by introducing a bifunctional cross linker that creates an artificial contact site between the two membranes. Other lipid transport proteins (LTPs) in the cell can then mediate lipid transport at these artificial contacts.

et al., 2015; Park et al., 2016). While mutants that individually abolish ERMES or Vps13 function are viable, loss of both ERMES and Vps13 function is lethal (Lang et al., 2015; Park et al., 2016). Several groups have identified mutations in the *VPS13* gene that compensate for the loss of ERMES, restoring normal growth (Lang et al., 2015; Park et al., 2016; van Leeuwen et al., 2016). These mutations create dominant, gain-of-function *VPS13* alleles, one of which is *VPS13-G718K*. One explanation for the ability of the dominant *VPS13* mutants to suppress the phenotypes associated with lack of ERMES is that the mutations increase Vps13-mediated delivery of lipids to mitochondria to obviate the need for ERMES.

The dominant *VPS13* mutations not only compensate for the loss of ERMES, they can act as intragenic suppressors of non-null *vps13* alleles as well (Park et al., 2016, 2021). For example, some patients with VPS13A disease carry a substitution of leucine 67 to proline in VPS13A. Mutating the corresponding leucine codon in yeast *VPS13* to proline creates the *vps13-L66P* allele that is synthetically lethal in combination with an ERMES mutant (Tomiyasu et al., 2011; Park et al., 2016). Introduction of a dominant gain-of-function *VPS13* mutation such as *G718K* into *vps13-L66P* restores growth in the absence of ERMES, perhaps by increasing levels of Vps13-mediated lipid transport. Similarly, when a cognate mutation to one in *VPS13D* identified in patients with cerebellar ataxia is introduced into yeast *VPS13* (*vps13-N2428S*), proper delivery of cargoes to the yeast vacuole is disrupted (Gauthier et al., 2018; Park et al., 2021). Introduction of the *G718K* mutation into the *vps13-N2428S* allele partially relieves this trafficking defect. Thus, in the context of the yeast cell, these mutations can promote the function of a mutant Vps13 protein at different contact sites, possibly by increasing the efficacy of lipid transfer.

An important point is that these suppressor mutations are relatively easy to obtain. Nineteen different suppressor mutations have been identified and they map throughout the N-terminal half of the Vps13 protein, particularly along the portion that forms the lipid transport channel (Lang et al., 2015; Park et al., 2016; van Leeuwen et al., 2016; Hanna et al., 2023). If these mutations promote a conformation that is permissive for lipid transfer, it may be possible to identify pharmacological agents that similarly enhance lipid transport by mimicking the effect of these mutations on Vps13 protein conformation (Figure 1B). Based on the yeast results, such agents would be expected to partially or fully compensate for the cellular effects of a non-null allele of *VPS13*.

Such transport-enhancing agents may be particularly useful for *VPS13D* disorders where the alleles found in patients thus far are primarily missense mutations (Gauthier et al., 2018; Seong et al., 2018). Knockouts of *VPS13D* in *Drosophila* or mice are embryonic lethal (Anding et al., 2018; Gauthier et al., 2018; Seong et al., 2018), which suggests that the human *vps13D* mutant alleles found in patients are likely partially functional and so a drug that increased their activity could be an effective treatment. For the other human *VPS13* family genes, most of the alleles isolated from patients are null mutations that eliminate the protein (Dobson-Stone et al., 2002; Seifert et al., 2009; Monfrini et al., 2022). Even in these instances, however, there is the possibility that activating one member of the VPS13 family might be able to partially compensate for the loss of another. This is particularly true for VPS13A and VPS13C, which are the most closely related pair evolutionarily and have some overlap in the contact sites they occupy (Kumar et al., 2018; Chen et al., 2022).

Strategy 2: bypass agents: induction of alternative contact sites

For patients who carry null mutants of VPS13 family genes, what is needed is not an agent that increases the activity of a mutant protein but one that restores lipid transfer in the absence of the protein entirely. Results from yeast have shown that such a 'bypass agent' is obtainable. The role of ERMES is to create both a connection between ER and mitochondrial membranes and to shuttle lipids between those membranes at this contact site (Kornmann and Walter, 2010). Kornmann and colleagues created cells containing a synthetic protein with an N-terminal transmembrane domain anchored in the ER and a C-terminal transmembrane in the mitochondrial outer membrane (Kornmann et al., 2009). This construct holds the two membranes in close apposition creating artificial contact sites. Remarkably, even though this construct has no capacity to transfer lipids, its expression is sufficient to suppress the phenotypes of loss of ERMES (Kornmann et al., 2009). Thus, artificially anchoring the two membranes together must allow other lipid transfer activities in the cell to mediate the necessary movement of lipids. Whether such a bypass is unique to ERMES or can also occur for other (e.g., VPS13-mediated) contacts is not known, but well worth exploring. In principle, artificial tethers targeted to appropriate pairs of membranes could act as bypass agents to restore lipid transfer in the absence of VPS13 proteins (Figure 1C).

Protein-based interorganelle tethers have already been shown to work in human cells (Varnai and Balla, 1998; Chang et al., 2013; Jing et al., 2020). However, the use of protein-based tethers would be difficult therapeutically as the problems associated with delivering and expressing the proteins in the appropriate tissues would be significant. What is needed is a chemical agent that can be used to connect two membranes *in vivo*. Recently, therapeutics have been developed for use in a different context that could be employed to create artificial contact sites.

Proteolysis targeting chimeras (PROTACs) have been developed as a means of targeting specific proteins for ubiquitin mediated degradation in the cell (Neklesa et al., 2017; Liu et al., 2022). These molecules consist of three moieties; a ligand that binds specifically to an E3 ligase, a linker region whose length can be varied, and a second ligand that binds to the protein that is to be targeted for degradation. This system has been developed to eliminate disease-causing proteins, for example activated kinases or misfolded proteins, from the cell by linking the target to the ubiquitin ligase and thereby increasing its rate of turnover. This approach has shown great promise and several different PROTAC-based treatments are currently in clinical trials (Liu et al., 2022; Weng et al., 2023).

A variety of linkers and ligands have already been developed (Weng et al., 2023). Importantly, as the proteins to be degraded are often well-established drug targets, the ligand moieties take advantage of known drugs with high affinity to specific molecules making the pharmacological efficacy of the PROTAC more likely (Weng et al., 2023). To adapt this system to contact sites is simply a matter of placing ligands that bind to two different integral membrane proteins of different organelles at the ends of the linker. For example placing ligands for a plasma membrane protein and an ER protein at either end of the linker would create a molecule that when added to cells should induce ER-Plasma membrane junctions.

Technical challenges for drug development

The dominant mutations identified in yeast are often substitutions of small residues such as glycine for large, charged residues such as arginine or glutamate (Lang et al., 2015; Park et al., 2016). Using structural models for the Vps13 proteins, it should be possible to design candidate molecules that bind and mimic the effects of introducing charges at these positions in the molecule (Batool et al., 2019). Even with a rational drug design approach, however, it will be necessary to screen through many candidate compounds. Thus, an important challenge will be to create cell-based assays for VPS13 protein function that allow for rapid screening of candidates. Currently, such assays exist for yeast, but appropriate cell lines and assays still need to be developed for the different human VPS13 family members.

For bypass agents, the use of the PROTAC platform would greatly speed the design of candidate molecules. For instance, ligands binding the plasma membrane protein CCR9 and the ER protein HMG-CoA reductase have already been incorporated into PROTACs (Li et al., 2020; Huber et al., 2022). Synthesis of a molecule with these ligands at either end should allow a rapid test of the ability of this approach to generate novel ER plasma membrane contacts. It should be noted, however, that these ligands might interfere with the function CCR9 and HMG-CoA reductase, respectively, creating unwanted effects. It will be important to ensure that the ligands used do not create cellular phenotypes on their own. Moreover, for protein-based interorganelle tethers it has been found that the length of the tether can have significant effects on its functionality (Varnai et al., 2007). Thus, it will be necessary not only to find appropriate ligands for each end of the PROTAC molecule but also to empirically test different lengths of linker. Again, the development of rapid phenotypic assays in knockout cell lines will be a critical tool for this process.

Discussion

Finally, to implement either of these strategies to address a specific disorder, more understanding of the cellular role of each VPS13 family protein is still required. For instance, in order to design PROTACs to connect the appropriate pair(s) of organelles, we will first need to know loss of which membrane contacts are relevant in each VPS13 family disease. However, this information is not necessary to begin developing and testing strategies to stimulate lipid transfer between any given pair of membranes. This will speed the development of treatments even as our understanding of the basis of these diseases continues to grow.

Data availability statement

The original contributions presented in the study are included in the article/supplementary material, further inquiries can be directed to the corresponding author.

Author contributions

AN: Writing – original draft, Writing – review & editing.

Funding

The author declares financial support was received for the research, authorship, and/or publication of this article. Work in the Neiman Lab is supported by NIH Grants GM072540 and GM145606 to AN.

Acknowledgments

The author thanks Nancy Hollingsworth and Jae-Sook Park for comments on the manuscript.

Conflict of interest

The author declares that the research was conducted in the absence of any commercial or financial relationships that could be construed as a potential conflict of interest.

Publisher's note

References

Anding, A. L., Wang, C., Chang, T. K., Sliter, D. A., Powers, C. M., Hofmann, K., et al. (2018). *Vps13D* encodes a ubiquitin-binding protein that is required for the regulation of mitochondrial size and clearance. *Curr. Biol.* 28, 287–295.e6. doi: 10.1016/j.cub.2017.11.064

Bankaitis, V. A., Johnson, L. M., and Emr, S. D. (1986). Isolation of yeast mutants defective in protein targeting to the vacuole. *Proc. Natl. Acad. Sci. U. S. A.* 83, 9075–9079. doi: 10.1073/pnas.83.23.9075

Batool, M., Ahmad, B., and Choi, S. (2019). A structure-based drug discovery paradigm. *Int. J. Mol. Sci.* 20:2783. doi: 10.3390/ijms20112783

Chang, C. L., Hsieh, T. S., Yang, T. T., Rothberg, K. G., Azizoglu, D. B., Volk, E., et al. (2013). Feedback regulation of receptor-induced Ca2+ signaling mediated by E-Syt1 and Nir2 at endoplasmic reticulum-plasma membrane junctions. *Cell Rep.* 5, 813–825. doi: 10.1016/j.celrep.2013.09.038

Chen, S., Mari, M., Parashar, S., Liu, D., Cui, Y., Reggiori, F., et al. (2020). Vps13 is required for the packaging of the ER into autophagosomes during ER-phagy. *Proc. Natl. Acad. Sci. U. S. A.* 117, 18530–18539. doi: 10.1073/pnas.2008923117

Chen, S., Roberts, M. A., Chen, C. Y., Markmiller, S., Wei, H. G., Yeo, G. W., et al. (2022). *VPS13A* and *VPS13C* influence lipid droplet abundance. *Contact* 5:251525642211256. doi: 10.1177/25152564221125613

Dobson-Stone, C., Danek, A., Rampoldi, L., Hardie, R. J., Chalmers, R. M., Wood, N. W., et al. (2002). Mutational spectrum of the CHAC gene in patients with chorea-acanthocytosis. *Eur. J. Hum. Genet.* 10, 773–781. doi: 10.1038/sj.ejhg.5200866

Gauthier, J., Meijer, I. A., Lessel, D., Mencacci, N. E., Krainc, D., Hempel, M., et al. (2018). Recessive mutations in *VPS13D* cause childhood onset movement disorders. *Ann. Neurol.* 83, 1089–1095. doi: 10.1002/ana.25204

Hanna, M., Guillen-Samander, A., and De Camilli, P. (2023). RBG motif bridge-like lipid transport proteins: structure, functions, and open questions. *Annu. Rev. Cell Dev. Biol.* 39, 409–434. doi: 10.1146/annurev-cellbio-120420-014634

Hayflick, S. J., Kruer, M. C., Gregory, A., Haack, T. B., Kurian, M. A., Houlden, H. H., et al. (2013). beta-propeller protein-associated neurodegeneration: a new X-linked dominant disorder with brain iron accumulation. *Brain* 136, 1708–1717. doi: 10.1093/brain/awt095

Holmes, S. E., O'Hearn, E., Rosenblatt, A., Callahan, C., Hwang, H. S., Ingersoll-Ashworth, R. G., et al. (2001). A repeat expansion in the gene encoding junctophilin-3 is associated with Huntington disease-like 2. *Nat. Genet.* 29, 377–378. doi: 10.1038/ng760

Huber, M. E., Toy, L., Schmidt, M. F., Vogt, H., Budzinski, J., Wiefhoff, M. F. J., et al. (2022). A chemical biology toolbox targeting the intracellular binding site of CCR9: fluorescent ligands, new drug leads and PROTACs. *Angew. Chem. Int. Ed. Engl.* 61:e202116782. doi: 10.1002/anie.202116782

Jing, J., Liu, G., Huang, Y., and Zhou, Y. (2020). A molecular toolbox for interrogation of membrane contact sites. *J. Physiol.* 598, 1725–1739. doi: 10.1113/JP277761

Kolehmainen, J., Black, G. C., Saarinen, A., Chandler, K., Clayton-Smith, J., Traskelin, A. L., et al. (2003). Cohen syndrome is caused by mutations in a novel gene, COH1, encoding a transmembrane protein with a presumed role in vesicle-mediated sorting and intracellular protein transport. *Am. J. Hum. Genet.* 72, 1359–1369. doi: 10.1086/375454

Kornmann, B., Currie, E., Collins, S. R., Schuldiner, M., Nunnari, J., Weissman, J. S., et al. (2009). An ER-mitochondria tethering complex revealed by a synthetic biology screen. *Science* 325, 477–481. doi: 10.1126/science.1175088

Kornmann, B., and Walter, P. (2010). ERMES-mediated ER-mitochondria contacts: molecular hubs for the regulation of mitochondrial biology. *J. Cell Sci.* 123, 1389–1393. doi: 10.1242/jcs.058636

Kumar, N., Leonzino, M., Hancock-Cerutti, W., Horenkamp, F. A., Li, P., Lees, J. A., et al. (2018). *VPS13A* and *VPS13C* are lipid transport proteins differentially localized at ER contact sites. *J. Cell Biol.* 217, 3625–3639. doi: 10.1083/jcb.201807019

Lang, A. B., John Peter, A. T., Walter, P., and Kornmann, B. (2015). ER-mitochondrial junctions can be bypassed by dominant mutations in the endosomal protein Vps13. *J. Cell Biol.* 210, 883–890. doi: 10.1083/jcb.201502105

Lesage, S., Drouet, V., Majounie, E., Deramecourt, V., Jacoupy, M., Nicolas, A., et al. (2016). Loss of *VPS13C* function in autosomal-recessive parkinsonism causes mitochondrial dysfunction and increases PINK1/Parkin-dependent Mitophagy. *Am. J. Hum. Genet.* 98, 500–513. doi: 10.1016/j.ajhg.2016.01.014

Li, M. X., Yang, Y., Zhao, Q., Wu, Y., Song, L., Yang, H., et al. (2020). Degradation versus inhibition: development of proteolysis-targeting chimeras for overcoming statin-induced compensatory upregulation of 3-Hydroxy-3-methylglutaryl coenzyme a reductase. *J. Med. Chem.* 63, 4908–4928. doi: 10.1021/acs.jmedchem.0c00339

Liu, Z., Hu, M., Yang, Y., Du, C., Zhou, H., Liu, C., et al. (2022). An overview of PROTACs: a promising drug discovery paradigm. *Mol. Biomed.* 3:46. doi: 10.1186/s43556-022-00112-0

Monfrini, E., Spagnolo, F., Canesi, M., Seresini, A., Rini, A., Passarella, B., et al. (2022). *VPS13C*-associated Parkinson's disease: two novel cases and review of the literature. *Parkinsonism Relat. Disord.* 94, 37–39. doi: 10.1016/j.parkreldis.2021.11.031

Neklesa, T. K., Winkler, J. D., and Crews, C. M. (2017). Targeted protein degradation by PROTACs. *Pharmacol. Ther.* 174, 138–144. doi: 10.1016/j.pharmthera.2017.02.027

Park, J. S., Hollingsworth, N. M., and Neiman, A. M. (2021). Genetic dissection of Vps13 regulation in yeast using human disease mutations. *Int. J. Mol. Sci.* 22:6200. doi: 10.3390/ijms22126200

Park, J. S., and Neiman, A. M. (2012). VPS13 regulates membrane morphogenesis during sporulation in *Saccharomyces cerevisiae*. *J. Cell Sci.* 125, 3004–3011. doi: 10.1242/jcs.105114

Park, J. S., Thorsness, M. K., Policastro, R., Mcgoldrick, L., Hollingsworth, N. M., Thorsness, P. E., et al. (2016). Yeast Vps13 promotes mitochondrial function and is localized at membrane contact sites. *Mol. Biol. Cell* 27, 2435–2449. doi: 10.1091/mbc.e16-02-0112

Rampoldi, L., Dobson-Stone, C., Rubio, J. P., Danek, A., Chalmers, R. M., Wood, N. W., et al. (2001). A conserved sorting-associated protein is mutant in chorea-acanthocytosis. *Nat. Genet.* 28, 119–120. doi: 10.1038/88821

Seifert, W., Holder-Espinasse, M., Kuhnisch, J., Kahrizi, K., Tzschach, A., Garshasbi, M., et al. (2009). Expanded mutational spectrum in Cohen syndrome, tissue expression, and transcript variants of *COH1*. *Hum. Mutat.* 30, E404–E420. doi: 10.1002/humu.20886

Seong, E., Insolera, R., Dulovic, M., Kamsteeg, E. J., Trinh, J., Bruggemann, N., et al. (2018). Mutations in *VPS13D* lead to a new recessive ataxia with spasticity and mitochondrial defects. *Ann. Neurol.* 83, 1075–1088. doi: 10.1002/ana.25220

Tomiyasu, A., Nakamura, M., Ichiba, M., Ueno, S., Saiki, S., Morimoto, M., et al. (2011). Novel pathogenic mutations and copy number variations in the *VPS13A* gene in patients with chorea-acanthocytosis. *Am. J. Med. Genet. B Neuropsychiatr. Genet.* 156B, 620–631. doi: 10.1002/ajmg.b.31206

Van Leeuwen, J., Pons, C., Mellor, J. C., Yamaguchi, T. N., Friesen, H., Koschwanez, J., et al. (2016). Exploring genetic suppression interactions on a global scale. *Science* 354:aag0839. doi: 10.1126/science.aag0839

Varnai, P., and Balla, T. (1998). Visualization of phosphoinositides that bind pleckstrin homology domains: calcium- and agonist-induced dynamic changes and relationship to myo-[3H]inositol-labeled phosphoinositide pools. *J. Cell Biol.* 143, 501–510. doi: 10.1083/jcb.143.2.501

Varnai, P., Toth, B., Toth, D. J., Hunyady, L., and Balla, T. (2007). Visualization and manipulation of plasma membrane-endoplasmic reticulum contact sites indicates the presence of additional molecular components within the STIM1-Orai1 complex. *J. Biol. Chem.* 282, 29678–29690. doi: 10.1074/jbc.M704339200

Weng, G., Cai, X., Cao, D., Du, H., Shen, C., Deng, Y., et al. (2023). PROTAC-DB 2.0: an updated database of PROTACs. *Nucleic Acids Res.* 51, D1367–D1372. doi: 10.1093/nar/gkac946

frontiers | Frontiers in Neuroscience

TYPE Brief Research Report
PUBLISHED 05 June 2024
DOI 10.3389/fnins.2024.1394478

OPEN ACCESS

EDITED BY
Anuska V. Andjelkovic,
University of Michigan, United States

REVIEWED BY
Nutan Sharma,
Harvard Medical School, United States
Roberto Rodríguez-Labrada,
Cuban Neuroscience Center, Cuba

*CORRESPONDENCE
Manuel J. Rodríguez
✉ marodriguez@ub.edu
Mercè Masana
✉ mmasana@ub.edu

†These authors have contributed equally to this work

RECEIVED 01 March 2024
ACCEPTED 20 May 2024
PUBLISHED 05 June 2024

CITATION
García-García E, Carreras-Caballé M, Coll-Manzano A, Ramón-Lainez A, Besa-Selva G, Pérez-Navarro E, Malagelada C, Alberch J, Masana M and Rodríguez MJ (2024) Preserved VPS13A distribution and expression in Huntington's disease: divergent mechanisms of action for similar movement disorders? *Front. Neurosci.* 18:1394478. doi: 10.3389/fnins.2024.1394478

Preserved VPS13A distribution and expression in Huntington's disease: divergent mechanisms of action for similar movement disorders?

Esther García-García[1,2,3], Maria Carreras-Caballé[1,2], Albert Coll-Manzano[1], Alba Ramón-Lainez[1,2,3], Gisela Besa-Selva[1,2,3], Esther Pérez-Navarro[1,2,3], Cristina Malagelada[1,2,3], Jordi Alberch[1,2,3,4], Mercè Masana[1,2,3*†] and Manuel J. Rodríguez[1,2,3*†]

[1]Department of Biomedical Sciences, School of Medicine and Health Sciences, Institute of Neurosciences, Universitat de Barcelona, Barcelona, Spain, [2]August Pi i Sunyer Biomedical Research Institute (IDIBAPS), Barcelona, Spain, [3]Centro de Investigación Biomédica en Red de Enfermedades Neurodegenerativas (CIBERNED), Instituto de Salud Carlos III, Barcelona, Spain, [4]Production and Validation Center of Advanced Therapies (Creatio), Faculty of Medicine and Health Science, University of Barcelona, Barcelona, Spain

VPS13A disease and Huntington's disease (HD) are two basal ganglia disorders that may be difficult to distinguish clinically because they have similar symptoms, neuropathological features, and cellular dysfunctions with selective degeneration of the medium spiny neurons of the striatum. However, their etiology is different. VPS13A disease is caused by a mutation in the VPS13A gene leading to a lack of protein in the cells, while HD is due to an expansion of CAG repeat in the huntingtin (Htt) gene, leading to aberrant accumulation of mutant Htt. Considering the similarities of both diseases regarding the selective degeneration of striatal medium spiny neurons, the involvement of VPS13A in the molecular mechanisms of HD pathophysiology cannot be discarded. We analyzed the VPS13A distribution in the striatum, cortex, hippocampus, and cerebellum of a transgenic mouse model of HD. We also quantified the VPS13A levels in the human cortex and putamen nucleus; and compared data on mutant Htt-induced changes in VPS13A expression from differential expression datasets. We found that VPS13A brain distribution or expression was unaltered in most situations with a decrease in the putamen of HD patients and small mRNA changes in the striatum and cerebellum of HD mice. We concluded that the selective susceptibility of the striatum in VPS13A disease and HD may be a consequence of disturbances in different cellular processes with convergent molecular mechanisms already to be elucidated.

KEYWORDS

chorea-acanthocytosis, VPS13A, huntingtin, Huntington's disease, movement disorders, basal ganglia, neurodegeneration

1 Introduction

Basal ganglia disorders are a heterogeneous group of neurodegenerative diseases that affect selectively a group of neuronal populations in cortical and subcortical circuitries. VPS13A disease (chorea-acanthocytosis, ChAc, OMIM: 200150; Jung et al., 2011; Peikert et al., 2023) and Huntington's disease (HD, OMIM: 143100; Ross et al., 2014) are two basal ganglia disorders that are often clinically difficult to distinguish because they have similar symptoms, magnetic resonance imaging findings (Suzuki et al., 2020) and neuropathological features with selective degeneration of the medium spiny neurons (MSNs) in the striatum (Liu et al., 2019). However, the etiology of both diseases is different. ChAc is a rare autosomal recessive neurodegenerative disease caused by a mutation in the VPS13A gene located on chromosome 9, which encodes the protein VPS13A (Ueno et al., 2001). Meanwhile, HD is an autosomal dominant disease that is due to an expansion of CAG repeat in the huntingtin (Htt) gene located on chromosome 4 (Ross et al., 2014). Thus, MSNs have a selective vulnerability to the lack of VPS13A (Henkel et al., 2008; Walterfang et al., 2011) and to the accumulation of mutant Htt (mHtt; Vonsattel and DiFiglia, 1998; Kassubek et al., 2004), while other neuronal populations in the striatum, such as interneurons, are more resistant. Therefore, the understanding of the mechanisms that make MSNs more vulnerable can be useful in developing therapeutical strategies to protect these neurons and their circuitries.

The low frequency of ChAc patients determines the little knowledge so far about the localization and function of VPS13A. This is a large ubiquitous protein highly expressed in the brain with a distinct VPS13A distribution that contributes to explaining the ChAc neuropathology (García-García et al., 2021). However, although the main neuropathological feature in ChAc patients is the selective degeneration of the caudate nucleus and putamen, the concentration of VPS13A in basal ganglia nuclei is weak (Kurano et al., 2007; García-García et al., 2021). Thus, the vulnerability of striatal neurons to VPS13A disease seems not to be related to the amount of protein present in the cell, but to specific striatal functional properties, circuitry, and MSN cell processes specifically affected by the lack of VPS13A.

VPS13A has a large variety of cellular functions that can affect the selective vulnerability of distinct neuronal populations. At the cellular level, VPS13A is a lipid transport protein localized in the contact sites between organelles (Kumar et al., 2018). Its lack of function has been associated with endocytic trafficking and lysosomal degradation impairment (Muñoz-Braceras et al., 2019), impaired autophagic degradation (Muñoz-Braceras et al., 2015), and abnormal calcium homeostasis (Pelzl et al., 2017). Furthermore, although VPS13A is not enriched in the synaptic compartment (Kurano et al., 2007; García-García et al., 2021), it is important for maintaining the neuronal optimal synaptic activity. Indeed, synaptic plasticity impairment and deficient glutamatergic and BDNF transmissions have been related to mouse corticostriatal VPS13A knockdown (García-García et al., 2023). In this line, enhanced neurite outgrowth and ramifications have been described in MSNs differentiated from hiPSC derived from fibroblast of ChAc (Stanslowsky et al., 2016), reinforcing the role of VPS13A in shaping neuronal dendritic morphology.

Interestingly, in HD, mHtt expression is also ubiquitous (Marques Sousa and Humbert, 2013). It accumulates in neurons as insoluble and hardly removable aggregates leading to synaptic abnormalities. Impairment of corticostriatal synaptic plasticity has been widely documented in HD mouse models and patients, with important glutamatergic and BDNF transmission disturbances in the molecular basis of these impairments (Canals et al., 2004; Del Toro et al., 2006). Furthermore, the accumulation of mHtt impairs a plethora of cell functions, including disruption of the ERK1/2 and the PKA signaling pathways (Saavedra et al., 2011; Tyebji et al., 2015). More interestingly mHtt also alters autophagy (Ravikumar et al., 2004), RNA splicing processes (Fernández-Nogales et al., 2016), and the rate of synthesis of selective proteins in the striatum (Creus-Muncunill et al., 2019), being these alterations at the basis of the molecular mechanisms of MSN dysfunction.

Considering all that, the involvement of VPS13A in the molecular mechanisms of HD pathophysiology cannot be discarded. The first step to approach this hypothesis is to depict the distribution of VPS13A in the HD brain, which should help to further understand its role in both basal ganglia synaptic plasticity and connectivity, and the ChAc neurodegenerative mechanisms. Thus, this study is focused on the analysis of the putative changes in VPS13A brain distribution induced by mHtt, especially in the striatum, cortex, hippocampus, and cerebellum.

2 Materials and methods

2.1 Human post-mortem nervous tissue

Human post-mortem tissue samples of the motor cortex and putamen were used to assess VPS13A concentration. Samples were collected at autopsy from individuals who had suffered a clinical history of HD ($n = 3$ female + 4 male, age: 54.4 (28–72) years; postmortem intervals of 4–18 h), and from non-HD controls ($n = 4$ female +2 male, age: 62.7 (39–81) years; postmortem intervals of 4–17 h; Table 1).

2.2 HD mouse model

Male and female R6/1 transgenic mice expressing the human exon-1 of mHtt containing 145 CAG repeats, and their corresponding wildtype (WT) littermates were obtained from Jackson Laboratory (Bar Harbor, ME, United States) and maintained in a B6CBA background. Animals were housed together in groups of mixed genotypes and kept under a 12:12 h light/dark cycle in a room at 19–22 °C and 40–60% humidity, with free access to food and water.

2.3 Mouse brain tissue sampling

Mice aged 20 weeks were used in the experiments. At this age, R6/1 mice show motor disturbances and synaptic plasticity impairment (Fernández-García et al., 2020; Kim et al., 2020). For immunohistochemical analysis, mice were anesthetized with a mixture of ketamine plus xylazine (100 + 10 mg/kg, i.p.) and transcardially perfused with ice-cooled 0.1 M PBS, followed by 4% paraformaldehyde (PFA). Then, brains were removed and fixed by immersion in 4% PFA at 4°C overnight. All PFA-fixed brains were

TABLE 1 Human post-mortem Huntington's disease samples used in this study.

Patient	Pathological diagnosis	Gender	Age (years)	CAG repeats	Brain area
1	Control	Female	74	-	STR & CTX
2	Control	Female	60	-	STR & CTX
3	Control	Male	76	-	STR & CTX
4	Control	Female	71	-	STR & CTX
5	Control	Female	81	-	STR & CTX
6	Control	Male	39	-	STR & CTX
7	HD, Vonsattel grade 3	Male	55	48	STR & CTX
8	HD, Vonsattel grade 3	Male	85	40	STR & CTX
9	HD, Vonsattel grade 3	Female	65	45	STR
10	HD, Vonsattel grade 3	Female	72	42	STR & CTX
11	HD, Vonsattel grade 3	Male	53	45	STR & CTX
12	HD, Vonsattel grade 2	Female	28	62	STR & CTX
13	HD, Vonsattel grade 4	Male	60	43	STR & CTX

STR, Striatum (Putamen); CTX, Motor Cortex.

cryoprotected with 30% sucrose in 0.1 M PBS and 0.02% sodium azide and frozen in dry ice-cooled isopentane. Specimens were stored at −80°C until sectioning. Sagittal serial sections were collected at 14 µm with a cryotome. For biochemical analysis, mice underwent euthanasia by cervical dislocation, and the brains were removed, dissected, and kept at −80°C.

2.4 Fluorescence *in situ* hybridization

A FISH procedure was performed using the RNAscope® 2.5 High Definition–Red Assay kit (Advanced Cell Diagnostics, Newark, CA, United States), following the instructions of the manufacturer and as previously reported in García-García et al. (2021). The target probe for the mouse Vps13a gene (Probe-Mm-Vps13a-E61-E71-C2, Advanced Cell Diagnostics, Newark, CA, United States) was hybridized for 2 h at 40°C, followed by a series of signal amplification and washing steps. Hybridizations were performed in a HybEZTM Hybridization System (Advanced Cell Diagnostics, Newark, CA, United States). Negative controls were performed with a negative control probe (targeting the DapB gene from the *Bacillus subtilis* strain SMY) provided by the kit. Specific hybridization signals were detected by fluorescence, and RNA staining was identified as red dots.

Images of the Vps13a expression staining were obtained with an inverted microscope (Leica DMI6000 B, Thermo Fisher Scientific, Waltham, MA, United States). For qualitative visual analysis of the intensity of Vps13a mRNA labeling in the slices, digital images were processed using an 8-bit 16-color lookup table with ImageJ 1.51a (National Institutes of Health, Bethesda, MD, United States).

2.5 Quantitative real-time PCR

The aqueous phase containing total RNA was isolated from the different mouse brain regions using QIAzol (Qiagen, Hilden, Germany), following the protocol of the manufacturer. Total RNA isolation, reverse transcription of RNA and qRT-PCR were performed as already described (García-García et al., 2021). PrimeTime qPCR assays were used as recommended by the provider (assay code Mm.PT.56a.8500899, sequence NM_173028(1) for Vps13a, and assay code Mm.PT.39a.1 sequence NM_008084 for GAPDH; IDT technologies, United States). The expression level was determined using a standard curve and normalized to housekeeper Gapdh gene mRNA levels. The ΔΔCt method was used to analyze the data.

2.6 Western blot

Tissues were homogenized in lysis buffer and protein samples were resolved in SDS-PAGE and NuPAGE gels as already published (García-García et al., 2023). Immunoblots were probed with anti-VPS13A (1:1500, Cat: HPA021662, Sigma-Aldrich, St. Louis, MI, United States). Immunoreactive bands were visualized using the Western blotting Luminol Reagent (Santa Cruz Biotechnology, Dallas, TX, United States). Images were acquired using Chemidoc™ (Bio-Rad, Hercules, CA, United States) and quantified by a computer-assisted densitometer (ImageLab™, Bio-Rad, Hercules, CA, United States).

2.7 Statistical analysis

All experiments were blinded and randomized. All results are reported as mean ± SEM. Normal distribution of data was assumed when the Shapiro–Wilk test was positive for normality. Statistical analyses were performed using either a two-tailed Student's t-test or one-way ANOVA followed by the Bonferroni test. Lineal regression models were generated to assess the relationship between the VPS13A levels in human brain samples and the HD Vonsattel's grade or the number of CAG repeats. All statistic tests were performed on GraphPad Prism 9.0 (GraphPad Software, San Diego). Differential expression datasets from Microarray and RNA-seq analysis were

identified in the Gene Expression Omnibus (GEO) repository from the National Center for Biotechnology Information (NCBI). The comparisons between control and HD conditions were performed with the GEO2R tool of the repository. In all analyses, values of $p < 0.05$ were considered statistically significant.

3 Results

To study the distribution of vps13a mRNA, we performed FISH on sagittal brain sections from WT and R6/1 mice at the age of 20 weeks. First, we focused on the brain regions of interest (Figure 1A) and we found different staining intensity profiles as previously published (García-García et al., 2021). We observed a staining enrichment in the cerebellum, notably in Purkinje cells and the granular layer; the pyramidal layers of the hippocampus and granular layer of dentate gyrus also presented high levels of staining. We found moderate staining in the somatosensory cortex and with wide expression along all cortical layers with a marked signal in layer V. Staining in the striatum was weak. We found no apparent differences in staining intensity between WT and R6/1 mice (Figure 1A).

We then analyzed the effects of mHtt on the VPS13A expression in the cortex, striatum, hippocampus, and cerebellum of 20-week-old R6/1 mice. After mRNA quantification by qRT-PCR, we found a significant 19% VPS13A expression decrease in the striatum and a 23% increase in the cerebellum of R6/1 mice when compared with WT animals (Figure 1B). However, these changes were not corroborated by western blot since we found no mHtt-induced changes in the VPS13A protein concentration in any of the four studied areas (Figure 1C).

We next analyzed whether this lack of significant VPS13A changes in symptomatic R6/1 mice was also present in the cerebral cortex and

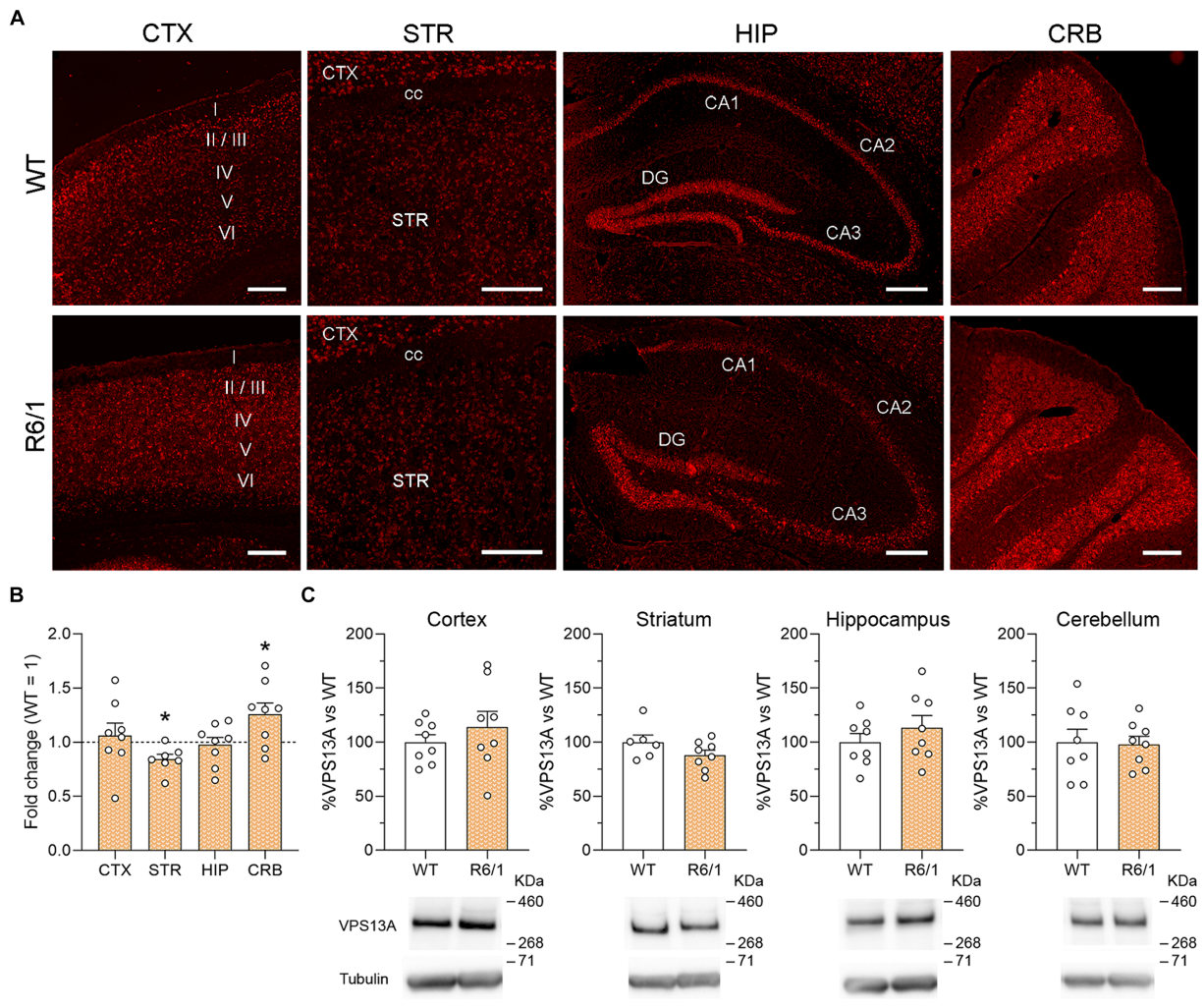

FIGURE 1
VPS13A mRNA and protein levels in representative brain regions of R6/1 mice. **(A)** Specific labeling of Vps13a mRNA in illustrative sagittal sections of striatum (STR), somatosensorial cortex (CTX), hippocampal formation (HIP) and cerebellum (CRB); cc, corpus callosum; STR, striatum; I, II, III, IV, V and VI are cortical layers; $n = 3$ WT and 3 R6/1 mice. Scale bar 250 µm. **(B)** Vps13a mRNA levels were analyzed by qRT-PCR in the striatum somatosensory cortex, striatum, hippocampus, and cerebellum. Values are expressed as mean ± SEM. Differences were analyzed by One-way ANOVA followed by the Bonferroni post-hoc test. *$p < 0.05$. Each point represents data from an individual mouse. $n = 8$ WT and 8 R6/1. **(C)** VPS13A protein levels were analyzed by western blot. Values are expressed as mean ± SEM. Differences were analyzed by Student's t-test. Each point represents data from an individual mouse. $n = 8$ Ctrl and 8 R6/1 (CTX, HIP and CRB) and 6 WT and 8 R6/1 (STR).

the putamen of HD patients. We found no significant changes in VPS13A levels in the motor cortex. However, we detected a significant 34% decrease in the putamen of HD patients compared with non-affected individuals by western blot (Figure 2A). The regression models showed no relationship between the levels of VPS13A protein with the HD Vonsattel's grade in the motor cortex or the putamen ($r^2 = 0.005$, $p = 0.893$ for the motor cortex and $r^2 = 0.098$, $p = 0.493$ for the putamen; Figure 2B). Finally, we found no significant correlation between the levels of VPS13A and the number of CAG repeats in the motor cortex ($r^2 = 0.023$, $p = 0.772$) or the putamen ($r^2 < 0.001$, $p = 0.994$; Figure 2C).

To validate these results, we finally assessed the involvement of the VPS13A gene expression changes in HD in a series of differential-expression datasets published in the GEO. We compared the VPS13A expression in either, the motor cortex of HD-patients vs. controls (Lin et al., 2016), the whole blood of HD patients vs. controls (Hu et al., 2011), the iPSC-derived MSNs of HD vs. control patients (Chiu et al., 2015), the striatum of R6/2 mice vs. WT mice (Labbadia et al., 2011),

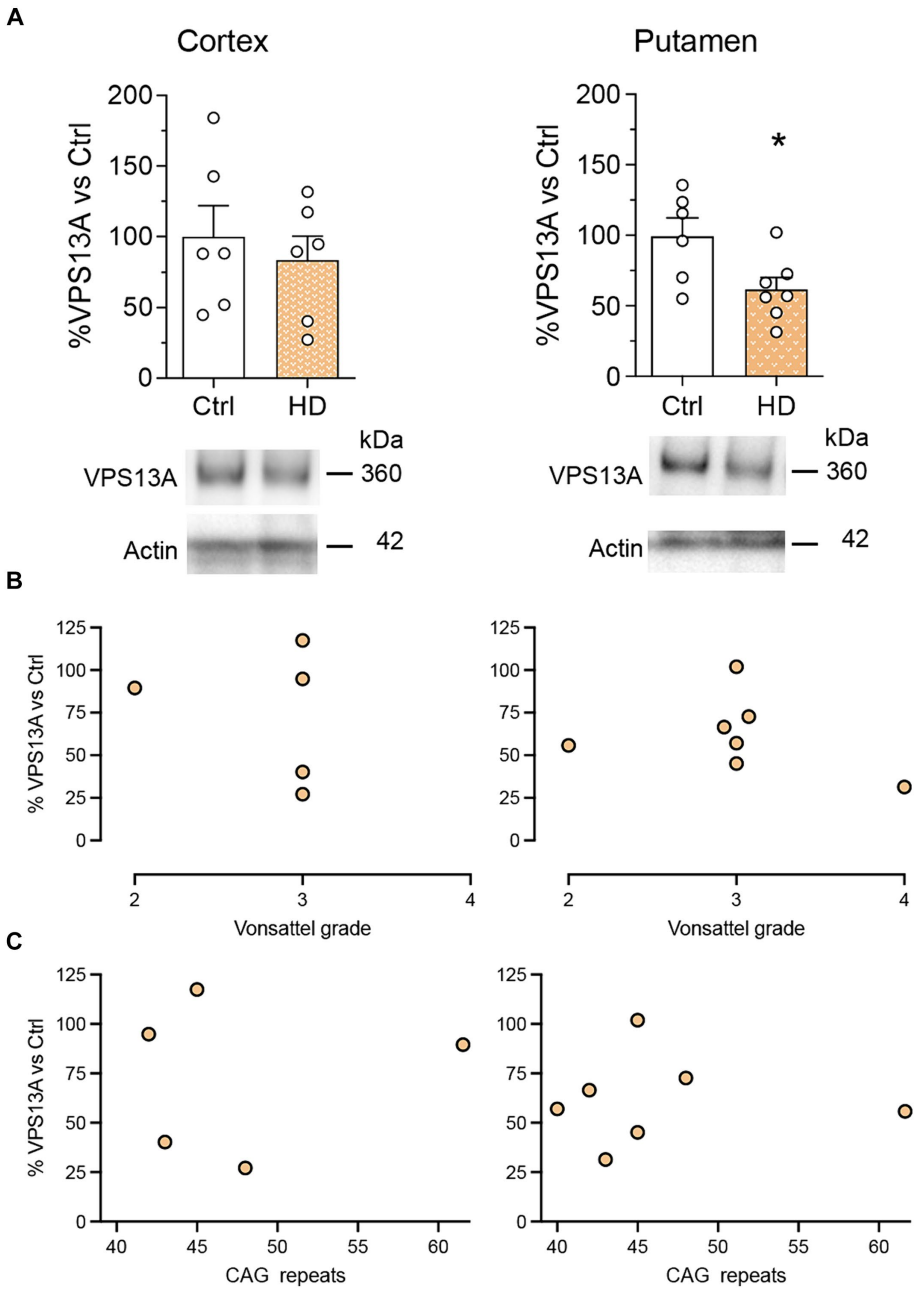

FIGURE 2
The levels of the VPS13A protein do not correlate with the HD condition. VPS13A protein levels were analyzed by western blot. **(A)** Representative immunoblots are shown. Values are expressed as mean ± SEM. Differences were analyzed by un-paired Student's *t*-test. $*p < 0.05$. Dot plots show the lack of correlation of the VPS13A levels in the motor cortex and the putamen with either the neuropathological stage (Vonsalttel grade) **(B)** or with the number of CAG repeats in the Htt gene **(C)**. Each point corresponds to the value from an individual sample. $n = 6$ Ctrl and 6 HD (cortex) and 6 Ctrl and 7 HD (putamen).

TABLE 2 Differential expression analyses of changes in VPS13A expression in the human and mouse HD datasets.

GEO dataset	Organism	Samples	LogFCh	Adj. *p*
GSE79666	Human	Motor cortex	0.0206	0.9690
GSE24250	Human	Whole blood	0.2008	0.9980
GSE59051	Human	iPSC-derived neurons	0.4195	0.5970
GSE29681	Mouse (R6/2 model)	Striatum	0.0876	0.8058
GSE11358	Mouse	STHdh cells	0.2790	0.7410

LogFCh, logarithm of the fold change; Adj. *p*, adjusted *p*-value.

and the conditionally immortalized HD STHdh$^{Q111/Q111}$ striatal neuronal progenitor cell line vs. conditionally immortalized WT STHdh$^{Q7/Q7}$ striatal neuronal progenitor cell line (Sadri-Vakili et al., 2007). According to the fold-change parameter of the VPS13A gene expression, with the *p*-value adjusted by the false discovery rate (Table 2), we found no significant HD effect in the VPS13A expression in any of the datasets analyzed.

4 Discussion

With the evidence from the results obtained, we found that mHtt accumulation only subtly alters VPS13A, with some significant changes in the mRNA and protein concentration in the striatum but does not influence the tissue distribution. This indicates that VPS13A is a very stable protein with crucial functions in neuronal functioning. Previous results found that VPS13A neuronal content is stable over time and that its concentration is not modulated by the overactivation of cholinergic, dopaminergic, or glutamatergic systems (García-García et al., 2021). Altogether, these data suggest that VPS13A has a stable presence and role in neurons with a fine regulation of protein levels that maintains its steady role.

Our results validate previous observations of the heterogeneous VPS13A brain distribution (Kurano et al., 2007; García-García et al., 2021). Of the four analyzed regions, the striatum showed the lowest expression, also in the HD brain, although it is the most affected area in ChAc patients, while the cerebellum showed the highest expression, also in the R6/1 mouse model of HD. The fact that mHtt does not modify the brain distribution of VPS13A indicates a lack of interdependence of both proteins. Consequently, it suggests that their respective mutations might trigger convergent pathological mechanisms affecting the weak cellular properties of the MSNs. Although the protein tissue distribution is unaffected, the decrease in protein levels in the putamen of HD patients suggests that a direct interaction of VPS13A with mHtt cannot be discarded. As proposed for many other proteins (Wanker et al., 2019), a pathological interaction of VPS13A with mHtt may limit its functionality and biological functions, leading to VPS13A dysfunction, subsequent deficient phospholipid homeostasis (Miltenberger-Miltenyi et al., 2023), and mitochondrial function impairment.

In this regard, both VPS13A and mHtt have been involved in some common cellular processes. For example, data suggest the VPS13A involvement in the protein degradation machinery and autophagy in ChAc pathophysiology (Muñoz-Braceras et al., 2015; Lupo et al., 2016; Vonk et al., 2017), a process that is also altered in HD (Ravikumar et al., 2004). However, among all these common pathophysiological processes, mitochondrial dysfunction stands out. Recent studies showed that VPS13A is localized at sites where the endoplasmic reticulum (ER) and mitochondria are in close contact to enable lipid transfer required for mitochondria and lipid-droplet-related processes in cell lines (Yeshaw et al., 2019). Interestingly, structural and functional changes in the ER-mitochondria contact sites leading to mitochondrial dysfunction (Shirendeb et al., 2011; Cherubini et al., 2020), and aberrant lipid homeostasis or calcium signaling (Aditi et al., 2016; Pchitskaya et al., 2018; Tshilenge et al., 2023) have been reported to contribute to the specific degeneration of the striatum in HD (Browne, 2008).

Additionally, despite the low expression of VPS13A and mHtt in the striatum, both VPS13A reduction and mHtt accumulation have been associated with striatal synaptic plasticity impairment (Parievsky et al., 2017; García-García et al., 2023) and a reduction of signaling molecules important for synaptic functioning such as BDNF and CX3CL1 (Canals et al., 2004; Giralt et al., 2009; Kim et al., 2020; Azman and Zakaria, 2022; García-García et al., 2023). Strong evidence links these two proteins with altered neuronal communication and deficient long-term depression induction in the corticostriatal circuitry of HD (Baydyuk et al., 2011; Besusso et al., 2013; Kim et al., 2020) Thus, defining the role of VPS13A in striatal synaptic plasticity and MSN communication may constitute a key point to understanding the specific striatal vulnerability not only in ChAc, but also in HD.

Finally, the low number of HD-patient samples and transgenic animals herein analyzed constitutes a limitation of the study, as it may cause a loss of statistical power to detect differences in VPS3A expression and protein. Keeping this in mind, we conclude that VPS13A brain distribution is not substantially affected by mHtt. Therefore, the selective susceptibility of MSN in both ChAc and HD might be a consequence of disturbances in convergent cellular processes and circuitry alterations with divergent molecular mechanisms. Further experiments are necessary to evaluate the role of the VPS13A function in mediating these convergent mechanisms that determine MSN-specific vulnerability in basal ganglia disorders.

Data availability statement

The raw data supporting the conclusions of this article will be made available by the authors, without undue reservation.

Ethics statement

Human tissue samples were obtained from the Neurological Tissue Bank of the Biobanc- Hospital Clínic-Institut d'Investigacions

Biomèdiques August Pi i Sunyer (IDIBAPS, Barcelona, Spain). The studies were conducted in accordance with the local legislation and institutional requirements. The participants provided their written informed consent to participate in this study. All animal procedures were conducted in accordance with the Spanish RD 53/2013 and European 2010/63/UE regulations for the care and use of laboratory animals and approved by the animal experimentation Ethics Committee of the Universitat de Barcelona (368/19) and Generalitat de Catalunya (11193).

Author contributions

EG-G: Writing – original draft, Methodology, Investigation, Formal analysis. MC-C: Writing – review & editing, Investigation, Formal analysis. AC-M: Writing – review & editing, Investigation, Formal analysis. AR-L: Writing – review & editing, Investigation, Formal analysis. GB-S: Writing – review & editing, Formal analysis. EP-N: Writing – review & editing, Resources, Investigation. CM: Writing – review & editing, Resources, Funding acquisition. JA: Writing – review & editing, Validation, Resources, Project administration, Funding acquisition. MM: Writing – review & editing, Validation, Project administration, Funding acquisition, Conceptualization. MR: Writing – original draft, Supervision, Funding acquisition, Data curation, Conceptualization.

Funding

The author(s) declare that financial support was received for the research, authorship, and/or publication of this article. This study was supported by grants from the Ministerio de Ciencia e Innovación (Spain), under projects no. PID2020-119386RB-I00 (JA and MR), no. PID2021-124896OA-I00 (MM), and no. SAF2017-88812-R and PID2020-119236RB-I00 /AEI/10.13039/501100011033/ (CM); Instituto de Salud Carlos III, Ministerio de Ciencia, Innovación y Universidades and European Regional Development Fund (ERDF) [CIBERNED, to JA], Spain; and ChAc Foundation (JA, MM and MR) Spain. Also, the project has been supported by María de Maeztu Unit of Excellence (CEX2021-001159), Institute of Neurosciences of the University of Barcelona, Ministry of Science, Innovation, and Universities. This research is part of NEUROPA. The NEUROPA Project has received funding from the European Union's Horizon 2020 Research and Innovation Program under Grant Agreement No. 863214 (MM).

Acknowledgments

We are very grateful to Carmen Andrade (Dept. Biomedical Sciences, UB) for her technical support on histological procedures, to Ana Maria Lopez (María de Maeztu Unit of Excellence, Institute of Neurosciences of the University of Barcelona, CEX2021-001159, Ministry of Science, Innovation and Universities) and Silvia Artigas (CIBERNED) for excellent mouse colony management.

Conflict of interest

The authors declare that the research was conducted in the absence of any commercial or financial relationships that could be construed as a potential conflict of interest.

Publisher's note

References

Aditi, K., Shakarad, M. N., and Agrawal, N. (2016). Altered lipid metabolism in Drosophila model of Huntington's disease. *Sci. Rep.* 6:31411. doi: 10.1038/SREP31411

Azman, K. F., and Zakaria, R. (2022). Recent advances on the role of brain-derived neurotrophic factor (BDNF) in neurodegenerative diseases. *Int. J. Mol. Sci.* 23:6827. doi: 10.3390/IJMS23126827

Baydyuk, M., Russell, T., Liao, G. Y., Zang, K., An, J. J., Reichardt, L. F., et al. (2011). TrkB receptor controls striatal formation by regulating the number of newborn striatal neurons. *Proc. Natl. Acad. Sci. USA* 108, 1669–1674. doi: 10.1073/PNAS.1004744108

Besusso, D., Geibel, M., Kramer, D., Schneider, T., Pendolino, V., Picconi, B., et al. (2013). BDNF-TrkB signaling in striatopallidal neurons controls inhibition of locomotor behavior. *Nat. Commun.* 4:2031. doi: 10.1038/NCOMMS3031

Browne, S. E. (2008). Mitochondria and Huntington's disease pathogenesis: insight from genetic and chemical models. *Ann. N. Y. Acad. Sci.* 1147, 358–382. doi: 10.1196/ANNALS.1427.018

Canals, J. M., Pineda, J. R., Torres-Peraza, J. F., Bosch, M., Martín-Ibañez, R., Muñoz, M. T., et al. (2004). Brain-derived neurotrophic factor regulates the onset and severity of motor dysfunction associated with enkephalinergic neuronal degeneration in Huntington's disease. *J. Neurosci.* 24, 7727–7739. doi: 10.1523/JNEUROSCI.1197-04.2004

Cherubini, M., Lopez-Molina, L., and Gines, S. (2020). Mitochondrial fission in Huntington's disease mouse striatum disrupts ER-mitochondria contacts leading to disturbances in Ca2+ efflux and reactive oxygen species (ROS) homeostasis. *Neurobiol. Dis.* 136:104741. doi: 10.1016/J.NBD.2020.104741

Chiu, F. L., Lin, J. T., Chuang, C. Y., Chien, T., Chen, C. M., Chen, K. H., et al. (2015). Elucidating the role of the A2A adenosine receptor in neurodegeneration using neurons derived from Huntington's disease iPSCs. *Hum. Mol. Genet.* 24, 6066–6079. doi: 10.1093/HMG/DDV318

Creus-Muncunill, J., Badillos-Rodríguez, R., Garcia-Forn, M., Masana, M., Garcia-Díaz Barriga, G., Guisado-Corcoll, A., et al. (2019). Increased translation as a novel pathogenic mechanism in Huntington's disease. *Brain* 142, 3158–3175. doi: 10.1093/brain/awz230

Del Toro, D., Canals, J. M., Ginés, S., Kojima, M., Egea, G., and Alberch, J. (2006). Mutant huntingtin impairs the post-Golgi trafficking of brain-derived neurotrophic factor but not its Val66Met polymorphism. *J. Neurosci.* 26, 12748–12757. doi: 10.1523/JNEUROSCI.3873-06.2006

Fernández-García, S., Conde-Berriozabal, S., García-García, E., Gort-Paniello, C., Bernal-Casas, D., García-Díaz Barriga, G., et al. (2020). M2 cortex-dorsolateral striatum stimulation reverses motor symptoms and synaptic deficits in Huntington's disease. *eLife* 9, 1–24. doi: 10.7554/eLife.57017

Fernández-Nogales, M., Santos-Galindo, M., Hernández, I. H., Cabrera, J. R., and Lucas, J. J. (2016). Faulty splicing and cytoskeleton abnormalities in Huntington's disease. *Brain Pathol.* 26, 772–778. doi: 10.1111/BPA.12430

García-García, E., Chaparro-Cabanillas, N., Coll-Manzano, A., Carreras-Caballé, M., Giralt, A., Del Toro, D., et al. (2021). Unraveling the spatiotemporal distribution of VPS13A in the mouse brain. *Int. J. Mol. Sci.* 22:13018. doi: 10.3390/IJMS222313018

García-García, E., Ramón-Lainez, A., Conde-Berriozabal, S., del Toro, D., Escaramis, G., Giralt, A., et al. (2023). VPS13A knockdown impairs corticostriatal

synaptic plasticity and locomotor behavior in a new mouse model of chorea-acanthocytosis. *Neurobiol. Dis.* 187:106292. doi: 10.1016/J.NBD.2023.106292

Giralt, A., Rodrigo, T., Martín, E. D., Gonzalez, J. R., Milà, M., Ceña, V., et al. (2009). Brain-derived neurotrophic factor modulates the severity of cognitive alterations induced by mutant huntingtin: involvement of phospholipaseCgamma activity and glutamate receptor expression. *Neuroscience* 158, 1234–1250. doi: 10.1016/J.NEUROSCIENCE.2008.11.024

Henkel, K., Walterfang, M., Velakoulis, D., Danek, A., and Kassubek, J. (2008). "Volumetric neuroimaging in Neuroacanthocytosis" in *Neuroacanthocytosis syndromes II*. eds. R. H. Walker, S. Saiki and A. Danek (Berlin Heidelberg: Springer), 175–185.

Hu, Y., Chopra, V., Chopra, R., Locascio, J. J., Liao, Z., Ding, H., et al. (2011). Transcriptional modulator H2A histone family, member Y (H2AFY) marks Huntington disease activity in man and mouse. *Proc. Natl. Acad. Sci. USA* 108, 17141–17146. doi: 10.1073/pnas.1104409108

Jung, H. H., Danek, A., and Walker, R. H. (2011). Neuroacanthocytosis syndromes. *Orphanet J. Rare Dis.* 6:68. doi: 10.1186/1750-1172-6-68

Kassubek, J., Landwehrmeyer, G. B., Ecker, D., Juengling, F. D., Muche, R., Schuller, S., et al. (2004). Global cerebral atrophy in early stages of Huntington's disease: quantitative MRI study. *Neuroreport* 15, 363–365. doi: 10.1097/00001756-200402090-00030

Kim, A., García-García, E., Straccia, M., Comella-Bolla, A., Miguez, A., Masana, M., et al. (2020). Reduced Fractalkine levels Lead to striatal synaptic plasticity deficits in Huntington's disease. *Front. Cell. Neurosci.* 14:163. doi: 10.3389/FNCEL.2020.00163

Kumar, N., Leonzino, M., Hancock-Cerutti, W., Horenkamp, F. A., Li, P. Q., Lees, J. A., et al. (2018). VPS13A and VPS13C are lipid transport proteins differentially localized at ER contact sites. *J. Cell Biol.* 217, 3625–3639. doi: 10.1083/JCB.201807019

Kurano, Y., Nakamura, M., Ichiba, M., Matsuda, M., Mizuno, E., Kato, M., et al. (2007). In vivo distribution and localization of chorein. *Biochem. Biophys. Res. Commun.* 353, 431–435. doi: 10.1016/J.BBRC.2006.12.059

Labbadia, J., Cunliffe, H., Weiss, A., Katsyuba, E., Sathasivam, K., Seredenina, T., et al. (2011). Altered chromatin architecture underlies progressive impairment of the heat shock response in mouse models of Huntington disease. *J. Clin. Invest.* 121, 3306–3319. doi: 10.1172/JCI57413

Lin, L., Park, J. W., Ramachandran, S., Zhang, Y., Tseng, Y. T., Shen, S., et al. (2016). Transcriptome sequencing reveals aberrant alternative splicing in Huntington's disease. *Hum. Mol. Genet.* 25, 3454–3466. doi: 10.1093/HMG/DDW187

Liu, J., Heinsen, H., Grinberg, L. T., Alho, E., Amaro, E., Pasqualucci, C. A., et al. (2019). Pathoarchitectonics of the cerebral cortex in chorea-acanthocytosis and Huntington's disease. *Neuropathol. Appl. Neurobiol.* 45, 230–243. doi: 10.1111/NAN.12495

Lupo, F., Tibaldi, E., Matte, A., Sharma, A. K., Brunati, A. M., Alper, S. L., et al. (2016). A new molecular link between defective autophagy and erythroid abnormalities in chorea-acanthocytosis. *Blood* 128, 2976–2987. doi: 10.1182/BLOOD-2016-07-727321

Marques Sousa, C., and Humbert, S. (2013). Huntingtin: here, there, everywhere! *J Huntington's Dis* 2, 395–403. doi: 10.3233/JHD-130082

Miltenberger-Miltenyi, G., Jones, A., Tetlow, A. M., Conceição, V. A., Crary, J. F., Ditzel, R. M., et al. (2023). Sphingolipid and phospholipid levels are altered in human brain in chorea-Acanthocytosis. *Mov. Disord.* 38, 1535–1541. doi: 10.1002/MDS.29445

Muñoz-Braceras, S., Calvo, R., and Escalante, R. (2015). TipC and the chorea-acanthocytosis protein VPS13A regulate autophagy in Dictyostelium and human HeLa cells. *Autophagy* 11, 918–927. doi: 10.1080/15548627.2015.1034413

Muñoz-Braceras, S., Tornero-Écija, A. R., Vincent, O., and Escalante, R. (2019). VPS13A is closely associated with mitochondria and is required for efficient lysosomal degradation. *Dis. Model. Mech.* 12:dmm036681. doi: 10.1242/DMM.036681

Parievsky, A., Moore, C., Kamdjou, T., Cepeda, C., Meshul, C. K., and Levine, M. S. (2017). Differential electrophysiological and morphological alterations of thalamostriatal and corticostriatal projections in the R6/2 mouse model of Huntington's disease. *Neurobiol. Dis.* 108, 29–44. doi: 10.1016/J.NBD.2017.07.020

Pchitskaya, E., Popugaeva, E., and Bezprozvanny, I. (2018). Calcium signaling and molecular mechanisms underlying neurodegenerative diseases. *Cell Calcium* 70, 87–94. doi: 10.1016/J.CECA.2017.06.008

Peikert, K., Dobson-Stone, C., Rampoldi, L., Miltenberger-Miltenyi, G., Neiman, A., De Camilli, P., et al. (2023). VPS13A disease. *Curated Reference Collection in Neurosci. Biobehav. Psychol.* 217–219. doi: 10.1016/B978-0-12-809324-5.00521-6

Pelzl, L., Elsir, B., Sahu, I., Bissinger, R., Singh, Y., Sukkar, B., et al. (2017). Lithium sensitivity of store operated Ca2+ entry and survival of fibroblasts isolated from chorea-Acanthocytosis patients. *Cell. Physiol. Biochem.* 42, 2066–2077. doi: 10.1159/000479901

Ravikumar, B., Vacher, C., Berger, Z., Davies, J. E., Luo, S., Oroz, L. G., et al. (2004). Inhibition of mTOR induces autophagy and reduces toxicity of polyglutamine expansions in fly and mouse models of Huntington disease. *Nat. Genet.* 36, 585–595. doi: 10.1038/NG1362

Ross, C. A., Pantelyat, A., Kogan, J., and Brandt, J. (2014). Determinants of functional disability in Huntington's disease: role of cognitive and motor dysfunction. *Mov. Disord.* 29, 1351–1358. doi: 10.1002/MDS.26012

Saavedra, A., Giralt, A., Rué, L., Xifró, X., Xu, J., Ortega, Z., et al. (2011). Striatal-enriched protein tyrosine phosphatase expression and activity in Huntington's disease: a STEP in the resistance to excitotoxicity. *J. Neurosci.* 31, 8150–8162. doi: 10.1523/JNEUROSCI.3446-10.2011

Sadri-Vakili, G., Bouzou, B., Benn, C. L., Kim, M. O., Chawla, P., Overland, R. P., et al. (2007). Histones associated with downregulated genes are hypo-acetylated in Huntington's disease models. *Hum. Mol. Genet.* 16, 1293–1306. doi: 10.1093/HMG/DDM078

Shirendeb, U., Reddy, A. P., Manczak, M., Calkins, M. J., Mao, P., Tagle, D. A., et al. (2011). Abnormal mitochondrial dynamics, mitochondrial loss and mutant huntingtin oligomers in Huntington's disease: implications for selective neuronal damage. *Hum. Mol. Genet.* 20, 1438–1455. doi: 10.1093/HMG/DDR024

Stanslowsky, N., Reinhardt, P., Glass, H., Kalmbach, N., Naujock, M., Hensel, N., et al. (2016). Neuronal dysfunction in iPSC-derived medium spiny neurons from chorea-Acanthocytosis patients is reversed by Src kinase inhibition and F-actin stabilization. *J. Neurosci.* 36, 12027–12043. doi: 10.1523/JNEUROSCI.0456-16.2016

Suzuki, F., Sato, N., Ota, M., Sugiyama, A., Shigemoto, Y., Morimoto, E., et al. (2020). Discriminating chorea-acanthocytosis from Huntington's disease with single-case voxel-based morphometry analysis. *J. Neurol. Sci.* 408:116545. doi: 10.1016/j.jns.2019.116545

Tshilenge, K. T., Aguirre, C. G., Bons, J., Gerencser, A. A., Basisty, N., Song, S., et al. (2023). Proteomic analysis of Huntington's disease medium spiny neurons identifies alterations in lipid droplets. *Molecular & Cellular Proteomics: MCP* 22:100534. doi: 10.1016/J.MCPRO.2023.100534

Tyebji, S., Saavedra, A., Canas, P. M., Pliassova, A., Delgado-García, J. M., Alberch, J., et al. (2015). Hyperactivation of D1 and A2A receptors contributes to cognitive dysfunction in Huntington's disease. *Neurobiol. Dis.* 74, 41–57. doi: 10.1016/J.NBD.2014.11.004

Ueno, S. I., Maruki, Y., Nakamura, M., Tomemori, Y., Kamae, K., Tanabe, H., et al. (2001). The gene encoding a newly discovered protein, chorein, is mutated in chorea-acanthocytosis. *Nat. Genet.* 28, 121–122. doi: 10.1038/88825

Vonk, J. J., Yeshaw, W. M., Pinto, F., Faber, A. I. E., Lahaye, L. L., Kanon, B., et al. (2017). Drosophila Vps13 is required for protein homeostasis in the brain. *PLoS One* 12:e0170106. doi: 10.1371/JOURNAL.PONE.0170106

Vonsattel, J. P. G., and DiFiglia, M. (1998). Huntington disease. *J. Neuropathol. Exp. Neurol.* 57, 369–384. doi: 10.1097/00005072-199805000-00001

Walterfang, M., Looi, J. C. L., Styner, M., Walker, R. H., Danek, A., Niethammer, M., et al. (2011). Shape alterations in the striatum in chorea-acanthocytosis. *Psychiatry Res.* 192, 29–36. doi: 10.1016/J.PSCYCHRESNS.2010.10.006

Wanker, E. E., Ast, A., Schindler, F., Trepte, P., and Schnoegl, S. (2019). The pathobiology of perturbed mutant huntingtin protein-protein interactions in Huntington's disease. *J. Neurochem.* 151, 507–519. doi: 10.1111/JNC.14853

Yeshaw, W. M., van der Zwaag, M., Pinto, F., Lahaye, L. L., Faber, A. I. E., Gómez-Sánchez, R., et al. (2019). Human VPS13A is associated with multiple organelles and influences mitochondrial morphology and lipid droplet motility. *eLife* 8:e43561. doi: 10.7554/ELIFE.43561

frontiers | Frontiers in Neuroscience

TYPE Mini Review
PUBLISHED 01 July 2024
DOI 10.3389/fnins.2024.1431400

OPEN ACCESS

EDITED BY
Kevin Peikert,
University Hospital Rostock, Germany

REVIEWED BY
Woong Sun,
Korea University, Republic of Korea
Pristyazhnyuk Inna,
Russian Academy of Sciences (RAS), Russia
Wenke Seifert,
Charité University Medicine Berlin, Germany

*CORRESPONDENCE
Fabrizio Vacca
✉ fabrizio.vacca@fa2.ch
Muhammad Ansar
✉ muhammad.ansar@fa2.ch

†These authors share last authorship

RECEIVED 11 May 2024
ACCEPTED 18 June 2024
PUBLISHED 01 July 2024

CITATION
Vacca F, Yalcin B and Ansar M (2024) Exploring the pathological mechanisms underlying Cohen syndrome.
Front. Neurosci. 18:1431400.
doi: 10.3389/fnins.2024.1431400

Exploring the pathological mechanisms underlying Cohen syndrome

Fabrizio Vacca[1]*, Binnaz Yalcin[2†] and Muhammad Ansar[1,3*†]

[1]Department of Ophthalmology, University of Lausanne, Jules Gonin Eye Hospital, Fondation Asile Des Aveugles, Lausanne, Switzerland, [2]Inserm UMR1231, Université de Bourgogne, Dijon, France, [3]Advanced Molecular Genetics and Genomics Disease Research and Treatment Centre, Dow University of Health Sciences, Karachi, Pakistan

Cohen Syndrome (CS) is a rare autosomal recessive disorder caused by biallelic mutations in the *VPS13B* gene. It is characterized by multiple clinical features, including acquired microcephaly, developmental delay, intellectual disability, neutropenia, and retinal degeneration. VPS13B is part of the bridge-like lipid transport (BLTP) protein family, which in mammals also includes VPS13A, -C, and -D. The proteins of this family are peripheral membrane proteins with different sub-cellular localization, but all share similar structural features and have been proposed to act as lipid transport proteins at organellar membrane contact sites. VPS13B is localized at the Golgi apparatus and is essential for the maintenance of organelle architecture. Here we present a review of the experimental data on the function of the protein at the cellular level, discussing the potential link with disease phenotype and review the studies on animal models recapitulating features of the human disease.

KEYWORDS

VPS13B, COH1, BLTP, Golgi, neurodevelopment, membrane contact sites, lipid transfer protein

Introduction

Cohen Syndrome (CS) (MIM: 216550) is a multisystemic genetic disease which was initially described five decades ago (Cohen et al., 1973). It is caused by biallelic mutations in the *VPS13B* gene. Over 660 pathogenic variants have been identified so far, mostly truncating loss-of-function (LoF) mutations.[1] It affects an estimated 50000 individuals worldwide, projected based on the prevalence of predicted LoF variants in *VPS13B* in the gnomAD database (Chen et al., 2024). Patients with CS suffer from many symptoms including developmental delay, intellectual disability, post-natal microcephaly, metabolic issues, neutropenia, severe myopia, and progressive loss of vision due to retinal degeneration (Kivitie-Kallio et al., 2000; Kivitie-Kallio and Norio, 2001). Brain structural abnormalities have been reported in some patients using cerebral magnetic resonance imaging (MRI). These include thick corpus callosum (Kivitie-Kallio et al., 1998; Mochida et al., 2004; Rejeb et al., 2017; Koehler et al., 2020), thin corpus callosum (Alipour et al., 2020), atrophy of the cerebellar vermis (Mochida et al., 2004; Waite et al., 2010), pontocerebellar atrophy (Katzaki et al., 2007), thinning of the cortex (Hu et al., 2021) and cerebral atrophy (Ghzawi et al., 2021). The disease-causing gene was identified in

1 www.ncbi.nlm.nih.gov/clinvar

2003 and originally named *COH1*, later renamed *VPS13B*, by homology with the yeast protein (Kolehmainen et al., 2003). In this mini-review, we outline the current experimental data that show potential pathological mechanisms of CS. This encompasses various models, including cell, neuronal, and animal models.

Cellular functions of VPS13B protein

VPS13B is one of the four mammalian genes (along with *VPS13A, -C, and -D*), homologous of the yeast *VPS13* (Velayos-Baeza et al., 2004). Of the four mammalian *VPS13* genes, *VPS13B* is the more evolutionary distant, proposed to have split very early from the other three in eukaryotic evolution. Recent clustering analyses suggest that the last eukaryotic common ancestor likely contained two *VPS13* paralogs: ancestral forms of *VPS13A/C/D* and *VPS13B* (Levine, 2022). These proteins are now recognized as part of a larger protein family denominated bridge-like lipid transfer protein (BLTP) which also includes the autophagy factor ATG2 and other few proteins (Neuman et al., 2022; Hanna et al., 2023). A remarkable structural feature of this protein family is the organization into a series of repeated units known as RBG (repeated beta-groove) units that compose the core of the hydrophobic tunnel and constitute the central backbone of the structure (Levine, 2022). The N- and C-terminal regions are the most conserved across different isoforms and contain accessory domains that likely play a crucial role in membrane interaction and lipid mobilization. VPS13B contains four folded accessory domains in the C-terminal region protruding from the rod-like structure formed by the RBG domains (Figure 1). Three of these domains are common across all VPS13 proteins: the arc-shaped Vps13 adaptor binding (VAB) domain, which is pivotal for protein–protein interactions; the ATC2-C domain, also known as the Gondola domain, composed of four amphipathic α-helices, also present in the lipid droplet proteins PLIN2 and GPAT4 and likely mediating interaction with lipid bilayers; a pleckstrin homology (PH) domain, which facilitates phosphoinositide binding. Additionally, the VPS13B protein uniquely contains a jellyroll/β-sandwich domain with an unclear function (Levine, 2022; Dall'Armellina et al., 2023; Hanna et al., 2023). BLTP proteins have been proposed to transfer lipids through a hydrophobic tunnel between adjacent organelle membranes at membrane-contact sites (MCS). This hypothesis is supported by experimental data from structural analyses, electron microscopy and biochemical studies (Kumar et al., 2018; Li et al., 2020; Cai et al., 2022). Evidence from specific cases, such as ATG2 in autophagosome expansion (Valverde et al., 2019) and yeast Vps13p in prospore formation, (Nakamura et al., 2021), suggests that these proteins contribute to membrane expansion by bulk lipid flow. However, no lipid selectivity has been definitively demonstrated to date. BLTP proteins are thought to connect two organelles with their N- and -C terminal domains, theoretically enabling them to serve also as scaffolding proteins at MCS.

VPS13A, -C, and -D are generally assumed to connect the endoplasmic reticulum (ER) to other organelles, as detailed by Hanna et al. (2023). However, no evidence currently exists to show that VPS13B connects to the ER. This is consistent with the lack of a FFAT motif in the N-terminal region, a motif that mediates ER interaction in other VPS13 proteins. Several reports show instead that VPS13B predominantly localizes to the Golgi complex. Interestingly, silencing RAB6, a VPS13B interactor, was found to partially prevent localization of VPS13B to the Golgi, highlighting its potential role in Golgi association (Seifert et al., 2015). Although it remains unclear whether VPS13B establishes connections between the Golgi and other

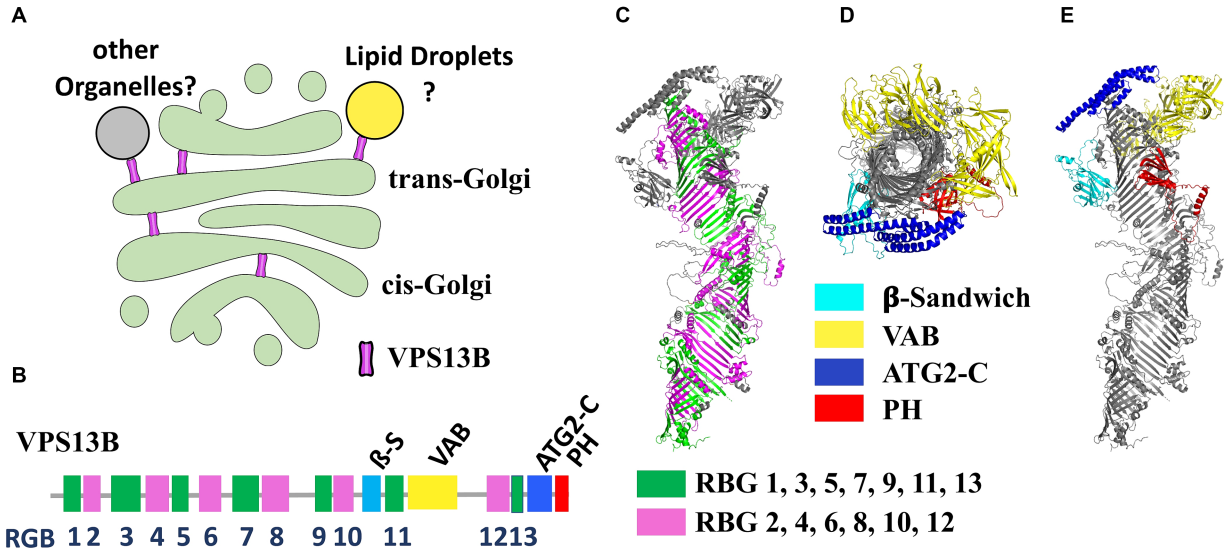

FIGURE 1
(A) Illustration of the potential localization of VPS13B within the Golgi complex according to available experimental evidences. **(B)** Scheme of the domain organization of the VPS13B polypeptide highlighting the position of the RBG repeats and the folded domains. **(C)** Side view of the predicted alphafold structure of VPS13B highlighting the RBG repeats forming the central scaffold of the protein (alternate RBG colored in green and magenta). RBG boundaries have been designed according to Levine (Levine, 2022). **(D,E)** Top view (from C-terminus) **(D)** of the same structure which clearly shows the tunnel going through the center of the protein and side view **(E)** highlighting the positions of the four folded domains. VPS13B Alphafold structure prediction was deposited by Samander et al. (DOI: 10.5281/zenodo.7626581).

organelles, immunofluorescence after hypotonic-mediated organelle swelling, indicates that VPS13B may localize at the interface between cis- and trans-Golgi membranes, potentially forming MCS between different Golgi cisternae (Ugur et al., 2023). VPS13B has also been found in association with lipid droplets, particularly in a subset of lipid droplets in close contact with the Golgi (Du et al., 2023; Figure 1). While localization in the Golgi complex seems well established and was observed with endogenous protein staining (Seifert et al., 2011, 2015; Zorn et al., 2022), other data mostly rely on over-expressed proteins, due to intrinsic technical challenges of visualizing the endogenous protein with available antibodies. Therefore, these localization findings should be interpreted cautiously.

Up to 100 VPS13B potential binding partners have been identified in high-throughput protein interaction screenings.[2] Some of these interactions have been validated through targeted experiments: for instance, RAB6, a GTPase which plays a prominent role in the regulation Golgi traffic (Seifert et al., 2015); and the SNARE proteins Syntaxin 6 (STX6) and Syntaxin 13 (STX13) (Koike and Jahn, 2019). STX6 is particularly notable due to its involvement in multiple vesicular trafficking pathways, including RAB6-dependent retrograde traffic from endosomes to the Golgi (Mallard et al., 2002; Ganley et al., 2008). Curiously, VPS13B was reported to bind selectively to vesicles positive for both STX6 and STX13 and is implicated in trafficking between early and recycling endosomes rather than the Golgi (Koike and Jahn, 2019). Moreover, Family With Sequence Similarity 177 Member A (FAM177A), a Golgi-localized protein of unknown function, has been proposed as a functional interactor of VPS13B. FAM177A is linked to a neurodevelopmental genetic disorder with phenotypic similarities to CS and exhibits a cellular phenotype similar to that of VPS13B (Ugur et al., 2023).

Golgi fragmentation as the central cellular defect in Cohen syndrome

Golgi fragmentation is a prominent and characteristic cellular defect observed in VPS13B-depleted cells (Seifert et al., 2011). A functional impairment of the Golgi is further supported by protein glycosylation defects in serum samples from CS patients (Duplomb et al., 2014). Although the correlation between VPS13B localization and Golgi fragmentation is strong, the exact role of VPS13B in this phenomenon as well as its broader role in maintaining Golgi morphology remains unclear. A recent study investigating the ability of missense variants to restore Golgi morphology further reinforces the association between Golgi fragmentation and CS pathogenicity (Zorn et al., 2022). Additionally, genome-wide CRISPR screening identified VPS13B among the top genes required for cholera toxin mediated intoxication, alongside other Golgi proteins (Gilbert et al., 2014). This finding implies a potential role in Golgi retrograde trafficking, although establishing a cause-and-effect relationship would require further investigations. The observation of Ugur et al. (2023) of a potential cis-to-trans Golgi bridging function of VPS13B aligns with this hypothesis. So far, the better-established inter-Golgi retrograde traffic mechanism is vesicle-mediated and is orchestrated by the Conserved Oligomeric Golgi (COG) complex in cooperation of set of Golgi SNARE proteins. Interestingly, the deletion of COG components often leads to Golgi fragmentation. Even if experimental evidences will be necessarily required to address VPS13B mechanistic function within the Golgi, we could speculate that it could be essential in facilitating retrograde traffic of even directly mediate the retrograde flow of some lipid species among the cisternae of the organelle.

Regardless of whether VPS13B directly causes Golgi fragmentation, this phenotype is likely linked to CS pathology. Although it is challenging to directly correlate Golgi impairment to neurodevelopmental features of CS because the Golgi apparatus is involved in many cellular processes, certain observations suggest a causal link. Similarities have been observed between CS and other diseases that affect Golgi morphology and trafficking, collectively known as "Golgipathies" (Passemard et al., 2017). These diseases include disorders impacting Golgi-associated retrograde protein (GARP) complex-mediated endosome-to-Golgi retrograde traffic (Feinstein et al., 2014; Gershlick et al., 2019); coating proteins involved in Golgi-to-ER traffic via COPI vesicles (Macken et al., 2021; Marom et al., 2021); Golgins like GM130 (Shamseldin et al., 2016), and tethering complexes facilitating bidirectional ER-Golgi traffic, such as Trafficking protein particle (TRAPP) (Sacher et al., 2019) and COG (D'Souza et al., 2020). Despite the heterogenicity of these conditions, they share key neurodevelopmental features with CS, such as postnatal microcephaly, often accompanied by dysgenesis of the corpus callosum. Unlike primary microcephaly, which mostly affects neurogenesis and migration during embryonic development, secondary (postnatal) microcephaly likely results from later events such as neuronal maturation, synaptogenesis and myelination.

Neuronal models of Cohen syndrome

Recent studies on neuronal models of CS investigated the correlation of VPS13B depletion or knockdown (KD) with neurodevelopmental abnormalities. In rat primary hippocampal neurons, VPS13B KD initially led to axonal elongation defects and misalignment of the Golgi complex with the direction of elongation, suggesting a correlation between Golgi defects and the neurodevelopmental phenotype (Seifert et al., 2015). Further investigations using human induced pluripotent stem cell (iPSC)-derived neurons have provided a valuable model for studying the neurodevelopmental features of CS. Lee et al. reported that neurons derived from a patient-derived iPSC normally differentiate into glutamatergic neurons but exhibit defective synaptogenesis and reduced expression of synaptic genes. Additionally, neurospheres generated from the same iPSC showed reduced size, potentially recapitulating microcephaly in CS patients (Lee et al., 2020a). The same laboratory also observed an increased autophagic flux both in fibroblasts and differentiated neurons (Lee et al., 2020b). In another study, iPSC-derived neurons from two CS patients using an alternative differentiation protocol revealed ultrastructural defects in several organelles beyond the Golgi, including altered morphology of ER and mitochondria, as well as increased MCS between these organelles. An impairment in autophagic flux was also noted, which aligns with elevated cellular stress and potential neurodegeneration (Shnaider et al., 2023). Given the well-known heterogenicity of iPSC lines, these studies (each using fibroblasts from only one or two patients) require

2 https://thebiogrid.org

further validation to fully establish how well they recapitulate the pathological mechanism of the disease at the cellular level. Nevertheless, *in vitro* neuronal cultures as well as brain or retinal organoids, that will be hopefully established in a near future, represent promising systems for investigating the cellular pathology of CS and exploring potential therapeutic targets.

Animal models of Cohen syndrome

CS has been also investigated in animal models over the past decade. These models recapitulate many of the features seen in human patients, offering an invaluable tool to explore the disease's pathological mechanisms and identify potential therapeutic strategies. An overview of model organisms used in CS research, along with their associated phenotypic traits, is summarized in Table 1.

The first animal model for CS was established in 2011, with a naturally occurring *VPS13B* variant identified in Border Collie dogs, displaying trapped neutrophil syndrome. Linkage analysis on a pedigree of dogs traced back to a single common ancestor and a candidate gene approach led to the identification of a recessive 4-bp deletion in exon 19 of the largest transcript of VPS13B, which results in premature truncation of the protein (Shearman and Wilton, 2011). Seven dogs harboring the deletion in the VPS13B gene exhibited phenotypic traits similar to those of human CS patients. With the exception of the truncal obesity absent in the pedigree and ophthalmic features, not examined in this study, these dogs showed the main characteristics of CS patients including developmental delay, intellectual disability, postnatal microcephaly, facial abnormalities (short philtrum, high narrow palate, prominent nasal bridge and prominent central upper incisors), along with hypotonia, delayed puberty, short stature, and neutropenia (Table 1). Intellectual disability was estimated in these dogs according to their reduced ability to learn simple tasks. According to the report, 43% of the dogs (3 out of 7) displayed a defective learning phenotype. It is worth mentioning that among the seven dogs, two died before reaching maturity, and their sex was not recorded.

In recent years, three mouse models for CS have been developed, all of which are null/knockout (KO) models. The first two were generated using CRISPR/Cas9 endonuclease-mediated gene disruption, while the third employed a traditional targeted strategy (details are provided in Table 1). The first model was engineered by the Toronto Centre for Phenogenomics, partner of the International Mouse Phenotyping Consortium (IMPC), which aims to produce knockout mice for every coding gene in the mouse genome (White et al., 2013). This first allele, designated as *Vps13b*$^{em1(IMPC)Tcp}$ was developed from a pure genetic background C57BL/6NCrl, a 2,348-bp deletion was introduced on mouse chromosome 15, resulting in the deletion of exons 2–4 of *Vps13b* gene. Phenotypic data of this model are available to the scientific community through the IMPC website.[3] Phenotypic data of 16 KO mice ($n=8$ per sex) revealed decreased exploration in new environment, reduced body length, abnormal lens and retina morphology, and male infertility (summarized in Table 1).

The second CS model, *Vps13b*^{em1Yosl}, was developed in the laboratory of Yong-Seok Lee at the Seoul National University College of Medicine. This model was engineered on a pure C57BL/6N genetic background by deleting exon 2 of *Vps13b*, specifically removing 156 bp that includes the start codon (Kim et al., 2019). Phenotypic data from male and female KO mice were combined ($n=12$ KO mice). These mice exhibited significant memory and cognitive impairments in the Morris water maze paradigm, reduced activity in the open field test, and decreased motor coordination in the rotarod test, evidenced by a shorter latency to fall. Intriguingly, the study indicated normal anxiety-like and social behaviors in this model. Importantly, no morphological changes, eye abnormalities, or developmental delays were observed in these mice (see Table 1).

The third model, denoted as *Vps13b*$^{tm1.2Ics}$, is the most extensively characterized model of CS. This model involved the deletion of exon 4 in the *Vps13b* gene (Da Costa et al., 2020; Lhussiez et al., 2020; Bonfante et al., 2021; Montillot et al., 2023). Unlike the two previous mouse models, it was developed on a mixed genetic background comprising C57BL/6N and C57BL/6J strains of mice, which are known to have genetic and phenotypic divergences (Simon et al., 2013). This model presented male infertility (Da Costa et al., 2020) and severe forms of cataracts (Lhussiez et al., 2020). In cranio-skeletal analysis using Skyscan 1174 micro-computed tomography, *Vps13b*$^{tm1.2Ics}$ mice displayed craniofacial abnormalities, mainly affecting the palate (narrowing and elevation) and the nasal region (elongation and widening of the nasal tip). These abnormalities were more pronounced in males than females (Bonfante et al., 2021).

Furthermore, brain anatomy and behavior were comprehensively assessed in *Vps13b*$^{tm1.2Ics}$ mice (Montillot et al., 2023). About half of the KO mice died during the first week of life, while the remaining mice had normal lifespan and presented core phenotypes of CS, including microcephaly, growth delay, hypotonia, altered memory, and enhanced sociability. A quantitative 2D histological assessment of 40 morphological parameters across 22 different brain regions (Mikhaleva et al., 2016; Collins et al., 2018; Nguyen et al., 2022) revealed that the hippocampus, crucial for memory and spatial orientation, was one of the most affected regions, with its volume reduced by around 40%. While both sexes were affected, certain neuroanatomical and behavioral phenotypes were less pronounced in females.

Discussion

In this review, we summarize two decades of experimental research on VPS13B and CS, spanning from basic cell biology to the more recent work on mouse models. The efforts in characterizing the mechanistic functions of VPS13B, along with the research on other members of the BLTP protein family, significantly enhanced our understanding of the basic functions of these proteins. Recent studies suggest a role in intra-Golgi traffic whose impairment leads to a partial disruption of the morphology of the organelle. The similarity of CS with other disorders caused by mutations in Golgi complex proteins suggests that Golgi dysfunction may play a role in disease etiology. However, many questions remain open about the precise function of VPS13B, including its lipid selectivity and its potential role beyond lipid transport as a scaffold protein or tethering factor at membrane contact sites. Addressing these questions is essential for developing a comprehensive understanding of the pathological mechanisms of CS.

Modeling the disease in physiologically relevant cellular models will also be crucial. Efforts have been made to investigate the role of VPS13B in neuronal development using iPSC-derived neuronal cells.

3 https://www.mousephenotype.org/

TABLE 1 Summary table of phenotypic characteristics linked to animal models of Cohen Syndrome.

Animal models of Cohen syndrome	Dog	Mouse	Mouse	Mouse			
Nomenclature/breed	Border Collies	*Vps13b* < em1(IMPC)Tcp>	*Vps13b* < em1Yosl>	Vps13b < tm1.2Ics>			
Genetic background	Not applicable	C57BL/6 NCrl	C57BL/6 N	Mixed C57BL/6 N-C57BL/6 J			
Sample size (control animals)	10 obligate carriers	419 M and 430 F	9 M/F combined	12 M	3 (sex unknown)	12 M and 9 F	16 M and 16 F
Sample size (mutant animals)	7 dogs (sex unknown)	8 M and 8 F	12 M/F combined	12 M	3 (sex unknown)	11 M and 5 F	16 M and 16 F
Phenotypes							
- Lethality	+	–	NA	NA	NA	NA	+
- Developmental delay	+	+	–	NA	NA	NA	+
- Behavior							
Intellectual disability	+	NA	+	NA	NA	NA	+
Abnormal social behaviors	NA	NA	–	NA	NA	NA	+
Abnormal anxiety-like behaviors	NA	NA	–	NA	NA	NA	+
- Abnormal locomotor activity	NA	+	+	NA	NA	NA	+
- Impaired motor coordination	NA	NA	+	NA	NA	NA	+
- Hypotonia	+	NA	+	NA	NA	NA	+
- Brain anatomy							
Postnatal microcephaly	+	NA	–	NA	NA	NA	+
Hippocampal hypoplasia	NA	NA	NA	NA	NA	NA	+
Other neuroanatomical phenotypes	NA	NA	NA	NA	NA	NA	+
- Eye							
Cataracts	NA	+	–	NA	+	NA	NA
Abnormal retina morphology	NA	+	–	NA	+	NA	NA
- Face							
High narrow palate	+	NA	NA	NA	NA	+	NA
Prominent nasal bridge	+	NA	NA	NA	NA	+	NA
- Skull shape anomalies	NA	NA	NA	NA	NA	NA	+
- Reproduction							
Male infertility	NA	+	NA	+	NA	NA	NA
Delayed puberty	+	NA	NA	NA	NA	NA	NA
- Short stature	+	+	–	NA	NA	NA	+
- Truncal obesity	–	–	NA	NA	NA	NA	NA
- Neutropenia	+	NA	NA	NA	NA	NA	NA
References	Shearman and Wilton (2011)	https://www.mousephenotype.org/data/genes/MGI:1916380	Kim et al. (2019)	Da Costa et al. (2020)	Lhussiez et al. (2020)	Bonfante et al. (2021)	Montillot et al. (2023)

NA, Not Available; Plus sign, presence; Minus sign, absence; em1, endonuclease-mediated mutation 1; IMPC, International Mouse Phenotyping Consortium; Tcp, Toronto Centre for Phenogenomics; Yosl, Yong-Seok Lee; tm1.2, targeted mutation 1.2; Ics, Mouse Clinical Institute; M, Male; F, Female.

While these findings are still preliminary and do not yet establish a direct correlation between observed cellular phenotypes and the *in vivo* features of the disease, they represent a promising approach for understanding the disease mechanisms at the cellular level.

The studies on mouse models have demonstrated reproducibility and high clinical relevance, mirroring several features of CS patients, such as developmental delay, secondary microcephaly, craniofacial gestalt, hypotonia, and positive-friendly behaviors. Importantly, mouse studies revealed previously unreported neuroanatomical features, including hippocampal and cerebellar atrophy attributed to early-life neuronal loss, which could be used as robust readouts of the disease. While both sexes were affected, mouse and human data suggest that VPS13B plays a more prominent role in males than females. Hence, it is crucial to consider sex as a biological variable in future pre-clinical studies on CS.

Author contributions

FV: Writing – original draft, Writing – review & editing. BY: Writing – original draft, Writing – review & editing. MA: Writing – original draft, Writing – review & editing.

Funding

The author(s) declare that financial support was received for the research, authorship, and/or publication of this article. We acknowledged the support of the Swiss National Science Foundation grants (320030_212959 and IZSTZ0_216615), Fondation ProVisu (Geneva, Switzerland) and the Million Dollar Bike Ride grant program by the Penn Medicine Orphan Disease Center. BY is an INSERM investigator, supported by grants from the Agence Nationale de la Recherche (ANR-18-CE12-0009 and ANR-22-CE12-0011), the IFCPAR/CEFIPRA (Indo-French Centre for Promotion of Advanced Research/Centre Franco-Indien pour la Promotion de la Recherche Avancée) grant no. 6503-J, the European Union through the WDR FEDER program, and by the University of Bourgogne Franche-Comté through an A.N.E.R. grant "Acceuil de Nouvelle Equipe de Recherche." The authors declare that this study received funding from AriBio Co. The funder was not involved in the study design, collection, analysis, interpretation of data, the writing of this article, or the decision to submit it for publication.

Conflict of interest

The authors declare that the research was conducted in the absence of any commercial or financial relationships that could be construed as a potential conflict of interest.

Publisher's note

References

Alipour, N., Salehpour, S., Tonekaboni, S. H., Rostami, M., Bahari, S., Yassaee, V., et al. (2020). Mutations in the Vps13B gene in Iranian patients with different phenotypes of Cohen syndrome. *J. Mol. Neurosci.* 70, 21–25. doi: 10.1007/s12031-019-01394-w

Bonfante, B., Faux, P., Navarro, N., Mendoza-Revilla, J., Dubied, M., Montillot, C., et al. (2021). A Gwas in Latin Americans identifies novel face shape loci, implicating Vps13B and a Denisovan introgressed region in facial variation. *Sci. Adv.* 7:eabc6160. doi: 10.1126/sciadv.abc6160

Cai, S., Wu, Y., Guillen-Samander, A., Hancock-Cerutti, W., Liu, J., and De Camilli, P. (2022). In situ architecture of the lipid transport protein Vps13C at Er-lysosome membrane contacts. *Proc. Natl. Acad. Sci. USA* 119:e2203769119. doi: 10.1073/pnas.2203769119

Chen, S., Francioli, L. C., Goodrich, J. K., Collins, R. L., Kanai, M., Wang, Q., et al. (2024). A genomic mutational constraint map using variation in 76,156 human genomes. *Nature* 625, 92–100. doi: 10.1038/s41586-023-06045-0

Cohen, M. M. Jr., Hall, B. D., Smith, D. W., Graham, C. B., and Lampert, K. J. (1973). A new syndrome with hypotonia, obesity, mental deficiency, and facial, oral, ocular, and limb anomalies. *J. Pediatr.* 83, 280–284. doi: 10.1016/S0022-3476(73)80493-7

Collins, S. C., Wagner, C., Gagliardi, L., Kretz, P. F., Fischer, M. C., Kessler, P., et al. (2018). A method for parasagittal sectioning for neuroanatomical quantification of brain structures in the adult mouse. *Curr. Protoc. Mouse Biol.* 8:e48. doi: 10.1002/cpmo.48

Da Costa, R., Bordessoules, M., Guilleman, M., Carmignac, V., Lhussiez, V., Courot, H., et al. (2020). Vps13b is required for acrosome biogenesis through functions in Golgi dynamic and membrane trafficking. *Cell. Mol. Life Sci.* 77, 511–529. doi: 10.1007/s00018-019-03192-4

Dall'armellina, F., Stagi, M., and Swan, L. E. (2023). In silico modeling human Vps13 proteins associated with donor and target membranes suggests lipid transfer mechanisms. *Proteins* 91, 439–455. doi: 10.1002/prot.26446

D'souza, Z., Taher, F. S., and Lupashin, V. V. (2020). Golgi incognito: from vesicle tethering to human disease. *Biochim. Biophys. Acta Gen. Subj.* 1864:129694. doi: 10.1016/j.bbagen.2020.129694

Du, Y., Hu, X., Chang, W., Deng, L., Ji, W. K., and Xiong, J. (2023). A possible role of Vps13B in the formation of Golgi-lipid droplet contacts associating with the ER. *Contact* 6:25152564231195718. doi: 10.1177/25152564231195718

Duplomb, L., Duvet, S., Picot, D., Jego, G., El Chehadeh-Djebbar, S., Marle, N., et al. (2014). Cohen syndrome is associated with major glycosylation defects. *Hum. Mol. Genet.* 23, 2391–2399. doi: 10.1093/hmg/ddt630

Feinstein, M., Flusser, H., Lerman-Sagie, T., Ben-Zeev, B., Lev, D., Agamy, O., et al. (2014). Vps53 mutations cause progressive cerebello-cerebral atrophy type 2 (PCCA2). *J. Med. Genet.* 51, 303–308. doi: 10.1136/jmedgenet-2013-101823

Ganley, I. G., Espinosa, E., and Pfeffer, S. R. (2008). A syntaxin 10-Snare complex distinguishes two distinct transport routes from endosomes to the trans-Golgi in human cells. *J. Cell Biol.* 180, 159–172. doi: 10.1083/jcb.200707136

Gershlick, D. C., Ishida, M., Jones, J. R., Bellomo, A., Bonifacino, J. S., and Everman, D. B. (2019). A neurodevelopmental disorder caused by mutations in the Vps51 subunit of the Garp and Earp complexes. *Hum. Mol. Genet.* 28, 1548–1560. doi: 10.1093/hmg/ddy423

Ghzawi, A., Hirbawi, H., Negida, A., and Abu-Farsakh, H. (2021). A case of a Jordanian male twin with Cohen's syndrome, with genetic analysis and muscle biopsy; case report. *Ann. Med. Surg.* 71:103014. doi: 10.1016/j.amsu.2021.103014

Gilbert, L. A., Horlbeck, M. A., Adamson, B., Villalta, J. E., Chen, Y., Whitehead, E. H., et al. (2014). Genome-scale Crispr-mediated control of gene repression and activation. *Cell* 159, 647–661. doi: 10.1016/j.cell.2014.09.029

Hanna, M., Guillen-Samander, A., and De Camilli, P. (2023). Rbg motif bridge-like lipid transport proteins: structure, functions, and open questions. *Annu. Rev. Cell Dev. Biol.* 39, 409–434. doi: 10.1146/annurev-cellbio-120420-014634

Hu, X., Huang, T., Liu, Y., Zhang, L., Zhu, L., Peng, X., et al. (2021). Identification of a novel Vps13B mutation in a Chinese patient with Cohen syndrome by whole-exome sequencing. *Pharmgenomics Pers. Med.* 14, 1583–1589. doi: 10.2147/PGPM.S327252

Katzaki, E., Pescucci, C., Uliana, V., Papa, F. T., Ariani, F., Meloni, I., et al. (2007). Clinical and molecular characterization of Italian patients affected by Cohen syndrome. *J. Hum. Genet.* 52, 1011–1017. doi: 10.1007/s10038-007-0208-4

Kim, M. J., Lee, R. U., Oh, J., Choi, J. E., Kim, H., Lee, K., et al. (2019). Spatial learning and motor deficits in vacuolar protein sorting-associated protein 13b (Vps13b) mutant mouse. *Exp. Neurobiol.* 28, 485–494. doi: 10.5607/en.2019.28.4.485

Kivitie-Kallio, S., Autti, T., Salonen, O., and Norio, R. (1998). Mri of the brain in the Cohen syndrome: a relatively large corpus callosum in patients with mental retardation and microcephaly. *Neuropediatrics* 29, 298–301. doi: 10.1055/s-2007-973581

Kivitie-Kallio, S., and Norio, R. (2001). Cohen syndrome: essential features, natural history, and heterogeneity. *Am. J. Med. Genet.* 102, 125–135. doi: 10.1002/1096-8628(20010801)102:2<125::AID-AJMG1439>3.0.CO;2-0

Kivitie-Kallio, S., Summanen, P., Raitta, C., and Norio, R. (2000). Ophthalmologic findings in Cohen syndrome. A long-term follow-up. *Ophthalmology* 107, 1737–1745. doi: 10.1016/S0161-6420(00)00279-7

Koehler, K., Schuelke, M., Hell, A. K., Schittkowski, M., Huebner, A., and Brockmann, K. (2020). A novel homozygous nonsense mutation of Vps13B associated with previously unreported features of Cohen syndrome. *Am. J. Med. Genet. A* 182, 570–575. doi: 10.1002/ajmg.a.61435

Koike, S., and Jahn, R. (2019). Snares define targeting specificity of trafficking vesicles by combinatorial interaction with tethering factors. *Nat. Commun.* 10:1608. doi: 10.1038/s41467-019-09617-9

Kolehmainen, J., Black, G. C., Saarinen, A., Chandler, K., Clayton-Smith, J., Träskelin, A. L., et al. (2003). Cohen syndrome is caused by mutations in a novel gene, Coh1, encoding a transmembrane protein with a presumed role in vesicle-mediated sorting and intracellular protein transport. *Am. J. Hum. Genet.* 72, 1359–1369. doi: 10.1086/375454

Kumar, N., Leonzino, M., Hancock-Cerutti, W., Horenkamp, F. A., Li, P., Lees, J. A., et al. (2018). Vps13A and Vps13C are lipid transport proteins differentially localized at ER contact sites. *J. Cell Biol.* 217, 3625–3639. doi: 10.1083/jcb.201807019

Lee, Y. K., Hwang, S. K., Lee, S. K., Yang, J. E., Kwak, J. H., Seo, H., et al. (2020a). Cohen syndrome patient iPSC-derived Neurospheres and forebrain-like glutamatergic neurons reveal reduced proliferation of neural progenitor cells and altered expression of synapse genes. *J. Clin. Med.* 9:1886. doi: 10.3390/jcm9061886

Lee, Y. K., Lee, S. K., Choi, S., Huh, Y. H., Kwak, J. H., Lee, Y. S., et al. (2020b). Autophagy pathway upregulation in a human ipsc-derived neuronal model of Cohen syndrome with Vps13B missense mutations. *Mol. Brain* 13:69. doi: 10.1186/s13041-020-00611-7

Levine, T. P. (2022). Sequence analysis and structural predictions of lipid transfer bridges in the repeating Beta groove (Rbg) superfamily reveal past and present domain variations affecting form, function and interactions of Vps13, Atg2, Ship164. *Hobbit. Tweek. Contact* 5:251525642211343. doi: 10.1177/25152564221134328

Lhussiez, V., Dubus, E., Cesar, Q., Acar, N., Nandrot, E. F., Simonutti, M., et al. (2020). Cohen syndrome-associated cataract is explained by Vps13B functions in Lens homeostasis and is modified by additional genetic factors. *Invest. Ophthalmol. Vis. Sci.* 61:18. doi: 10.1167/iovs.61.11.18

Li, P., Lees, J. A., Lusk, C. P., and Reinisch, K. M. (2020). Cryo-Em reconstruction of a Vps13 fragment reveals a long groove to channel lipids between membranes. *J. Cell Biol.* 219:e202001161. doi: 10.1083/jcb.202001161

Macken, W. L., Godwin, A., Wheway, G., Stals, K., Nazlamova, L., Ellard, S., et al. (2021). Biallelic variants in Copb1 cause a novel, severe intellectual disability syndrome with cataracts and variable microcephaly. *Genome Med.* 13:34. doi: 10.1186/s13073-021-00850-w

Mallard, F., Tang, B. L., Galli, T., Tenza, D., Saint-Pol, A., Yue, X., et al. (2002). Early/recycling endosomes-to-TGN transport involves two Snare complexes and a Rab6 isoform. *J. Cell Biol.* 156, 653–664. doi: 10.1083/jcb.200110081

Marom, R., Burrage, L. C., Venditti, R., Clement, A., Blanco-Sanchez, B., Jain, M., et al. (2021). Copb2 loss of function causes a coatopathy with osteoporosis and developmental delay. *Am. J. Hum. Genet.* 108, 1710–1724. doi: 10.1016/j.ajhg.2021.08.002

Mikhaleva, A., Kannan, M., Wagner, C., and Yalcin, B. (2016). Histomorphological phenotyping of the adult mouse brain. *Curr. Protoc. Mouse Biol.* 6, 307–332. doi: 10.1002/cpmo.12

Mochida, G. H., Rajab, A., Eyaid, W., Lu, A., Al-Nouri, D., Kosaki, K., et al. (2004). Broader geographical spectrum of Cohen syndrome due to Coh1 mutations. *J. Med. Genet.* 41:e87. doi: 10.1136/jmg.2003.014779

Montillot, C., Skutunova, E., Ayushma, D., Dubied, M., Lahmar, A., Nguyen, S., et al. (2023). Characterization of Vps13b-mutant mice reveals neuroanatomical and behavioral phenotypes with females less affected. *Neurobiol. Dis.* 185:106259. doi: 10.1016/j.nbd.2023.106259

Nakamura, T. S., Suda, Y., Muneshige, K., Fujieda, Y., Okumura, Y., Inoue, I., et al. (2021). Suppression of Vps13 adaptor protein mutants reveals a central role for Pi4P in regulating prospore membrane extension. *PLoS Genet.* 17:e1009727. doi: 10.1371/journal.pgen.1009727

Neuman, S. D., Levine, T. P., and Bashirullah, A. (2022). A novel superfamily of bridge-like lipid transfer proteins. *Trends Cell Biol.* 32, 962–974. doi: 10.1016/j.tcb.2022.03.011

Nguyen, S., Kannan, M., Gaborit, M., Collins, S. C., and Yalcin, B. (2022). Quantitative neuroanatomical phenotyping of the embryonic mouse brain. *Curr. Protoc.* 2:e509. doi: 10.1002/cpz1.509

Passemard, S., Perez, F., Colin-Lemesre, E., Rasika, S., Gressens, P., and El Ghouzzi, V. (2017). Golgi trafficking defects in postnatal microcephaly: the evidence for "Golgipathies". *Prog. Neurobiol.* 153, 46–63. doi: 10.1016/j.pneurobio.2017.03.007

Rejeb, I., Jilani, H., Elaribi, Y., Hizem, S., Hila, L., Zillahrdt, J. L., et al. (2017). First case report of Cohen syndrome in the Tunisian population caused by Vps13B mutations. *BMC Med. Genet.* 18:134. doi: 10.1186/s12881-017-0493-5

Sacher, M., Shahrzad, N., Kamel, H., and Milev, M. P. (2019). Trappopathies: an emerging set of disorders linked to variations in the genes encoding transport protein particle (Trapp)-associated proteins. *Traffic* 20, 5–26. doi: 10.1111/tra.12615

Seifert, W., Kuhnisch, J., Maritzen, T., Horn, D., Haucke, V., and Hennies, H. C. (2011). Cohen syndrome-associated protein, Coh1, is a novel, giant Golgi matrix protein required for Golgi integrity. *J. Biol. Chem.* 286, 37665–37675. doi: 10.1074/jbc.M111.267971

Seifert, W., Kuhnisch, J., Maritzen, T., Lommatzsch, S., Hennies, H. C., Bachmann, S., et al. (2015). Cohen syndrome-associated protein Coh1 physically and functionally interacts with the small Gtpase Rab6 at the Golgi complex and directs neurite outgrowth. *J. Biol. Chem.* 290, 3349–3358. doi: 10.1074/jbc.M114.608174

Shamseldin, H. E., Bennett, A. H., Alfadhel, M., Gupta, V., and Alkuraya, F. S. (2016). Golga2, encoding a master regulator of golgi apparatus, is mutated in a patient with a neuromuscular disorder. *Hum. Genet.* 135, 245–251. doi: 10.1007/s00439-015-1632-8

Shearman, J. R., and Wilton, A. N. (2011). A canine model of Cohen syndrome: trapped neutrophil syndrome. *BMC Genomics* 12:258. doi: 10.1186/1471-2164-12-258

Shnaider, T. A., Khabarova, A. A., Morozova, K. N., Yunusova, A. M., Yakovleva, S. A., Chvileva, A. S., et al. (2023). Ultrastructural abnormalities in induced pluripotent stem cell-derived neural stem cells and neurons of two Cohen syndrome patients. *Cells* 12:2702. doi: 10.3390/cells12232702

Simon, M. M., Greenaway, S., White, J. K., Fuchs, H., Gailus-Durner, V., Wells, S., et al. (2013). A comparative phenotypic and genomic analysis of C57bl/6J and C57bl/6N mouse strains. *Genome Biol.* 14:R82. doi: 10.1186/gb-2013-14-7-r82

Ugur, B., Schueder, F., Shin, J., Hanna, M. G., Wu, Y., Leonzino, M., et al. (2023). Vps13B is localized at the cis-trans Golgi complex interface and is a functional partner of Fam177A1. *bioRxiv*. doi: 10.1101/2023.12.18.572081

Valverde, D. P., Yu, S., Boggavarapu, V., Kumar, N., Lees, J. A., Walz, T., et al. (2019). Atg2 transports lipids to promote autophagosome biogenesis. *J. Cell Biol.* 218, 1787–1798. doi: 10.1083/jcb.201811139

Velayos-Baeza, A., Vettori, A., Copley, R. R., Dobson-Stone, C., and Monaco, A. P. (2004). Analysis of the human Vps13 gene family. *Genomics* 84, 536–549. doi: 10.1016/j.ygeno.2004.04.012

Waite, A., Somer, M., O'Driscoll, M., Millen, K., Manson, F. D. C., and Chandler, K. E. (2010). Cerebellar hypoplasia and Cohen syndrome: a confirmed association. *Am. J. Med. Genet. A* 152A, 2390–2393. doi: 10.1002/ajmg.a.33569

White, J. K., Gerdin, A. K., Karp, N. A., Ryder, E., Buljan, M., Bussell, J. N., et al. (2013). Genome-wide generation and systematic phenotyping of knockout mice reveals new roles for many genes. *Cell* 154, 452–464. doi: 10.1016/j.cell.2013.06.022

Zorn, M., Kuhnisch, J., Bachmann, S., and Seifert, W. (2022). Disease relevance of rare Vps13B missense variants for neurodevelopmental Cohen syndrome. *Sci. Rep.* 12:9686. doi: 10.1038/s41598-022-13717-w

frontiers | Frontiers in Neuroscience

TYPE Brief Research Report
PUBLISHED 18 July 2024
DOI 10.3389/fnins.2024.1406969

OPEN ACCESS

EDITED BY
Kevin J. O'Donovan,
United States Military Academy,
United States

REVIEWED BY
Joan-lluis Vives-Corrons,
Josep Carreras Leukaemia Research Institute (IJC), Spain
Immacolata Andolfo,
University of Naples Federico II, Italy

*CORRESPONDENCE
Lars Kaestner
✉ lars_kaestner@me.com

RECEIVED 25 March 2024
ACCEPTED 15 May 2024
PUBLISHED 18 July 2024

CITATION
Hernández CA, Peikert K, Qiao M, Darras A, de Wilde JRA, Bos J, Leibowitz M, Galea I, Wagner C, Rab MAE, Walker RH, Hermann A, van Beers EJ, van Wijk R and Kaestner L (2024) Osmotic gradient ektacytometry – a novel diagnostic approach for neuroacanthocytosis syndromes. *Front. Neurosci.* 18:1406969. doi: 10.3389/fnins.2024.1406969

Osmotic gradient ektacytometry – a novel diagnostic approach for neuroacanthocytosis syndromes

Carolina A. Hernández[1], Kevin Peikert[2,3,4], Min Qiao[5,6], Alexis Darras[5], Jonathan R. A. de Wilde[1], Jennifer Bos[1], Maya Leibowitz[7], Ian Galea[7], Christian Wagner[5,8], Minke A. E. Rab[1,9], Ruth H. Walker[10,11], Andreas Hermann[2,3,12], Eduard J. van Beers[13], Richard van Wijk[1] and Lars Kaestner[5,6]*

[1]Department of Central Diagnostic Laboratory - Research, University Medical Center Utrecht, trecht University, Utrecht, Netherlands, [2]Translational Neurodegeneration Section "Albrecht Kossel", Department of Neurology, University Medical Center Rostock, University of Rostock, Rostock, Germany, [3]Center for Transdisciplinary Neurosciences Rostock (CTNR), University Medical Center Rostock, Rostock, Germany, [4]United Neuroscience Campus Lund-Rostock (UNC), Rostock, Germany, [5]Dynamics of Fluids, Experimental Physics, Saarland University, Saarbrücken, Germany, [6]Heoretical Medicine and Biosciences, Medical Faculty, Saarland University, Homburg, Germany, [7]Clinical Neurosciences, Clinical and Experimental Sciences, Faculty of Medicine, University of Southampton, Southampton, United Kingdom, [8]Physics and Materials Science Research Unit, University of Luxembourg, Esch-sur-Alzette, Luxembourg, [9]Department of Hematology, Erasmus University Medical Center, Rotterdam, Netherlands, [10]Department of Neurology, James J. Peters Veterans Affairs Medical Center, Bronx, NY, United States, [11]Department of Neurology, Mount Sinai School of Medicine, New York City, NY, United States, [12]Deutsches Zentrum für Neurodegenerative Erkrankungen (DZNE) Rostock/Greifswald, Rostock, Germany, [13]Center for Benign Hematology, Thrombosis and Hemostasis - Van Creveldkliniek, University Medical Center Utrecht, Utrecht University, Utrecht, Netherlands

Introduction: The unique red blood cell (RBC) properties that characterize the rare neuroacanthocytosis syndromes (NAS) have prompted the exploration of osmotic gradient ektacytometry (Osmoscan) as a diagnostic tool for these disorders. In this exploratory study, we assessed if Osmoscans can discriminate NAS from other neurodegenerative diseases.

Methods: A comprehensive assessment was conducted using Osmoscan on a diverse group of patients, including healthy controls (*n*=9), neuroacanthocytosis syndrome patients (*n*=6, 2 VPS13A and 4 XK disease), Parkinson's disease patients (*n*=6), Huntington's disease patients (n=5), and amyotrophic lateral sclerosis patients (*n*=4). Concurrently, we collected and analyzed RBC indices and patients' characteristics.

Results: Statistically significant changes were observed in NAS patients compared to healthy controls and other conditions, specifically in osmolality at minimal elongation index (O_{min}), maximal elongation index (EI_{max}), the osmolality at half maximal elongation index in the hyperosmotic part of the curve (O_{hyper}), and the width of the curve close to the osmolality at maximal elongation index (O_{max}-width).

Discussion: This study represents an initial exploration of RBC properties from NAS patients using osmotic gradient ektacytometry. While specific parameters exhibited differences, only O_{hyper} and O_{max}-width yielded 100% specificity for other neurodegenerative diseases. Moreover, unique correlations between Osmoscan parameters and RBC indices in NAS versus controls were identified, such as osmolality at maximal elongation index (O_{max}) vs. mean cellular hemoglobin content (MCH) and minimal elongation index (EI_{min}) vs. red blood cell distribution width (RDW). Given the limited sample size, further studies are essential to establish diagnostic guidelines based on these findings.

KEYWORDS

VPS13A disease, XK disease, neurodegeneration, RBC deformability, ektacytometry, Osmoscan, acanthocytes

1 Introduction

Neuroacanthocytosis syndromes (NAS) comprise the neurodegenerative disorders VPS13A disease (formerly known as chorea-acanthocytosis) and XK disease (formerly known as McLeod syndrome) (Walker et al., 2023). Autosomal recessive VPS13A disease is caused by mutations in the *Vacuolar Protein Sorting 13 Homolog A* (*VPS13A*) gene and may present with progressive cognitive impairment, psychiatric symptoms, various movement disorders, muscle weakness, and epilepsy. In addition, the disease is characterized by acanthocytosis – the presence of morphologically altered red blood cells (RBCs) displaying thorn-like protrusions (Ueno et al., 2001; Rampoldi et al., 2002; Lupo et al., 2016). X-linked XK disease is caused by mutations in the *XK* gene typically leading to the absence of the Kx blood antigen. Manifestations of XK disease are very similar to VPS13A disease except for, e.g., the usually later onset and prominent cardiac involvement (Danek et al., 2001; Peikert et al., 2022a). As in VPS13A disease, acanthocytosis is a very common, but not obligatory feature (Peikert et al., 2022b). Recent studies have shown that VPS13A (bridge-like lipid transfer protein) and XK (scramblase) form a protein complex which may be the molecular basis of the phenotypical similarities in the symptoms of the related disorders (Park and Neiman, 2020; Guillén-Samander et al., 2022; Park et al., 2022; Ryoden et al., 2022).

Hence, RBCs are clearly affected in NAS (Storch et al., 2005; Siegl et al., 2013; Cluitmans et al., 2015; Peikert et al., 2022b). It is not clear whether the acanthocytes are a byproduct of the disease, directly resulting from the genetic defect, or a secondary effect. It is also unknown whether they play a role in disease progression (Franceschi et al., 2014; Adjobo-Hermans et al., 2015). It is known that RBC from NAS patients have an altered deformability (Darras et al., 2021; Rabe et al., 2021; Reichel et al., 2022; Recktenwald et al., 2022a). These properties are obviously important in the circulation of the microvasculature (Barshtein et al., 2016, 2017).

Osmotic gradient ektacytometry is another method for measuring RBC deformability, in addition to the previously mentioned microfluidic approaches (Bianchi et al., 2015; Lazarova et al., 2017; Zaninoni et al., 2018). The Laser Optical Rotational Red Cell Analyzer (Lorrca, RR Mechatronics, The Netherlands) is a device established for diagnostic parameters of RBC-related diseases (Costa et al., 2016; Kaestner and Bianchi, 2020). We tested if such an osmotic gradient ektacytometry approach could be used as a diagnostic tool for NAS. An easy method for an initial NAS screening is of utmost importance since NAS patients receive their diagnosis often very late. It is not uncommon for a correct diagnosis of NAS, which are ultra-rare diseases, to be made years or even decades after the initial symptoms appear. Obviously, the genetic confirmation is required for a definitive diagnosis (Walker and Danek, 2021), but an easy inexpensive 'pre-test' would be an extremely useful screening tool for both patients and clinicians.

2 Materials and methods

2.1 Patient samples

Peripheral blood was collected into EDTA tubes (Sarstedt, Germany) for healthy control samples ($n = 9$) and VPS13A disease patients ($n = 2$), XK disease patients ($n = 4$), carriers of VPS13A mutations ($n = 3$), carriers of the XK mutations ($n = 4$), Parkinson's disease (PD) patients ($n = 6$), Huntington's disease (HD) patients ($n = 5$) and amyotrophic lateral sclerosis (ALS) patients ($n = 4$) patients. The study was approved by the review boards of the 'Ärztekammer des Saarlandes', permission number 51/18, as well as of the University of Rostock (A 2019–0134), and performed in accordance with the Declaration of Helsinki. Part of the study was carried out under national (UK) research ethics committee approval 11/SC/0204 and institutional approval ERGO 41084.

2.2 Osmotic gradient ektacytometry

Osmoscans were performed by osmotic gradient ektacytometry on the Lorrca (RR Mechatronics, The Netherlands), according to the manufacturer's instructions (Costa et al., 2016; Lazarova et al., 2017; Zaninoni et al., 2018). The Osmoscan was performed using a standardised final RBC dilution of 20,000 cells per µL of reagent. For the Osmoscan an osmotic gradient is created by the device by mixing two polyvinylpyrolidone (PVP) solutions with similar, physiological pH and viscosity, but different osmotic values.

For this study: Osmo LOW: 54 mOsm/kg, viscosity: 26.19 cP, Osmo HIGH: 776 mOsm/kg, viscosity: 28.76 cP was used. Data collection started at 60 mOsm/kg and continued until approximately 600 mOsm/kg. Red blood cell deformability was measured at a shear of 30 Pa, every second. The osmotic gradient gradually changes as a result of a varying mix of low and high osmotic reagent in the Couette flow system. The laser beam diffraction pattern (the A and B axis of the elliptical pattern) was measured. Deformability was expressed as the Elongation Index (EI), and calculated by the formula (A-B)/(A + B) representing the average shape change of the total RBC population under shear. The (local) minimum in elongation index (EI) in the hypo-osmotic part of the curve defines the values EI_{min} and the corresponding osmolarity as O_{min}. O_{min} negatively correlates with the membrane surface-to-volume ratio of the RBCs: if the surface-to-volume ratio decreases, O_{min} increases. The (global) maximum EI of the curves define EI_{max} and as the corresponding value O_{max}. If cell surface-to-volume decreases, EI_{max} decreases. The value of half EI_{max} in the hyperosmotic part of the curve defines EI_{hyper} and the corresponding osmolarity O_{hyper}. An additional parameter is the area under the curve (AUC), which is correlated with the decrease in membrane deformability. Furthermore, we introduce two new parameters recently described (Wilde et al., 2023), called O_{max}-width and O_{min}-width, which are defined as the width of the curve at ±5%

of EI_{max} and at ±5% of EI_{min}. The values of O_{max}-width recently showed a relation to the high intracellular viscosity of the RBC and limited ability to lose water to the environment (Wilde et al., 2023). Meanwhile O_{min}-width has been correlated to RBC population volume variability, disease severity and osmotic fragility (Wilde et al., 2023).

2.3 Red blood cell indices

A complete RBC count including reticulocyte counts was measured by the central laboratory of the Saarland University Hospital (Flormann et al., 2022) or in the haematology department of Southampton General Hospital on an automated XN10 system (Sysmex, Japan).

2.4 Statistics

The various parameters of RBC and Osmoscan analyses were thoroughly examined using standard statistical methods, including ordinary one-way ANOVA and Tukey's multiple comparison test, with a confidence interval set at 95%. The correlation heatmap was constructed using the non-parametric Spearman correlation, incorporating a two-tailed *p*-value within a 95% confidence interval. For specific correlations, linear regressions were employed. It is important to note that all of these statistical analyses were executed and visualized using GraphPad Prism. This comprehensive approach aimed to provide a robust understanding of the relationships and variations within the studied parameters, ensuring a thorough and reliable interpretation of the data.

3 Results

3.1 Patient selection and characteristics

Since both VPS13A and XK disease are very rare diseases with an estimated incidence of 1:1,000,000 and 1:10,000,000, respectively, we used the occasion of the '11th International Meeting on Neuroacanthocytosis Syndromes' (Kaestner, 2023), which was a joint scientific and patient meeting, to recruit two VPS13A disease patients and four XK disease patients as well as three *VPS13A* and four *XK* mutation carriers. The basic demographic characteristics of the patients are listed in Table 1. To allow a judgment for differential diagnosis, we compared the NAS patients to patients suffering from other neurodegenerative diseases, in particular, Parkinson's disease (PD), Huntington's disease (HD) and Amyotrophic lateral sclerosis (ALS) patients. The characteristics of these patients as well as the healthy controls are also summarized in Table 1.

3.2 Osmotic gradient ektacytometry

We investigated the differences in RBC deformability using the Osmoscan for patient samples from VPS13A disease, XK disease, HD, PD and ALS patients and compared it to healthy donors, in addition to carriers of VPS13A disease and XK disease. The results are summarised in Figure 1. In the graphs of Figures 1A–D, deformability vs. osmolality curves are plotted, whereas Figures 1E–L shows the statistical evaluation of particular parameters derived from the curves exemplified in Figures 1A–D.

Figure 1A depicts representative examples of Osmoscan curves from the RBCs of a healthy donor and a NAS patient. Furthermore, this panel contains annotations for the particular parameters, which are statistically evaluated. Figure 1B shows the Osmoscan curves from RBCs of both VPS13A disease patients and all four XK-disease patients, all showing the same shape characteristics justifying their pooling into one NAS group for further statistical analysis. Similarly, Figure 1C shows two VPS13A and XK disease mutation carriers measured together with nine healthy control samples, also showing the same characteristics. Figure 1D depicts representative examples from the NAS group in comparison to RBC samples from other neurodegenerative patients, in particular PD, HD and ALS.

For EI_{min} and AUC corresponding to Figures 1E–I, respectively, the curves of the NAS RBCs seem to differ from healthy control patients but this difference does not reach significance ($p = 0.15$;

TABLE 1 Patient characteristics.

		Healthy controls	Mutation carriers	NAS	HD	PD	ALS	*p*-value
Number		9	7	6	5	6	4	
Specifications			4 XK; 3 VPS13A	4 XK; 2 VPS13A	CAG repeats in the HTT gene ≧ 40	sporadic PD cases	sporadic ALS cases	
Age	Mean	54.6	64.9	51.1	65.7	69.6	63.3	0.14 (Kruskal-Wallis test)
	Min	38.4	45.4	33.6	54.1	46.2	50.1	
	Max	77.0	80.4	70.0	75.1	81.2	72.7	
	SD	14.8	12.6	13.2	9.3	12.1	11.0	
Sex	Male	4	0	6	2	4	4	0.003 (Chi-square)
	Female	5	7	0	3	2	0	

NAS, neuroacanthocytosis syndrome; HD, Huntington's disease; PD, Parkonson's disease; ALS, amyotrophic lateral sclerosis; CAG, codes for glutamine.

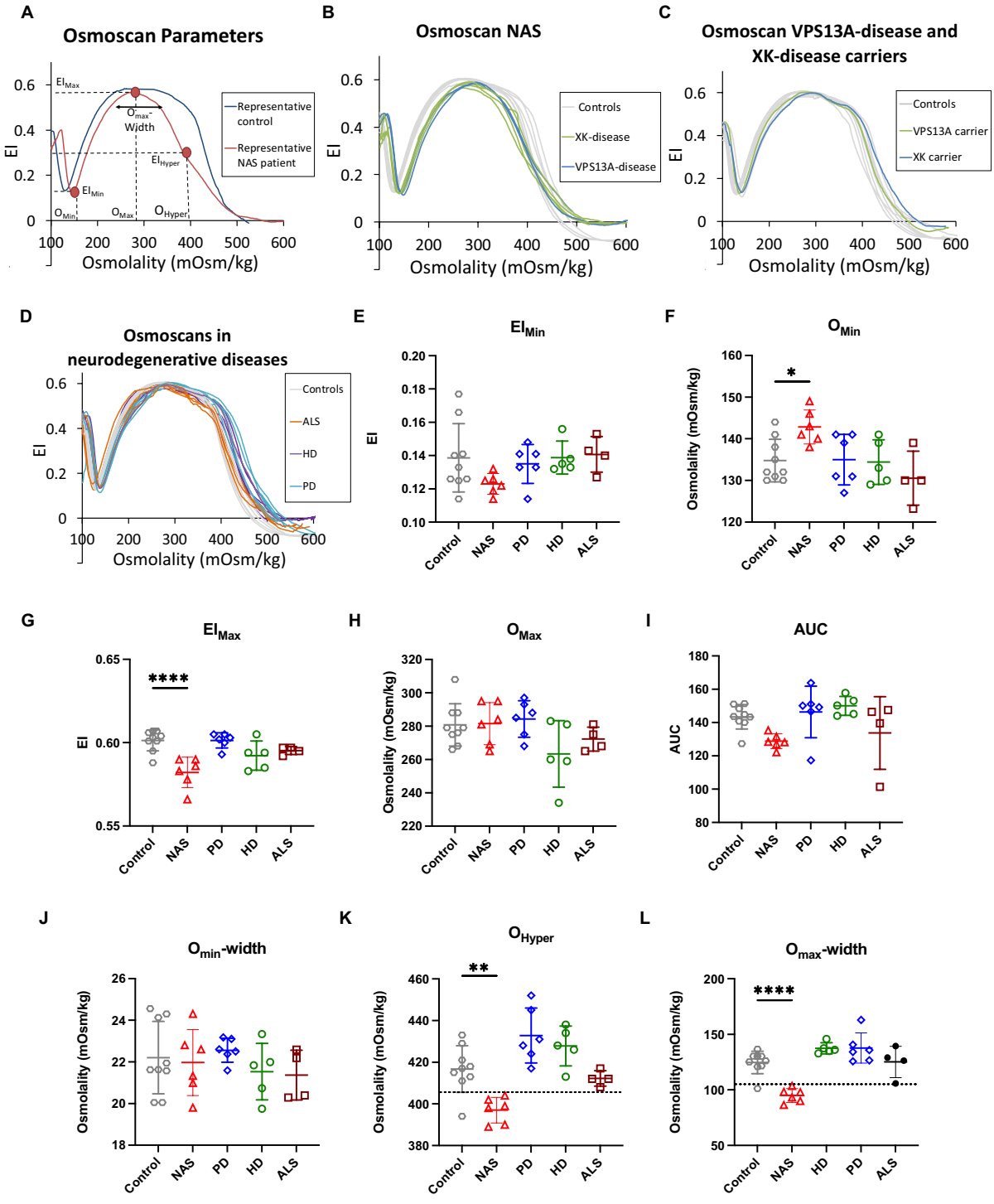

FIGURE 1
Ektacytometry data. Panel **(A)** shows representative Osmoscan curves of a NAS patient sample compared to a healthy control donor. In addition, characteristic parameters of the curve are annotated. Panel **(B)** provides the Osmoscan curves of both VPS13A disease patients and all 4 XK disease patients, showing their similarity and justifying to pool these patients in a NAS group for statistical analysis. Panel **(C)** depicts representative Osmoscan curves for both, *VPS13A* and *XK* mutation carriers showing their similarity. Panel **(D)** plots all Osmoscan curves of patients from all investigated neurodegenerative diseases except NAS to indicate the lack of difference between control curves and the neurodegenerative disorders HD, PD and ALS. In panels **(A–D)** each curve represents an individual patient or a healthy volunteer. Panels **(E–L)** show the statistical analysis of the characteristic parameters annotated in panel A. These are EI_{min}, O_{min}, EI_{max}, O_{max}, AUC, O_{min}-width, O_{hyper} and O_{max}-width, respectively. Plotted are the individual values with indication of the mean and the standard error of mean (SEM). Significance was checked with an ordinary one-way ANOVA test, and 1–4 stars correspond to *p*-values lower than 0.05, 0.01, 0.001, and 0.0001, respectively.

$p = 0.08$). In contrast, a significant difference was seen in the O_{min}, EI_{max}, O_{hyper} and in O_{max}-width in NAS patients vs. healthy controls (Figures 1F,G,K,L). Interestingly, for O_{hyper} and O_{max}-width one could find threshold values allowing discrimination between controls and NAS patients (dotted lines in Figures 1K,L, respectively) with only one false positive value from healthy controls and no false positive among

the other patients. In addition, no statistically significant difference was observed for any ektacytometric parameter when comparing HD, PD and ALS vs. healthy controls.

3.3 Red blood cell indices and their correlation with ektacytometry parameters

In addition, for all patients, a complete RBC count including a reticulocyte count was performed. The results are summarized in Figures 2A–I. With very few exceptions, which are the RBC distribution width (RDW) for the XK disease patients and the reticulocyte hemoglobin content for the *VPS13A* mutation carriers and the ALS patients, all measured indices were on average within the reference range (grey areas in Figures 2A–I). Differences in RBC number, hemoglobin concentration and hematocrit (Figures 2A–C, respectively) were most likely due to age and gender differences (typically, the mutation carriers were the mothers of the male patients).

Only very few parameters showed significant differences between the compared groups. Most of them were related to particular low values of the PD patients (RBC number – Figure 2A, hemoglobin concentration – Figure 2B, hematocrit – Figure 2C and mean cellular hemoglobin concentration (MCHC) – Figure 2F). However, the above-mentioned increase of RDW in XK disease patients also showed significant differences in carriers as well as ALS patients (Figure 2G). However, since the patient groups were heterogenous and not very large, such differences were likely caused by age or comorbidities rather than by the disease itself. In addition, Supplementary Table S1 provides the blood count parameters with a *p*-value for the comparison with the healthy control group.

Furthermore, we tested for correlations among all measured parameters (Figure 2J) especially the putative correlation between Osmoscan parameters and RBC indices (yellow framed areas in Figure 2J) for healthy controls and NAS patients. The correlation plot of selected parameters, namely, EI_{min} vs. RDW and O_{max} vs. MCH is provided in Figures 2K,L, respectively.

4 Discussion

4.1 Interpretation of the presented data

Deformability characteristics of RBCs have been widely used as biomarkers to determine membrane integrity and cellular viability, e.g., for disorders such as sickle cell disease (Mozar et al., 2016; Parrow et al., 2017; Connes et al., 2018; Gutierrez et al., 2021), diabetes (McMillan et al., 1978; Hanss et al., 1983; Williamson et al., 1985; Caimi and Presti, 2004) or COVID19 (Kubánková et al., 2021; Recktenwald et al., 2022b) but also in the context of RBC quality for transfusion purposes (Card et al., 1983; Barshtein et al., 2016, 2017; Lopes et al., 2023). Specifically, in NAS, membrane deformability changes have been explored along with their effect on microcirculation (Darras et al., 2021; Rabe et al., 2021; Reichel et al., 2022; Recktenwald et al., 2022a).

Although ektacytometry was already used to assess RBC deformability of NAS patients in the past (Bosman, 2018; Lazari et al., 2020), to the best of our knowledge, Osmoscans have not been explored for these neurological conditions yet. Here, we demonstrate the method's applicability and utility for NAS by showing significant differences in several Osmoscan parameters. The best discrimination was found for O_{hyper} and O_{max}-width, which refers to the hydration status of the RBCs. Importantly NAS patients could be distinguished from both healthy control donors as well as other patients with neurodegenerative diseases (HD, PD and ALS).

4.2 Classification of the data in the diagnostic context

As outlined in the Introduction, it would be extremely useful to have an easy method for an initial NAS screening. It would be even better to have markers for the monitoring of the disease state and its progression, and for monitoring the effect of therapeutic interventions. Here we discuss to which extent osmotic gradient ektacytometry may fulfil such requirements and how it compares to other RBC-based techniques.

This is to the best of our knowledge the first approach to investigate blood samples of NAS patients by Osmoscans. Therefore, it can only be seen as an initial approach for discriminating differences in the parameters O_{hyper} – Figure 1K and O_{max}-width – Figure 1L. Both O_{hyper} and O_{max}-width provided only one false positive value for controls (11%) and none in the other neurodegenerative diseases (differential diagnosis). Although these initial results are very promising, sample size was small, and further studies with more patients are required to substantiate these results and inform diagnostic guidelines.

Inspired by one of the reviewers, it is suggested that the osmoscan may help differentiate between NAS patients and patients with PIEZO1 mutations [hereditary xerocytosis (HX)]. While HX patients show a left shift of their osmoscan curve (Kaestner and Bianchi, 2020), the NAS curves differ from HX in the sense that in NAS the O_{min} of the osmoscan is increased, rather than typically decreased (in HX). This results in a narrower width, which is also reflected in the significant difference in the O_{max}-width parameter (Figure 1L).

Other RBC properties may be used diagnostically or as a biomarker to identify or follow NAS patients. These parameters are in particular the acanthocyte count, the erythrocyte sedimentation rate (ESR) and data derived from microfluidic approaches. Table 2 compares the different approaches including known conditions and properties of the particular techniques. The acanthocyte count is the oldest method that is purely based on the RBC shape, classifying a certain percentage of acanthocytes. This method, regardless of whether based on conventional dry blood smears or on optimized wet smears (Storch et al., 2005), proved to be challenging in practice. In patients, the number of acanthocytes can vary over time, including total absence (Malandrini et al., 1993; Sorrentino et al., 1999; Bayreuther et al., 2010). Furthermore, echinocytes can be mistaken for acanthocytes (Peikert et al., 2022b) and the method is prone to human bias (Darras et al., 2021). The situation slightly improves when 3D-imaging and shape classification based on machine learning is applied (Rabe et al., 2021; Simionato et al., 2021). Therefore the acanthocyte count as a biomarker for NAS patients can be seen as controversial.

The other methods listed in Table 2 (ESR, microfluidics and ektacytometry) have in common a more integrated read-out, which not only considers RBC shape but their deformability. Furthermore, they are recent putative biomarkers for NAS (see first line in Table 2). In this respect all of them need further investigation, studies with larger sample sizes, and therefore we are unable to favor or even recommend one of these methods as a gold-standard. Nevertheless, for each of the methods we like to highlight one up-to-date unique

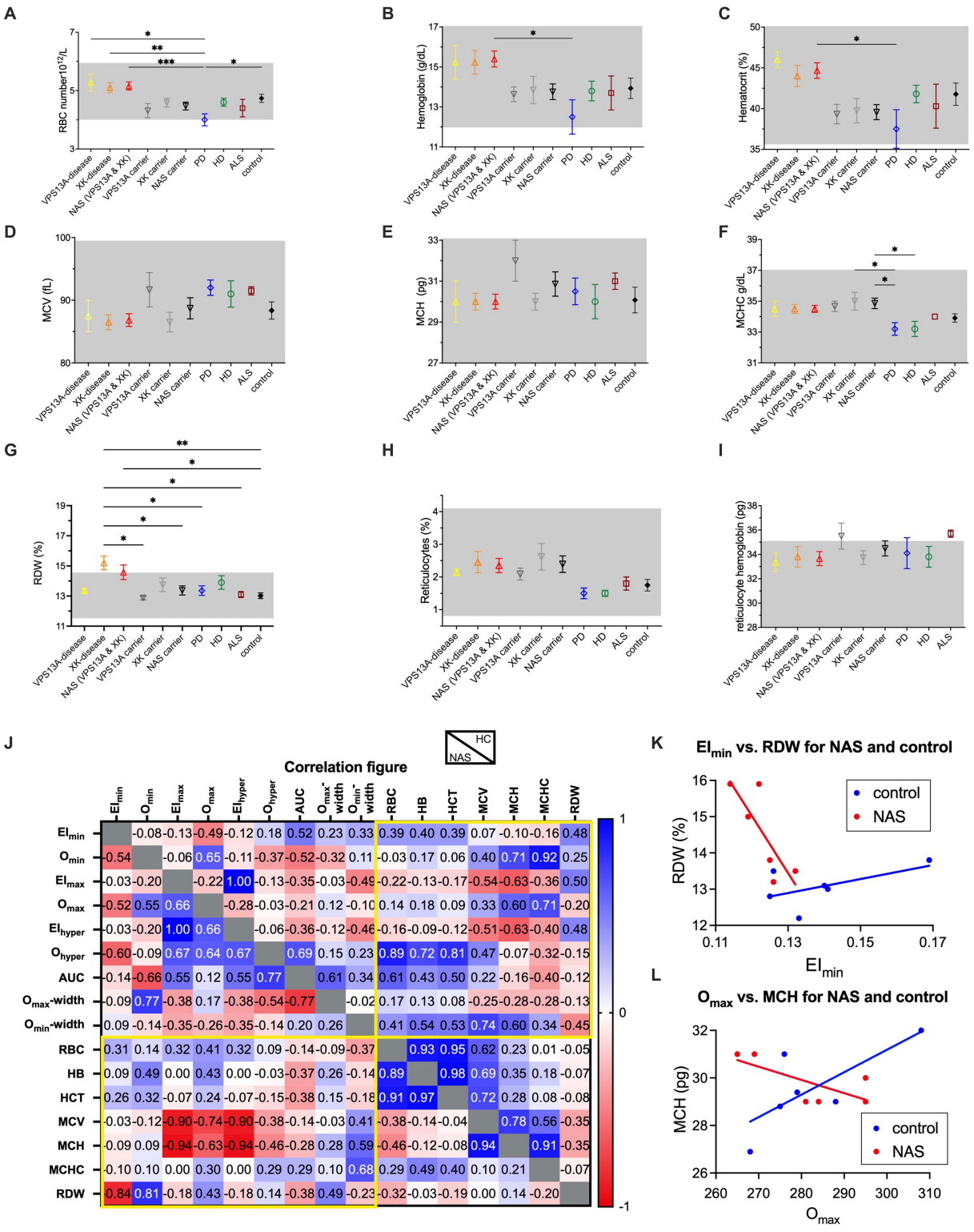

FIGURE 2
RBC indices of the different patient groups and mutation carriers and correlations with the ektacytometry parameters. Panels **(A–I)** present the RBC number per blood volume, the hemoglobin concentration of the blood, the hematocrit, the mean RBC volume (MCV), the mean RBC hemoglobin content, the mean RBC hemoglobin concentration, the RBC distribution width (RDW), the percentage of reticulocytes and the mean reticulocyte hemoglobin content, respectively. Data are based on 2 VPS13A disease patients, 4 XK disease patients, 3 *VPS13A* mutation carriers, 4 *XK* mutation carriers, 6 PD patients, 5 HD patients, 4 ALS patients and 9 controls. The NAS patients as well as the NAS mutation carriers are based on pooled respective subgroups (VPS13A and XK disease). Plotted are the mean values with the standard error of mean (SEM). Significance was checked with an Ordinary one-way ANOVA test, and 1–4 stars correspond to *p*-values lower than 0.05, 0.01, 0.001, and 0.0001, respectively. Panel **(J)** is a color-coded correlation matrix for healthy controls (HC) and pooled NAS patients of the values presented in Figures 1E–L and panels **(A–G)**. Selected correlation blots for EI_{min} vs. RDW and O_{max} vs. MCH are provided in panels K and L, respectively.

TABLE 2 Comparison of RBC-based diagnostic measures for NAS.

Criterion	Acanthocyte count	Prolonged Erythrocyte sedimentation rate	Microfluidic assay	Ektacytometry
References	Storch et al. (2005), Darras et al. (2021), Peikert et al. (2022b)	Darras et al. (2021), Rabe et al. (2021), John et al. (2023)	Rabe et al. (2021), Recktenwald et al. (2022a), Reichel et al. (2022)	This paper
Diagnostic power	Limited (improved in automated 3D classification)	Good discrimination to controls, specificity still needs to be shown	Good discrimination to controls, specificity still needs to be shown	Discrimination at detectable limit, statistics limited to this paper
Correlation with severeness or disease state	No evidence	Unknown	Unknown	Unknown
Blood sample volume	50 µL	Typically, 1.5 mL	5 µL	200 µL
Routine devices available	Blood smear examination at different levels of automation (3D is not routine)	Several levels of automation available; parameters easy adaptable for manual devices	Yes (Erysense by Cysmic GmbH, Saarbrücken, Germany)	Yes (Lorrca by RR Mechatronics, Zwaag, The Netherlands)
Possibility of multiplexing/throughput	Unlikely	In principle yes, but needs (software) adaptation of existing technologies	In principle yes, but needs hardware developments of existing technologies	Challenging
Implementation in clinical settings	Difficult, prone to bias, needs repeated training	Easy, though requires instrument upgrade	Medium, institution should set standard for diagnostic workup and quality control	Medium, institution should be regular user of instrument and set standard for diagnostic workup and quality control

property that is in support for the particular approach. A significant strength of the Westergren ESR is the broad availability of this established method, including automated devices for its quantification in central haematological laboratories. It requires only a different read-out mode (a longer time and preferentially the kinetics of the sedimentation (Darras et al., 2021, 2022; Dasanna et al., 2022). The big advantage of the microfluidic approach is the small sample volume, which would very well work with samples from finger needle prick not requiring venous blood sampling (Recktenwald et al., 2022a). In this report, we present a comparison with respect to other neurodegenerative diseases for Osmoscans (currently lacking for ESR and microfluidics).

All the three methods discussed (ESR, microfluidics, and Osmoscan), are based to a large extent on RBC deformability. Therefore, all of them may develop into a diagnostic marker/biomarker. However, different deployment scenarios, such as a diagnostic screen in a large population, the follow-up of particular patients or the comparison of patients, may all require special conditions (sample volume, sample numbers, time and expenses per test) and this may determine the method of choice.

Data availability statement

The original contributions presented in the study are included in the article/Supplementary material, further inquiries can be directed to the corresponding author.

Ethics statement

The studies involving humans were approved by the review boards of the 'Ärztekammer des Saarlandes', permission number 51/18, as well as of the University of Rostock (A 2019-0134). Part of the study was carried out under national (UK) research ethics committee approval 11/SC/0204 and institutional approval ERGO 41084. The studies were conducted in accordance with the local legislation and institutional requirements. The participants provided their written informed consent to participate in this study.

Author contributions

CH: Formal analysis, Visualization, Writing – original draft, Data curation, Investigation, Methodology. KP: Data curation, Investigation, Funding acquisition, Resources, Writing – review & editing. MQ: Data curation, Investigation, Writing – review & editing. AD: Data curation, Investigation, Writing – review & editing. JW: Writing – review & editing, Methodology. JB: Methodology, Writing – review & editing. ML: Resources, Writing – review & editing. IG: Resources, Writing – review & editing. CW: Writing – review & editing, Funding acquisition, Project administration, Supervision. MR: Writing – review & editing, Methodology. RW: Writing – review & editing, Resources. AH: Funding acquisition, Supervision, Writing – review & editing. EB: Supervision, Writing – review & editing, Methodology, Project administration. RW: Methodology, Project administration, Supervision, Writing – review & editing, Funding acquisition. LK: Funding acquisition, Project administration, Supervision, Writing – review & editing, Conceptualization, Formal analysis, Visualization, Writing – original draft.

Funding

The author(s) declare that financial support was received for the research, authorship, and/or publication of this article. This study was supported by the European Framework Horizon 2020 under grant

agreement number 860436 (EVIDENCE) and European Framework Horizon Europe under grant agreement number 101120168 (INNOVATION). KP is supported by the Rostock Academy of Science (RAS) and Andreas Hermann by the "Hermann und Lilly Schilling-Stiftung für medizinische Forschung im Stifterverband."

Acknowledgments

We are grateful to Glenn (†) and Ginger Irvine as the founders of the Advocacy for Neuroacanthocytosis Patients (www.naadvocacy.org) and to Susan Wagner and Joy Willard-Williford as representatives of the NA Advocacy USA (www.naadvocacyusa.org).

Conflict of interest

The authors declare that the research was conducted in the absence of any commercial or financial relationships that could be construed as a potential conflict of interest.

The author(s) declared that they were an editorial board member of Frontiers, at the time of submission. This had no impact on the peer review process and the final decision.

Publisher's note

Supplementary material

The Supplementary material for this article can be found online at: https://www.frontiersin.org/articles/10.3389/fnins.2024.1406969/full#supplementary-material

References

Adjobo-Hermans, M. J. W., Cluitmans, J. C. A., and Bosman, G. J. C. G. M. (2015). Neuroacanthocytosis: observations, theories and perspectives on the origin and significance of Acanthocytes. *Tremor Other Hyperkinet. Mov.* 5:328. doi: 10.7916/d8vh5n2m

Barshtein, G., Goldschmidt, N., Pries, A. R., Zelig, O., Arbell, D., and Yedgar, S. (2017). Deformability of transfused red blood cells is a potent effector of transfusion-induced hemoglobin increment: A study with β-thalassemia major patients. *Am. J. Hematol.* 92, E559–E560. doi: 10.1002/ajh.24821

Barshtein, G., Pries, A. R., Goldschmidt, N., Zukerman, A., Orbach, A., Zelig, O., et al. (2016). Deformability of transfused red blood cells is a potent determinant of transfusion-induced change in recipient's blood flow. *Microcirculation* 23, 479–486. doi: 10.1111/micc.12296

Bayreuther, C., Borg, M., Ferrero-Vacher, C., Chaussenot, A., and Lebrun, C. (2010). Choréo-acanthocytose sans acanthocytes. *Rev. Neurol.* 166, 100–103. doi: 10.1016/j.neurol.2009.03.005

Bianchi, P., Zaninoni, A., Fermo, E., Vercellati, C., Paola, M. A., Zanella, A., et al. (2015). Diagnostic power of laser assisted optical rotational cell analyzer (LoRRca MaxSis) evaluated in 118 patients affected by hereditary hemolytic anemias. *Blood* 126:942. doi: 10.1182/blood.v126.23.942.942

Bosman, G. J. C. G. M. (2018). Disturbed red blood cell structure and function: an exploration of the role of red blood cells in neurodegeneration. *Front. Med.* 5:146. doi: 10.3389/fmed.2018.00198

Caimi, G., and Presti, R. L. (2004). Techniques to evaluate erythrocyte deformability in diabetes mellitus. *Acta Diabetol.* 41, 99–103. doi: 10.1007/s00592-004-0151-1

Card, R. T., Mohandas, N., and Mollison, P. L. (1983). Relationship of post-transfusion viability to deformability of stored red cells. *Br. J. Haematol.* 53, 237–240. doi: 10.1111/j.1365-2141.1983.tb02016.x

Cluitmans, J. C. A., Tomelleri, C., Yapici, Z., Dinkla, S., Bovee-Geurts, P., Chokkalingam, V., et al. (2015). Abnormal red cell structure and function in neuroacanthocytosis. *PLoS One* 10:e0125580. doi: 10.1371/journal.pone.0125580

Connes, P., Renoux, C., Romana, M., Abkarian, M., Joly, P., Martin, C., et al. (2018). Blood rheological abnormalities in sickle cell anemia. *Clin. Hemorheol. Microcirc.* 68, 165–172. doi: 10.3233/ch-189005

Costa, L. D., Suner, L., Galimand, J., Bonnel, A., Pascreau, T., Couque, N., et al. (2016). Diagnostic tool for red blood cell membrane disorders: assessment of a new generation ektacytometer. *Blood cells Mol. Dis.* 56, 9–22. doi: 10.1016/j.bcmd.2015.09.001

Danek, A., Rubio, J. P., Rampoldi, L., Ho, M., Dobson-Stone, C., Tison, F., et al. (2001). McLeod neuroacanthocytosis: genotype and phenotype. *Ann. Neurol.* 50, 755–764. doi: 10.1002/ana.10035

Darras, A., Dasanna, A. K., John, T., Gompper, G., Kaestner, L., Fedosov, D. A., et al. (2022). Erythrocyte sedimentation: collapse of a high-volume-fraction soft-particle gel. *Phys. Rev. Lett.* 128:088101. doi: 10.1103/physrevlett.128.088101

Darras, A., Peikert, K., Rabe, A., Yaya, F., Simionato, G., John, T., et al. (2021). Acanthocyte sedimentation rate as a diagnostic biomarker for neuroacanthocytosis syndromes: experimental evidence and physical justification. *Cells* 10:788. doi: 10.3390/cells10040788

Dasanna, A. K., Darras, A., John, T., Gompper, G., Kaestner, L., Wagner, C., et al. (2022). Erythrocyte sedimentation: effect of aggregation energy on gel structure during collapse. *Phys. Rev. E* 105:024610. doi: 10.1103/physreve.105.024610

Flormann, D., Qiao, M., Murciano, N., Iacono, G., Darras, A., Hof, S., et al. (2022). Transient receptor potential channel vanilloid type 2 in red cells of cannabis consumer. *Am. J. Hematol.* 97, E180–E183. doi: 10.1002/ajh.26509

Franceschi, L. D., Bosman, G. J. C. G. M., and Mohandas, N. (2014). Abnormal red cell features associated with hereditary neurodegenerative disorders: the neuroacanthocytosis syndromes. *Curr. Opin. Hematol.* 21, 201–209. doi: 10.1097/moh.0000000000000035

Guillén-Samander, A., Wu, Y., Pineda, S. S., García, F. J., Eisen, J. N., Leonzino, M., et al. (2022). A partnership between the lipid scramblase XK and the lipid transfer protein VPS13A at the plasma membrane. *Proc. Natl. Acad. Sci.* 119:e2205425119. doi: 10.1073/pnas.2205425119

Gutierrez, M., Shamoun, M., Seu, K. G., Tanski, T., Kalfa, T. A., and Eniola-Adefeso, O. (2021). Characterizing bulk rigidity of rigid red blood cell populations in sickle-cell disease patients. *Sci. Rep.* 11:7909. doi: 10.1038/s41598-021-86582-8

Hanss, M., Attali, J. R., Helou, C., and Lemarie, J. C. (1983). Erythrocytes deformability and diabetes. *Clin. Hemorheol. Microcirc.* 3, 383–391. doi: 10.3233/ch-1983-3404

John, T., Kaestner, L., Wagner, C., and Darras, A. (2023). Early stage of erythrocyte sedimentation rate test: fracture of a high-volume-fraction gel. *PNAS Nexus* 3:pgad416. doi: 10.1093/pnasnexus/pgad416

Kaestner, L. (2023). Proceedings of the eleventh international meeting on neuroacanthocytosis syndromes. *Tremor Other Hyperkinet. Mov.* 13:41. doi: 10.5334/tohm.826

Kaestner, L., and Bianchi, P. (2020). Trends in the development of diagnostic tools for red blood cell-related diseases and anemias. *Front. Physiol.* 11:387. doi: 10.3389/fphys.2020.00387

Kubánková, M., Hohberger, B., Hoffmanns, J., Fürst, J., Herrmann, M., Guck, J., et al. (2021). Physical phenotype of blood cells is altered in COVID-19. *Biophys. J.* 120, 2838–2847. doi: 10.1016/j.bpj.2021.05.025

Lazari, D., Leal, J. K. F., Brock, R., and Bosman, G. (2020). The relationship between aggregation and deformability of red blood cells in health and disease. *Front. Physiol.* 11:288. doi: 10.3389/fphys.2020.00288

Lazarova, E., Gulbis, B., Van Oirschot, B., and Van Wijk, R. (2017). Next-generation osmotic gradient ektacytometry for the diagnosis of hereditary spherocytosis: interlaboratory method validation and experience. *Clin. Chem. Lab. Med.* 55, 394–402. doi: 10.1515/cclm-2016-0290

Lopes, M. G. M., Recktenwald, S. M., Simionato, G., Eichler, H., Wagner, C., Quint, S., et al. (2023). Big data in transfusion medicine and artificial intelligence analysis for red blood cell quality control. *Transfus. Med. Hemother.* 50, 163–173. doi: 10.1159/000530458

Lupo, F., Tibaldi, E., Matte, A., Sharma, A. K., Brunati, A. M., Alper, S. L., et al. (2016). A new molecular link between defective autophagy and erythroid abnormalities in chorea-acanthocytosis. *Blood* 128, 2976–2987. doi: 10.1182/blood-2016-07-727321

Malandrini, A., Fabrizi, G. M., Palmeri, S., Ciacci, G., Salvadori, C., Berti, G., et al. (1993). Choreo-acanthocytosis like phenotype without acanthocytes: clinicopathological case report. *Acta Neuropathol.* 86, 651–658. doi: 10.1007/bf00294306

McMillan, D. E., Utterback, N. G., and Puma, J. L. (1978). Reduced erythrocyte deformability in diabetes. *Diabetes* 27, 895–901. doi: 10.2337/diab.27.9.895

Mozar, A., Connes, P., Collins, B., Hardy-Dessources, M.-D., Romana, M., Lemonne, N., et al. (2016). Red blood cell nitric oxide synthase modulates red blood cell deformability in sickle cell anemia. *Clin. Hemorheol. Microcirc.* 64, 47–53. doi: 10.3233/ch-162042

Park, J.-S., Hu, Y., Hollingsworth, N. M., Miltenberger-Miltenyi, G., and Neiman, A. M. (2022). Interaction between VPS13A and the XK scramblase is important for VPS13A function in humans. *J. Cell Sci.* 135:jcs260227. doi: 10.1242/jcs.260227

Park, J.-S., and Neiman, A. M. (2020). XK is a partner for VPS13A: a molecular link between chorea-Acanthocytosis and McLeod syndrome. *Mol. Biol. Cell* 31, 2425–2436. doi: 10.1091/mbc.e19-08-0439-t

Parrow, N. L., Tu, H., Nichols, J., Violet, P.-C., Pittman, C. A., Fitzhugh, C., et al. (2017). Measurements of red cell deformability and hydration reflect HbF and HbA2 in blood from patients with sickle cell anemia. *Blood Cells Mol. Dis.* 65, 41–50. doi: 10.1016/j.bcmd.2017.04.005

Peikert, K., Hermann, A., and Danek, A. (2022a). XK-associated McLeod syndrome: nonhematological manifestations and relation to VPS13A disease. *Transfus. Med. Hemother.* 49, 4–12. doi: 10.1159/000521417

Peikert, K., Storch, A., Hermann, A., Landwehrmeyer, G. B., Walker, R. H., Simionato, G., et al. (2022b). Commentary: acanthocytes identified in Huntington's disease. *Front. Neurosci.* 16:1049676. doi: 10.3389/fnins.2022.1049676

Rabe, A., Kihm, A., Darras, A., Peikert, K., Simionato, G., Dasanna, A. K., et al. (2021). The erythrocyte sedimentation rate and its relation to cell shape and rigidity of red blood cells from chorea-acanthocytosis patients in an off-label treatment with Dasatinib. *Biomol. Ther.* 11:727. doi: 10.3390/biom11050727

Rampoldi, L., Danek, A., and Monaco, A. P. (2002). Clinical features and molecular bases of neuroacanthocytosis. *J. Mol. Med.* 80, 475–491. doi: 10.1007/s00109-002-0349-z

Recktenwald, S. M., Lopes, M. G. M., Peter, S., Hof, S., Simionato, G., Peikert, K., et al. (2022a). Erysense, a lab-on-a-Chip-based point-of-care device to evaluate red blood cell flow properties with multiple clinical applications. *Front. Physiol.* 13:884690. doi: 10.3389/fphys.2022.884690

Recktenwald, S. M., Simionato, G., Lopes, M. G., Gamboni, F., Dzieciatkowska, M., Meybohm, P., et al. (2022b). Cross-talk between red blood cells and plasma influences blood flow and omics phenotypes in severe COVID-19. *eLife* 11:e81316. doi: 10.7554/elife.81316

Reichel, F., Kräter, M., Peikert, K., Glaß, H., Rosendahl, P., Herbig, M., et al. (2022). Changes in blood cell deformability in chorea-Acanthocytosis and effects of treatment with Dasatinib or Lithium. *Front. Physiol.* 13:852946. doi: 10.3389/fphys.2022.852946

Ryoden, Y., Segawa, K., and Nagata, S. (2022). Requirement of Xk and Vps13a for the P2X7-mediated phospholipid scrambling and cell lysis in mouse T cells. *Proc. Natl. Acad. Sci.* 119:e2119286119. doi: 10.1073/pnas.2119286119

Siegl, C., Hamminger, P., Jank, H., Ahting, U., Bader, B., Danek, A., et al. (2013). Alterations of red cell membrane properties in nneuroacanthocytosis. *PLoS One* 8:e76715. doi: 10.1371/journal.pone.0076715

Simionato, G., Hinkelmann, K., Chachanidze, R., Bianchi, P., and Fermo, E., Wijk, R. van van Wijk, R., Leonetti, M., Wagner, C., Kaestner, L., and Quint, S. (2021). Red blood cell phenotyping from 3D confocal images using artificial neural networks. *PLoS Comput. Biol.* 17,:e1008934. doi: 10.1371/journal.pcbi.1008934

Sorrentino, G., Renzo, A. D., Miniello, S., Nori, O., and Bonavita, V. (1999). Late appearance of acanthocytes during the course of chorea-acanthocytosis. *J. Neurol. Sci.* 163, 175–178. doi: 10.1016/s0022-510x(99)00005-2

Storch, A., Kornhass, M., and Schwarz, J. (2005). Testing for acanthocytosis. *J. Neurol.* 252, 84–90. doi: 10.1007/s00415-005-0616-3

Ueno, S., Maruki, Y., Nakamura, M., Tomemori, Y., Kamae, K., Tanabe, H., et al. (2001). The gene encoding a newly discovered protein, chorein, is mutated in chorea-acanthocytosis. *Nat. Genet.* 28, 121–122. doi: 10.1038/88825

Walker, R. H., and Danek, A. (2021). "Neuroacanthocytosis" – overdue for a taxonomic update. *Tremor Other Hyperkinet. Mov.* 11:1. doi: 10.5334/tohm.583

Walker, R. H., Peikert, K., Jung, H. H., Hermann, A., and Danek, A. (2023). Neuroacanthocytosis syndromes: the clinical perspective. *Contact* 6:25152564231210340. doi: 10.1177/25152564231210339

Wilde, J. R. A. D., Boesveld, M. E., Vuren, A. J.Van, and Solinge, W. W. Vn, Beers, E. J. V., Bartels, M., et al. (2023). Novel biomarkers for assessing clinical severity in hereditary spherocytosis - application of routine and advanced diagnostic tests. *Blood* 142,:2453. doi: 10.1182/blood-2023-189034

Williamson, J. R., Gardner, R. A., Boylan, C. W., Carroll, G. L., Chang, K., Marvel, J. S., et al. (1985). Microrheologic investigation of erythrocyte deformability in diabetes mellitus. *Blood* 65, 283–288. doi: 10.1182/blood.v65.2.283.283

Zaninoni, A., Fermo, E., Vercellati, C., Consonni, D., Marcello, A. P., Zanella, A., et al. (2018). Use of laser assisted optical rotational cell analyzer (LoRRca MaxSis) in the diagnosis of RBC membrane disorders, enzyme defects, and congenital Dyserythropoietic anemias: a monocentric study on 202 patients. *Front. Physiol.* 9:451. doi: 10.3389/fphys.2018.00451

frontiers | Frontiers in Neurology

TYPE Case Report
PUBLISHED 25 July 2024
DOI 10.3389/fneur.2024.1377377

OPEN ACCESS

EDITED BY
Luigi M. Romito,
IRCCS Carlo Besta Neurological Institute Foundation, Italy

REVIEWED BY
Amar Patel,
Yale University, United States
Manuel J. Rodriguez,
University of Barcelona, Spain
Ruth Walker,
United States Department of Veterans Affairs, United States

*CORRESPONDENCE
Hongfeng Liang
✉ 447547418@qq.com
Chunye Zheng
✉ 1064569514@qq.com

†These authors have contributed equally to this work

RECEIVED 02 February 2024
ACCEPTED 15 July 2024
PUBLISHED 25 July 2024

CITATION
Xu Y, Yu J, Gao Y, Su Q, Xie H, Liang H and Zheng C (2024) A case of chorea-acanthocytosis with significant improvement of symptoms at one year with deep brain stimulation: case report and literature review.
Front. Neurol. 15:1377377.
doi: 10.3389/fneur.2024.1377377

A case of chorea-acanthocytosis with significant improvement of symptoms at one year with deep brain stimulation: case report and literature review

Yan Xu[1†], Jiabin Yu[2†], Yimeng Gao[1†], Qiaozhen Su[2], Haitao Xie[2], Hongfeng Liang[2*] and Chunye Zheng[2*]

[1]The Second Clinical College of Guangzhou University of Chinese Medicine, Guangzhou, China, [2]Department of Neurology, Guangdong Provincial Hospital of Traditional Chinese Medicine, Guangzhou, China

Chorea-acanthocytosis (ChAc) is a rare, neurodegenerative disorder caused by mutations in the VPS13A gene. In this article, we report on a 32-year-old man diagnosed with ChAc, with involuntary movements of the mouth and trunk, drooling of the mouth, slurred speech, and abnormal vocalizations as the main clinical manifestations. Three weeks after implantation of globus pallidus internal (GPi)-deep brain stimulation (DBS), the patient's symptoms improved significantly. For example, articulation is clear, involuntary trunk movements and salivation have largely disappeared, and abnormal vocalizations have been significantly reduced. After 1 year of follow-up, the improvement in involuntary movement symptoms is essentially the same as before. As far as we know, we are the first to report the relief of involuntary vocalizations in a patient with GPi-DBS treatment, and that salivation and involuntary trunk movements have almost disappeared, and all other symptoms are significantly relieved, which is rare in previous cases. All of the above proves that the treatment of our case with DBS was very successful and that longer term follow-up is critical. We also hope that our case will provide new references and therapeutic ideas for the future treatment of patients with ChAc.

KEYWORDS

chorea-acanthocytosis, involuntary movement, abnormal vocalizations, globus pallidus internal, deep brain stimulation

Introduction

Chorea-acanthocytosis (ChAc) is an extremely rare autosomal recessive neurodegenerative disorder caused by mutations in VPS13A, which is located on 9q21, and is a subtype of neuroacanthocytosis syndrome (1). Its main clinical features include progressive movement disorders, seizures, psychiatric symptoms, cognitive deficits, etc., and orofacial dyskinesia is one of its most prominent features, and there may be self-injurious behavior (2, 3). The prevalence of the disease is about 1: 1,000,000, and most patients with ChAc have elevated creatine phosphokinase (CK) levels, in addition to the fact that ChAc is mainly characterized by peripheral blood acanthocytosis (4). Magnetic Resonance Imaging (MRI) of the brain generally shows bilateral symmetrical atrophy of the caudate nucleus. Clinical treatment

options for ChAc are currently greatly limited and only limited improvement from symptomatic and supportive therapy (5). Previous studies have found that GPi-DBS not only improves dystonia and choreiform symptoms in ChAc patients, but may also be the best option for ChAc patients with predominantly orofacial and submandibular dystonia (6–8). At the same time, we also reviewed the relevant literature to explore the characteristics and advantages of GPi-DBS treatment of ChAc, in hopes of creating a reference for future ChAc treatments.

Case presentation

A 32-year-old man presented in September 2022 with involuntary movements of the corners of the mouth, drooling of the mouth (noticeable during eating or drinking), frequent involuntary vocalizations (similar to grunting) slurred speech, occasional involuntary forward flexion, and an unsteady gait. The patient's choreic symptoms had significantly worsened after 6 months, such as more frequent involuntary movements of the corners of the mouth and involuntary movements of the limbs, occasional involuntary forward flexion of the trunk with a slight tilt to the right when walking, and the number of abnormal vocalizations made increased. Moreover, he developed new symptoms, involuntary turning of the neck and shrugging of the shoulders, involuntary grimacing, and lacking fluency in swallowing. The patient had no other typical symptoms, such as cognitive, psychiatric, neuropathic, or myopathic symptoms or seizures. A physical examination of the patient revealed dysarthria, occasional choking on food or water, decreased sensation of the posterior pharyngeal wall bilaterally, reduced pharyngeal reflexes on both sides

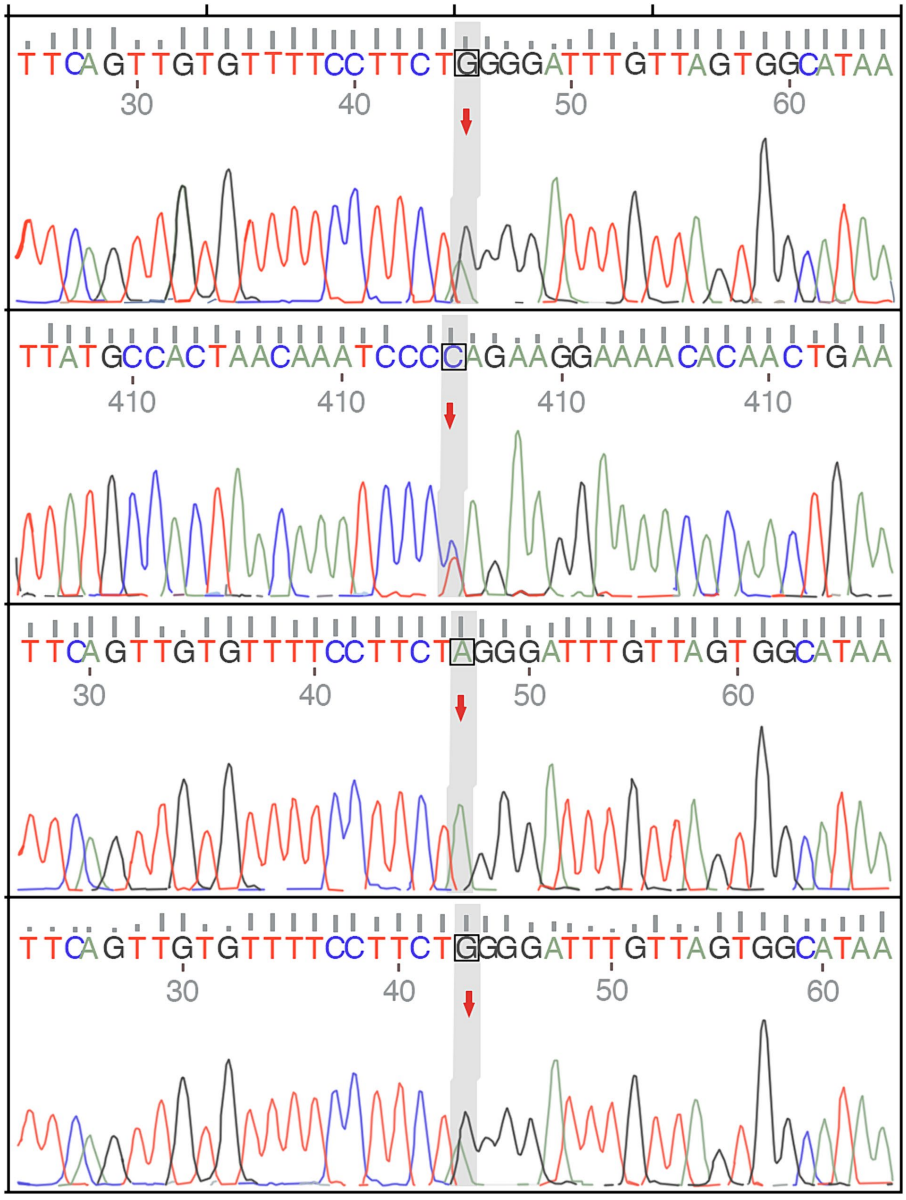

FIGURE 1
The genetic examination results of the patient and show a single nucleotide variant and a small fragment insertion–deletion variant.

of the pharyngeal wall, slow elevation of the soft palate bilaterally in the region, a slight decrease in muscle tone in the extremities, and muscle strength of the limbs of Grade 5. Furthermore, his knee-jerk and achilles tendon reflexes were diminished. Laboratory tests indicated the presence of 9% acanthocytes in the blood smear, while serum ceruloplasmin levels were within the normal range at 284 mg/L (normal values range from 150–600 mg/L). The cranial MR suggests atrophy of the caudate nucleus on the left side of the cranium. According to the electromyogram results, abnormalities in the measured tibial nerve H-reflex suggest damage to the lumbosacral nerve root. Nerve conduction and electro-neurography of the remaining extremities showed no significant abnormalities. The genetic examination results (Figure 1) showed the patient had two heterozygous mutations in the VPS13A gene, mutation 1 (c.7253A > G, p.Asn2481Ser, source of variation: father) was located in the coding region: nucleotide 7,253 was mutated from adenine to guanine resulting in a mutation of amino acid 2,481 from asparagine to serine. Mutation 2 (c.8908-2A > G, source of variation: mother) was located at the classical splice site: the second nucleotide upstream of nucleotide 8,908 was mutated from adenine to guanine, and this mutation may result in aberrant splicing of the exon, which could lead to aberrant mRNA splicing affecting the normal structure and function of the translated protein product. And these mutations not were reported previously.

In the process of tracing the patient's history, we found that there was no family history of neurological disease. In the past six months, the patient has tried a variety of drugs in other hospitals. In January 2023, the patient took tiapride hydrochloride (0.1 g/tid) and pramipexole (0.125 mg/tid). However, the symptoms did not improve. In one month, the patient accepted diazepam (5 mg/bid) and haloperidol (1 mg/bid), and the involuntary movements of the corners of the mouth began to improve, but as the patient continued to take the medication, the symptoms returned to the beginning. We tried treating the patient with levodopa and benserazide hydrochloride (0.125 mg/tid) after admission, but the symptoms did not improve. We also tried using Chinese medicine recipes for the patient. After taking Prof. Huang's experienced Ge-Gen -Decoction, his drooling symptoms improved slightly, and other symptoms had not improved, but he wanted a greater improvement in the treatment effect. In the

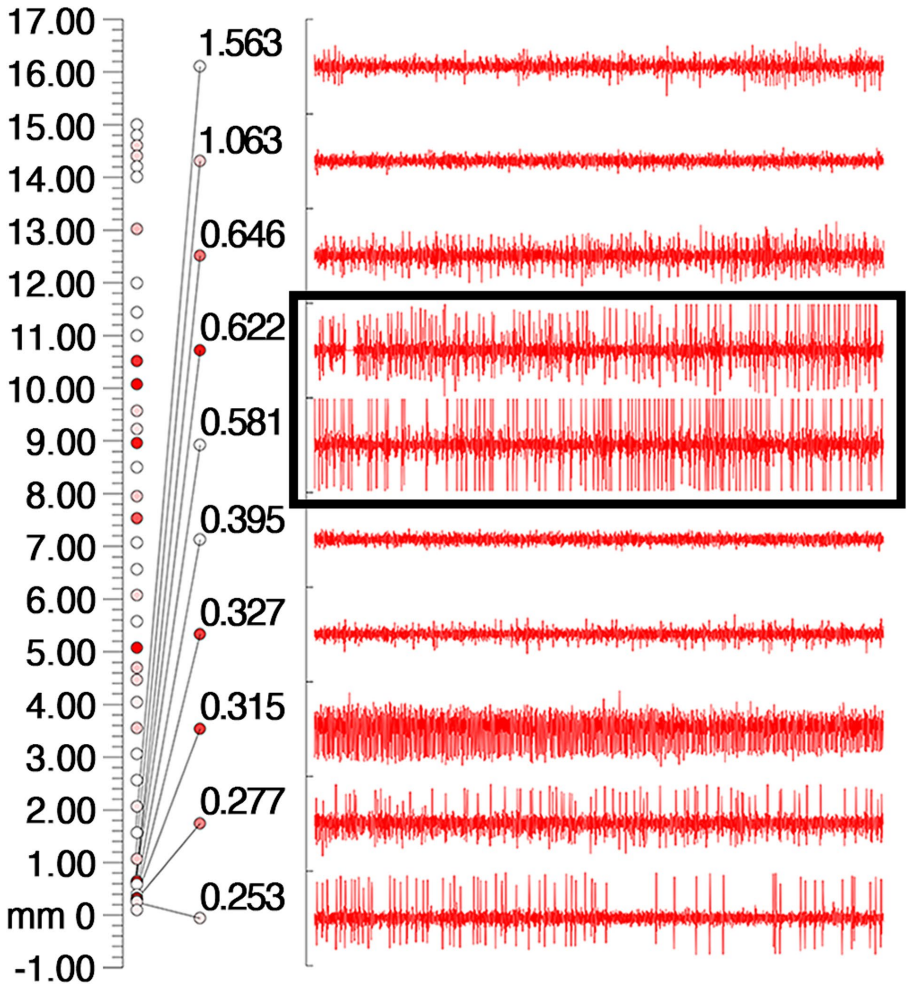

FIGURE 2
Intraoperative electrophysiologic monitoring unit observed cellular discharges typical of GPi. The coordinates on the leftmost side of the picture, the number 0 indicates the preset depth of the target point, the number 17 indicates 17 mm above the target point, and the cellular discharges are continuously recorded from the number 17 downwards, and the cellular discharges are the most typical and obvious in the black box, and then 0.622 mm and 0.531 mm above the target point. The different colored circles are related to the background sound (the sound during intraoperative testing of the nuclei), with the higher the background sound the redder the color.

TABLE 1 Target Coordinates and detailed stimulation parameters of the patient.

Location	X (mm)	Y (mm)	Z (mm)	Ring	Arc	Current	Pluse width (μs)	Frequency (Hz)
Left	122.8	99.5	101.0	54.7°	109.4°	2.0 V	120	135
Right	89.1	99.7	104.2	54.1°	75.4°	2.0 V	120	135

end, we recommend that patients try GPi-DBS therapy after careful consideration.

On March 23, 2023, we performed stereotactic deep brain electrode placement, as shown in Figure 2. In the first half of the procedure, deep brain electrodes are implanted while the patient is awake. Intraoperative electrophysiologic recordings of the GPi nuclei were satisfactory and in the correct position, and the location parameters are detailed in Table 1. After completing the first half of the procedure, we performed a Computed Tomography (CT) scan, fused the CT data with the preoperative implantation plan, and began implanting the peripheral pulse generator under general anesthesia after confirming the accuracy of the implantation position (Figure 3). We selected the corresponding parameters after a comprehensive evaluation based on the patient's intraoperative symptom improvement and tolerance level (9). The frequency of the intraoperative test was 130 Hz, and the pulse width was 60 μs. In the third week after surgery (April 13, 2023), the patient returned to the hospital and DBS was turned on, and the stimulation parameters also started from low current and low frequency, and were slowly adjusted upward, while observing the patients' symptom relief changes, and finally selecting the appropriate stimulation frequency and current (Table 1). Respectively, we assessed the patient's pre-operative and post-operative Montreal Cognitive Assessment scores of 27 and 26(>26 normal cognitive functions). And we also assessed the patient's pre-operative total Unified Huntington's Disease Rating Scale (UHDRS) motor score of 53 and at post-operative week 3, a total UHDRS motor score of 21. After 1 year of follow-up, the improvement in involuntary movement symptoms is essentially the same as before. Ultimately, the patient's choreic symptoms improved significantly, and a significant reduction in abnormal vocalizations.

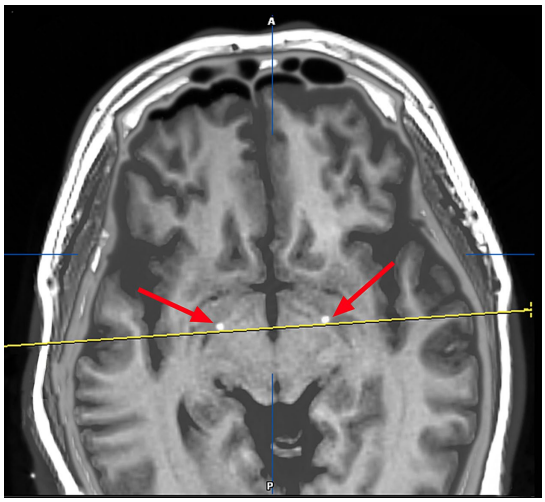

FIGURE 3
Image after fusion of preoperative MR plan and postoperative CT and it is a postoperative image fusion, suggesting that the stimulation electrode is precisely located in the GPI nucleus.

Literature review

Through literature reviewed in the PubMed database from 1978 to 2023, a total of 35 patients treated with DBS were identified. In the end, 21 patients were included, as detailed in Table 2, after removing reports with grossly incomplete information or inaccessible literature. The first attempt to treat ChAc with DBS was made by Wihl et al. (21), however, the patients failed to benefit from DBS treatment. Since then, approximately 30 patients have been successfully treated with DBS for ChAc, with varying results and frequency of treatment. Significant remission of chorea and dystonia was achieved in all patients, with variable results for improvements in symptoms such as dysarthria and dysphagia. This could be related to different stimulus frequencies, pulse widths, or current intensities in individual patients.

Discussion

Neuroacanthocytosis (NA) is a neurological syndrome associated with acanthocytosis, and its identification, diagnosis, and nomenclature have evolved. It was mainly used to characterize ChAc, McLeod syndrome (MLS), and Huntington's disease-like 2 (HDL2) between 2001–2017, and it is understood that the current understanding of NA includes diseases caused by mutations in the VPS13A and XK genes (22, 23). However, there is a significant overlap in clinical symptoms, laboratory investigations, and imaging manifestations between the two subtypes. Genetic diagnosis is the primary method of differentiation. XK disease is a genetic disorder caused by mutations in the XK gene on the X chromosome that result in the loss or dysfunction of the encoded protein (24). The presentation of XK disease is characterized by muscular involvement, such as skeletal muscle myopathy, and peripheral neuropathy, and it can also affect other organ systems. Particularly, involvement of the heart may be a characteristic feature of the disease (25, 26).

ChAc is the most common type of neuroacanthocytosis. It may also be called VPS13A disease and is caused by pathogenic variants in the gene (27). The peak age of onset of the disease is 30–40 years of age, with progressive exacerbation of symptoms (28). Choreiform movements were the most prevalent clinical symptom in the disease (88%), followed by orofacial dystonia (80%), which includes increased facial expressions such as grimacing, smacking of the tongue, and biting of the tongue and lips (29, 30). Laboratory tests probably reveal an increase in the percentage of peripheral blood acanthocytes, which is a hint of the diagnosis of ChAc (31). Moreover, serum CK levels are significantly elevated. An Electromyogram is dominated by neuroaxonal damage and myopathic changes. Besides, cranial imaging may show symmetrical bilateral atrophy of the caudate. In this case, the patient was genetically tested and had classic choreic symptoms, so the ChAc diagnosis was clear.

TABLE 2 Summary of characteristics of ChAc patients with previously treated with DBS.

Time/ Author	Age/ Sex	VPS13A mutations	Main symptoms	Current	Pluse width (μs)	Fre (Hz)	UHDR (pre-op)	Follow-up (m)	UHDRS (post-op)	Outcome
2009/Ruiz et al. (10)	35/F	NA	Oromandibular dyskinesia, dysarthria, irregular choreic gait with truncal spasm	(L)4.4 V (R)4.2 V	180	130	24	NA	14	Rapid relief of tension disorder and chorea symptoms, dysarthria did not improved
2012/Shin et al. (11)	39/F	+	Whole body involuntary movement, orolingual dyskinesia with tongue protrusion and lip biting, involuntary head banging	(L)3.0 V (R)2.9 V	90	130	44	13	12	Dystonia, bradykinesia, choreic movements of the limbs and trunk had significantly improved, no improvement in chewing and biting of lips and tongue
2012/Li et al. (7)	39/M	NA	Orofacial and lingual dyskinesia, shoulder shrugging, neck stretching and tongue biting, chorea of the lower limbs and trunk	(L)3.5 V (R)3.5 V	60	40	36	9	13	Obvious improvement in chorea symptoms and dysphagia, mild improvements in dystonia with 40 Hz stimulation of the GPi, both chorea and dystonia were exacerbated by 130 Hz GPi stimulation.
	30/M	NA	Orofacial and lingual dyskinesia with tongue biting, generalized chorea and trunk spasms, difficulties in writing, speaking, swallowing, and walking	(L)3.5 V (R)3.5 V	60	40	53	5	27	
2013/ Kefalopoulou et al. (12)	54/M	NA	Orofacial dyskinesias and feeding dystonia, violent trunk spasms	(L)2.5 V (R)2.5 V	60	130	40	NA	23	Upper limb dexterityand truncal dips improved markedly, no improvement in feeding dystonia
	43/M	NA	Oromandibular dyskinesias, dysarthria, violent choreic movements of upper and lower limbs, lurching gait and poor balance	(L)2.5 V (R)2.5 V	90	130	74	NA	50	Significant improvement in choreic movement, walking and truncal spasms
2015/Nakano et al. (13)	43/M	NA	Involuntary movements of the tongue and all extremities	(L)3.0–3.5 V (R)3.0–3.5 V	60–90	160	52	12	31	The dexterity of the upper extremities improved markedly
	40/M	NA	Dysarthria and oromandibular dyskinesia, progressive violent choreic movement of all extremities, trunk spasm and head-drop	(L)3.0–3.5 V (R)3.0–3.5 V	60–90	160	50	12	36	Decreased limb movement, dysarthria and slight head-drop did not improved
2015/Lee et al. (14)	36/M	+	Slurred speech, orofacial olingual dyskinesia, biting tongue and lip, and choreiform movements of the head and neck	(L)2.9 V (R)2.3 V	60	130	59	6	36–34	Marked improvement in choreic movements, biting tongue and lip
2016/ Fernández-Pajarín et al. (15)	43/M	+	Abnormal movements of the orofacial region, upper limbs and trunk	(L)4 mA (R)4 mA	212	60	39	12	13	Marked improvement in orofacial dyskinesias and limb choreic movements

(Continued)

10.3389/fneur.2024.1377377

TABLE 2 (Continued)

Time/ Author	Age/ Sex	VPS13A mutations	Main symptoms	Current	Pluse width (μs)	Fre (Hz)	UHDR (pre-op)	Follow-up (m)	UHDRS (post-op)	Outcome
Author	Age/ Sex	VPS13A	Main Symptoms	Current	Pluse width (μs)	Fre (Hz)	UHDRS (pre-op)	Follow-up (m)	UHDRS (post-op)	Outcome
2018/Liu et al. (16)	35/M	+	Clenching and biting, dysphagia, slurred speech, involuntary head and limb	(L)2.6–3.5 mA (R)2.6–3.6 mA	70–100	150–165	62	12	18	Clinical improvement
	37/M	+	Biting, dysphagia, twitching limbs and trunk weakness and numbness of hands, myocardial infarction	(L)2.5–3.8 mA (R)2.5–3.3 mA	80–140	150–175	42	12	12	
	37/M	+	Biting, tongue involuntary movements, vocal tics, involuntary limb movements, generalized tonic–clonic seizure attack	(L)2.0–3.0 mA (R)2.0–3.0 mA	60–80	135–165	24	12	8	
	35/M	+	Biting, tongue involuntary movements involuntary limb movements, generalized tonic–clonic seizure attack	(L)2.5 mA (R)2.5 mA	90	160	22	12	8	
	36/F	+	licking lips, pouting, biting, dysphagia, chorea, gait instability	(L)2.0–2.7 mA (R)2.0–2.7 mA	90–100	150	48	12	14	Clinical improvement
	33/F	+	Biting, slurred speech, trembling legs and twitching arms, generalized tonic–clonic seizure attack	(L)0.0–1.6 mA (R)1.8–2.5 mA	60	130–145	16	12	6	
2018/Doshi et al. (17)	77/F	NA	Orofacial dyskinesias, neck dyskinesias	(L)3.0 V (R)3.0 V	90	130	36	NA	13	Dyskinesias were completely resolved
2019/Richard et al. (18)	31/M	+	Orolingual hyperkinesia, dysarthria, truncal and extremities chorea, gait instability, hyporeflexia, bradykinesia	(L)2.6 V (R)2.6 V	60	100	13	6	4	Speech, chorea and swallowing are ameliorated
2019/Wang et al. (19)	43/F	NA	Dysphagia, dysarthria, involuntary tongue protrusion, biting lip, and teeth grinding	(L)2.2 V (R)2.2 V	60	130	61	12	31	Significantly improvement in dysarthria, chorea and dyskinesia
2020/Wu et al. (20)	35/F	+	Involuntary movements of tongue, lower jaw, neck, trunk, and lower limbs, biting tongue and lip	(L)3.0 V (R)3.15 V	60	160	51	12	27	Remarkable remission in tongue biting, dysarthria, and gait abnormality
	35/M	+	Oromandibular dystonia, involuntary jaw movement, and upper limb right limb affecting handwriting.	(L)3.0 V (R)2.95 V	50	130	40	12	22	Remission of involuntary orofacial movements

NO., number; M, male; F, female; VPS13A, VPS13A mutations; Fre, frequency; Hz, hertz; NA, not available; UHDRS, unified Huntington's disease rating scale score; pre-op, pre-operative; m, month; post-op, post-operative; +, yes.

10.3389/fneur.2024.1377377

At present, ChAc disease has no specific treatment, medications (such as dopamine blockers and VMAT2 inhibitors) can improve dyskinesia or rather chorea significantly, however not all of the symptoms of ChAc respond, and there may be side effects. Therefore, it is crucial to develop effective therapeutic approaches and evaluate treatment outcomes for ChAc patients. DBS is a widely used mainstream treatment for the treatment of movement disorders (9, 32). However, due to ChAc rarity, determining DBS therapeutic efficacy and safety remains challenging. A study was conducted to compare short- and long-term DBS treatment outcomes in fifteen ChAc patients, and the study found significant improvement in both chorea and dystonia, but results for dysarthria and swallowing were mixed. Additionally, akinesia did not improve among the patients (8). It is worth noting that we found most patients experience symptomatic relief with medium to high-frequency stimulation when summarizing the previous literature (Table 2), but Li et al. (7) reported two patients whose symptoms were relieved by low-frequency 40 Hz stimulation, on the contrary, both chorea and dystonia were exacerbated by 130 Hz GPi stimulation. We also found that most patients had pulse widths between 60 and 90 μs, with only two patients exceeding 150 μs and the stimulation current was between 2.5–3.0 volt (V) in most patients and 2.0–4.0 mA in some patients. The rational choice of stimulation frequency, pulse width, and current size for DBS treatment needs more research to verify, and we hope to make the treatment of the disease by DBS more standardized in the future.

In our case, the patient exhibited significant improvement in choreiform symptoms, It greatly improved the patient's overall quality of life. To our knowledge, this is the first reported case of relief of involuntary vocalization symptoms through GPi-DBS treatment. Our patient had similar symptoms to a previously reported patient who experienced involuntary vocalizations (9). However, the patient in that report did not benefit from GPi-DBS stimulation. Fortunately, our patient responded well to the GPi-DBS treatment, with a reduction in involuntary vocalization, and movements of the trunk almost disappeared.

In conclusion, the patient's symptoms have improved with DBS, particularly chorea, involuntary vocalization, and salivation at the corners of the mouth. It is reasonable to consider DBS as a safe treatment option for ChAc patients. However, the current reports on DBS for ChAc patients are mainly derived from a limited number of case reports and some small-sample retrospective studies from around the world. Therefore, further studies are still needed to confirm its efficacy and safety. Additionally, we believe that it is necessary to conduct long-term postoperative follow-ups of ChAc patients to continuously improve the treatment program and enhance their quality of life.

Data availability statement

The datasets presented in this article are not readily available because of ethical and privacy restrictions. Requests to access the datasets should be directed to the corresponding authors.

Ethics statement

Ethical review and approval was not required for the study on human participants in accordance with the local legislation and institutional requirements. Written informed consent from the patients/participants or patients/participants' legal guardian/next of kin was not required to participate in this study in accordance with the national legislation and the institutional requirements. Written informed consent was obtained from the individual(s) for the publication of any potentially identifiable images or data included in this article.

Author contributions

YX: Investigation, Writing – original draft, Methodology. JY: Formal analysis, Methodology, Resources, Writing – original draft. YG: Data curation, Writing – original draft. QS: Conceptualization, Methodology, Resources, Writing – review & editing. HX: Methodology, Supervision, Validation, Writing – review & editing. HL: Conceptualization, Data curation, Validation, Writing – review & editing. CZ: Conceptualization, Resources, Writing – review & editing.

Funding

The author(s) declare financial support was received for the research, authorship, and/or publication of this article. The Fifth Batch of National Training Programme for Excellent Clinical Talents in Traditional Chinese Medicine (National TCM Human Education Letter [2022] no. 1); Guangdong Provincial Hospital of Traditional Chinese Medicine Famous Chinese Medicine Experts Academic Experience Inheritance Workshop Project (Second Hospital of Traditional Chinese Medicine [2014] no. 89).

Acknowledgments

Our authors deeply appreciate the editors and reviewers for their help with the manuscript.

Conflict of interest

The authors declare that the research was conducted in the absence of any commercial or financial relationships that could be construed as a potential conflict of interest.

Publisher's note

References

1. Kaestner L. Proceedings of the eleventh international meeting on Neuroacanthocytosis syndromes. *Tremor Other Hyperkinet Mov (N Y)*. (2023) 13:41. doi: 10.5334/tohm.826

2. Huang S, Zhang J, Tao M, Lv Y, Xu L, Liang Z. Two case reports of chorea-acanthocytosis and review of literature. *Eur J Med Res*. (2022) 27:22. doi: 10.1186/s40001-022-00646-7

3. Walker RH. Untangling the thorns: advances in the Neuroacanthocytosis syndromes. *J Mov Disord*. (2015) 8:41–54. doi: 10.14802/jmd.15009

4. Jung HH, Danek A, Walker RH. Neuroacanthocytosis syndromes. *Orphanet J Rare Dis*. (2011) 6:68. doi: 10.1186/1750-1172-6-68

5. Peikert K, Danek A, Hermann A. Current state of knowledge in chorea-Acanthocytosis as core Neuroacanthocytosis syndrome. *Eur J Med Genet*. (2018) 61:699–705. doi: 10.1016/j.ejmg.2017.12.007

6. Wu Y, Xu YY, Gao Y, Li JM, Liu XW, Wang MQ, et al. Deep brain stimulation for chorea-acanthocytosis: a systematic review. *Neurosurg Rev*. (2022) 45:1861–71. doi: 10.1007/s10143-022-01735-1

7. Li P, Huang R, Song W, Ji J, Burgunder JM, Wang X, et al. Deep brain stimulation of the globus pallidus internal improves symptoms of chorea-acanthocytosis. *Neurol Sci*. (2012) 33:269–74. doi: 10.1007/s10072-011-0741-y

8. Miquel M, Spampinato U, Latxague C, Aviles-Olmos I, Bader B, Bertram K, et al. Short and long term outcome of bilateral pallidal stimulation in chorea-acanthocytosis. *PLoS One*. (2013) 8:e79241. doi: 10.1371/journal.pone.0079241

9. Mulroy E, Vijiaratnam N, De Roquemaurel A, Bhatia KP, Zrinzo L, Foltynie T, et al. A practical guide to troubleshooting pallidal deep brain stimulation issues in patients with dystonia. *Parkinsonism Relat Disord*. (2021) 87:142–54. doi: 10.1016/j.parkreldis.2021.05.017

10. Garcia Ruiz PJ, Ayerbe J, Bader B, Danek A, Sainz MJ, Cabo I, et al. Deep brain stimulation in chorea acanthocytosis. *Mov Disord*. (2009) 24:1546–7. doi: 10.1002/mds.22592

11. Shin H, Ki CS, Cho AR, Lee JI, Ahn JY, Lee JH, et al. Globus pallidus interna deep brain stimulation improves chorea and functional status in a patient with chorea-acanthocytosis. *Stereotact Funct Neurosurg*. (2012) 90:273–7. doi: 10.1159/000338216

12. Kefalopoulou Z, Zrinzo L, Aviles-Olmos I, Bhatia K, Jarman P, Jahanshahi M, et al. Deep brain stimulation as a treatment for chorea-acanthocytosis. *J Neurol*. (2013) 260:303–5. doi: 10.1007/s00415-012-6714-0

13. Nakano N, Miyauchi M, Nakanishi K, Saigoh K, Mitsui Y, Kato A. Successful combination of Pallidal and thalamic stimulation for intractable involuntary movements in patients with Neuroacanthocytosis. *World Neurosurg*. (2015) 84:1177.e1–7. doi: 10.1016/j.wneu.2015.06.052

14. Lee JH, Cho WH, Cha SH, Kang DW. Globus pallidus interna deep brain stimulation for chorea-acanthocytosis. *J Korean Neurosurg Soc*. (2015) 57:143–6. doi: 10.3340/jkns.2015.57.2.143

15. Fernández-Pajarín G, Sesar A, Ares B, Jiménez-Martín I, Blanco-Arias P, Corredera E, et al. Deep brain bilateral pallidal stimulation in chorea-acanthocytosis caused by a homozygous VPS13A mutation. *Eur J Neurol*. (2016) 23:e4–5. doi: 10.1111/ene.12833

16. Liu Z, Liu Y, Wan X, Yang Y, Wang L, Dou W, et al. Pallidal deep brain stimulation in patients with chorea-Acanthocytosis. *Neuromodulation*. (2018) 21:741–7. doi: 10.1111/ner.12763

17. Doshi P, Chamankar N. Globus pallidus internal deep-brain stimulation in a patient with Neuroacanthocytosis with drug-induced parkinsonism. *Stereotact Funct Neurosurg*. (2018) 96:276. doi: 10.1159/000492234

18. Richard A, Hsu J, Baum P, Alterman R, Simon DK. Efficacy of deep brain stimulation in a patient with genetically confirmed chorea-Acanthocytosis. *Case Rep Neurol*. (2019) 11:199–204. doi: 10.1159/000500951

19. Wang KL, Hess CW, Xu D, Zhang JG, Hu W, Meng FG. High frequency bilateral Globus pallidus Interna deep brain stimulation can improve both chorea and dysarthria in chorea-acanthocytosis. *Parkinsonism Relat Disord*. (2019) 62:248–50. doi: 10.1016/j.parkreldis.2019.01.008

20. Wu Y, Li H, Zhang C, Sun B, Li D, Wu Y. Subthalamic nucleus deep brain stimulation in two siblings with chorea-acanthocytosis. *Neurol Sci*. (2020) 41:1623–5. doi: 10.1007/s10072-020-04246-3

21. Wihl G, Volkmann J, Allert N, Lehrke R, Sturm V, Freund HJ. Deep brain stimulation of the internal pallidum did not improve chorea in a patient with neuro-acanthocytosis. *Mov Disord*. (2001) 16:572–5. doi: 10.1002/mds.1109

22. Rubio JP, Danek A, Stone C, Chalmers R, Wood N, Verellen C, et al. Chorea-acanthocytosis: genetic linkage to chromosome 9q21. *Am J Hum Genet*. (1997) 61:899–908. doi: 10.1086/514876

23. Walker RH, Peikert K, Jung HH, Hermann A, Danek A. Neuroacanthocytosis syndromes: the clinical perspective. *Contact (Thousand Oaks)*. (2023) 6:25152564231210339. doi: 10.1177/25152564231210339

24. Roulis E, Hyland C, Flower R, Gassner C, Jung HH, Frey BM. Molecular basis and clinical overview of McLeod syndrome compared with other Neuroacanthocytosis syndromes: a review. *JAMA Neurol*. (2018) 75:1554–62. doi: 10.1001/jamaneurol.2018.2166

25. Quick S, Heidrich FM, Winkler MV, Winkler AH, Ibrahim K, Linke A, et al. Cardiac manifestation is evident in chorea-acanthocytosis but different from McLeod syndrome. *Parkinsonism Relat Disord*. (2021) 88:90–5. doi: 10.1016/j.parkreldis.2021.05.015

26. Ampoldi L, Danek A, Monaco AP. Clinical features and molecular bases of neuroacanthocytosis. *J Mol Med (Berl)*. (2002) 80:475–91. doi: 10.1007/s00109-002-0349-z

27. Walker RH, Danek A. "Neuroacanthocytosis"—overdue for a taxonomic update. *Tremor Other Hyperkinet Mov (N Y)*. (2021) 11:1. doi: 10.5334/tohm.583

28. Liu J, Bader B, Danek A. Neuroacanthocytosis in China: a review of published reports. *Tremor Other Hyperkinet Mov (N Y)*. (2014) 4:248. doi: 10.5334/tohm.226

29. Burbaud P, Rougier A, Ferrer X, Guehl D, Cuny E, Arne P, et al. Improvement of severe trunk spasms by bilateral high-frequency stimulation of the motor thalamus in a patient with chorea-acanthocytosis. *Mov Disord*. (2002) 17:204–7. doi: 10.1002/mds.1260

30. Bader B, Walker RH, Vogel M, Prosiegel M, McIntosh J, Danek A. Tongue protrusion and feeding dystonia: a hallmark of chorea-acanthocytosis. *Mov Disord*. (2010) 25:127–9. doi: 10.1002/mds.22863

31. Reichel F, Kräter M, Peikert K, Glaß H, Rosendahl P, Herbig M, et al. Changes in blood cell deformability in chorea-Acanthocytosis and effects of treatment with Dasatinib or Lithium. *Front Physiol*. (2022) 13:852946. doi: 10.3389/fphys.2022.852946

32. Starr PA, Vitek JL, Bakay RA. Deep brain stimulation for movement disorders. *Neurosurg Clin N Am*. (1998) 9:381–402. doi: 10.1016/S1042-3680(18)30273-0

frontiers | Frontiers in Genetics

TYPE Case Report
PUBLISHED 21 August 2024
DOI 10.3389/fgene.2024.1421952

OPEN ACCESS

EDITED BY
Xiaoling Xuei,
Indiana University School of Medicine,
United States

REVIEWED BY
Diou Luo,
Iowa State University, United States
Ruth Walker,
United States Department of Veterans Affairs,
United States
Adrian Danek,
Ludwig Maximilian University of Munich,
Germany

*CORRESPONDENCE
Sarah Wiethoff,
sarah.wiethoff@ukmuenster.de

RECEIVED 23 April 2024
ACCEPTED 30 July 2024
PUBLISHED 21 August 2024

CITATION
Dambietz CA, Doescher A, Heming M, Schirmacher A, Schlüter B, Schulte-Mecklenbeck A, Thomas C, Wiendl H, Meyer zu Hörste G and Wiethoff S (2024) Case report: Clinical, genetic and immunological characterization of a novel *XK* variant in a patient with McLeod syndrome.
Front. Genet. 15:1421952.
doi: 10.3389/fgene.2024.1421952

Case report: Clinical, genetic and immunological characterization of a novel *XK* variant in a patient with McLeod syndrome

Christine Anna Dambietz[1], Andrea Doescher[2], Michael Heming[1], Anja Schirmacher[3], Bernhard Schlüter[3], Andrea Schulte-Mecklenbeck[1], Christian Thomas[4], Heinz Wiendl[1], Gerd Meyer zu Hörste[1] and Sarah Wiethoff[1]*

[1]Department of Neurology with Institute of Translational Neurology, University Hospital Münster, Münster, Germany, [2]DRK Blutspendedienst NSTOB, Institute Bremen-Oldenburg, Springe, Germany, [3]Central Laboratory, University Hospital Münster, Münster, Germany, [4]Institute of Neuropathology, University Hospital Münster and University of Münster, Münster, Germany

Introduction: Pathogenic variants in the *XK* gene are associated with dysfunction or loss of XK protein leading to McLeod syndrome (MLS), a rare X-linked neuroacanthocytosis syndrome with multisystemic manifestation. Here we present clinical, genetic and immunological data on a patient originally admitted to our clinic for presumed post-COVID-19 syndrome, where thorough clinical work-up revealed a novel frameshift deletion in *XK* causal for the underlying phenotype. We additionally review the clinicogenetic spectrum of reported McLeod cases in the literature.

Methods: We performed in-depth clinical characterization and flow cytometry of cerebrospinal fluid (CSF) in a patient where multi-gene panel sequencing identified a novel hemizygous frameshift deletion in *XK*. Additionally, Kell (K) and Cellano (k) antigen expression was analysed by Fluorescence-activated Cell Sorting (FACS). *KEL* gene expression was examined by RNA sequencing.

Results: A novel hemizygous frameshift deletion in the *XK* gene resulting in premature termination of the amino acid chain was identified in a 46-year old male presenting with decrease in physical performance and persisting fatigue after COVID-19 infection. Examinations showed raised creatine kinase (CK) levels, neuropathy and clinical features of myopathy. FACS revealed the K-k+ blood type and reduced Cellano density. CSF flow cytometry showed elevation of activated T Cells.

Abbreviations: ACMG, American College of Medical Genetics and Genomics; cDNA, Complementary desoxyribonucleic acid; CK, Creatine kinase; CNS, Central nervous system; COS cells, *CV-1 in origin carrying SV40* cells; COVID-19, Coronavirus disease 2019; CSF, Cerebrospinal fluid; Cys, Cysteine; ER. Endoplasmic reticulum; FACS, Fluorescence-activated Cell Sorting; Gly, Glycine; GOT, Glutamic oxaloacetic transaminase; Ig, Immunoglobulin; K, Kell antigen; k, Cellano antigen; LDH, Lactate dehydrogenase; MRI, Magnetic resonance imaging; MUP, Motor unit action potential; NK, Natural killer cell; PCR, Polymerase chain reaction; RBC, Red blood cell; Rh, Rhesus; RNA, Ribonucleic acid; SARS-CoV-2, Severe acute respiratory syndrome coronavirus type 2; STIR, Short Tau Inversion Recovery sequence; Trp, Tyrptophane; U/l, Unit per liter

Conclusion: In-depth clinical, genetic, immunological and ribonucleic acid (RNA) expression data revealed axonal neuropathy, myopathy and raised levels of activated CSF-T-lymphocytes in a patient with a previously unpublished frameshift deletion in the *XK* gene.

KEYWORDS

***XK* gene, McLeod syndrome, neuropathy, myopathy, Kell system, neurogenetic disease, intrathecal immunity, flow cytometry**

Introduction

Pathogenic variants in the *XK* gene are associated with MLS, a rare X-linked neuroacanthocytosis syndrome affecting mainly males (Roulis et al., 2018). Mainly private pathogenic variants (small deletions, frameshift variants, missense variants and insertions) have been identified in *XK* (Jung et al., 2004) as well as extended deletions spanning beyond the *XK* gene (Roulis et al., 2018). The *XK* gene, located in the Xp21.1 region of the X-chromosome, codes for the transmembrane XK protein which forms a heterodimer with the Kell protein (Figure 1A). It is known to express the antigen Kx on red blood cells (RBCs) and support the expression of Kell protein antigens. Recent evidence suggests XK forming a complex with chorein/*VPS13A*, a likely hint for shared pathophysiological mechanisms in clinical resemblance of MLS and *VPS13A* disease (chorea acanthocytosis) (Peikert et al., 2022). Identified genetic changes in *XK* result in dysfunction or loss of the XK protein which is associated with changes in skeletal structure of different cells, e.g., erythrocytes (Ballas et al., 1990; Lee et al., 1991; Terada et al., 1999). Clinical findings associated with *XK* variants comprise a multisystemic spectrum disorder including acanthocytosis, haemolysis, anaemia, spleno- and hepatomegaly, cardiomyopathy, myopathy, neuropathy, dystonia, choreatic movement disorders as well as neuropsychiatric disorders and cognitive decline. Symptoms usually manifest in males around their fourth decade and progress slowly. Females can rarely be affected, generally displaying a milder phenotype (Danek et al., 2001; Roulis et al., 2018).

In this case report we present the clinical, genetic and immunological characterization of a patient with a yet unpublished, but pathogenic deletion in *XK*. We display the restriction of Kell antigen expression resulting from the identified deletion to support its pathogenicity, and we review 44 further cases identified from the literature with multisystemic MLS adding to a better understanding of this rare disease with variable phenotypic presentation.

Methods

Molecular genetic analysis

Genetic analysis of blood was performed using a customised myopathy multi-gene panel [Twist Version one analysed with varvis® (version 1.19)] covering candidate genes for myopathy and muscular dystrophy. Evaluation of results, clinicogenetic correlation and classification of variants followed the four eyes principle and *American College of Medical Genetics and Genomics* (ACMG) guidelines.

Fluorescence-activated Cell Sorting (FACS) and flow cytometry

To analyse expression of Kell protein antigens Kell (K, K1) and Cellano (k, K2) on RBCs, FACS analysis of whole blood was performed with anti-K and anti-k antibodies. Additional flow cytometry of cerebrospinal fluid (CSF) was performed to analyse the subcomposition of cells in the CSF.

Rh flow cytometry

Additional FACS was performed to analyse the expression of Kell protein antigens Kell (K) and Cellano (k) on RBCs.

Gene expression analysis

Analysis of *KEL* gene expression was performed by real-time polymerase chain reaction (real-time PCR) using a validated expression assay (TaqMan™ Gene Expression Assay) with specific primers and StepOne™T software (version 2.2.2. Applied Biosystems 2011) for RNA quantification analysis. Detailed methods including primer sequences and a list of genes included in the myopathy multi gene panel can be found in Supplementary Data S1.

Case description

A 46-year old male patient presented to the neurology department of the University Hospital Münster with muscular weakness, decreasing physical performance and exercise intolerance following mild coronavirus disease 19 (COVID-19). Prior to presentation, physical examination, laboratory tests, electrocardiogram, echocardiography, body plethysmography, lung diffusion testing and chest X-ray had been performed and gave no evidence of cardiac or pulmonary dysfunction. Laboratory results showed elevated creatine kinase (CK), transaminases and positive Severe acute respiratory syndrome coronavirus type 2 (SARS-COV-2) immunoglobulins of class M and G (IgM and IgG). A cardiac magnetic resonance imaging (MRI) showed no signs indicative of post-COVID-19 myocarditis, displaying a regular sized left ventricle with mild septal hypertrophy and normal cardiac output. The patient reported to not have noticed any kind of muscular weakness, myalgia, stiffness or muscular atrophy prior to COVID-19 infection. However, elevated CK (up to 2,500 U/l) had been noted on routine blood screens

10.3389/fgene.2024.1421952

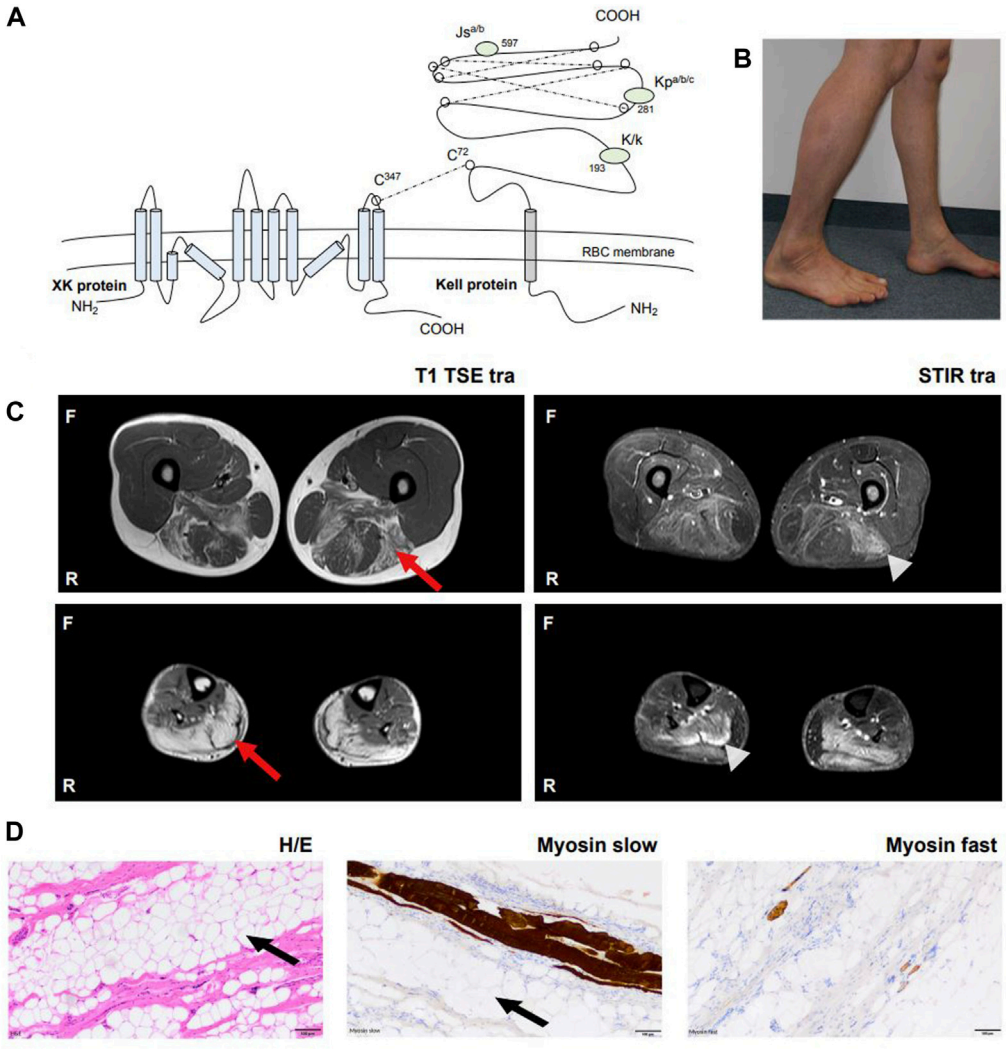

FIGURE 1
Overview of *XK* pathophysiology and clinical manifestation in our patient. **(A)** The *XK* gene codes for the XK protein which consists of ten transmembrane domains and forms a heterodimer with the Kell protein via a disulfide bond (Cys^{347}_{XK} – Cys^{72}_{Kell}). The XK protein is expressed in many tissues, including RBCs, bone marrow, brain and other neuronal tissues. The *KEL* gene codes for the Kell protein, which is a glycoprotein of 732 amino acids. The Kell protein is expressed on RBCs, bone marrow, testes and fetal liver. The protein expresses 25 antigens, the best known Kell blood group antigens are Kell (K) and Cellano (k) located at amino acid position 193, Kp at amino acid position 281 and Js at amino acid position 597. **(B)** Photograph. The patient's lower legs with dominant atrophy of the left gastrocnemius muscle. **(C)** Whole body muscle MRI. Bilateral fatty oedematous atrophy of adductors, hamstring muscles and calves with T1 hyperintensity (red arrow). Hyperintensity in STIR sequences revealed recent oedema in the above muscles (light grey arrowhead). Muscles in other parts of the body were not affected. **(D)** Histological examination after biopsy of the left gastrocnemius muscle with hematoxylin and eosin staining, myosin slow and myosin fast staining revealed severe atrophy of skeletal muscle with vacant fat (black arrow) and surplus of connective tissue, but without signs of inflammation, rimmed vacuoles or ragged red fibers. No other specific structural or immunohistochemical abnormalities were detected. Abbreviations: Cys, cysteine; MRI, Magnetic resonance imaging; F, front; H/E, hematoxylin eosin staining; R, righthand side; RBCs, red blood cells; STIR, Short Tau Inversion Recovery sequence.

before but had not triggered neurological or further work-up. The patient reported muscular weakness most pronounced in legs and feet upon low physical exertion persisting after his COVID-19 disease. There was no myalgia at rest, during or after exercise. Medical history included allergic rhinoconjunctivitis and restless legs syndrome (RLS) and there was no intake of regular medication or known substance abuse. The diagnosis of RLS has been made about 20 years ago. The patient reported an urge to move his legs especially in the evening and at night with occasional sleep disturbance and alleviation upon movement. Symptomatic therapy has not been necessary according to our patient. Other unintended movement disorders throughout daytime or sleep disorders have not been reported or observed by our patient. Regarding the precise description of the patient's complaints, all obligatory criteria are fulfilled to make a diagnosis of RLS (referring to the International RLS Study Group). We did not interpret his RLS as prodromal chorea. There was no family history for neuromuscular/neurological diseases. The mother of the patient had difficulties walking. She had a long-known spinal stenosis, but clinical examination showed normal reflex status, no muscle wasting, no fasciculation and no pareses. The neurological examination of our patient revealed slight

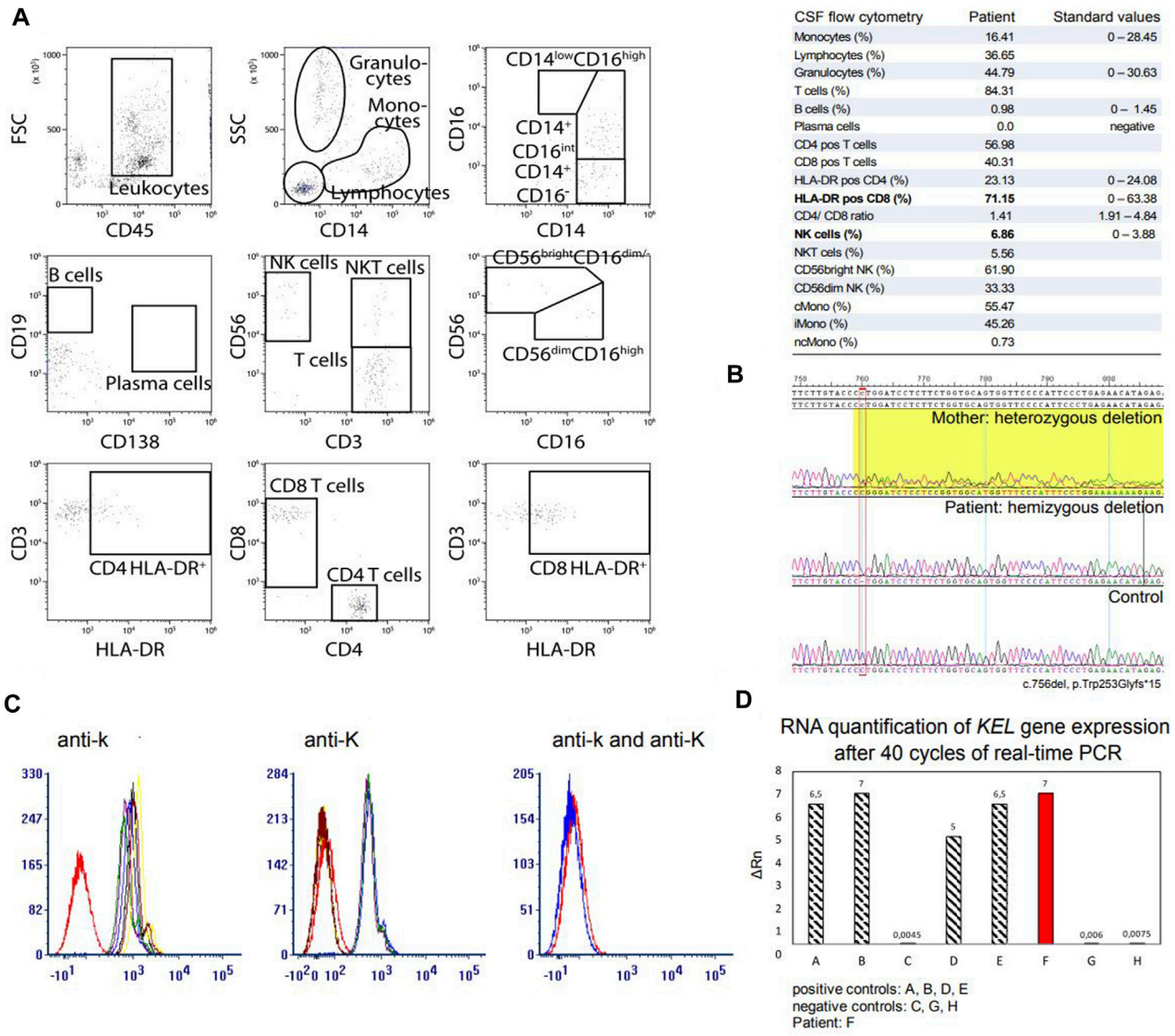

CSF flow cytometry	Patient	Standard values
Monocytes (%)	16.41	0 – 28.45
Lymphocytes (%)	36.65	
Granulocytes (%)	44.79	0 – 30.63
T cells (%)	84.31	
B cells (%)	0.98	0 – 1.45
Plasma cells	0.0	negative
CD4 pos T cells	56.98	
CD8 pos T cells	40.31	
HLA-DR pos CD4 (%)	23.13	0 – 24.08
HLA-DR pos CD8 (%)	**71.15**	0 – 63.38
CD4/ CD8 ratio	1.41	1.91 – 4.84
NK cells (%)	**6.86**	0 – 3.88
NKT cels (%)	5.56	
CD56bright NK (%)	61.90	
CD56dim NK (%)	33.33	
cMono (%)	55.47	
iMono (%)	45.26	
ncMono (%)	0.73	

FIGURE 2
CSF flow cytometry analysis, molecular genetic analysis and *KEL* gene expression analysis in our patient. **(A)** CSF flow cytometry. Flow cytometry analysis of the patient's CSF revealed elevation of HLA-DR+CD8+ T cells with a CD4/CD8 ratio of 1.4 and elevation of NKs. **(B)** Sanger sequencing of the *XK* gene revealed a novel deletion at position 756, resulting in a frameshift deletion and a premature termination of the amino acid chain (exon 3; c.756del, p.Trp253Glyfs*15). Segregation analysis in the mother revealed that they carry the same *XK* deletion. **(C)** Fluorescence-activated Cell Sorting was performed to analyse the expression of Kell antigens Kell (K) and Cellano (k) on erythrocytes. Five samples of fresh EDTA and two samples of RBCs were detected with antibodies (a) anti-k and (b) anti-K. Our patient is marked in red. (c) Presentation of the Kell antigens Cellano (k) and Kell (K) in our patient. **(D)** *KEL* gene expression assay. Real-time PCR was performed using the TaqMan Gene Expression Assay. Our patient with the novel *XK* deletion (F) showed no restriction in expression of the *KEL* gene on RNA level. Abbreviations: CD56^{bright} NK, CD56^{bright} natural killer cells; CD56^{dim} NK, CD56^{dim} natural killer cells; cMono, classical monocytes; CSF, cerebrospinal fluid; del, deletion; EDTA, Ethylenediaminetetraacetic acid; Gly, glycine; HLA-DR pos, activated cells; iMono, intermediate monocytes; ncMono, non-classical monocytes; NK, natural killer cells; NKT, natural killer T cells; PCR, polymerase chain reaction; RBCs, red blood cells; RNA, ribonucleic acid; Trp, tryptophane.

weakness in abduction of the right hip (4/5), in dorsal extension and plantar flexion of both feet (4/5) and atrophy of the left calf muscle with regular muscle strength in the upper limbs. Figure 1B shows difference in calf circumference with a slimmer left lower leg and atrophy of the gastrocnemius muscle. No permanent sensory deficits were reported and clinical examination revealed mild reduction of vibration sense in the right lower leg (3/8 right malleolus, 4/8 right knee) while deep tendon reflexes were intact. Cranial nerve status and speech were normal. A *flexible endoscopic evaluation of swallowing* assessment was normal with no signs of dysphagia. Gait testing revealed Trendelenburg sign on the right side and walking on tiptoes and heels was impeded. Balance was intact and no involuntary movement disorders were observed. There were no signs of formal or content-related cognitive abnormalities and a neuropsychological screening revealed unsuspicious results regarding common screening instruments (*Bayer Activities of Daily Living Scale* B-ADL (1,16), *Hospital Anxiety and Depression Scale* HADS-D (anxiety: 7, depression: 1), *Montreal Cognitive Assessment* MoCa (29/30), *Symbol Digit Modalities test* SDMT (58). Laboratory results

showed elevation of CK at all different time points of consultation (max. 4,163 U/l; reference: <174 U/l), Glutamic oxaloacetic transaminase (GOT) (max. 138 U/l; reference: 10–50 U/l) and lactate dehydrogenase (LDH) (max. 590 U/l; reference: 135–225 U/l) which prompted further diagnostic work-up with regards to myopathy and muscular dystrophies. GOT and LDH can be co-elevated in muscular dystrophies but can also be elevated in primary cardiac and hepatic diseases and can hint towards early stages of cardiomyopathy or hepatopathy respectively. Interestingly, anti-PM-Scl100 antibodies were detected in a specific myositis panel. Other antinuclear antibodies, antineutrophil cytoplasmic antibodies and rheumatoid factors were negative. Blood group profile revealed blood group type A, Rhesus D positivity (CcD.Ee) and K-k+ (kk) type. Further immunohaematological characterization was not possible due to technical and logistical reasons at time of manuscript publication but is scheduled in due course. Whole body muscle MRI showed bilateral fatty and oedematous atrophy of adductors, hamstrings and both calves (Figure 1C). MRI of the lumbar spine showed multisegmental degeneration with spinal narrowing at L3/4 and L4/5 but no significant neural foraminal constrictions or myelopathy (Supplementary Figure S1A). Electrophysiological investigations revealed axonal polyneuropathy with motor and sensory involvement, fasciculations and pathological spontaneous activity but formally normal motor unit action potentials (MUPs) in left vastus muscle, left tibial anterior muscle and left gastrocnemius muscle. Evoked potentials indicated an afferent sensory disorder of the left arm and both legs. Biopsy of the right gastrocnemius muscle showed severe atrophy of skeletal muscle without signs of inflammation, rimmed vacuoles or ragged red fibres. No other specific structural or immunohistochemical abnormalities were detected (Figure 1D). Lumbar puncture was performed after first admission at our department (10 months after the patient's COVID-19 disease). CSF standard analysis showed no abnormalities in total cell count or protein and no intrathecal immunoglobulin synthesis. CSF flow cytometry revealed a slight elevation of HLA-DR $CD4^+$ (27.8%, reference <24%) and HLA-DR $CD8^+$ cells (75.5%, reference <63,4%), a CD4/CD8 ratio of 1.4 and an elevation of natural killer cells (NKs) (5,8%) (Figure 2A). Multi-gene panel sequencing including common candidate genes for myopathy or muscular dystrophy revealed a novel hemizygous deletion (c.756del, p.Trp253Glyfs*15) of the *XK* gene (Figure 2B). In order to examine its impact, we performed FACS analysis of blood which revealed negativity for Kell (K) and a reduced density of Cellano (k) antigen on the patient's erythrocytes in comparison to healthy controls (Figure 2C). Real-time PCR revealed no restriction of *KEL* gene expression in our patient (Figure 2D). For an overview of clinical work-up of our patient, please see Supplementary Figure 1B.

Discussion

Here, we present a case of MLS with a novel deletion in the *XK* gene.

Dominant features at presentation were raised CK, muscular weakness and atrophy, decreasing physical performance and exercise intolerance which the patient had only noted after COVID-19 disease. However, thorough work-up revealed longer-standing changes including neuropathy, muscle atrophy with fatty involution and raised CK, indicating longer-standing neuropathy and myopathy most likely due to the underlying genetic defect in the *XK* gene. Routine myositis screening revealed positive anti-PM-Scl100 antibodies which can be associated with overlapping polymyositis, scleroderma (Reichlin et al., 1984; Mahler M et al., 2005) or other autoimmune diseases (Lackner et al., 2020) and had triggered muscle biopsy for exclusion of myositis prior to the genetic diagnostic work-up. In light of absence of other antibody-positivity and changes indicative for inflammatory muscle disease in MRI and muscle histopathology, we interpreted these antibody findings as false positive/non-specific.

The identified novel deletion in *XK* leads to a frameshift and exchange of tryptophan (Trp) to glycine (Gly) at position number 253, resulting in a premature termination of the amino acid chain. The identified change is highly conserved, rare and has not yet been reported in the literature. Segregation analysis revealed the same deletion in the patient's mother, identifying her as heterozygous carrier.

In order to analyse potential pathogenicity of the novel deletion we performed FACS which revealed reduced expression of k antigen in our patient compared to healthy controls. Negativity for the Kell (K) antigen has been shown to not be related to *XK* variation versus wildtype (Allen et al., 1961) but is most common in the overall population (92.5%) (Ristovska et al., 2022). We then investigated whether the *KEL* gene expression was diminished on RNA level. Real-time PCR showed no restriction of *KEL* specific RNA, indicating that the downregulation of Kell antigen expression associated with the identified *XK* deletion must be impeded in a later step of protein or antigen presentation. Russo *et al.* identified the assembly and transfer mechanisms of Kell and XK protein in an *in vivo* system (Russo et al., 1998). Physiologically, Kell and XK protein occur as a dimer complex, linked by a disulphide bond between cysteine (Cys) molecules, Kell Cys^{72} and XK Cys^{347}, which is formed in the endoplasmic reticulum (ER) (Russo et al., 1998; Russo et al., 1999). It is unknown whether pathogenic variants in *XK* impact on the formation or stability of this disulphide bond. After assembly in the ER, the complex is transferred to the cell's membrane and the Golgi compartment. The transport and expression of recombinant Kell and XK protein in *CV-1 in origin carrying SV40* (COS) cells in *in vivo* experiments appeared to be independent of the other protein (Russo et al., 1999), but clinical reports have shown that Kell protein expression and Kell antigen presentation are significantly diminished in patients with defect or loss of the XK protein. Intracellular proteins or enzymes that are involved in Kell/XK complex formation, transport and presentation on erythrocytes' membranes have not been identified yet. It hence remains of great interest to further analyse intracellular processes and identify differences in patients with physiologically intact XK protein and in patients with pathogenic *XK* gene changes.

Exacerbation or, as in our case, subjective onset of clinical symptoms after infection (as in this case SARS-CoV-2) has to our knowledge not been investigated before in patients with MLS. For our patient, the onset of initially unspecific symptoms such as fatigue, decrease of physical performance and perception of unspecific muscle weakness was subjectively referred to COVID-19

disease. Consequently, he was admitted under presumption of post-COVID-19 syndrome. He hence underwent thorough diagnostic work-up, including examination of CSF where routine parameters revealed no abnormalities. However, CSF flow cytometry revealed elevation of HLA-DR$^+$CD4$^+$ and HLA-DR$^+$CD8$^+$ cells and elevation of NKs. HLA-DR$^+$CD4$^+$ and HLA-DR$^+$CD8$^+$ cells represent activation of T-lymphocytes in the central nervous system (CNS). Activated lymphocytes and NKs in the CSF are associated with immunological processes and have been found in autoimmune and inflammatory CNS diseases (Strunk et al., 2018; Gross et al., 2021). Here, the finding of elevated activated T cells and NKs indicate an immune-cell-mediated response in the CNS which *might* trigger a greater susceptibility to perception of muscular weakness and reduced physical strength after COVID-19 disease that then led to subjective notification of first symptoms of *XK*-disease in our patient. However, further analyses including CSF flow cytometry in patients with pathogenic variants in *XK* with or without prior SARS-CoV-2 infection are warranted.

Our patient displayed clinically dominating muscular weakness and neuropathy with lack of acanthocytosis, hepatopathy, cardiomyopathy or cognitive and psychiatric impairment to date. We hence wondered whether the location of the reported deletion correlates with specific clinical symptoms and if pathogenic changes in close proximity to the herein identified novel deletion might show clinical resemblance. Therefore, we performed a systematic analysis of patients reported in the literature with pathogenic *XK* gene changes, including nucleotide changes, insertions, deletions and gross deletions of *XK* gene. We enquired PubMed searching for the following keywords: *XK*, McLeod syndrome, gene variants/changes, deletion, insertion, missense mutation; as well as cited manuscripts in the respective publications. We only included patients where sufficient clinical/phenotypic data was available for clinicogenetic correlation which left us with 44 cases amenable to our analysis. Supplementary Table S1 gives an overview of the observed *XK* variants and their clinical manifestation. The spectrum of respective clinical symptoms could not be assigned to a specific type or localization of reported variants only. However, patients with pathogenic variants in exon 3 and in close proximity to the novel deletion of our patient (c.756del, p.Trp253Glyfs*15) did manifest with neuropathy and myopathy, frequently displaying areflexia, elevated CK and acanthocytosis without hepatopathy or cardiomyopathy. Neuropsychiatric symptoms and movement disorders were variably present in a subset of these.

As previously reported in the literature, symptoms may manifest successively over time and it cannot be ruled out that cognitive decline, a movement disorder or acanthocytosis might appear over time in our patient, strengthening the importance of follow-up exams in rare neurogenetic conditions. Informing and explaining the diagnosis of *XK* disease to our patient, we called his attention to possible manifestation of further neurological symptoms in the future, the risk of transfusion reactions and multi-systemic manifestation such as cardiomyopathy. Following our patient up, we will focus on his motor and sensory functions, possible emergence of movement disorders and his cognitive and emotional state. Additionally, cardiac MRI showed mild septal hypertrophy in our patient and cardiomyopathy can be a prominent feature of MLS, thus cardiac follow-up examination and practice management will be of high importance as well as proactive information and avoidance of potential elevated risk of transfusion reactions in this disease.

Conclusion

Here, we report a novel deletion in *XK* in a patient with elevated creatine kinase, signs of myopathy and neuropathy as well as raised levels of activated T-lymphocytes in CSF. We performed a clinicogenetic review of a selection of reported genetically confirmed MLS cases in the literature and confirmed the broad multisystemic, but individually variable phenotypic presentation that cannot be predicted by location or type of genetic variant alone. We showed that the *XK* deletion in our patient results in diminished expression of the Kell blood group antigen Cellano (k), however, real-time PCR revealed no restriction of *KEL* gene expression on RNA level. It remains of great interest to identify the exact pathogenic mechanisms of Kell blood group antigen expression in the presence of XK protein and the impact of pathogenic *XK* gene variation leading to clinical manifestation in future studies of this rare disease.

Data availability statement

The datasets presented in this study can be found in online repositories. The names of the repository/repositories and accession number(s) can be found in the article/Supplementary Material.

Ethics statement

Ethical approval was not required for the studies involving humans because this study was performed according to the local ethics policies and in line with the Declaration of Helsinki. The studies were conducted in accordance with the local legislation and institutional requirements. The participants provided their written informed consent to participate in this study. Written informed consent was obtained from the individual(s) for the publication of any potentially identifiable images or data included in this article.

Author contributions

CD: Data curation, Investigation, Resources, Visualization, Writing–original draft, Conceptualization. AD: Formal Analysis, Methodology, Writing–review and editing, Investigation. MH: Data curation, Software, Writing–review and editing. AS: Formal Analysis, Investigation, Methodology, Writing–review and editing. BS: Supervision, Validation, Writing–review and editing, Data curation. AS-M: Data curation, Formal Analysis, Validation, Writing–review and editing. CT: Formal Analysis, Investigation, Writing–review and editing, Validation. HW: Supervision, Validation, Writing–review and editing. GM: Conceptualization, Project administration, Resources, Supervision, Validation, Writing–review and editing. SW: Conceptualization, Project

administration, Resources, Supervision, Validation, Writing–original draft, Writing–review and editing, Visualization.

Funding

The author(s) declare that no financial support was received for the research, authorship, and/or publication of this article.

Acknowledgments

We thank our patient (and his mother) for participating in this case report.

Conflict of interest

The authors declare that the research was conducted in the absence of any commercial or financial relationships that could be construed as a potential conflict of interest.

Publisher's note

Supplementary material

The Supplementary Material for this article can be found online at: https://www.frontiersin.org/articles/10.3389/fgene.2024.1421952/full#supplementary-material

SUPPLEMENTARY FIGURE S1
Diagnostic work-up of our patient. **(A)** MRI of lumbar spine. Multisegmental degeneration with spinal narrowing at L3/4 and L4/5 (white arrow) without significant neural foraminal constrictions or myelopathy. Abbreviations: CK, creatine kinase; MRI, magnetic resonance imaging. **(B)** Timeline of the diagnostic work-up of our patient.

References

Allen, F. H., Jr., Krabbe, S. M., and Corcoran, P. A. (1961). A new phenotype (McLeod) in the Kell blood-group system. *Vox Sang.* 6, 555–560. doi:10.1111/j.1423-0410.1961.tb03203.x

Ballas, S. K., Bator, S. M., Aubuchon, J. P., Marsh, W. L., Sharp, D. E., and Toy, E. M. (1990). Abnormal membrane physical properties of red cells in McLeod syndrome. *Transfusion* 30 (8), 722–727. doi:10.1046/j.1537-2995.1990.30891020333.x

Danek, A., Rubio, J. P., Rampoldi, L., Ho, M., Dobson-Stone, C., Tison, F., et al. (2001). McLeod neuroacanthocytosis: genotype and phenotype. *Ann. Neurol.* 50 (6), 755–764. doi:10.1002/ana.10035

Gross, C. C., Schulte-Mecklenbeck, A., Madireddy, L., Pawlitzki, M., Strippel, C., Räuber, S., et al. (2021). Classification of neurological diseases using multi-dimensional CSF analysis. *Brain* 144 (9), 2625–2634. doi:10.1093/brain/awab147

Jung, H. H., Danek, A., Walker, R. H., Frey, B. M., and Peikert, K. (2004). "McLeod neuroacanthocytosis syndrome," in *GeneReviews®*. Editors M. P. Adam, J. Feldman, G. M. Mirzaa, R. A. Pagon, S. E. Wallace, L. J. H. Bean, et al. (Seattle (WA): University of Washington, Seattle), 1993–2024.

Lackner, A., Tiefenthaler, V., Mirzayeva, J., Posch, F., Rossmann, C., Kastrati, K., et al. (2020). The use and diagnostic value of testing myositis-specific and myositis-associated autoantibodies by line immuno-assay: a retrospective study. *Ther. Adv. Musculoskelet. Dis.* 12, 1759720X20975907. doi:10.1177/1759720X20975907

Lee, S., Zambas, E. D., Marsh, W. L., and Redman, C. M. (1991). Molecular cloning and primary structure of Kell blood group protein. *Proc. Natl. Acad. Sci. U. S. A.* 88 (14), 6353–6357. doi:10.1073/pnas.88.14.6353

Mahler M, R. R., Dähnrich, C., Blüthner, M., and Fritzler, M. J. (2005). Clinical evaluation of autoantibodies to a novel PM/scl peptide antigen. *Arthritis Res. Ther.* 7 (3), R704–R713. doi:10.1186/ar1729

Peikert, K., Hermann, A., and Danek, A. (2022). XK-associated McLeod syndrome: nonhematological manifestations and relation to VPS13A disease. *Transfus. Med. Hemother* 49 (1), 4–12. doi:10.1159/000521417

Reichlin, M. M. P., Targoff, I., Bunch, T., Arnett, F., Sharp, G., Treadwell, E., et al. (1984). Antibodies to a nuclear/nucleolar antigen in patients with polymyositis overlap syndromes. *J. Clin. Immunol.* 4 (1), 40–44. doi:10.1007/BF00915286

Ristovska, E., Bojadjieva, T. M., Velkova, E., Dimceva, A. H., Todorovski, B., Tashkovska, M., et al. (2022). Rare blood groups in ABO, Rh, Kell systems - biological and clinical significance. *Pril. Makedon. Akad. Nauk. Umet. Odd. Med. Nauki* 43 (2), 77–87. doi:10.2478/prilozi-2022-0021

Roulis, E., Hyland, C., Flower, R., Gassner, C., Jung, H. H., and Frey, B. M. (2018). Molecular basis and clinical overview of McLeod syndrome compared with other neuroacanthocytosis syndromes: a review. *JAMA Neurol.* 75 (12), 1554–1562. doi:10.1001/jamaneurol.2018.2166

Russo, D., Lee, S., and Redman, C. (1999). Intracellular assembly of Kell and XK blood group proteins. *Biochim. Biophys. Acta* 1461 (1), 10–18. doi:10.1016/s0005-2736(99)00148-0

Russo, D., Redman, C., and Lee, S. (1998). Association of XK and Kell blood group proteins. *J. Biol. Chem.* 273 (22), 13950–13956. doi:10.1074/jbc.273.22.13950

Strunk, D., Schulte-Mecklenbeck, A., Golombeck, K. S., Meyer Zu Hörste, G., Melzer, N., Beuker, C., et al. (2018). Immune cell profiling in the cerebrospinal fluid of patients with primary angiitis of the central nervous system reflects the heterogeneity of the disease. *J. Neuroimmunol.* 321, 109–116. doi:10.1016/j.jneuroim.2018.06.004

Terada, N., Fujii, Y., Ueda, H., Kato, Y., Baba, T., Hayashi, R., et al. (1999). Ultrastructural changes of erythrocyte membrane skeletons in chorea-acanthocytosis and McLeod syndrome revealed by the quick-freezing and deep-etching method. *Acta Haematol.* 101 (1), 25–31. doi:10.1159/000040917

frontiers | Frontiers in Neuroscience

TYPE Original Research
PUBLISHED 09 September 2024
DOI 10.3389/fnins.2024.1408105

OPEN ACCESS

EDITED BY
Peter Koulen,
University of Missouri–Kansas City,
United States

REVIEWED BY
Jose Laffita Mesa,
Karolinska Institutet (KI), Sweden
Christopher D. Stephen,
Harvard Medical School, United States

*CORRESPONDENCE
Ruth H. Walker
✉ ruth.walker@mssm.edu

RECEIVED 27 March 2024
ACCEPTED 09 August 2024
PUBLISHED 09 September 2024

CITATION
Walker RH, Barreto M, Bateman JR, Bustamante ML, Chiu G, Feitell S, Frey BM, Guerra P, Guerrero S, Jung HH, Maldonado F, Meyer E, Miranda M, McFarland E, Oates P, Ochoa G, Olsson K, Paucar M, Proschle JA, Sammler EM, Troncoso M, Wu-Wallace R, Young L, Vege S, Westhoff CM and Danek A (2024) The protean presentations of XK disease (McLeod syndrome): a case series with new observations and updates on previously reported families.
Front. Neurosci. 18:1408105.
doi: 10.3389/fnins.2024.1408105

The protean presentations of XK disease (McLeod syndrome): a case series with new observations and updates on previously reported families

Ruth H. Walker[1,2]*, Mariana Barreto[3], James R. Bateman[4,5], M. Leonor Bustamante[3,6], Graham Chiu[7], Scott Feitell[8], Beat M. Frey[9], Patricio Guerra[10], Sofia Guerrero[11], Hans H. Jung[12], Fernando Maldonado[13], Eduardo Meyer[9], Marcelo Miranda[3,14], Emelie McFarland[4], Patricia Oates[8], Gorka Ochoa[15], Karin Olsson[16], Martin Paucar[16,17], Jonatan Alvarez Proschle[18], Esther M. Sammler[19], Monica Troncoso[20], Rachel Wu-Wallace[4,21], Leo Young[4], Sunitha Vege[15], Connie M. Westhoff[15] and Adrian Danek[22]

[1]Department of Neurology, James J. Peters Veterans Affairs Medical Center, New York, NY, United States, [2]Department of Neurology, Mount Sinai School of Medicine, New York, NY, United States, [3]Diagnosis Foundation, Santiago, Chile, [4]Mental Health Service Line and the Mental Illness Research, Education, and Clinical Center, W.G. (Bill) Hefner Salisbury Veterans Affairs Medical Center, Salisbury, NC, United States, [5]Department of Neurology, Wake Forest University School of Medicine, Winston-Salem, NC, United States, [6]Human Genetics Program, Faculty of Medicine, Biomedical Sciences Institute, University of Chile, Santiago, Chile, [7]Rheumatologist, Palmerston North, New Zealand, [8]Rochester Regional Health, Sands-Constellation Heart Institute, Rochester, NY, United States, [9]Regional Blood Transfusion Service, Swiss Red Cross, Zurich, Switzerland, [10]School of Medicine, University San Sebastián, Puerto Montt, Chile, [11]Hospital De Castro, Los Lagos, Chile, [12]Department of Neurology, University Hospital, Zurich, Switzerland, [13]Servicio Salud Reloncaví, Puerto Montt, Chile, [14]Clínica Meds, Lo Barnechea, Chile, [15]New York Blood Center Enterprises, New York, NY, United States, [16]Department of Neurology, Karolinska University Hospital, Stockholm, Sweden, [17]Department of Clinical Neuroscience, Karolinska Institutet, Stockholm, Sweden, [18]Independent Researcher, Puerto Varas, Chile, [19]University of Dundee, School of Medicine, Dundee, Scotland, [20]Hospital San Borja Arriaran, University of Chile, Santiago, Chile, [21]UCLA Semel Institute for Neuroscience & Human Behavior, Los Angeles, CA, United States, [22]Department of Neurology, LMU University Hospital, LMU Munich, Munich, Germany

XK disease is a very rare, multi-system disease, which can present with a wide spectrum of symptoms. This disorder can also be identified pre-symptomatically with the incidental detection of serological abnormalities when typing erythrocytes in peripheral blood, or on other routine laboratory testing. Increasing awareness of this disorder and improved access to genetic testing are resulting in increasing identification of affected patients and families. Here we provide updates to some previously-reported families and patients and provide additional clinical details. We also report four new cases with a variety of presentations, one of whom had a novel mutation.

KEYWORDS

McLeod, XK, chorea, acanthocytosis, neurodegeneration

Introduction

XK disease, formerly known as McLeod syndrome, is a primarily neurodegenerative disorder which additionally affects cardiac and skeletal muscle, peripheral nervous system, liver, and spleen (Jung et al., 1993). Inheritance is X-linked, typically affecting middle-aged men, although occasionally carrier females develop symptoms. Most neurological manifestations are movement disorders, typically chorea, tics, but also parkinsonism and dystonia, however seizures and neuropsychiatric symptoms can be presenting features. Psychiatric symptoms can include psychosis, delusions, depression, obsessive-compulsive features, and others. Subjects are increasingly being identified by incidental genomic screening in addition to the detection of elevated transaminases and creatine kinase (CK), red blood cell (RBC) acanthocytosis, or by weak expression of Kell blood group system antigens with absence of Kx antigen, i.e. the McLeod phenotype, when typing of red blood cells by blood transfusion centers (Lee et al., 2000; Redman et al., 1999). If subjects are transfused with Kell+ blood they may develop anti-Kell antibodies which can result in massive hemolysis of subsequent Kell+ transfusions, thus transfusion with appropriately matched blood type is critical. The acanthocytosis does not appear to result in major hematologic consequences apart from a mild hemolytic anemia. The diagnosis can be made either by RBC phenotyping or by identification of a pathogenic variant of XK. If the diagnosis is made initially by genetic methodology, RBC phenotyping should also be performed for confirmation (Jung et al., 1993).

We present details of two families; one large kinship from Chile related to two affected brothers who have been previously reported (Gantenbein et al., 2011; Miranda et al., 2012; Miranda et al., 2007), and the family and neurological history of a patient previously published in brief (Floch et al., 2021; Boppana et al., 2023; Lim et al., 2022). We also present clinical details of a patient whose blood was examined as part of blood analyses from a series of patients with VPS13A disease (chorea-acanthocytosis) and XK disease (Siegl et al., 2013). We report the first case of XK disease diagnosed in a person of African ancestry, who had a novel mutation. This patient suffered from severe behavioral issues which were primarily eating-related, and we discuss the strategies employed to manage these issues. We also describe two unrelated patients with an identical mutation and widely differing presentations, emphasizing the apparent absence of genotype-phenotype correlations; one of these presented with a sleep disorder, recognized to be a clinically significant feature of XK disease (Lim et al., 2022; Danek et al., 2001; Munter et al., 2023), and the other with a seizure disorder and severe depression.

Methods

We obtained the latest clinical information regarding previously published subjects, in addition to those recently identified. All subjects gave permission for publication of their clinical data.

Case series

Family 1

In this large family with significant consanguinity, a pathogenic variant in the *XK* gene, c.856_860del (p.Leu286Tyrfs*16), (previously termed 938-942delCTCTA) was originally identified in two members of, this pedigree (Figure 1). These individuals have been previously reported in detail; VI-1 [(Miranda et al., 2012) case 2 (Miranda et al., 2007); patient C (Gantenbein et al., 2011)] and VI-2 [case 1 (Miranda et al., 2007)]. The family had emigrated in 1857 from Höchstberg in current Baden-Württemberg, Germany, as part of a wave of German emigration to Chile.

IV-1:There is no clinical information about the patient but it is assumed that he was affected, being an obligate carrier.

IV-2: This 76-year-old man had a 10-year history of chorea and a 2-year history of seizures. Cognitively he was clinically normal. Peripheral blood smear demonstrated acanthocytosis.

IV-5: This woman was reported to suffer from muscular atrophy. Further details are not available.

IV-7: This woman who was an obligate mutation carrier was reported to suffer from progressive blindness. Further details are not available.

IV-8: At 87 years old this woman was found to have pigmentary retinopathy (RP) and dementia.

V-1, V-3, V,6; These women were obligate mutation carriers and were reported to have abnormal neurological features, however details are not available.

V-2: This woman was observed to have a peripheral neuropathy. Her CK was normal; and she had 1-2 acanthocytes/field on peripheral blood smear.

V-4: This woman was an obligate mutation carrier. At 39 years old she was neurologically asymptomatic and had a normal neurological examination except for decreased vibratory sensation in lower extremities. Electrophysiology revealed a moderate, axonal-predominant sensory-motor polyneuropathy. CK was normal, however she had acanthocytosis on peripheral blood smear.

V-7: This man presented with chorea and cognitive decline at age 49. Total CK was 1964 IU/L (normal $<$ 250 IU/L). Brain MRI identified mild diffuse atrophy, predominantly supratentorial, and microangiopathic in appearance. Echocardiogram was normal. On examination he had mild chorea of the lower extremities, oral dyskinesia, and mild dysarthria.

VI-1 and VI-2: The clinical details of these brothers are published in detail elsewhere [VI-1 (Miranda et al., 2012), case 2 (Miranda et al., 2007), patient C (Gantenbein et al., 2011); VI-2, case 1 (Miranda et al., 2007)]. Briefly, VI-1 developed chorea at the age of 47 which later progressed to parkinsonism, in addition to mild cognitive issues, obsessive-compulsive features, and emotional lability. IV-2 presented with paranoid psychosis at age 23 and chorea 6 years later, albeit following the use of anti-psychotic medications.

VI -3: This woman was reported to suffer from *anorexia nervosa*. No further details are available.

VI-4: This 29-year-old woman was neurologically asymptomatic, and normal on neurological examination apart from decreased vibratory sensation in lower extremities. Magnetic

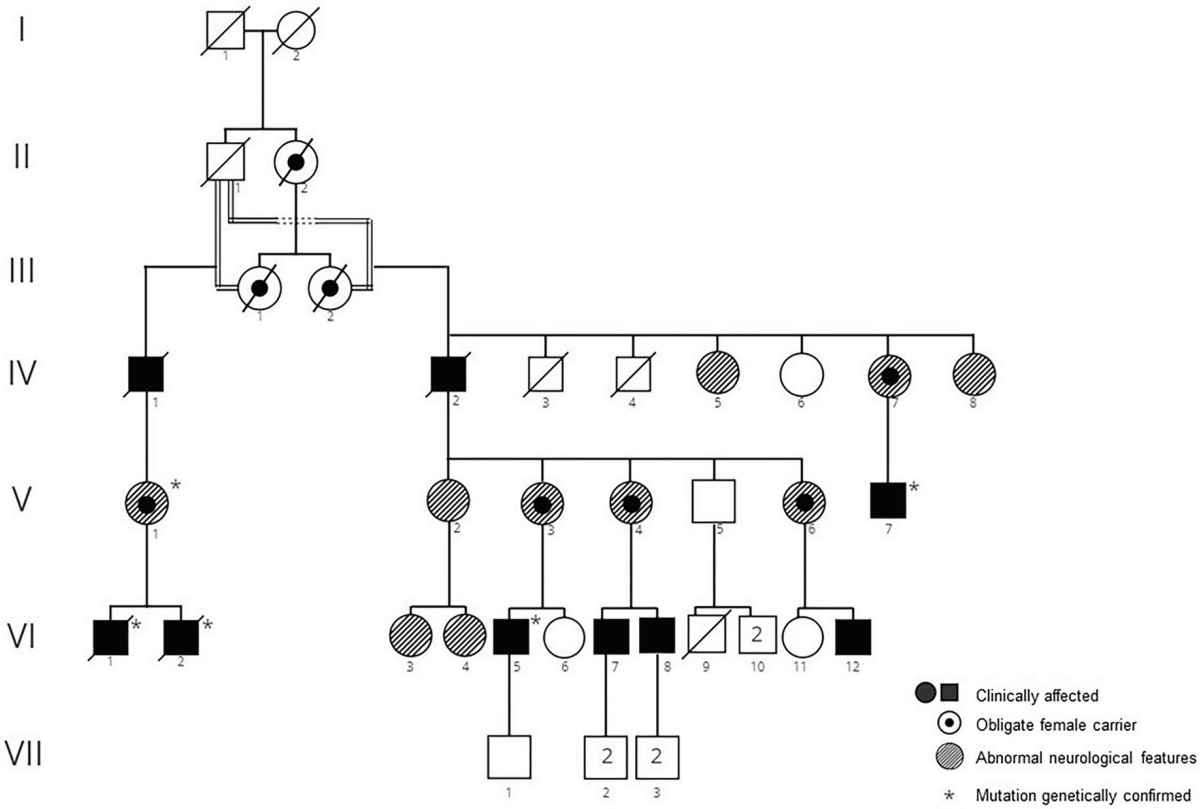

FIGURE 1
Pedigree of family 1. Clinically affected men, obligate carrier women, and women with atypical neurologic featurs are shown.

resonance imaging (MRI) was reported to show moderate cerebellar atrophy. Her CK was normal.

VI-5: This man first noticed abnormal movements when he was 15 years old. At age 36 he continues to work at a high cognitive level without difficulties. He reported some mild obsessive-compulsive behaviour such as checking and counting. On examination he was cognitively normal with a Montreal Cognitive Assessment (MoCA) score of 28. There was mild chorea, motor tics, and his gait was impaired with frequent stumbling and tripping. Deep tendon reflexes were absent throughout. No feeding dystonia was observed and there was no history of seizures. CK was markedly elevated (5000 IU/L; (normal < 250 IU/L); only 6% acanthocytes were found in the peripheral blood smear after osmotic stress. Brain MRI showed very mild caudate atrophy.

VI-7: This man was neurologically asymptomatic at the age of 20, with a normal neurological examination except for decreased vibratory sensation in lower extremities. Electrophysiology demonstrated moderate, axonal-predominant sensory-motor polyneuropathy. CK was markedly elevated at 4,524 IU/L (normal < 250 IU/L), and acanthocytosis was reported in peripheral blood.

VI-8: At 13 years old this boy was evaluated for the incidental laboratory finding of elevated transaminases. Intelligence and psychomotor milestones in infancy were normal. His main symptom was fatigue. Muscle strength and deep tendon reflexes were normal; the only neurological abnormality was a decrease in vibration sense in both legs. Electrophysiology revealed a moderate, axonal-predominant sensory-motor polyneuropathy. CK was 1,213 IU/L (normal < 250 IU/L); there was RBC acanthocytosis (Figure 2). He continued to be neurologically asymptomatic at the age of 17, although there was persistent CK elevation (11,827 IU/L). He was subsequently lost to medical follow-up.

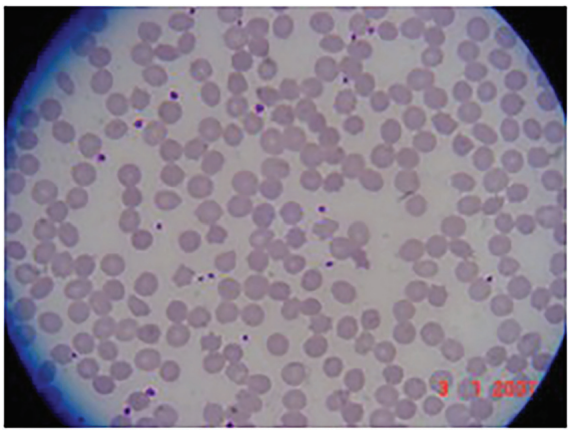

FIGURE 2
Acanthocytosis in patient VI-8. Peripheral blood smear showing acanthocytes.

VI-12: This man is severely affected and is bedridden 15 years after symptom onset. Further details are not available.

Family 2

This family (Figure 3) was of northern European ancestry. Several other family members were reported to have cardiac disease and were potentially also affected, based upon serological testing of RBCs, however further clinical details are not available. II-1 died in his sleep aged 54. II-6 was reported to have died at age 20 from a cardiac cause. No affected females are reported.

I-1: In his early 50s this man developed muscle weakness, tics, severe depression, and was found to have the McLeod RBC phenotype. He died at the age of 60 due to cardiac disease, possibly related to ventricular tachycardia.

III-1: This 44-year-old man presented with severe congestive heart failure (CHF) with an ejection fraction of 10% and runs of non-sustained supraventricular tachycardia. He had been found at the age of 6 to have the McLeod RBC phenotype, following the diagnosis of his maternal grandfather (I-1). Neurological examination at age 44 demonstrated intact strength and reflexes, with no involuntary movements. His CHF was satisfactorily managed with an implantable cardioverter defibrillator (AICD) (Boppana et al., 2023). A sleep study demonstrated severe periodic limb movements of sleep (PLMS) and sleep apnea (case 6 (Lim et al., 2022)). CK was normal (225 IU/L; normal 32–267 IU/L); aspartate aminotransaminase (AST) was normal (34 IU/L; normal 0–35 IU/L), while alanine aminotransferase (ALT) was mildly elevated (71 IU/L, normal 0–35 IU/L). Brain MRI was unremarkable.

Sequencing of *XK* identified a pathogenic mutation c.577A > T encoding for a premature stop codon (p.Lys193Ter) (case 2 (Floch et al., 2021)).

Case A

This 57-year-old white male (presumptively of Northern European ancestry) was first noted to have 33% acanthocytosis on peripheral blood film. One year later, he was presented with acute but transient dysphagia, and was noted to have continuous choreoathetoid movements affecting all four limbs, trunk, and head, in addition to wasting of intrinsic muscles of the hands and feet. Cognitive functioning was preserved, however, he displayed symptoms of schizophreniform psychosis, most notably the belief that he had a clairvoyant ability to communicate with his deceased brother. (It is unknown as to whether his brother was also affected.) In addition to the acanthocytosis, a raised CK was the only abnormal blood result.

Nerve conduction testing confirmed presence of a severe sensory motor axonal peripheral polyneuropathy with only mild neurogenic changes, and no myopathic features. Sural and superficial peroneal sensory responses were bilaterally absent, as were ulnar sensory responses.

Brain MRI showed mild generalized atrophy and minor signal abnormalities in the caudate nucleus, and an incidental pituitary macroadenoma. 24-h-electrocardiogram and echocardiogram were normal.

Over the next 3 years, prior to his death, there were major issues with mood, labile affect, and delusions, the latter of which he denied. His myopathy progressed with severe distal wasting of all four limbs, he became wheelchair-dependent, and developed parkinsonism in combination with choreathetoid movements. His cognitive functioning deteriorated, and he developed increased emotional lability and suicidal ideation.

Targeted genetic testing following identification of the McLeod RBC phenotype identified a point mutation in exon 3, c.1023G > A which encodes for a premature stop codon. This mutation was previously reported in an unrelated patient (Supple et al., 2001).

This subject' blood was analyzed as part of a study of erythrocyte membrane properties in patients with acanthocytosis due to various neurogenetic disorders (including VPS13A disease and pantothenate kinase-associated neurodegeneration [PKAN]) (Siegl et al., 2013). As his was the single sample with XK disease, no statistical comparison with the other disorders or controls was possible.

Case B

A 59-year-old Black American man had a progressive history of involuntary movements and behavioral issues. He reported difficulties with verbal disinhibition and tics beginning in his 40's, which had a significant impact on his interpersonal relationships. The family was African-American with no family history of neurological issues.

Neurological examination at age 54 showed generalized chorea, with motor impersistence. Deep tendon reflexes were trace in all extremities and plantar response was flexor bilaterally. All other neurological aspects were normal. Speech was soft and he tended to repeat himself. Gait was unsteady and staggering.

He was reported to violently act out his dreams, which was attributed to his diagnosis of PTSD following military service. He was very paranoid and there were many instances of severe behavioral disturbances resulting in multiple legal issues with trespassing and larceny. He had compulsive vomiting and was admitted to a long-term care facility as he was unable to live at home due to hoarding, defecating, and urinating in the home with no interest or acknowledgment of the need to clean, bathe, or eat properly.

At age 58, he was seen for psychotherapy to address multiple psychiatric symptoms and complaints. Presenting problems included symptoms related to trauma and depression including nightmares, negative alterations with beliefs and emotional state, irritability, concentration, sleep disturbance, shame, anhedonia, sadness, psychomotor agitation, and feelings of worthlessness. He also endorsed obsessive and perseverative thoughts about food. Behaviorally, he exhibited unwanted eating and feeding symptoms including food hoarding, binge eating, vomiting, and reactions of anger when food was taken away from him. Eating symptoms were complicated by his reported difficulties with extreme polydipsia, hyperphagia, and dysphagia. Despite placement of a feeding tube and nighttime feedings, he continued to have vomiting and malnutrition. He primarily described feelings of distress and shame surrounding vomiting and vocal tics, which negatively impacted his ability to socialize with others.

Psychotherapy treatment focused on increasing self-esteem by separating his self-identity from his medical symptoms and use of coping strategies, specifically positive imagery, to decrease vocal tics which were exacerbated by stress. He reported benefits from these interventions. Due to sanitary concerns from food hoarding as well as behavior towards staff regarding food, he was placed on a behavioral modification plan that specified mealtimes, snack limits, rewards for good behavior, as well as rules for room cleaning, treatment of staff, and other floor mates (e.g., not stealing food from

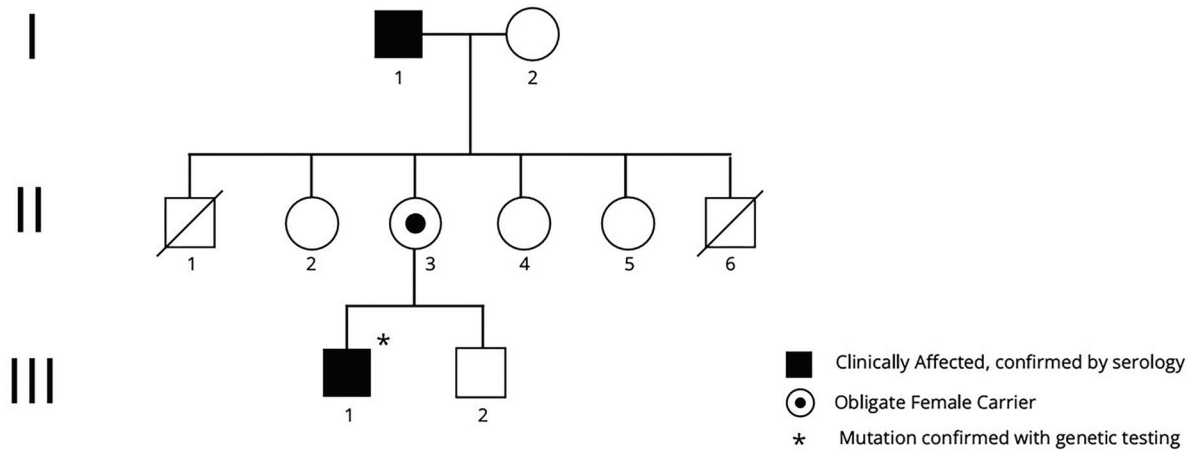

FIGURE 3
Pedigree of family 2. Clinically affected men, in whom the diagnosis was serologically confirmed, are shown, with the obligate carrier woman. Male subjects II-1 and II-6 both died of causes likely related to XK disease.

other long-stay individuals). Staff reported a decrease in behavioral difficulties when enforcing the behavior plan.

Peripheral blood smear was reported to show 15–20% acanthocytes; CK was elevated at 1629 IU/L, as was AST. Brain MRI showed caudate atrophy. He had a reported history of atypical chest pain but echocardiography was normal.

He carried a diagnosis of "neuroacanthocytosis" for many years until genetic sequencing was performed and identified a novel mutation in *XK*, c.484C > T encoding for a premature stop codon (p.Gln162Ter). RBC antigen typing showed weak expression of Kell system antigens and Kx- phenotype (Table 1), indicating a McLeod phenotype.

Case C

A 42-year-old man of Scottish and English ancestry was referred to a rheumatologist for evaluation of elevated CK which had been present for at least 12 years. There was no family history of neurological disorders. He had reported having "restless legs syndrome" for 10 years, with recent worsening of involuntary movements during the day. He did not report any issues with thinking or memory. His main complaint was of very restless and active sleep. On examination constant fasciculations were noted of his calf muscles in addition to subtle involuntary foot movements; strength and sensation were intact, deep tendon reflexes were reduced.

Brain MRI was uninterpretable due to his involuntary movements. 30% acanthocytosis was noted on peripheral blood smear. He had persistently raised troponin T of 28–62 ng/L (normal - 0–13 ng/L) and cardiac MRI showed global impairment of systolic function (left ventricular ejection fraction 55%), with a calcium coronary computed tomography (CT) score of 0. A sleep study was performed following reports of severe abnormal movements during sleep, and demonstrated REM sleep behavior disorder (RBD) and obstructive sleep apnea (body mass index [BMI] 28.3). Continuous positive airway pressure (CPAP) was not tolerated and worsened his involuntary movements.

Targeted genetic testing following identification of the McLeod RBC phenotype showed c.397C > T in exon 2 of *XK* encoding for a premature stop codon (p.Arg133Ter) (Table 1). This mutation was not found in his mother, thus this appears to be a *de novo* mutation. His 3 brothers had normal Kell and XK antigen expression.

Case D

This 52-year-old Finnish man with no family history of neurological disease, presented with generalized seizures at age 38. He suffered from recurrent severe depressive episodes and suicidality and was referred for weakness, myalgia, progressive balance difficulties and involuntary movements. The time course for the onset of the involuntary movements was not clearly defined, however these worsened around age 46. Upon examination he had no deficits on comprehensive cognitive evaluation. Examination of eye movements revealed broken smooth pursuit with horizontal end-gaze nystagmus, mild slowness of saccades in both vertical and horizontal directions and hypometric saccades. There was mild chorea of the extremities and trunk, humming, and moderate dysarthria. He had distal muscle atrophy and mild, generalized weakness, absent deep tendon reflexes, and a normal sensory examination; there was no feeding dystonia, dysphagia or weight loss.

Laboratory tests revealed elevated CK, myoglobin, and lactate dehydrogenase levels but no signs of hemolysis. Brain MRI showed caudate atrophy, cortical atrophy (Figure 4), and mildly increased iron accumulation in globus pallidus. Cardiac evaluation was unremarkable. On electrophysiological study he had a sensorimotor axonal neuropathy, and biopsy from the right tibialis anterior muscle a mild myopathy.

His seizures were refractory to treatment with carbamazepine and subsequently lamotrigine, but were ultimately controlled on a combination of valproic acid, perampanel and cenobamate. His depression has also been refractory to treatment with an antidepressant.

On peripheral blood smear only 2% of erythrocytes were acanthocytes. On targeted genetic testing he was found to have c.397C > T, p.R133X in exon 2 of *XK* (Blueprints Genetics, Finland). This variant was absent in his mother and brother, thus was a *de novo* mutation. Kell antigens were absent or weakly

TABLE 1 Summary of mutations, their serological effects, and relevant previous publications related to each case.

	Mutation	Effect of mutation	Erythrocyte phenotype	ISBT erythrocyte phenotype	Previous publications
Family 1	c.856_860del	p.Leu286Tyrfs*16	Kx 0, K1 0, K2 +, K3 0, K4 0	XK-1; KEL:-1,2,-3,-4	Gantenbein et al., 2011; Miranda et al., 2007; Miranda et al., 2012
Family 2	c.577A > T	p.Lys193Ter	K–k+w Kp(a–b+w) Kx-	XK-1; KEL:-1,2w,-3,4w	Boppana et al., 2023; Floch et al., 2021; Lim et al., 2022
Case A	c.1023G > A	p.Trp341Ter	Kx absent (no other information available)	XK:-1	Siegl et al., 2013
Case B	c.484C > T	p.Gln162Ter	K $k+^{w}$, Kp(a $b+^{w}$), Js(a $b+^{w}$) Kx–	XK:-1; KEL:-1,2w,-3,4w,-6,7w	N/A
Case C	c.397C > T	p.Arg133Ter	K+/$k-^{wk}$, Kp(a-$b+^{wk}$) and Kx-; very weak expression of k and Kp^{b}	XK:-1; KEL:1,2w,-3,4w	N/A
Case D	c.397C > T	p.Arg133Ter	Absent K, Kpa, and Kpb; weak expression of k	KEL:-1,2,3w,4w	N/A

We include the revised RBC nomenclature as per the International Society of Blood Transfusion (IBST).

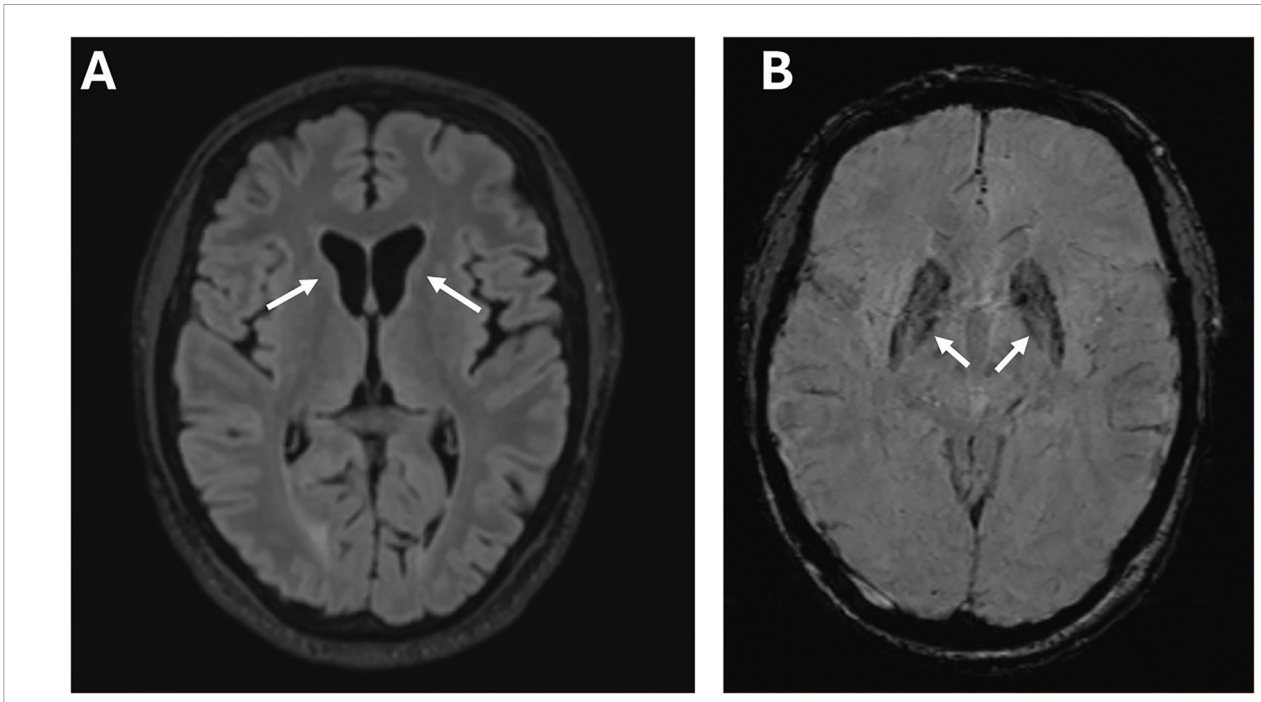

FIGURE 4
Imaging features of Case D. Brain MRI of case D at age 53 years, showing marked atrophy of the caudate nuclei bilaterally in a T1-weighted scan (arrows) **(A)**; susceptibility-weighted images (SWI) sequence showing abnormally increased iron deposition in the globus pallidus (arrows) **(B)**.

expressed, and Kx was absent (Table 1), consistent with the McLeod phenotype.

Discussion

XK disease is an X-linked recessive disorder which can resemble other progressive neurodegenerative disorders, specifically Huntington's disease (HD). The diagnosis can be suspected when patients with chorea or other movement disorders are also noted to have seizures, myopathy, or peripheral neuropathy, with laboratory findings or elevated CK, transaminases, or acanthocytes. There continues to be no evidence of a genotype-phenotype correlation. Even within families, such as Family 1, there is a spectrum of symptoms, which can be cognitive, psychiatric, or neurological.

We highlight here the multi-faceted aspects of XK disease: Presentations include dysphagia (case A), severe psychiatric and behavioral issues (cases B, D), seizures (case D), and disordered sleep (case C).

Case B is remarkable for the severity of his psychiatric and behavioral issues. Psychiatric issues in XK disease can vary widely; in many patients these are minimal, however occasional patients

with severe issues are reported (Jung and Haker, 2004), similar to those in this and case D. Management can be very challenging, however cognitive-behavioral therapy (CBT) appears to have been relatively beneficial for this patient.

Case C was being evaluated for chronic CK elevation, and his main neurological presentation was with a sleep disorder. Both this patient and case B were noted to have RBD early in their disease course.

A spectrum of sleep disorders, including PLMS, RBD, and sleep apnea, has been identified as a significant cause of morbidity and mortality in XK disease (Danek et al., 2001; Lim et al., 2022; Munter et al., 2023). Prospective laboratory sleep studies may be informative in people diagnosed with XK disease especially given the contributions of sleep disorders to cardiac and cognitive impairment.

Case D presented with seizures, and subsequently with severe psychiatric issues, with less prominent chorea and other features. His seizures were initially resistant to treatment but were ultimately controlled with complex polypharmacy. His presentation and disease course have been strikingly different from that of case C, with whom he shares a genetic variant. This variant, p.Arg133Ter (R133X), so far the most commonly-occurring variant, and has been reported previously in a number of unrelated patients from Europe (Danek et al., 2001; Torres et al., 2022; Dotti et al., 2000; Klempíř et al., 2008; Bansal et al., 2008; Díaz-Manera et al., 2018) (n = 8) and one Japanese patient (Murakami et al., 2019; Urata et al., 2019).

Of note, the specifics of the McLeod RBC phenotype can be variable with the same genetic variant, although this can be challenging to compare due to variations in testing antibodies used. The phenotypic variability of red blood cells as assessed by conventional serology is mainly due to technical issues (subjective read-out of hemagglutination assays, gel versus tube technique, variable avidity of polyclonal antibodies). This might be avoided by flow cytometry or fluorescence-activated cell sorting (FACS) assessment of red blood cells, because the applied monoclonal antibodies are more standardized. In addition FACS analysis recognizes double red cell population of Kx+/Kx- red cells in female carriers (Miranda et al., 2007; Jung et al., 2001).

Most patients reported have been of northern European ancestry, with a small number being East Asian or Hispanic. Case B is the first patient reported with African ancestry and has a novel mutation, however, variants of *XK* often appear to be limited to individual families. We suspect that the absence of diagnosis of XK in individuals of African ancestry is unlikely to be due to a genetic factor, and is more likely to be due to disparities in health care access and implementation.

Sporadic *de novo* pathogenic variants in *XK* are rare events among XK disease reports; gonadal mosaicism is a plausible alternative to sporadic occurrence in patients C and D.

In general, female mutation carriers appear to be asymptomatic. A few affected women have been documented (Jung et al., 2001; Gandhi et al., 2008; Ho et al., 1996), likely due to skewed X chromosome inactivation. Family 1 contained a number of women presenting with various neurological findings, some of which were atypical for XK disease, including cerebellar atrophy on brain MRI and retinitis pigmentosa. Some of these women were obligate carriers of the causative mutation, while for others (e.g. IV-8), their genetic status was unknown. The relationship of these symptoms, and the significance of a heterozygous *XK* mutation in women remains to be elucidated. Dementia obviously can be due to a large number of causes, however it was reported in the mother of two brothers with XK disease, with neuropathology showing hippocampal TDP-43 pathology and mild Alzheimer's-type pathology (Dulski et al., 2016).

Compulsive behaviors in general are less frequently reported in XK disease, in comparison with VPS13A disease, where they tend to be more prominent (Walterfang et al., 2011; Walker et al., 2006). Various other features of both diseases can be present in both but tend to be less prominent and more variable in appearance in XK than in VPS13A disease, such as feeding dystonia (Gantenbein et al., 2011), chorea, and cognitive impairment. Conversely, features which tend to be more prominent and debilitating in XK disease than VPS13A include myopathy (Hewer et al., 2007), and cardiac disease (Oechslin et al., 2009).

With the increased availability of WGS/WES more patients are being diagnosed incidentally prior to the appearance of clinically significant neurological symptoms, however, it is of note that all of the cases reported here underwent targeted genetic sequencing, in most cases following identification of the McLeod RBC phenotype. The diagnosis of XK disease may eventually be corroborated by the combination of variable central nervous system, neuromuscular and cardiac manifestation in combination with elevated CK, although these may be absent or very mild, even in later years (Walker et al., 2007). As appropriate interpretation of these genetic results requires clinical context, it is critical that practitioners outside the realm of neurology become aware of the spectrum of symptoms potentially attributable to XK disease (for example, the minimal impairment of case VI-5 from Family 1). In particular, sleep-related symptoms are important contributing factors to morbidity and mortality and are potentially manageable. Regular cardiac monitoring should be performed, in addition to consideration of implications for blood transfusion (Jung et al., 1993). It appears that all mutations so far identified as pathogenic will eventually lead to clinical manifestations, albeit variable in severity (Walker et al., 2007) (i.e. disease penetrance is complete and only mitigated by patient age). Identification of mutation carriers at a young age drives the incentive to develop molecular therapies prior to clinical disease manifestation, to ensure safety of blood transfusions is needed, and also to obviate unnecessary investigations such as liver or muscle biopsy.

Data availability statement

The original contributions presented in the study are included in the article/supplementary material, further inquiries can be directed to the corresponding author.

Ethics statement

Ethical approval was not required for the study involving humans in accordance with the local legislation and institutional requirements. Written informed consent to participate in this study was not required from the participants or the participants' legal guardians/next of kin in accordance with the national legislation and the institutional requirements. Written informed consent

was obtained from the individual(s) for the publication of any potentially identifiable images or data included in this article.

Author contributions

RW: Conceptualization, Data curation, Investigation, Writing – original draft, Writing – review and editing. MB: Data curation, Writing – review and editing, JB: Data curation, Writing – review and editing. MLB: Data curation, Writing – review and editing. GC: Data curation, Writing – review and editing. SF: Data curation, Writing – review and editing. BF: Data curation, Writing – review and editing. PG: Data curation, Writing – review and editing. SG: Data curation, Writing – review and editing. HJ: Data curation, Writing – review and editing. FM: Data curation, Writing – review and editing. EdM: Data curation, Writing – review and editing. MM: Data curation, Writing – review and editing. EmM: Data curation, Writing – review and editing. PO: Data curation, Writing – review and editing. GO: Data curation, Writing – review and editing. KO: Data curation, Writing – review and editing. MP: Data curation, Writing – review and editing. JP: Data curation, Writing – review and editing. ES: Data curation, Writing – review and editing. MT: Data curation, Writing – review and editing. RW-W: Data curation, Writing – review and editing. LY: Data curation, Writing – review and editing. SV: Data curation, Writing – review and editing. CW: Writing – review and editing. AD: Writing – review and editing.

Acknowledgments

We thank the patients and families for their participation in these studies, and for giving permission to publish their clinical details. We thank Hallie Lee-Stroka of the New York Blood Center for performing the serology typing of Case III-1 of Family 2.

Conflict of interest

The authors declare that the research was conducted in the absence of any commercial or financial relationships that could be construed as a potential conflict of interest.

The authors declared that they were an editorial board member of Frontiers, at the time of submission. This had no impact on the peer review process and the final decision.

Publisher's note

References

Bansal, I., Jeon, H., Hui, S., Calhoun, B., Manning, D., Kelly, T., et al. (2008). Transfusion support for a patient with McLeod phenotype without chronic granulomatous disease and with antibodies to Kx and Km. *Vox Sang* 94, 216–220.

Boppana, H., Thakkar, S., Patel, H., Bou Chaaya, R., and Feitell, S. (2023). A case of McLeod's syndrome presenting with severe decompensated heart failure. *Methodist. DeBakey Cardiovasc. J.* 19, 75–78. doi: 10.14797/mdcvj.1164

Danek, A., Rubio, J., Rampoldi, L., Ho, M., Dobson-Stone, C., Tison, F., et al. (2001). McLeod neuroacanthocytosis: Genotype and phenotype. *Ann. Neurol.* 50, 755–764.

Díaz-Manera, J., Sotoca-Fernández, J., Alonso-Jiménez, A., Marzo, M., Gallardo, E., Segovia-Simón, S., et al. (2018). Mcleod syndrome is a new cause of axial muscle weakness. *Muscle Nerve*. 58, E5–E8. doi: 10.1002/mus.26086

Dotti, M., Battisti, C., Malandrini, A., Federico, A., Rubio, J., Circiarello, G., et al. (2000). McLeod syndrome and neuroacanthocytosis with a novel mutation in the XK gene. *Mov. Disord.* 15, 1282–1284.

Dulski, J., Soltan, W., Schinwelski, M., Rudzinska, M., Wojcik-Pedziwiatr, M., Wictor, L., et al. (2016). Clinical variability of neuroacanthocytosis syndromes-a series of six patients with long follow-up. *Clin. Neurol. Neurosurg.* 147, 78–83. doi: 10.1016/j.clineuro.2016.05.028

Floch, A., Lomas-Francis, C., Vege, S., and Westhoff, C. (2021). Three new XK alleles; two associated with a McLeod RBC phenotype. *Transfusion (Paris)* 61, E69–E70. doi: 10.1111/trf.16650

Gandhi, S., Hardie, R., and Lees, A. (2008). "An Update on the Hardie Neuroacanthocytosis series," in *Neuroacanthocytosis syndromes II [Internet]*, eds R. Walker, S. Saiki, and A. Danek (Berlin: Springer), 43–51. doi: 10.1007/978-3-540-71693-8_3

Gantenbein, A., Damon-Perričre, N., Bohlender, J., Chauveau, M., Latxague, C., Miranda, M., et al. (2011). Feeding dystonia in McLeod syndrome. *Mov. Disord. Off. J. Mov. Disord. Soc.* 26, 2123–2126.

Hewer, E., Danek, A., Schoser, B., Miranda, M., Reichard, R., Castiglioni, C., et al. (2007). McLeod myopathy revisited: More neurogenic and less benign. *Brain J. Neurol.* 130, 3285–3296. doi: 10.1093/brain/awm269

Ho, M., Chalmers, R., Davis, M., Harding, A., and Monaco, A. P. (1996). A novel point mutation in the McLeod syndrome gene in neuroacanthocytosis. *Ann. Neurol.* 39, 672–675.

Jung, H., and Haker, H. (2004). Schizophrenia as a manifestation of X-linked Mcleod-neuroacanthocytosis syndrome. *J. Clin. Psychiatry* 65, 722–723. doi: 10.4088/jcp.v65n0520c

Jung, H., Danek, A., Walker, R., Frey, B., and Peikert, K. (1993). "McLeod neuroacanthocytosis syndrome," in *GeneReviews® [Internet]*, eds M. P. Adam, J. Feldman, G. M. Mirzaa, R. A. Pagon, S. E. Wallace, L. J. Bean, et al. (Seattle, WA: University of Washington).

Jung, H., Hergersberg, M., Kneifel, S., Alkadhi, H., Schiess, R., Weigell-Weber, M., et al. (2001). McLeod syndrome: A novel mutation, predominant psychiatric manifestations, and distinct striatal imaging findings. *Ann. Neurol.* 49, 384–392.

Klempíř, J., Roth, J., Zárubová, K., Písačka, M., Špačková, N., and Tilley, L. (2008). The McLeod syndrome without acanthocytes. *Parkinsonism Relat. Disord.* 14, 364–366.

Lee, S., Russo, D., and Redman, C. (2000). The Kell blood group system: Kell and XK membrane proteins. *Semin. Hematol.* 37, 113–121.

Lim, M., Sarva, H., Hiller, A., Feitell, S., Oates, P., Barone, D., et al. (2022). Sleep disorders in McLeod syndrome: A case series. *Parkinsonism Relat. Disord.* 102, 86–88.

Miranda, M., Castiglioni, C., Frey, B., Hergersberg, M., Danek, A., and Jung, H. (2007). Phenotypic variability of a distinct deletion in McLeod syndrome. *Mov. Disord. Off. J. Mov. Disord. Soc.* 22, 1358–1361. doi: 10.1002/mds.21536

Miranda, M., Jung, H., Danek, A., and Walker, R. (2012). The chorea of McLeod syndrome: Progression to hypokinesia. *Mov. Disord. Off. J. Mov. Disord. Soc.* 27, 1701–1702. doi: 10.1002/mds.25224

Munter, D., Peikert, K., Veit, T., Hermann, A., Nowak, L., Kahnert, K., et al. (2023). Polysomnographic findings in the ultra-rare McLeod syndrome: Further documentation of sleep apnea as possible feature. *J. Clin. Sleep. Med.* 20, 339–344. doi: 10.5664/jcsm.10854

Murakami, T., Abe, D., Matsumoto, H., Tokimura, R., Abe, M., Tiksnadi, A., et al. (2019). A patient with McLeod syndrome showing involvement of the central sensorimotor tracts for the legs. *BMC Neurol.* 19:301. doi: 10.1186/s12883-019-1526-9

Oechslin, E., Kaup, D., Jenni, R., and Jung, H. (2009). Cardiac abnormalities in McLeod syndrome. *Int. J. Cardiol.* 132, 130–132.

Redman, C., Russo, D., and Lee, S. (1999). Kell, Kx and the McLeod syndrome. *Baillieres Best Pract. Res. Clin. Haematol.* 12, 621–635.

Siegl, C., Hamminger, P., Jank, H., Ahting, U., Bader, B., Danek, A., et al. (2013). Alterations of red cell membrane properties in neuroacanthocytosis. *PLoS One* 8:e76715. doi: 10.1371/journal.pone.0076715

Supple, S., Iland, H., Barnett, M., and Pollard, J. D. (2001). A spontaneous novel XK gene mutation in a patient with McLeod syndrome. *Br. J. Haematol.* 115, 369–372. doi: 10.1046/j.1365-2141.2001.03121.x

Torres, V., Painous, C., Santacruz, P., Sánchez, A., Sanz, C., Grau-Junyent, J., et al. (2022). Very long time persistent HyperCKemia as the first manifestation of Mcleod syndrome: A case report. *Mov. Disord. Clin. Pract.* 9, 821–824. doi: 10.1002/mdc3.13502

Urata, Y., Nakamura, M., Sasaki, N., Shiokawa, N., Nishida, Y., Arai, K., et al. (2019). Novel pathogenic XK mutations in McLeod syndrome and interaction between XK protein and chorein. *Neurol. Genet.* 5:e328. doi: 10.1212/NXG.0000000000000328

Walker, R., Danek, A., Uttner, I., Offner, R., Reid, M., and Lee, S. (2007). McLeod phenotype without the McLeod syndrome. *Transfusion (Paris)* 47, 299–305.

Walker, R., Liu, Q., Ichiba, M., Muroya, S., Nakamura, M., Sano, A., et al. (2006). Self-mutilation in chorea-acanthocytosis: Manifestation of movement disorder or psychopathology? *Mov. Disord. Off. J. Mov. Disord. Soc.* 21, 2268–2269.

Walterfang, M., Evans, A., Looi, J., Jung, H., Danek, A., Walker, R., et al. (2011). The neuropsychiatry of neuroacanthocytosis syndromes. *Neurosci. Biobehav. Rev.* 35, 1275–1283.

frontiers | Frontiers in Neuroscience

TYPE Case Report
PUBLISHED 02 October 2024
DOI 10.3389/fnins.2024.1409366

OPEN ACCESS

EDITED BY
Joan-lluis Vives-Corrons,
Josep Carreras Leukaemia Research Institute (IJC), Spain

REVIEWED BY
Paola Bianchi,
IRCCS Ca 'Granda Foundation Maggiore Policlinico Hospital, Italy
Immacolata Andolfo,
University of Naples Federico II, Italy
Roberta Russo,
University of Naples Federico II, Italy
Giampaolo Minetti,
University of Pavia, Italy

*CORRESPONDENCE
Martin Paucar
martin.paucar-arce@regionstockholm.se

†These authors have contributed equally to this work

RECEIVED 29 March 2024
ACCEPTED 02 September 2024
PUBLISHED 02 October 2024

CITATION
Paucar M, Wincent J, Rubin C, Peikert K, Kyhle J, Hertegård S, Möller R, Beshara S and Svenningsson P (2024) Case report: Neuroacanthocytosis associated with novel variants in the *VPS13A* gene with concomitant nucleotide expansion for CANVAS and assessment with osmotic gradient ektacytometry.
Front. Neurosci. 18:1409366.
doi: 10.3389/fnins.2024.1409366

Case report: Neuroacanthocytosis associated with novel variants in the *VPS13A* gene with concomitant nucleotide expansion for CANVAS and assessment with osmotic gradient ektacytometry

Martin Paucar[1,2]*, Josephine Wincent[3,4], Charlotta Rubin[5], Kevin Peikert[6,7,8], Josefin Kyhle[9], Stellan Hertegård[10,11], Riita Möller[11,12], Soheir Beshara[3,13†] and Per Svenningsson[1,2†]

[1]Department of Clinical Neuroscience, Karolinska Institutet, Stockholm, Sweden, [2]Department of Neurology, Karolinska University Hospital, Stockholm, Sweden, [3]Department of Molecular Medicine and Surgery, Karolinska Institutet, Stockholm, Sweden, [4]Department of Clinical Genetics, Karolinska University Hospital, Stockholm, Sweden, [5]Department of Clinical Nutrition, Karolinska University Hospital, Stockholm, Sweden, [6]Translational Neurodegeneration Section "Albrecht Kossel," Department of Neurology, University Medical Center Rostock, University of Rostock, Rostock, Germany, [7]Center for Transdisciplinary Neurosciences Rostock, University Medical Center Rostock, Rostock, Germany, [8]United Neuroscience Campus Lund-Rostock, Rostock, Germany, [9]Department of Speech and Language, Karolinska University Hospital, Stockholm, Sweden, [10]Department of Clinical Science, Intervention and Technology, Karolinska Institutet, Stockholm, Sweden, [11]Department of Otolaryngology, Karolinska University Hospital, Stockholm, Sweden, [12]Department of Medical Biology and Biostatistics, Karolinska Institutet, Stockholm, Sweden, [13]Department of Clinical Chemistry, Karolinska University Hospital, Stockholm, Sweden

Background and objectives: The diseases historically known as neuroacanthocytosis (NA) conditions include *VPS13A* disease (formerly chorea-acanthocytosis) and *XK* disease (formerly McLeod syndrome). Here we report a patient with a hyperkinetic syndrome associated with variants in *VPS13A* with a concomitant homozygous nucleotide expansion in Replication factor C, subunit 1 (*RFC1*) and evaluate the role of ektacytometry for the assessment of acanthocytes.

Methods: Investigations included clinical assessments, neuroimaging studies, laboratory analyses, blood smears, ektacytometry, psychometric evaluation, and genetic analyses. Using ektacytometry, an osmoscan curve is obtained yielding a diffraction pattern as a measure of average erythrocyte deformability from circular at rest to elliptical at a high shear stress. The pattern allows the derivation of several parameters (mainly EI-max, O-min and O-Hyper points). Samples from two other patients with genetically proven *VPS13A* disorder and *XK* disease and varying numbers of acanthocytes as well as from a fourth with acanthocytosis due to liver failure were also analyzed.

Case presentation: The patient has impulsivity, chorea and disabling feeding dystonia refractory to treatment and 15% acanthocytes in peripheral blood. Genetic workup revealed compound heterozygous variants c.1732_1733del; p.(V578Ffs*9) and c.8282C > A, p.(S2761*) in *VPS13A* with absence of

chorein in the blood, the latter variant is novel. In addition, he harbors a homozygous nucleotide expansion in the *RFC1* gene, reported in cerebellar ataxia, neuropathy, vestibular areflexia syndrome (CANVAS). However, the patient does not display ataxia yet. Ektacytometry revealed significantly reduced erythrocyte deformability in this patient and in another man with *VPS13A* disease. In contrast, the patient with *XK* disease had 2% acanthocytes and mild abnormalities on ektacytometry. In the three cases, ektacytometry yielded a specific pattern, different from acanthocytosis due to liver failure.

Conclusion: Pathogenicity of the *VPS13A* variants is confirmed by absence of chorein, long-term follow up is required to evaluate any synergistic impact of for the underlying CANVAS mutation. New generation ektacytometry provides an objective measurement of erythrocytes' rheological properties and may serve as a complement to blood smears. Finally, ektacytometry's ability to detect deformability of erythrocytes in NA seems to depend on the degree of acanthocytosis.

KEYWORDS

neuroacanthocytosis, ektacytometry, *VPS13A*, *VPS13A* disease, feeding dystonia

Background

VPS13A disease (formerly known as chorea-acanthocytosis) and *XK* disease (formerly McLeod syndrome) are the conditions historically known as the core neuroacanthocytosis (NA) syndromes (Walker et al., 2023; Walker and Danek, 2021; Peikert et al., 2002; Jung et al., 2004). The percentage of acanthocytes in both *VPS13A* disease and *XK* disease is variable (5–50%) under the course of disease, > 6.3% acanthocytes in peripheral blood is considered abnormal. To reduce the risk for false positive and negative cases, acanthocytosis is assessed with a specific protocol (Storch et al., 2005). The red blood cells membrane properties are determined by membrane structure, which in turn, identifies membrane deformability, mechanical stability and permeability. These rheological properties can be measured by osmotic gradient ektacytometry. Data on ektacytometry in NA syndromes is still very limited (De Franceschi et al., 2014; Cluitmans et al., 2015; Lazari et al., 2020; Ballas et al., 1990; Hernández et al., 2024).

Patient and methods

Investigations included clinical assessments, neuroimaging studies, laboratory analyses, blood smears, ektacytometry, psychometric evaluation, and genetic analyses. A Western blot analysis for chorein, with two different antibodies (Anti-VPS13A, HPA021662, Sigma-Aldrich, rabbit and Anti-VPS13A, PA5-54483, Invitrogen, rabbit), was performed according to the protocol described by Dobson-Stone et al. (2004). Briefly, one antibody targets an epitope located in middle of the protein (Invitrogen), and the second one targets an epitope in the C-terminus (Sigma). Absence of bands with both antibodies reflects lack of chorein expression, even of a truncated protein. Blood samples from a man with genetically proven *VPS13A* disease previously reported by Paucar et al. (2015), from a man with *XK* disease harboring the recurrent variant c.397C > T; p.R133X in *XK* (Dotti et al., 2000; Klempír et al., 2008; Murakami et al., 2019) and from a woman with liver failure and acanthocytosis were also included for comparison.

Blood smear and ektacytometry

In all cases, the presence of acanthocytes was assessed according to the protocol for wet blood smears proposed by Storch et al. (2005). Erythrocytes were also studied using new generation osmotic gradient ektacytometry (LoRRca® Maxis; RR Mechatronics). By mixing low and high osmolar solutions, an osmotic gradient was established, and the laser diffraction pattern was recorded. Few microliters of blood were suspended in 5 ml of isotonic Polyvinylpyrrolidone solution (PVP) (RR Mechatronics) and mixed carefully. Osmoscan curve was performed, and the following variables were obtained: the minimal osmolality (O-min), where 50% of RBC are lysed in a hypoosmotic environment and its corresponding minimal elongation index (EI-min), the maximal elongation index (EI-max) at optimal osmolality (O-max), the hyperosmotic osmolality (O-hyper), where half of the maximal elongation index (EI-hyper) is reached, and the area under the osmoscan curve (AUC) was calculated.

Massive parallel sequencing and Sanger sequencing

Massive parallel sequencing (MPS) of the patient was performed using a 30× PCR-free paired-end WGS protocol on an Illumina NovaSeq 6000 platform as described previously

(Magnusson et al., 2020). A gene panel of 956 genes associated with movement disorders and neuromuscular disease was analyzed. The variants were prioritized based on conservation, frequency in internal and public databases, and pattern of inheritance. The ranked variants were then visualized in the Scout analysis platform (Stranneheim et al., 2021). Both *VPS13A* variants, confirmed in the patient by PCR and Sanger sequencing, were segregated in the parents. The Sanger sequencing was performed by standard methods on an ABI 3730 PRISM® DNA Analyzer. Primer sequences available upon request. The homozygous *RFC1* expansion was confirmed by PCR amplification covering the repeat region.

Results

Case presentation

This is a 36-year-old man (index case, patient A) born to healthy and non-consanguineous Finnish parents, the pedigree is presented in Figure 1A. One sibling, affected by obesity, hypertension, and reduced systolic function had limited compliance to medication, died suddenly at age 31 years some years before the index case came to our center for evaluation. The cause of death could not be determined, his DNA was not available for analyses. The patient was referred due to personality change, impulsivity, slurred speech, progressive involuntary movements, and severe eating difficulties. The patient had involuntary lingual movements with tongue protrusion induced by eating, with frequent biting of the lips and tongue. The patient has been using dental guards but bit off these devices. Fiberoptic endoscopic evaluation of swallowing revealed oropharyngeal dysphagia. The patient reported weight loss, involuntary leaning of the trunk backward but denies falls, he has not required walking aids, and has been able to engage in winter sports (skiing and skating on ice). Upon exam he displayed moderate chorea in the face, perioral region and extremities as well as feeding and truncal dystonia. There were no signs of lingual motor impersistence. He could walk and run and performed tandem gait without difficulties. There were no signs of dysmetria, or nystagmus, vestibular-ocular reflex (VOR) was normal on video head impulse test (vHIT). He had areflexia, plantar responses were flexor; muscle tone, strength and sensation were normal. There was no evidence of muscle atrophy either. Eye movements were characterized by broken smooth pursuit and mild slowness of vertical saccades. Horizontal optokinetic nystagmus (OKN), amplitude and speed on vertical OKN were normal. The last exam yielded 29 points in the Unified Huntington's Disease Rating Scale-Total Motor Score (UHDRS-TMS) protocol. Several drugs (different neuroleptics alone and combined, tetrabenazine, trihexyphenidyl, and dantrolene) were tried for feeding dystonia without any benefit. Botulinum injections were applied to the pterygoid muscles but not to the tongue base since this pose the risk of worsening his dysphagia. The patient was offered a gastrostomy, but he decided to delay the procedure. His last BMI was 23.5, his diet consists almost exclusively of oral nutrition supplements. The patient declined to use psychotropic medicines. The cognitive evaluation revealed difficulties performing the Luria test, a recent neuropsychological assessment found clear variations ranging from significantly below average-to-average performance. Clearly low performances were found in verbal episodic memory, both learning and retrieval of verbal material as well as verbal working memory. Likewise, executive abilities, such as word flow and flexibility (ability to switch between concepts in visual tempo-demanding tasks) were below average. The work pace in various tasks was also slower than expected. There were no signs of hemolysis except a mild reduction of haptoglobin levels. CK levels and EMG were normal, a neurography demonstrated incipient sensory neuropathy whereas his EEG was normal (Clinical findings are summarized in Table 1). The MRI of the brain shows caudate atrophy and increased iron accumulation in this structure (Figures 1B, C), his cardiac evaluation (echocardiography and ECG) was unremarkable.

TABLE 1 Summary of clinical findings in a man with pathogenic biallelic new variants in *VPS13A* and a homozygous nucleotide expansion in *RFC1*.

Parameter	Findings
Motor features	Chorea and severe feeding dystonia
Other neurological features	No
Psychiatric features	Impulsivity
Cognition	Mild executive difficulties
Seizures	No
Genetic variants	*VPS13A* c.1732_1733, p.(Val578Phefs*9)[a] c.8282 C > A, p.(Ser2761*)[b] Homozygous pentanucleotide expansion in *RFC1*
Diagnosis	*VPS13A* disease
Ektacytometry	Clearly abnormal
Degree of acanthocytosis (%)	15%
ENeG/EMG	Abnormal values on ENeG
Neuroimaging	Caudate atrophy Increased iron levels in the caudate nuclei
Hemolysis	No[c]
CK	Normal
Myoglobulin	Normal
Transaminases	Normal

AST, aspartate aminotransferase; BG, basal ganglia; ENeG, electroneurography; ND, no determined. [a]This variant is found in 2 individuals (Finns) in gnomAD, CADD = 32. [b]This variant is absent in gnomAD. CADD = 45. [c]Only haptoglobin was mildly reduced, but other tests for hemolysis (blood cell count, reticulocytes, lactate dehydrogenase, and bilirubin) were all normal.

Genetics and biochemistry

The patient was initially investigated for Huntington's disease (HD) but lacked pathological CAG expansions in the *HTT* gene. MPS identified compound heterozygous truncating variants in *VPS13A*. The variant c.1732_1733del; p.(V578Ffs*9) (CADD 32) was inherited from the patient's father and was previously reported in the heterozygous state in two individuals (Finns) in gnomAD v2.1.1 corresponding to a carrier frequency of 1/11000. The second variant c.8282C > A, p.(S2761*), (CADD 45) was

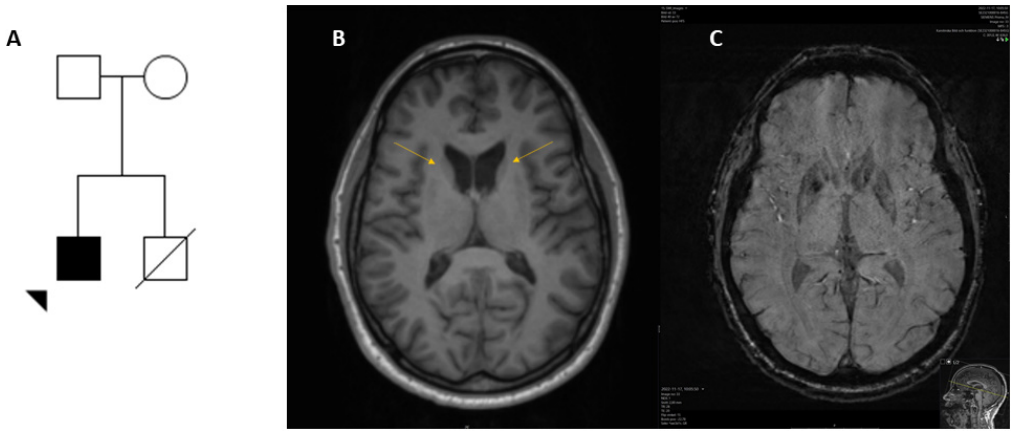

FIGURE 1
Pedigree and neuroimaging of a man with *VPS13A* disease and carrier for a homozygous nucleotide expansion in *RFC1*. The patient (arrowhead) is of Finnish descendancy, each parent carries a variant in *VPS13A* **(A)**. Neuroimaging at age 35 years, T2 weighted axial image **(B)** displaying caudate atrophy (arrows) and subsequent widening of the ventricles and a SWI sequence with increased iron levels in the same structure **(C)**. Motion artifacts limited assessment of the putamen.

inherited from the patient's mother and was absent from gnomAD v2.1.1 Chorein/VPS13A protein was not detected by Western blot (Supplementary Figure 1). In addition, the patient carries a homozygous nucleotide expansion in the Replication Factor C, Subunit 1 (*RFC1*) gene.

Blood smears, ektacytometry and blood count

In blood smears from patient A, 15% acanthocytes were found, and ektacytometry revealed significantly reduced deformability in erythrocytes (Figure 2, curve A). Similar results were shown in another male patient with *VPS13A* disease (Hernández et al., 2024) with a similar count of acanthocytes in peripheral blood (Figure 2, curve B). In contrast, ektacytometry for the patient with *XK* disease, harboring 2% acanthocytes, revealed only mild abnormalities (Figure 2, curve C). In both cases, the most affected measurement in ektacytometry was the "O hyper" point. In contrast, acanthocytosis due to alcoholic liver failure yielded a completely different curve (Figure 2, curve D). Data from complete blood count are presented in Table 2. The genetic data was further studied regarding variants in the *PIEZO1* and *SPTA1* genes, that may yield altered curves. No pathogenic variants in either gene were found in patient A or for patient D (with advanced liver cirrhosis). Patients B and C went through targeted genetic testing for *VPS13A* and *XK* disease only, thus testing for other genetic erythrocyte membrane defects than for NA syndromes was not part of their work-up.

Discussion

This is the first time a patient of Finnish origin is reported as affected by a *VPS13A* disease. Both *VPS13A* variants reported here are new in the context of *VPS13A* disease. Homozygous nucleotide expansions in *RFC1* are the underlying cause of cerebellar ataxia, neuropathy and vestibular areflexia syndrome (CANVAS). In this case, the only feature suggesting a *RFC1*-related disorder was incipient neuropathy. On the other hand, neuropathy is a common trait among patients with *VPS13A* disease. Long-term follow up is warranted to determine any synergistic effect of this dual pathology. Feeding dystonia, a hallmark of *VPS13A* disease, is particularly challenging to treat (Bader et al., 2010) as reported here. The risk for cardiomyopathy and ventricular arrhythmias in *XK* disease is well known, recently a study demonstrated that cardiomyopathy can also be a feature in *VPS13A* disease (Quick et al., 2021). The index case's late brother who died suddenly and unexpectedly did not have any known neurological symptoms according to his relatives, a genetic investigation was not possible to carry out. Normal CK level in our patient is of note since this protein is elevated in the majority of patients with *VPS13A* disease (Peikert et al., 2002).

The morphology of erythrocytes is maintained by membrane lipids, proteins, and spectrin–actin membrane-skeleton. Cellular membranes comprise lipid bilayers that consist of glycerophospholipids, sphingolipids and cholesterol where phosphatidylcholine, phosphatidylethanolamine and phosphatidylserine (PtdSer) are among the major glycerophospholipids as well as phosphatidylserine (PtdIns) as one of the relatively minor glycerophospholipids (Sakuragi and Nagata, 2023).

The VPS13 protein family members (A–D) have been recently identified to be located at membrane contact sites acting in bulk lipid transfer (Leonzino et al., 2021). Mutations in the corresponding genes for the *VPS13* protein family members are of clinical importance as mutations in each protein lead to a specific neurological disorder (Peikert et al., 2002). However, acanthocytosis has only been identified in *VPS13A* disease giving rise to remarkable phenotypic similarities with *XK* disease, that is a genetically distinct disorder (Walker et al., 2023). XK on the other hand, was described as a transmembrane protein linked to the Kell protein by a disulfide bond in erythrocytes. XK and Kell seem, though, not linked in both brain and skeletal muscle (Spesivtseva et al., 2023). XKr8, however, was shown to function as a lipid scramblase and its

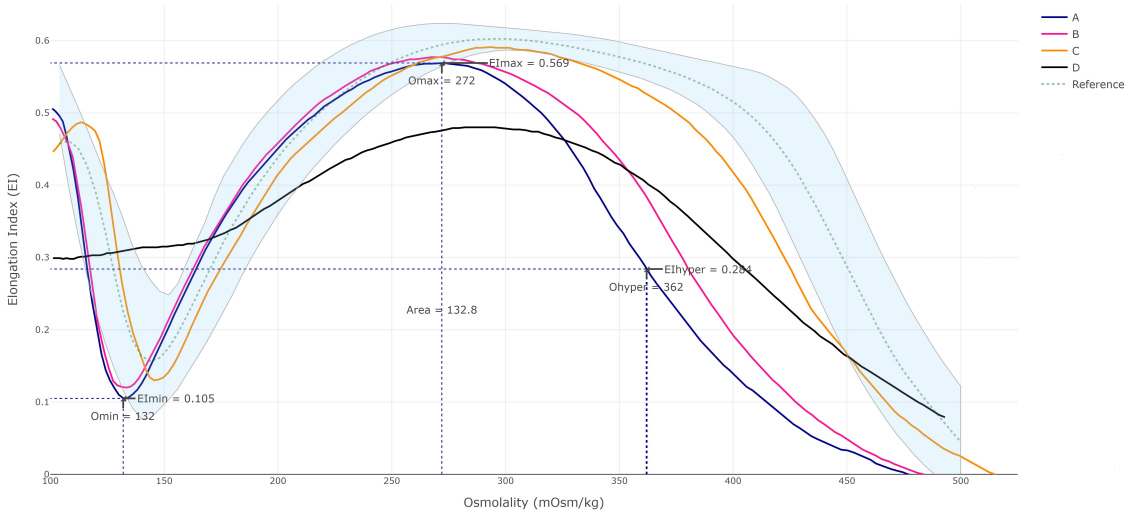

FIGURE 2
Ektacytometry data. Osmoscan profiles in the patient reported here with *VPS13A* disease **(A)**; another male patient with *VPS13A* disease with 12% acanthocytes **(B)**; a man with *XK* disease with 2% acanthocytes **(C)**; and in a female patient with liver failure and about 50% acanthocytes **(D)**. Continuous line represents the deformability of each patient and shaded area the control group. The patient samples were analyzed as single measurement each, but data are shown to be comparable with those previously presented (Ballas et al., 1990). The control group was established using data from 22 healthy controls and further verified using samples from additional 31 healthy subjects. Samples from 10 patients diagnosed with hereditary spherocytosis were included in the evaluation to discriminate the two different groups. Precision and sample stability testing were run according to internal laboratory procedures, the method was verified during spring 2023.

TABLE 2 **Complete blood count of the reported cases.**

Parameter and diagnosis	*VPS13A* disease (patient A)	*VPS13A* disease (patient B)	*XK* disease (patient C)	Liver cirrhosis (patient D)	Reference range
B-Hb	146	135	155	54	134–170 g/L
B-RBCs	4.9	4.5	4.6	1.6	4.2–5.7 10^{12}/L
B-Hct	0.45	0.37	0.42	0.16	0.39–0.50
B-MCV	92	85	89	103	82–98 fL
Erc(B)-MCH	30	31	33	34	27–33 pg
Erc(B)-MCHC	324	365	369	338	317–357 g/L
Erc(B)-RDW	< 18	< 18	< 18	> 18*	< 18%
Reticulocyte count	142*	60	104	236*	28–115 10^{9}/L
Leukocyte count	5.7	4.5	8.6	25.5*	3.5–8.8 10^{9}/L
Platelet count	159	178	307	129*	145–348 10^{9}/L

Erc(B)-RDW > 18% is considered pathologic and is reported as anisocytosis. Patient A is the case described in this work.

role in apoptotic PtdSer exposure was subsequently identified (Suzuki et al., 2014). The reduced levels of PtdSer subspecies in the inner membrane leaflet of McLeod erythrocytes (with absent XK protein) had been already described by Redman et al. (1989). Further, VPS13A participates in regulating the phosphorylation of PtdIns on the plasma membrane of the erythrocytes. The level of PtdIns regulates the interaction between the plasma membrane and membrane-skeleton (Park et al., 2015).

Studying the pathophysiology of diseases due to mutations of the VPS13 protein family members, other lipid transfer proteins, and proteins related by a common function, such as XK, may indicate that these are all part of a group of disorders with a common mechanism of impaired bulk lipid transport (Walker et al., 2023).

The mechanism/s of the abnormal red cell membrane structure that results in acanthocytosis in *VPS13A* disease and *XK* disease is/are not fully understood. Several hypotheses are postulated among which is the disturbances in the phosphorylation-controlled binding between the integral membrane protein complexes and the membrane-skeleton (De Franceschi et al., 2014) and of depolymerized cortical actin due to absence or significant reduction in chorein encoded by *VPS13A* (Föller et al., 2012).

However, it now appears likely that VPS13 and XK proteins are functionally linked. At the plasma membrane, VPS13A interacts with the scramblase XK. This complex may be involved in lipid transport between the endoplasmic reticulum and plasma

membrane as well as lipid scrambling between the two leaflets of the plasma membrane (Guillén-Samander et al., 2022). Erythrocytes lack organelles when circulating in peripheral blood, however, it is possible that abnormal lipid metabolism and organellar transfer during maturation (erythropoiesis) affects their membrane composition.

This complex function in membrane lipid homeostasis and survival resulting perhaps from deficient PtdSer and/or PtdIns exposure at the plasma membrane may explain the phenotypic similarities between the two disorders including formation of acanthocytes (Walker et al., 2023).

Ektacytometry is a widely used tool for assessing erythrocyte deformability and hydration status, giving a different pattern for each type of erythrocyte membrane defects (Da Costa et al., 2016; Andolfo et al., 2016). The significant change in ektacytometry data was mostly observed in the left shift of the O-hyper point, which reflects the stiffness of erythrocytes. A mild decrease in deformability was also noted in index patient as well as patient with neuroacanthocytosis with similar acanthocyte percentage in peripheral blood. The changes seen were closely related to the number of acanthocytes identified in patients with *VPS13A* disease and *XK* disease. These changes were, however, not reflected on hematological parameters. Rheologic abnormalities on four patients with *XK* disease reported by Ballas et al. (1990) are similar to our findings. Reichel et al. (2022) also found reduced erythrocyte deformability in *VPS13A* disease by means of microfluidic techniques. Data on ektacytometry for *VPS13A* disease and pantothenate kinase-associated neurodegeneration (PKAN), another condition also associated with acanthocytosis, is also limited (De Franceschi et al., 2014; Cluitmans et al., 2015). A report on ektacytometry of neuroacanthocytosis cases did not provide details on underlying genotype (Lazari et al., 2020). In contrast, spur cell anemia in liver failure is thought to be due to exogenous factors not related to membrane structure since transfused cells tend to undergo similar morphological alterations as well (Shah et al., 2023). That explains the fact that changes observed in ektacytometry displayed a completely different pattern in acanthocytosis caused by liver failure.

Ektacytometry is an objective tool to evaluate erythrocyte deformability. Our report, despite cross-sectional single measurements of few patients, adds on the utility of this tool for assessment of patients with *VPS13A* and *XK* diseases (Walker and Danek, 2021). This tool may constitute a promising complement especially when blood smears are inconclusive. Taken together, our data suggest an ektacytometry-based fingerprint for *VPS13A* disease, but larger studies are required to validate our findings.

Patient perspective

The patient with *VPS13A* disease reported here provided oral and written consent for this work in the context of research approved by the Swedish Ethical Review Authority. The course of disease is progressive and feeding dystonia is highly disabling. Gastrostomy in a near future, is a reasonable and necessary option for this patient. The other patients whom blood was tested for acanthocytosis did also provide oral and written consent.

Data availability statement

The original contributions presented in this study are included in this article/Supplementary material, further inquiries can be directed to the corresponding author.

Ethics statement

The studies involving humans were approved by the Swedish Ethical Review Authority. The studies were conducted in accordance with the local legislation and institutional requirements. The participants provided their written informed consent to participate in this study. Written informed consent was obtained from the individual(s) for the publication of any potentially identifiable images or data included in this article. Written informed consent was obtained from the participant/patient(s) for the publication of this case report.

Author contributions

MP: Conceptualization, Data curation, Formal analysis, Funding acquisition, Investigation, Methodology, Project administration, Resources, Software, Supervision, Validation, Visualization, Writing – original draft, Writing – review & editing. JW: Formal analysis, Methodology, Software, Validation, Writing – review & editing. CR: Conceptualization, Formal analysis, Investigation, Validation, Writing – review & editing. KP: Conceptualization, Data curation, Formal analysis, Investigation, Methodology, Supervision, Validation, Visualization, Writing – review & editing. JK: Data curation, Investigation, Methodology, Writing – review & editing. SH: Investigation, Methodology, Validation, Writing – review & editing. RM: Investigation, Methodology, Validation, Writing – review & editing. SB: Conceptualization, Data curation, Formal analysis, Investigation, Methodology, Project administration, Resources, Software, Supervision, Validation, Visualization, Writing – original draft, Writing – review & editing. PS: Data curation, Formal analysis, Funding acquisition, Investigation, Project administration, Resources, Supervision, Writing – review & editing.

Funding

The authors declare financial support was received for the research, authorship, and/or publication of this article. MP's research was funded by the Stockholm Region and by the Promobilia Foundation. PS was a Wallenberg Clinical Scholar.

Acknowledgments

We are grateful to the patients for their kind participation, and to psychologist Eva Nordström for performing the cognitive evaluation on the reported patient.

Conflict of interest

The authors declare that the research was conducted in the absence of any commercial or financial relationships that could be construed as a potential conflict of interest.

Publisher's note

All claims expressed in this article are solely those of the authors and do not necessarily represent those of their affiliated organizations, or those of the publisher, the editors and the reviewers. Any product that may be evaluated in this article, or claim that may be made by its manufacturer, is not guaranteed or endorsed by the publisher.

Supplementary material

The Supplementary Material for this article can be found online at: https://www.frontiersin.org/articles/10.3389/fnins.2024.1409366/full#supplementary-material

References

Andolfo, I., Russo, R., Gambale, A., and Iolascon, A. (2016). New insights on hereditary erythrocyte membrane defects. *Haematologica* 101, 1284–1294. doi: 10.3324/haematol.2016.142463

Bader, B., Walker, R., Vogel, M., Prosiegel, M., McIntosh, J., and Danek, A. (2010). Tongue protrusion and feeding dystonia: A hallmark of chorea-acanthocytosis. *Mov. Disord.* 25, 127–129. doi: 10.1002/mds.22863

Ballas, S., Bator, S., Aubuchon, J., Marsh, W., Sharp, D., and Toy, E. (1990). Abnormal membrane physical properties of red cells in McLeod syndrome. *Transfusion* 30, 722–727. doi: 10.1046/j.1537-2995.1990.30891020333.x

Cluitmans, J., Tomelleri, C., Yapici, Z., Dinkla, S., Bovee-Geurts, P., Chokkalingam, V., et al. (2015). Abnormal red cell structure and function in neuroacanthocytosis. *PLoS One* 10:e0125580. doi: 10.1371/journal.pone.0125580

Da Costa, L., Suner, L., Galimand, J., Bonnel, A., Pascreau, T., Couque, N., et al. (2016). Society of hematology and pediatric immunology (SHIP) group; French society of hematology (SFH). Diagnostic tool for red blood cell membrane disorders: Assessment of a new generation ektacytometer. *Blood Cells Mol. Dis.* 56, 9–22. doi: 10.1016/j.bcmd.2015.09.001

De Franceschi, L., Bosman, G., and Mohandas, N. (2014). Abnormal red cell features associated with hereditary neurodegenerative disorders: The neuroacanthocytosis syndromes. *Curr. Opin. Hematol.* 21, 201–209. doi: 10.1097/MOH.0000000000000035

Dobson-Stone, C., Velayos-Baeza, A., Filippone, L., Westbury, S., Storch, A., Erdmann, T., et al. (2004). Chorein detection for the diagnosis of chorea-acanthocytosis. *Ann. Neurol.* 56, 299–302. doi: 10.1002/ana.20200

Dotti, M., Battisti, C., Malandrini, A., Federico, A., Rubio, J., Circiarello, G., et al. (2000). McLeod syndrome and neuroacanthocytosis with a novel mutation in the XK gene. *Mov. Disord.* 15, 1282–1284.

Föller, M., Hermann, A., Gu, S., Alesutan, I., Qadri, S., Borst, O., et al. (2012). Choreinsensitive polymerization of cortical actin and suicidal cell death in chorea-acanthocytosis. *FASEB J.* 26, 1526–1534.

Guillén-Samander, A., Wu, Y., Pineda, S., García, F., Eisen, J., Leonzino, M., et al. (2022). partnership between the lipid scramblase XK and the lipid transfer protein VPS13A at the plasma membrane. *Proc. Natl. Acad. Sci. U.S.A.* 119:e2205425119. doi: 10.1073/pnas.2205425119

Hernández, C., Peikert, K., Qiao, M., Darras, A., de Wilde, J., Bos, J., et al. (2024). Osmotic gradient ektacytometry - a novel diagnostic approach for neuroacanthocytosis syndromes. *Front. Neurosci.* 18:1406969. doi: 10.3389/fnins.2024.1406969

Jung, H., Danek, A., Walker, R., Frey, B., and Peikert, K. (2004). "McLeod neuroacanthocytosis syndrome," in *GeneReviews® [Internet]*, eds M. Adam, J. Feldman, G. Mirzaa, R. Pagon, S. Wallace, L. Bean, et al. (Seattle, WA: University of Washington).

Klempír, J., Roth, J., Zárubová, K., Písacka, M., Spacková, N., and Tilley, L. (2008). The McLeod syndrome without acanthocytes. *Parkinsonism Relat. Disord.* 14, 364–366.

Lazari, D., Freitas Leal, J., Brock, R., and Bosman, G. (2020). The relationship between aggregation and deformability of red blood cells in health and disease. *Front. Physiol.* 11:288. doi: 10.3389/fphys.2020.00288

Leonzino, M., Reinisch, K. M., and De Camilli, P. (2021). Insights into VPS13 properties and function reveal a new mechanism of eukaryotic lipid transport. *Biochim. Biophys. Acta* 1866:159003. doi: 10.1016/j.bbalip.2021.159003

Magnusson, M., Eisfeldt, J., Nilsson, D., Rosenbaum, A., Wirta, V., Lindstrand, A., et al. (2020). Loqusdb: Added value of an observations database of local genomic variation. *BMC Bioinform.* 21:273. doi: 10.1186/s12859-020-03609-z

Murakami, T., Abe, D., Matsumoto, H., Tokimura, R., Abe, M., Tiksnadi, A., et al. (2019). patient with McLeod syndrome showing involvement of the central sensorimotor tracts for the legs. *BMC Neurol.* 19:301. doi: 10.1186/s12883-019-1526-9

Park, J., Halegoua, S., Kishida, S., and Neiman, A. M. (2015). A conserved function in phosphatidylinositol metabolism for mammalian Vps13 family proteins. *PLoS One* 10:e0124836. doi: 10.1371/journal.pone.0124836

Paucar, M., Lindestad, P. Å, Walker, R. H., and Svenningsson, P. (2015). Teaching video neuroimages: Feeding dystonia in chorea-acanthocytosis. *Neurology* 85, e143–e144.

Peikert, K., Dobson-Stone, C., Rampoldi, L., Miltenberger-Miltenyi, G., Neiman, A., De Camilli, P., et al. (2002). "VPS13A disease," in *GeneReviews® [Internet]*, eds M. Adam, J. Feldman, G. Mirzaa, R. Pagon, S. Wallace, L. Bean, et al. (Seattle, WA: University of Washington).

Quick, S., Heidrich, F., Winkler, M., Winkler, A., Ibrahim, K., Linke, A., et al. (2021). Cardiac manifestation is evident in chorea-acanthocytosis but different from McLeod syndrome. *Parkinsonism Relat. Disord.* 88, 90–95. doi: 10.1016/j.parkreldis.2021.05.015

Redman, C., Huima, T., Robbins, E., Lee, S., and Marsh, W. (1989). Effect of phosphatidylserine on the shape of McLeod red cell acanthocytes. *Blood* 74, 1826–1835.

Reichel, F., Kräter, M., Peikert, K., Glaß, H., Rosendahl, P., Herbig, M., et al. (2022). Changes in blood cell deformability in chorea-acanthocytosis and effects of treatment with dasatinib or lithium. *Front. Physiol.* 13:852946. doi: 10.3389/fphys.2022.852946

Sakuragi, T., and Nagata, S. (2023). Regulation of phospholipid distribution in the lipid bilayer by flippases and scramblases. *Nat. Rev. Mol. Cell Biol.* 24, 576–596. doi: 10.1038/s41580-023-00604-z

Shah, P., Grewal, U., and Hamad, H. (2023). *Acanthocytosis: StatPearls*. Treasure Island, FL: StatPearls Publishing.

Spesivtseva, A., Gvarzhdec, N., Autlev, K., Kruchinin, E., and Kuznetsov, I. (2023). Diseases of the neuroacanthocytosis group: A systematic review of clinical cases and difficulties in their diagnosis. *Adv. Life Sci.* 10, 335–340.

Storch, A., Kornhass, M., and Schwarz, J. (2005). Testing for acanthocytosis A prospective reader-blinded study in movement disorder patients. *J. Neurol.* 252, 84–90. doi: 10.1007/s00415-005-0616-3

Stranneheim, H., Lagerstedt-Robinson, K., Magnusson, M., Kvarnung, M., Nilsson, D., Lesko, N., et al. (2021). Integration of whole genome sequencing into a healthcare setting: High diagnostic rates across multiple clinical entities in 3219 rare disease patients. *Genome Med.* 13:40.

Suzuki, J., Imanishi, E., and Nagata, S. (2014). Exposure of phosphatidylserine by Xk-related protein family members during apoptosis. *J. Biol. Chem.* 289, 30257–30267.

Walker, R., and Danek, A. (2021). "Neuroacanthocytosis" – overdue for a taxonomic update. *Tremor Other Hyperkinet. Mov.* 11:1. doi: 10.5334/tohm.583

Walker, R., Peikert, K., Jung, H., Hermann, A., and Danek, A. (2023). Neuroacanthocytosis syndromes: The clinical perspective. *Contact* 6:25152564231210339. doi: 10.1177/25152564231210339

frontiers | Frontiers in Neuroscience

TYPE Original Research
PUBLISHED 11 December 2024
DOI 10.3389/fnins.2024.1488133

OPEN ACCESS

EDITED BY
Kevin Peikert,
University Hospital Rostock, Germany

REVIEWED BY
Saurabh Srivastav,
Texas Children's Hospital, United States
Muhammad Ansar,
Fondation Asile des Aveugles, Switzerland

*CORRESPONDENCE
Wenke Seifert
✉ wenke.seifert@charite.de

RECEIVED 29 August 2024
ACCEPTED 18 October 2024
PUBLISHED 11 December 2024

CITATION
Schottmann G, Martínez Almudéver C, Knop JCM, Suk EK, Meyer Z, Kohlhase J, Himmelreich N, Kühnisch J, Ott C-E and Seifert W (2024) Impact of genetic test interpretation on a *VPS13B* missense variant in Cohen syndrome.
Front. Neurosci. 18:1488133.
doi: 10.3389/fnins.2024.1488133

Impact of genetic test interpretation on a *VPS13B* missense variant in Cohen syndrome

Gudrun Schottmann[1], Carmen Martínez Almudéver[2], Julia C. M. Knop[2], Eun Kyung Suk[3], Zianka Meyer[4], Jürgen Kohlhase[5], Nastassja Himmelreich[6,7], Jirko Kühnisch[8,9], Claus-Eric Ott[10] and Wenke Seifert[2]*

[1]Zentrum für Sozial-und Neuropädiatrie (DBZ), Vivantes Klinikum Neukölln, Berlin, Germany, [2]Institute of Cell Biology and Neurobiology, Charité - Universitätsmedizin Berlin, corporate member of Freie Universität Berlin und Humboldt-Universität zu Berlin, Berlin, Germany, [3]Praxis für Humangenetik, Berlin, Germany, [4]Diagenom GmbH, Rostock, Germany, [5]Zentrum für Humangenetik, SYNLAB MVZ Humangenetik Freiburg, Tübingen, Germany, [6]Zentrum für Humangenetik Tübingen, Tübingen, Germany, [7]CeGaT, Tübingen, Germany, [8]Experimental and Clinical Research Center (ECRC), a cooperation been the Max Delbrück Center for Molecular Medicine in the Helmholtz Association and Charité—Universitätsmedizin Berlin, Berlin, Germany, [9]Institute of Physiology, Brandenburg Medical School (MHB) Theodor Fontane, Brandenburg an der Havel, Germany, [10]Institute for Medical Genetics and Human Genetics, Charité—Universitätsmedizin Berlin, corporate member of Freie Universität Berlin und Humboldt Universität zu Berlin, Berlin, Germany

Introduction: Cohen syndrome (CS) is an early-onset pediatric neurodevelopmental disorder characterized by postnatal microcephaly and intellectual disability. An accurate diagnosis for individuals with CS is crucial, particularly for their caretakers and future prospects. CS is predominantly caused by rare homozygous or compound heterozygous pathogenic variants in the vacuolar protein sorting-associated 13B (*VPS13B*) gene, which disrupt protein translation and lead to a loss of function (LoF) of the encoded VPS13B protein.

Methods: The widespread incorporation of next-generation sequencing approaches in genetic diagnostics increases the number of individuals carrying *VPS13B* mutant alleles. At the same time, it increases the detection of variants of unknown clinical significance, necessitating further functional pathogenicity validation.

Results: In this study, we present a family with two CS patients. Within this family, four rare *VPS13B* variants were detected: c.710G > C, p.Arg237Pro; c.6804delT, p.Phe2268Leufs*24; c.7304C > T, p.Ala2435Val; and c.10302T > A, p.Tyr3434*. These variants challenge the interpretation of their disease-causing role. Specifically, the variants c.6804delT, p.Phe2268Leufs*24 and c.710G > C, p.Arg237Pro were detected in trans configuration and are considered to be causing CS genetically. The functional characterization of the missense variant c.710G > C, p.Arg237Pro shows diminished localization at the Golgi complex, highlighting its clinical relevance and supporting its classification by the American College of Medical Genetics and Genomics (ACMG) as likely pathogenic, class 4.

Discussion: Overall, we emphasize the need for combining genetic and functional testing of VPS13B missense variants to ensure accurate molecular diagnosis and personalized medical care for CS patients.

KEYWORDS

VPS13B, Cohen syndrome, missense variant, functional testing, Golgi complex

Introduction

In recent decades, human genetics has enabled the rapid and comprehensive identification of genetic variants and their association with neurological diseases (Satam et al., 2023). However, we emphasize the importance of systematic phenotyping and functional studies, especially when the interpretation of variants of unknown significance (VUS) leaves uncertainty regarding their pathogenic character.

In this study, we present two brothers with the phenotype of Cohen syndrome (CS, MIM: #216550). CS is a rare autosomal recessive genetic condition that is primarily characterized by developmental delay, postnatal microcephaly, and distinctive facial gestalt with wave-shaped eyelids and a short philtrum (Kolehmainen et al., 2003; El Chehadeh-Djebbar et al., 2013). The clinical diagnosis of CS is facilitated by the presence of progressive retinal dystrophy and/or neutropenia. Additional facultative clinical signs include myopia, childhood hypotonia, joint laxity, a cheerful disposition, and autism spectrum disorder (ASD)-like behavior (Katzaki et al., 2007; Gueneau et al., 2014). Genetically, CS is predominantly caused by splice site mutations, frameshift indels, or nonsense variants, which typically results in a complete loss of function (LoF) of the encoded vacuolar protein sorting-associated 13B (VPS13B) (Seifert et al., 2009). VPS13B belongs to the VPS13 family of bridge-like lipid transfer proteins, suggesting that it facilitates lipid transport between adjacent membranes (Vacca et al., 2024; Mochida et al., 2004; Hanna et al., 2023). At the cellular level, VPS13B is primarily localized to the Golgi complex. It plays a crucial role in preserving the morphology and function of the Golgi, potentially influencing membrane organization and intracellular membrane transport (Vacca et al., 2024; Seifert et al., 2011). Recent studies using neuronal models, including iPSC-derived neurons and animal models of CS, have indicated that VPS13B depletion is linked to neurodevelopmental abnormalities, such as axonal elongation defects, defective synaptogenesis, and increased autophagic flux (Seifert et al., 2015; Lee et al., 2020; Lee et al., 2020). However, a clear genotype–phenotype correlation or functional correlation regarding the differences in the clinical expression of CS has not yet been established.

In contrast, the interpretation of *VPS13B* missense variants is challenging due to the lack of biochemical and pathomechanistic characterization of most VPS13B protein regions. Although *in silico* analysis supports predictions of pathogenicity, functional evidence provides much stronger validation for the pathogenic character of a genetic variant. To overcome this limitation, we established a cellular detection assay that measures the subcellular distribution of the encoded VPS13B protein in the Golgi apparatus and the cytosol after immunostaining (Zorn et al., 2022). In this study, we employed a quantitative subcellular analysis of VPS13B mutant protein distribution to classify the familial *VPS13B* missense VUS, thereby validating the genetic diagnosis for CS.

Methods

Family consent

Written informed consent for genetic testing and the use of data for publication was obtained from each participant. Parental consent was secured for both siblings under 18 years of age.

Genetic testing

DNA was isolated from peripheral EDTA blood. Both patients underwent initial Sanger sequencing of the entire coding region of the *VPS13B* gene (exon 2–62, including 20 bp of the 3′ and 5′ intron regions) using standard procedures with a 3130XL Genetic Analyzer (Applied Biosystems). All details can be obtained upon request. Quadro analysis of the *VPS13B* gene using NGS-based whole exome sequencing was performed on both patients and their parents to reevaluate the variants, technically confirm allelic distribution, and ascertain the *de novo* status. Enrichment of the coding regions, adjacent intronic regions, and other non-coding, disease-relevant regions of the *VPS13B* candidate region was performed using *in-solution* hybridization. For exome capture, we used enrichment kits from Twist Bioscience. High-throughput sequencing was conducted using the Illumina NovaSeq 6,000/NovaSeq X Plus System. Adapter sequences were removed using Skewer, a tool designed for trimming high-throughput sequencing reads. The resulting sequences were aligned to the human reference genome (hg19) using the Burrows–Wheeler Aligner sequences. The sequences that were not uniquely aligned or were identified as duplicates, most likely due to PCR amplification, were removed to ensure data accuracy. Sequencing data were processed using Illumina bcl2fastq2 software, which converts raw BCL files generated by the sequencer into FASTQ files for further analysis. The remaining high-quality sequences were annotated for sequence variants using various internal and external databases, including the Illumina database and the VPS13B MANE PLUS CLINICAL transcript ENST00000358544, NM_017890.5, comprising 12,069 bp. However, in this study, all variants were aligned to the ubiquitously expressed and conserved variant *VPS13B* ENST00000357162.7, NM_152564.5, comprising 11,994 bp and encoding 3,997 amino acids (aa) as the reference.

Reagents and antibodies

All reagents were obtained from Sigma-Aldrich, Roth or Merck, unless stated otherwise. The following commercial antibody was used: Mouse anti-GM130 (BD Transductions Laboratories, Cat. No. 610822). Rabbit anti-VPS13B (442) was described earlier (Seifert et al., 2011). Secondary antibodies for immunofluorescence included donkey anti-mouse-Cy3, anti-rabbit-Cy3, and anti-rabbit-Cy2 (all from Dianova GmbH). 6-Diamidino-2-phenylindole (DAPI) (Invitrogen) was used for nuclear DNA staining.

Cloning of the *VPS13B* variant expression vectors by site-directed mutagenesis

Missense variants were annotated using the *VPS13B* transcript [Ensembl, ENST00000357162.6 (VPS13B-202); RefSeq, NM_152564.5]. For transient expression, the full-length human *VPS13B* construct encoding the VPS13B missense variant p.Arg237Pro (pcDNA3.1_VPS13B-mutR237P) was cloned using site-directed mutagenesis PCR (Reikofski and Tao, 1992). Briefly, the full-length wild-type human construct pcDNA3.1_VPS13B-wt (Seifert et al., 2011) was amplified using primer pairs containing the corresponding missense variants in VPS13B using PrimeSTAR GXL DNA Polymerase (NEB Inc.) according to the manufacturer's instructions. The PCR products were subsequently treated with the KLD enzyme mix (NEB Inc.), which eliminated the

methylated pcDNA3.1_VPS13B-wt vectors and prepared them for the DNA ligation reaction. The integrity and correct mutagenesis of all cloned vectors were confirmed through Sanger sequencing.

Cell culture and transfection

HeLa-cells (ATCC) were cultured at 37°C in a 5% CO_2 atmosphere using DMEM culture medium supplemented with 5% FCS and 1% glutamine. Transient transfection of the expression vectors was performed at approximately 50% confluence using Lipofectamine (Invitrogen, Thermo Fisher) according to the manufacturer's instructions. The variant of interest was pcDNA3.1_VPS13B-mutArg237Pro, while pcDNA3.1_VPS13B-mutAla590Thr and pcDNA3.1_hVPS13B-mutGlu2704Arg served as negative and positive controls, respectively. Cell harvesting for further analysis was performed 24–48 h post-transfection.

Immunofluorescence

For visualization of intracellular protein expression and localization, the cells were cultured on coverslips and, if required, transfected (see above). The cells on the coverslips were fixed using 3% (w/v) paraformaldehyde in 1x PBS at 4°C and permeabilized in 0.5% (v/v) Triton X-100 and 1% (w/v) BSA in 1x PBS. Primary antibodies were incubated in 1% (w/v) BSA diluted in 1x PBS for at least 8 h at 4°C. After rinsing with PBS, secondary antibodies were incubated in 1% (w/v) BSA diluted in 1x PBS for 2 h at 4°C. Subsequently, the coverslips were attached to slides using ImmuMount (ThermoFisher). The visualization was performed using a spinning disk microscope (Zeiss), with a comparable cellular imaging level and identical imaging conditions.

ImageJ and statistical analysis

Image analysis and Golgi enrichment were performed using ImageJ. Two different regions of interest (ROIs) were defined for each cell separately, as previously described (Zorn et al., 2022). Briefly, one ROI outlining the cell border measured the total VPS13B immunofluorescence of the cell (total cell ROI), while the second ROI outlining the GM130-positive Golgi structure (Golgi ROI) measured the Golgi-associated immunofluorescence of VPS13B. The percentage of Golgi-associated VPS13B fluorescence compared to the total VPS13 cell fluorescence intensity was calculated. The graphical representation and statistical analysis were carried out using GraphPad Prism software. The VPS13B variants pcDNA3.1_VPS13B-mutAla590Thr and pcDNA3.1_hVPS13B-mutGlu2704Arg were previously described (Zorn et al., 2022) and included in the study as Golgi enrichment-affecting negative and positive controls for the VPS13B missense variant, respectively.

In silico prediction and variant classification for the evaluation of pathogenicity

All variant pathogenicity prediction algorithms and the ACMG classification (ACMG/ACGS 2020 guidelines, version 4.01) were conducted as previously described (Zorn et al., 2022). Truncating *VPS13B* variants were classified as decribed (Abou Tayoun et al., 2018).

Results

Patients and family

Here, we report the phenotype of two brothers with clinical manifestations indicating CS.

Patient 1 was born at term (41 weeks) via spontaneous delivery, with a relatively low birth weight of 3,030 g (P16, −1.01 SD). He exhibited respiratory adaptation disorder and muscular hypotonia. A cranial MRI scan at birth revealed a structurally unremarkable brain with slightly enlarged cerebrospinal fluid spaces. After birth, the patient developed postnatal microcephaly, with a head circumference of 41 cm at the age of 1 (<P1, −5.19 SD), and a psychomotor developmental delay. All developmental milestones were met at delayed time points. The patient was able to sit independently at the age of 1.5 years, walked independently by the age of 4, and has remained non-verbal to date. Myopia was diagnosed at the age of 4. He is usually in a friendly mood and shows limited understanding of simple content. Moreover, within the first year, the patient was noted to have recurrent bronchial infections and neutropenia. Other symptoms included feeding difficulties, small genitalia, and bilateral undescended testis.

Patient 2, the younger brother, was born via spontaneous delivery at term after a pregnancy complicated by maternal diabetes requiring insulin therapy. At 6 months of age, developmental delay, muscular hypotonia, and feeding difficulties became evident. He developed distinct postnatal microcephaly and, despite intensive supportive therapy, showed slow developmental progress. He was able to sit unaided at 21 months and has been walking with support since the age of 3 years. Sleeping disorders and feeding difficulties have been ongoing to this day. The boy frequently shows high irritability and exhibits autistic features, including reduced eye contact, stereotypical movements, and social withdrawal. His mother reports that he often appears to be in his own world and lacks a recognizable need for social contact, which is in line with previous reports of autistic features in CS (Table 1).

Sequencing results

Chromosomal analysis and microarray comparative genomic hybridization (CGH) were unremarkable, indicating no major chromosomal abnormalities. Initial Sanger sequencing of the *VPS13B* gene was performed based on the clinically distinct phenotype of CS in Patient 1. Further molecular testing of both patients and the parents was performed using candidate region *in-solution* hybridization enrichment and high-throughput sequence analysis using the Illumina NovaSeq 6000/NovaSeq X Plus System. Next-generation sequencing-based copy number variations were calculated based on the sequences that could be assigned to a genomic position using an internally developed method based on sequencing depth. No genomic copy number imbalances were detected that could explain the patients' phenotype. Further annotation of the high-throughput sequencing data using various internal and external databases for the sequence variants in the candidate region of *VPS13B* confirmed two pathogenic

TABLE 1 Summary of the clinical characteristics of both related brothers with CS.

CS features	Patient 1	Patient 2
Age at clinical assessment	8 y	3 y 3 m
Facial dysmorphism	+	+
Postnatal microcephaly	+	+
Growth chart		
At birth: gestational age/weight/length/head circumference	41 w/3030 g/n.s./n.s.	40 w/3130 g/48 cm/34 cm
Actual: age/weight/length/head circumference	8 y/26.2 kg/121.5 cm/46.7 cm	3 y/10.2 kg/85 cm/43.9 cm
Developmental delay	+	+
Head control	Unknown	4 m
Sitting unsupported	18 m	21 m
Walking unsupported	4 y	Supported walking at 3y
Speaking words	Non-verbal	Non-verbal
Autistic features	–	+
Myopia/retinopathy	+/–	–/–
Neutropenia	+	–
Congenital muscular hypotonia	+	+
Other	Recurrent infections, feeding difficulties until age 4 (improving since the age of 4), bilateral nondescensus testis, and small genitalia	Cranial flattening right >left, constant feeding difficulties, and sleeping difficulties

+ present, – absent, and n.s., not specified.

heterozygous variants and two heterozygous VUS in the older patient (Patient 1): c.6804delT, p.Phe2268fs*24 (Rafiq et al., 2015); c.10302T > A, p.Tyr3434*; c.710G > C, p. Arg237Pro; and c.7304C > T, p.Ala2435Val. In the younger patient (Patient 2), sequencing of the candidate region of *VPS13B* identified one pathogenic heterozygous variant and two heterozygous VUS: c.6804delT, p.Phe2268fs*24 (Rafiq et al., 2015); c.710G > C, p. Arg237Pro; and c.7304C > T, p.Ala2435Val. Subsequent analysis of the parents suggested that the mother carried the pathogenic variant c.6804delT, p.Phe2268fs*24 and the VUS c.7304C > T, p.Ala2435Val, which were inherited by both brothers. The second pathogenic variant, c.10302T > A, p.Tyr3434*, in Patient 1, was not inherited from the mother or the father, suggesting a *de novo* agent, germ cell mosaicism, or a somatic event. The father carried the heterozygous *VPS13B* VUS c.710G > C, p. Arg237Pro, which was inherited by both brothers (Figure 1; Table 2).

Variant pathogenicity prediction algorithms

To understand the complex genetic and clinical data, we interpreted the *VPS13B* variants according to the ACMG standards and guidelines (Deignan et al., 2019). The Phe2268Leufs*24 variant has been previously reported to cause CS (Table 2, ClinVarID: 817631) (Rafiq et al., 2015; Zare Ashrafi et al., 2023). The p.Tyr3434* variant was detected in Patient 1, and it is classified as a pathogenic variant due to its deleterious nature. However, this variant did not co-segregate with the CS phenotype within the family, likely indicating a *de novo* mutation, germ cell mosaicism, or a somatic event. Paternity and maternity for both patients were confirmed. The missense variants were further processed using standard computational and predictive *in silico* algorithms. In this study, the major difference between both missense variants was predicted using SNPs&GO analyses (Calabrese et al., 2009), which indicated a disease-causing prediction for p.Arg237Pro and a neutral character for p.Ala2435Val (Table 2). The disease-causing prediction of pArg237Pro was further supported by its conservation down *to Xenopus tropicalis* (Figure 1B), while p.Ala2435Val was excluded as a cause of the CS phenotype due to its co-segregation as a complex maternal allele with p.Phe2268Leufs*24. Overall, the segregation of p.Arg237Pro with the CS phenotype suggested that this missense variant caused autosomal recessive CS in both affected brothers, along with the p.Phe2268Leufs*24 variant.

Golgi localization

To date, the analysis of cellular VPS13B distribution is the only simple and reliable method to investigate the effects of *VPS13B* missense variants (Zorn et al., 2022). This method involves cloning the respective missense variant into a mammalian expression vector (pcDNA3.1_VPS13B) and subsequent overexpression in standard cell cultures, such as HeLa cells (Zorn et al., 2022). Using this approach, we showed that the wild-type VPS13B protein localizes to the Golgi complex, as indicated by its co-localization with the Golgi matrix protein GM130 (Figure 2A). As controls, we analyzed two previously reported *VPS13B* missense variants regarding their subcellular localization (Zorn et al., 2022). The p.Ala590Thr variant exhibited a subcellular distribution similar to the wild-type VPS13B protein and was therefore used as a negative control. In contrast, the p.Gly2704Arg variant showed reduced localization to the Golgi complex and was used as a positive control, indicating a disruption in subcellular targeting. The analysis of the p.Arg237Pro variant revealed a significant reduction in Golgi enrichment of the mutated VPS13B protein (Figures 2A,B). It is important to note that the overall area covered by the Golgi complex

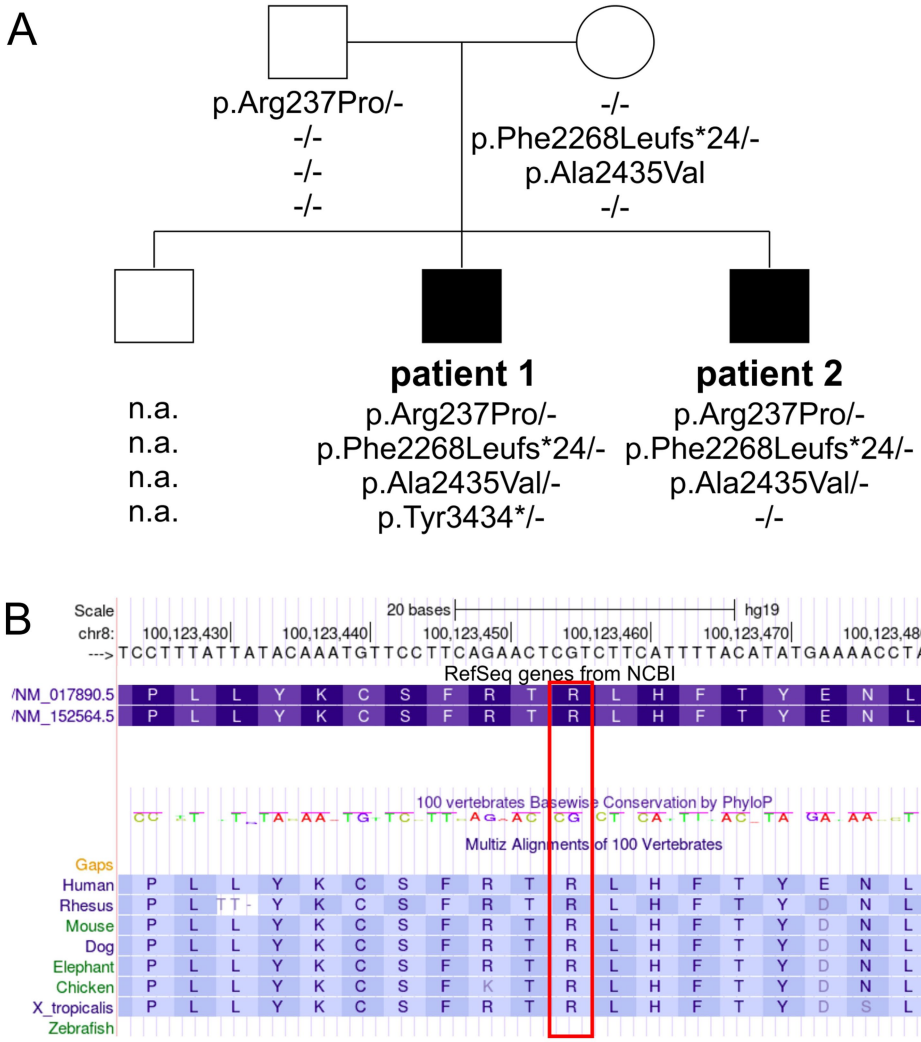

FIGURE 1
Pedigree and genetic findings in the family with CS. (A) Squares and circles symbolize males and females, respectively. Filled symbols indicate affected individuals, while unfilled symbols represent healthy individuals. The *VPS13B* genotypes are depicted below each symbol (n.a., no DNA available). (B) A partial screenshot of the *VPS13B* gene region on chr8:100,123,423–100,123,486 from the UCSC genome browser shows the conservation plot of the VPS13B p.Arg237 variant (highlighted in a red box), with conservation extending down to *Xenopus tropicalis*.

was not affected; therefore, all variants are comparable to the wild-type VPS13B protein in this respect (Figure 2C).

Discussion

CS is a rare neurodevelopmental autosomal recessive condition mainly characterized by developmental delay and postnatal microcephaly. In this study, we present a family with two affected brothers who exhibit the obligate clinical CS signs, such as postnatal microcephaly, developmental delay, and distinctive facial gestalt. When we compared the two brothers, we found divergent clinical signs: for example, certain autistic features were exhibited by Patient 2 whereas myopia and neutropenia were detected in Patient 1 only. Genetic testing of *VPS13B* in the family revealed two LoF variants, p.Phe2268fs*and p.Tyr3434*, as well as two missense variants, p.Arg237Pro and p.Ala2435Val. The heterozygous variant p.Phe2268fs*24 was found to be present in both Patient 1 and Patient 2, which was inherited from their phenotypically unaffected mother. This variant was recently associated with CS and classified as pathogenic (class 5) according to the ACMG criteria (Deignan et al., 2019). The heterozygous variant p.Ala2435Val was also found to be present in both Patient 1 and Patient 2, which was inherited from their phenotypically unaffected mother. The co-segregation of p.Ala2435Val with the heterozygous p.Phe2268fs*24 in all three individuals suggested the presence of a complex VPS13B allele. Based on this, p.Ala2435Val was classified as a VUS (class 3) according to the ACMG guidelines, and current evidence suggests that it may not have a pathogenic impact. Patient 1 had the heterozygous LoF variant p.Tyr3434*, which had not been previously described. This variant appeared *de novo* in Patient 1 and was classified as pathogenic

TABLE 2 Variant pathogenicity interpretation was conducted according to the ACMG standards and guidelines (Richards et al., 2015).

Variant (Protein change)	Arg237Pro	Phe2268Leufs*24	Ala2435Val	Tyr3434*
Population data				
Database (dbSNP)	n.d.	n.d.	rs752558975	n.d.
gnomAD allele frequency	n.d.	n.d.	0.000003098	n.d.
gnomAD allele count	0 Arg237Cys: 26/1601682 Arg237His: 18/1601318	0	5/1614036	0
gnomAD number of homozygotes	0 Arg237Cys: 0 Arg237His: 0	0	0	0
Computational and predictive *in silico* algorithms				
Character	Missense	Frameshift	Missense	stop
Grantham score	103	n.a.	64	n.a.
Mutation taster (*p*-value)	0.999999996377372	1 (NMD)	0.999999927453442	1 (NMD)
PolyPhen-2 (HumVar)	0.997 (pathogenic)	n.a.	0.997 (pathogenic)	n.a.
MutPred 2 probability	0.914 (pathogenic)	n.a.	0.627 (likely pathogenic)	n.a.
SNPs&GO—PhD-SNP	0.940 (disease)	n.a.	0.132 (neutral)	n.a.
SNPs&GO—SNPs&GO	0.769 (disease)	n.a.	0.030 (neutral)	n.a.
SIFT Score	0.00 (intolerant)	n.a.	0.00 (intolerant)	n.a.
Affected PROSITE and ELM Motifs	ELME000012, ELME000063, ELME000136, ELME000137, ELME000159, ELME000358	Truncation/NMD, LoF expected	ELME000052, ELME000159, ELME000358	Truncation/NMD, LoF expected
Functional data—*in vitro* data (cell culture)				
Golgi localization	Decreased	Not tested	Not tested	Not tested
Segregation data				
Co-segregation within the family (autosomal recessive)	Yes	Yes	No	No
Allelic data				
	Paternal allele	Maternal allele	Maternal allele	Paternal allele (*de novo*)
Literature				
	Unpublished	Rafiq et al. (2015)	Unpublished	Unpublished

(Continued)

10.3389/fnins.2024.1488133

10.3389/fnins.2024.1488133

TABLE 2 (Continued)

Variant (Protein change)	Arg237Pro	Phe2268Leufs*24	Ala2435Val	Tyr3434*
ACMG categories				
Population data	**PM2**	**PM2**	**PM2**	**PM2**
Predictive data	**PP3**	**PVS1**	**Inconsistent**	**PVS1**
Functional data	**PS3**	**n.a.**	**n.a.**	**n.a.**
Segregation	**PP1**	**PP1**	**n.a.**	**n.a.**
De novo data	**n.a.**	**n.a.**	**n.a.**	**PS2**
Allelic data	**PM3**	**PM3**	**BP2**	**n.a. (ambiguous for familiar CS diagnosis)**
Reinterpretation according to the ACMG	**Likely pathogenic (class 4)**	**Pathogenic (class 5)**	**Low VUS (class 3)**	**Pathogenic (class 5)**

For population data, the gnomAD database was used (Chen et al., 2024). To obtain computational and predictive *in silico* data, we applied analyses using different tools: Grantham (Grantham, 1974), MutationTaster (Schwarz et al., 2014), PolyPhen-2 (Adzhubei et al., 2013), SNP&GO (Calabrese et al., 2009), MutPred2 (Pejaver et al., 2020), and the SIFT Score (Kumar et al., 2009). Functional data for p.Arg237Pro were obtained using *in vitro* analyses in HeLa cells (refer to Figure 2). Allelic data were obtained from the pedigree and the segregation of the CS phenotype, along with the previously identified genotype of the individuals within the family. The literature was searched for previously published genotypes. The reinterpretation of all variants was performed according to the ACMG standards and guidelines (Deignan et al., 2019). n.a., not applicable and n.d., not documented.

(class 5) due to the presence of a premature stop codon. The rare heterozygous *variant* p.Arg237Pro was found to be present in both Patient 1 and Patient 2 and was inherited from their phenotypically unaffected father. So far, this variant has been annotated in ClinVar as a VUS. Our analysis activated the ACMG criteria PM2, PP3, and PM3 for this variant. Importantly, diminished Golgi enrichment in the subcellular analysis of VPS13B p.Arg237Pro allowed for the additional activation of the PS3 term, resulting in the ACMG classification as likely pathogenic, class 4. In addition, a comparable substitution at the same amino acid position (p.Arg237His) has previously been described as a variant of uncertain significance in a compound heterozygous context, based on a trio exome analysis of a patient with CS (Liu et al., 2021). The combination of genetic and functional analyses helps to elucidate how different variants affect protein function, which will be crucial in the future for explaining phenotypic variability. Overall, genetic analysis suggested that CS in both Patients 1 and 2 was caused by the compound heterozygous VPS13B variants p.Phe2268fs*24 and p.Arg237Pro. We speculated that the *de novo* event p.Tyr3434* dominated the missense variant p.Arg237Pro in Patient 1, resulting in a complete *VPS13B* LoF and, consequently, a CS phenotype that includes neutropenia. Furthermore, we hypothesized that an incomplete LoF of *VPS13B*, due to exon-skipping splice variants, larger in-frame indels, and missense variants of uncertain significance (VUS), likely contributes to the phenotypic complexity and heterogeneity of both CS and *VPS13B*-associated ASD-like behavior (Zorn et al., 2022; Afridi et al., 2024; AbdelAleem et al., 2023). This hypothesis was supported by the altered CS phenotype observed in Patient 2 with ASD-like behavior. Together, this also suggests that establishing a phenotype–genotype correlation will improve patient management by anticipating specific clinical manifestations.

VPS13B missense variants have been rarely linked to CS due to low detection rates and limited biological evidence. A total of 4,973 coding missense variants have been reported to date, of which 109 have been found in homozygosity. The clinical significance of these variants in ClinVar is categorized as follows: 27 classified as benign/likely benign, 42 with conflicting interpretations, 28 as variants of uncertain significance (VUS), and 12 without sufficient documentation. According to data from the patient cohort, literature, and ClinVar, 42 missense variants of VPS13B have been associated with CS so far (Zorn et al., 2022). VPS13B missense variants have also been linked to autism spectrum disorders (ASDs), as noted in a previous study (Yu et al., 2013). The connection between VPS13B and ASD, particularly in patients with CS, raises questions about whether some variants may contribute to ASD-like behavior (Rafiq et al., 2015; Ionita-Laza et al., 2014; Howlin, 2001). Further exploration of this possibility could help identify more specific clinical subtypes of CS, potentially allowing for personalized care and management strategies. Notably, the majority of established CS-causing VSP13B missense variants cluster within or near the Vps13 adaptor binding (VAB) domain, which facilitates the membrane recruitment of the VPS13B C-terminus to the Golgi complex (Zorn et al., 2022; Levine, 2022). The cell biological contribution of the previously described N-terminal missense variant VPS13B p.Arg237Pro, which localizes to the highly conserved N-terminal VPS13 region (VPS13_N, also known as RBG2), to CS and the

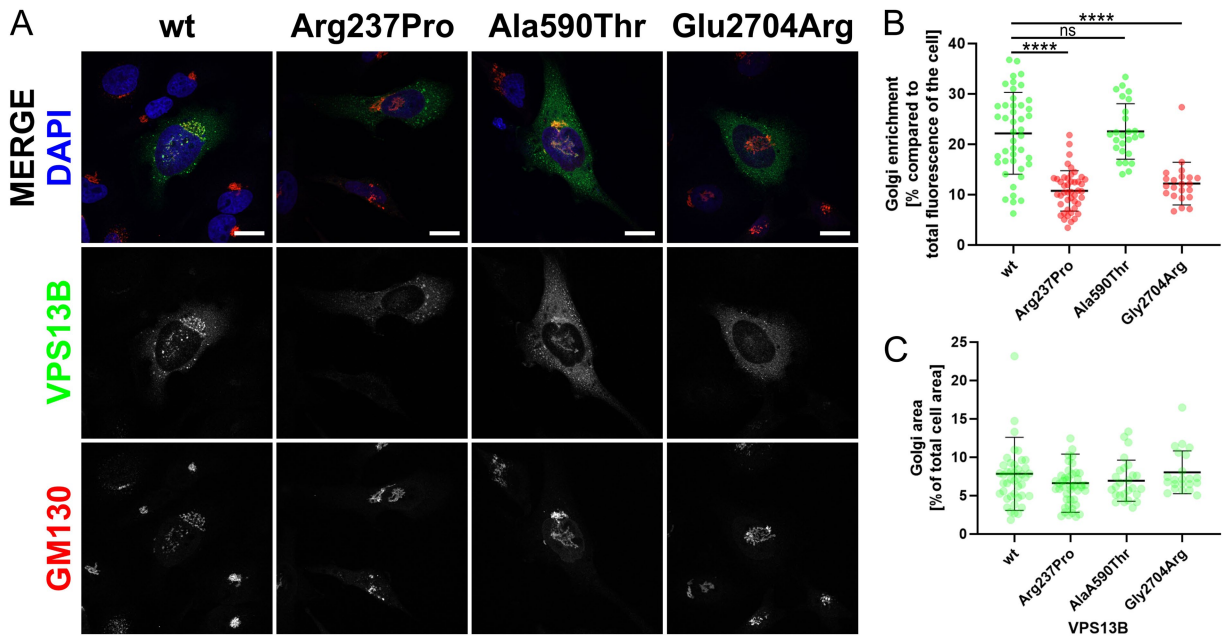

FIGURE 2
Golgi localization. (A) *HeLa* cells were transfected with different pcDNA3.1_VPS13B constructs, encoding either wild-type (wt) or mutated VPS13B (missense variants p.Arg237Pro, p.Ala590Thr, p.Glu2704Arg). Twenty-four hours post-transfection, all cells were processed for immunostaining of VPS13B (green) and GM130 (red). Imaging was performed using a Zeiss spinning disk microscope. Nuclei were stained with DAPI (blue). The scale bar represents 20 μm. (B) Quantitative analysis of the subcellular Golgi enrichment of VPS13B was conducted using ImageJ. Two ROIs were defined for each analyzed cell: one total cell ROI, drawn around the cell area, and one Golgi ROI, drawn around the GM130-positive Golgi area. Statistical analysis was conducted on the Golgi enrichment by calculating the percentage of the VPS13B fluorescence intensity at the Golgi compared to the total cellular fluorescence intensity. (C) Analysis of the Golgi area of VPS13B was conducted using ImageJ. Both ROIs were used to measure the area. Statistical analysis was performed by calculating the percentage of the occupied Golgi area compared to the total cellular area.

ADS-like behavior is currently unclear (Levine, 2022; Velayos-Baeza et al., 2004). The VPS13B region around the position p.Arg237 is highly conserved in vertebrates. The human VPS13_N domain has not been characterized; however, a study utilizing cryo-electron microscopy analyzed the VPS13 N-terminal regions of the fungi *Chaetomium thermophilum* and yeast *Saccharomyces cerevisiae* (Li et al., 2020). The VPS13 N-terminal region was postulated to mediate the lipid membrane attachment toward the donor lipid membrane. Mutation of critical hydrophobic amino acids into charged amino acids in the Vps13p N-terminal region of *S. cerevisiae* reduced yeast sporulation, indicating defective lipid transport (Li et al., 2020). Overall, genetic analysis of VPS13B p.Arg237Pro suggested that the VPS13_N domain is critical for VPS13B function, impacts VPS13B Golgi enrichment, and may affect the stability of the VPS13B lipid membrane complex.

In conclusion, while phenotyping and genetic testing are powerful tools for the initial identification of genetic variants, functional studies are indispensable for the accurate interpretation of missense variants. By combining these strengths, especially in the era of NGS, rigorous functional analysis will enhance our ability to diagnose accurately and consequently improve our understanding of molecular pathomechanisms. Furthermore, this study highlights the importance of integrating accurate genetic testing, comprehensive evaluation, and functional analyses to elucidate the complex phenotype–genotype correlation and the pathogenic mechanisms underlying CS. Such integration not only improves accurate diagnosis but also helps identify new therapeutic targets and improve personalized patient care. To increase understanding of CS and related neurodevelopmental disorders, future research should focus on larger cohort studies to better assess the prevalence and spectrum of VPS13B variants. Functional assays, particularly *in vitro* and *in vivo* models, are essential for validating the effects of newly identified missense variants on VSP13B function and may help uncover the molecular mechanisms driving phenotypic variability. In addition, longitudinal studies, including standardized clinical assessments and precise phenotyping of patients with CS, may assist in identifying potential genetic modifiers.

Data availability statement

The original contributions presented in the study are included in the article/supplementary material, further inquiries can be directed to the corresponding author.

Ethics statement

Ethical approval was not required for the study involving human samples in accordance with the local legislation and institutional requirements. Written informed consent for participation in this study was provided by the each adult and participants' legal guardians.

Author contributions

GS: Investigation, Writing – original draft. CM: Formal analysis, Writing – original draft, Data curation. JKo: Data curation, Formal analysis, Writing – original draft. ES: Investigation, Writing – original draft. ZM: Data curation, Methodology, Writing – original draft. JK: Writing – review & editing. NH: Data curation, Investigation, Methodology, Writing – original draft. JKü: Formal analysis, Validation, Writing – original draft, Writing – review & editing. C-EO: Investigation, Writing – original draft. WS: Conceptualization, Formal analysis, Funding acquisition, Investigation, Project administration, Resources, Supervision, Validation, Writing – original draft, Writing – review & editing.

Funding

The author(s) declare that financial support was received for the research, authorship, and/or publication of this article. CM received an ERASMUS scholarship for the duration of the project. For cell biological research on VPS13B, WS was funded by a DFG grant (SE2266_1-1).

Acknowledgments

We would like to thank Magdalena Feldhahn, CeGaT, Tübingen, Germany, for bioinformatical support.

Conflict of interest

ES was employed by company Praxis für Humangenetik. ZM was employed by company Diagenom GmbH. JK was employed by company Zentrum für Humangenetik, SYNLAB MVZ Humangenetik Freiburg. NH was employed by companies Zentrum für Humangenetik Tübingen and CeGaT.

The remaining authors declare that the research was conducted in the absence of any commercial or financial relationships that could be construed as a potential conflict of interest.

Publisher's note

References

AbdelAleem, A., Haddad, N., Al-Ettribi, G., Crunk, A., and Elsotouhy, A. (2023). Cohen syndrome and early-onset epileptic encephalopathy in male triplets: two disease-causing mutations in VPS13B and NAPB. *Neurogenetics* 24, 103–112. doi: 10.1007/s10048-023-00710-2

Abou Tayoun, A. N., Pesaran, T., DiStefano, M. T., Oza, A., Rehm, H. L., Biesecker, L. G., et al. (2018). Recommendations for interpreting the loss of function PVS1 ACMG/AMP variant criterion. *Hum. Mutat.* 39, 1517–1524. doi: 10.1002/humu.23626

Adzhubei, I., Jordan, D. M., and Sunyaev, S. R. (2013). Predicting functional effect of human missense mutations using PolyPhen-2. *Curr. Prot.* 7:Unit7.20. doi: 10.1002/0471142905.hg0720s76

Afridi, T. U. K., Fatima, A., Satti, H. S., Akram, Z., Yousafzai, I. K., Naeem, W. B., et al. (2024). Exome sequencing in four families with neurodevelopmental disorders: genotype-phenotype correlation and identification of novel disease-causing variants in VPS13B and RELN. *Mol. Gen. Genomics.* 299:55. doi: 10.1007/s00438-024-02149-y

Calabrese, R., Capriotti, E., Fariselli, P., Martelli, P. L., and Casadio, R. (2009). Functional annotations improve the predictive score of human disease-related mutations in proteins. *Hum. Mutat.* 30, 1237–1244. doi: 10.1002/humu.21047

Chen, S., Francioli, L. C., Goodrich, J. K., Collins, R. L., Kanai, M., Wang, Q., et al. (2024). A genomic mutational constraint map using variation in 76,156 human genomes. *Nature* 625, 92–100. doi: 10.1038/s41586-023-06045-0

Deignan, J. L., Chung, W. K., Kearney, H. M., Monaghan, K. G., Rehder, C. W., Chao, E. C., et al. (2019). Points to consider in the reevaluation and reanalysis of genomic test results: a statement of the American College of Medical Genetics and Genomics (ACMG). *Genet. Med.* 21, 1267–1270. doi: 10.1038/s41436-019-0478-1

El Chehadeh-Djebbar, S., Blair, E., Holder-Espinasse, M., Moncla, A., Frances, A. M., Rio, M., et al. (2013). Changing facial phenotype in Cohen syndrome: towards clues for an earlier diagnosis. *Eur. J. Hum. Genet.* 21, 736–742. doi: 10.1038/ejhg.2012.251

Grantham, R. (1974). Amino acid difference formula to help explain protein evolution. *Science* 185, 862–864. doi: 10.1126/science.185.4154.862

Gueneau, L., Duplomb, L., Sarda, P., Hamel, C., Aral, B., Chehadeh, S. E., et al. (2014). Congenital neutropenia with retinopathy, a new phenotype without intellectual deficiency or obesity secondary to VPS13B mutations. *Am. J. Med. Genet. A* 164A, 522–527. doi: 10.1002/ajmg.a.36300

Hanna, M., Guillén-Samander, A., and De Camilli, P. (2023). RBG motif bridge-like lipid transport proteins: structure, functions, and open questions. *Annu. Rev. Cell Dev. Biol.* 39, 409–434. doi: 10.1146/annurev-cellbio-120420-014634

Howlin, P. (2001). Autistic features in Cohen syndrome: a preliminary report. *Dev. Med. Child Neurol.* 43, 692–696. doi: 10.1111/j.1469-8749.2001.tb00143.x

Ionita-Laza, I., Capanu, M., De Rubeis, S., McCallum, K., and Buxbaum, J. D. (2014). Identification of rare causal variants in sequence-based studies: methods and applications to VPS13B, a gene involved in Cohen syndrome and autism. *PLoS Genet.* 10:e1004729. doi: 10.1371/journal.pgen.1004729

Katzaki, E., Pescucci, C., Uliana, V., Papa, F. T., Ariani, F., Meloni, I., et al. (2007). Clinical and molecular characterization of Italian patients affected by Cohen syndrome. *J. Hum. Genet.* 52, 1011–1017. doi: 10.1007/s10038-007-0208-4

Kolehmainen, J., Black, G. C., Saarinen, A., Chandler, K., Clayton-Smith, J., Träskelin, A. L., et al. (2003). Cohen syndrome is caused by mutations in a novel gene, COH1, encoding a transmembrane protein with a presumed role in vesicle-mediated sorting and intracellular protein transport. *Am. J. Hum. Genet.* 72, 1359–1369. doi: 10.1086/375454

Kumar, P., Henikoff, S., and Ng, P. C. (2009). Predicting the effects of coding non-synonymous variants on protein function using the SIFT algorithm. *Nat. Protoc.* 4, 1073–1081. doi: 10.1038/nprot.2009.86

Lee, Y. K., Hwang, S. K., Lee, S. K., Yang, J. E., Kwak, J. H., Seo, H., et al. (2020). Cohen syndrome patient iPSC-derived Neurospheres and forebrain-like glutamatergic neurons reveal reduced proliferation of neural progenitor cells and altered expression of synapse genes. *J. Clin. Med.* 9:1886. doi: 10.3390/jcm9061886

Lee, Y. K., Lee, S. K., Choi, S., Huh, Y. H., Kwak, J. H., Lee, Y. S., et al. (2020). Autophagy pathway upregulation in a human iPSC-derived neuronal model of Cohen syndrome with VPS13B missense mutations. *Mol. Brain* 13:69. doi: 10.1186/s13041-020-00611-7

Levine, T. P. (2022). Sequence analysis and structural predictions of lipid transfer bridges in the repeating Beta groove (RBG) superfamily reveal past and present domain variations affecting form, function and interactions of VPS13, ATG2, SHIP164, hobbit and Tweek. *Contact (Thousand Oaks)* 5:251525642211343. doi: 10.1177/25152564221134328

Li, P., Lees, J. A., Lusk, C. P., and Reinisch, K. M. (2020). Cryo-EM reconstruction of a VPS13 fragment reveals a long groove to channel lipids between membranes. *J. Cell Biol.* 219:1161. doi: 10.1083/jcb.202001161

Liu, Y., Liu, X., Qin, D., Zhao, Y., Cao, X., Deng, X., et al. (2021). Clinical utility of next-generation sequencing for developmental disorders in the rehabilitation department: experiences from a single Chinese center. *J. Mol. Neurosci.* 71, 845–853. doi: 10.1007/s12031-020-01707-4

Mochida, G. H., Rajab, A., Eyaid, W., Lu, A., Al-Nouri, D., Kosaki, K., et al. (2004). Broader geographical spectrum of Cohen syndrome due to COH1 mutations. *J. Med. Genet.* 41:e87. doi: 10.1136/jmg.2003.014779

Pejaver, V., Urresti, J., Lugo-Martinez, J., Pagel, K. A., Lin, G. N., Nam, H. J., et al. (2020). Inferring the molecular and phenotypic impact of amino acid variants with MutPred2. *Nat. Commun.* 11:5918. doi: 10.1038/s41467-020-19669-x

Rafiq, M. A., Leblond, C. S., Saqib, M. A., Vincent, A. K., Ambalavanan, A., Khan, F. S., et al. (2015). Novel VPS13B mutations in three large Pakistani Cohen syndrome families suggests a Baloch variant with autistic-like features. *BMC Med. Genet.* 16:41. doi: 10.1186/s12881-015-0183-0

Reikofski, J., and Tao, B. Y. (1992). Polymerase chain reaction (PCR) techniques for site-directed mutagenesis. *Biotechnol. Adv.* 10, 535–547. doi: 10.1016/0734-9750(92)91451-J

Richards, S., Aziz, N., Bale, S., Bick, D., das, S., Gastier-Foster, J., et al. (2015). Standards and guidelines for the interpretation of sequence variants: a joint consensus recommendation of the American College of Medical Genetics and Genomics and the Association for Molecular Pathology. *Genet. Med.* 17, 405–424. doi: 10.1038/gim.2015.30

Satam, H., Joshi, K., Mangrolia, U., Waghoo, S., Zaidi, G., Rawool, S., et al. (2023). Next-generation sequencing technology: current trends and advancements. *Biology (Basel)* 12:997. doi: 10.3390/biology12070997

Schwarz, J. M., Cooper, D. N., Schuelke, M., and Seelow, D. (2014). MutationTaster2: mutation prediction for the deep-sequencing age. *Nat. Methods* 11, 361–362. doi: 10.1038/nmeth.2890

Seifert, W., Holder-Espinasse, M., Kühnisch, J., Kahrizi, K., Tzschach, A., Garshasbi, M., et al. (2009). Expanded mutational spectrum in Cohen syndrome, tissue expression, and transcript variants of COH1. *Hum. Mutat.* 30, E404–E420. doi: 10.1002/humu.20886

Seifert, W., Kuhnisch, J., Maritzen, T., Horn, D., Haucke, V., and Hennies, H. C. (2011). Cohen syndrome-associated protein, COH1, is a novel, giant Golgi matrix protein required for Golgi integrity. *J. Biol. Chem.* 286, 37665–37675. doi: 10.1074/jbc.M111.267971

Seifert, W., Kuhnisch, J., Maritzen, T., Lommatzsch, S., Hennies, H. C., Bachmann, S., et al. (2015). Cohen syndrome-associated protein COH1 physically and functionally interacts with the small GTPase RAB6 at the Golgi complex and directs neurite outgrowth. *J. Biol. Chem.* 290, 3349–3358. doi: 10.1074/jbc.M114.608174

Vacca, F., Yalcin, B., and Ansar, M. (2024). Exploring the pathological mechanisms underlying Cohen syndrome. *Front. Neurosci.* 18:1431400. doi: 10.3389/fnins.2024.1431400

Velayos-Baeza, A., Vettori, A., Copley, R. R., Dobson-Stone, C., and Monaco, A. P. (2004). Analysis of the human VPS13 gene family. *Genomics* 84, 536–549. doi: 10.1016/j.ygeno.2004.04.012

Yu, T. W., Chahrour, M. H., Coulter, M. E., Jiralerspong, S., Okamura-Ikeda, K., Ataman, B., et al. (2013). Using whole-exome sequencing to identify inherited causes of autism. *Neuron* 77, 259–273. doi: 10.1016/j.neuron.2012.11.002

Zare Ashrafi, F., Akhtarkhavari, T., Fattahi, Z., Asadnezhad, M., Beheshtian, M., Arzhangi, S., et al. (2023). Emerging epidemiological data on rare intellectual disability syndromes from analyzing the data of a large Iranian cohort. *Arch. Iran. Med.* 26, 186–197. doi: 10.34172/aim.2023.29

Zorn, M., Kuhnisch, J., Bachmann, S., and Seifert, W. (2022). Disease relevance of rare VPS13B missense variants for neurodevelopmental Cohen syndrome. *Sci. Rep.* 12:9686. doi: 10.1038/s41598-022-13717-w

frontiers | Frontiers in Neuroscience

TYPE Review
PUBLISHED 28 April 2025
DOI 10.3389/fnins.2025.1534061

OPEN ACCESS

EDITED BY
Andreas Hermann,
University Hospital Rostock, Germany

REVIEWED BY
Jay Penney,
University of Prince Edward Island, Canada
Sean Munro,
University of Cambridge, United Kingdom

*CORRESPONDENCE
Laura Elizabeth Swan
✉ laura.swan@liverpool.ac.uk

RECEIVED 25 November 2024
ACCEPTED 14 March 2025
PUBLISHED 28 April 2025

CITATION
Swan LE (2025) VPS13 and bridge-like lipid transporters, mechanisms, and mysteries. *Front. Neurosci.* 19:1534061. doi: 10.3389/fnins.2025.1534061

VPS13 and bridge-like lipid transporters, mechanisms, and mysteries

Laura Elizabeth Swan*

Department of Biochemistry, Cell and Systems Biology, University of Liverpool, Liverpool, United Kingdom

Bridge-like lipid transporters (BLTPs) have recently been revealed as key regulators of intraorganellar lipid trafficking, with their loss being associated with defective synaptic signalling and congenital neurological diseases. This group consists of five protein subfamilies [BLTP1-3, autophagy-related 2 (ATG2), and vacuolar protein sorting 13 (VPS13)], which mediate minimally selective lipid transfer between cellular membranes. Deceptively simple in both structure and presumed function, this review addresses open questions as to how bridge-like transporters work, the functional consequences of bulk lipid transfer on cellular signalling, and summarises some recent studies that have shed light on the surprising level of regulation and specificity found in this family of transporters.

KEYWORDS

BLTP, VPS13, ATG2, scramblase activity, lipid transfer activity, membrane contacts

Introduction

For several decades, subcellular organelles were considered distinct entities, whose membrane lipid content could only be changed by the action of organelle-targeted enzymes, by subcellular sorting performed by adaptor proteins bending and sorting lipids into specific geometries to be scissioned and trafficked away from its parent organelle, or by admixture of organelle membranes via mechanisms such as SNARE-mediated fusion. Excitingly, recent decades have revealed the existence of non-vesicular lipid transfer by specialised transporters at proteinaceous organelle-to-organelle junctions (membrane contacts) whereby selected membrane lipids are exchanged across a narrow organelle-to-organelle gap.

In the last few years, genetic studies combined with structural insight from protein modelling (Braschi et al., 2022; Neuman et al., 2022a) revealed a significant group of structurally similar proteins, where the lipid transporter, rather than fostering an exchange mechanism, forms a physical bridge that spans the gap between a donor and a receiver organelle. These bridge-like transfer proteins (BLTPs) are formed by multiple repeats of one motif: a repeating beta groove (RBG) (Neuman et al., 2022a), which forms an extremely long semi-open tube with a hydrophobic interior (Li et al., 2020). These repeats and the tube they form are half-open to solvent, whereby lipids are conducted from one end to the other of the organelle gap by a single protein. This gap can span as much as ~30 nm between organelles and is known to have critical roles in establishing membrane function. Our current understanding of the function of BLTPs is relatively crude: they are thought to be comparatively unselective in the lipids they transport and to act essentially as a 'firehose' delivering phospholipids to their target membranes. However, as our understanding of these mechanisms develops, researchers have found a surprising amount of subtlety as to how each of the five members of the BLTP family functions, and how lipid transfer via each of these transporters leads to signalling and trafficking deficits in human patients and model organisms.

Understanding the properties, regulation, and function of this class of proteins will provide significant insight into how organelles maintain their identity, along with transmembrane cargo and adaptors, while allowing response to physiological changes. This review discusses some of the key open questions concerning the nature and function of these proteins and presents current evidence as to how this family of proteins works to drive organelle function.

The structure of bridge-like transporters

The group of bridge-like transporters (BLTPs) form a small, but well-conserved (Table 1) group of five protein groups(Braschi et al., 2022; Neuman et al., 2022a) BLTP1-3, autophagy-related 2 (ATG2) and vacuolar protein sorting 13 (VPS13), and their paralogues. The group shares some common features: an N-terminal Chorein domain [a scoop-shaped domain with a hydrophobic interior, whose evolutionary origins may extend as far back as a common ancestry with bacteria (Neuman et al., 2022a; Levine, 2019)], which directly funnels into the interior of anywhere from 6 to 17 repeats of the Repeating Beta Groove (RBG) motif (Neuman et al., 2022a; Levine, 2022). The RBG motif is a five antiparallel beta-stranded repeat that curves into a U or 'taco' shape and terminates in an unstructured loop, which when repeated, spans the distance between donor and acceptor membrane. BLTPs show extensive and conserved cytosolic loops and patches that decorate the cytosolic length of the tube formed by the RBG repeats (Dall'Armellina et al., 2023), but few specific interactors of these patches are known. At both the N- and C-termini of these proteins, which form the interfaces with donor and acceptor membranes, the proteins become more specialised among individual family members. Nearly every member of this family has been associated with human disease (Ugur et al., 2020; see Table 2), highlighting the important physiological role that this form of lipid transport plays.

Very loosely, the BLTP family of proteins can be split into two groups: BLTP1-3, which do not have extensive C-terminal interfaces with adaptor proteins, and ATG2/VPS13 families (designated BLTP4/BLTP5 respectively), which have extensive C-terminal specialisations that form a platform to recruit multiple adaptor factors on their target membrane. For a cartoon of the domain structures of BLTP family proteins, see Figure 1. A model of their association with membranes is presented in Figure 2.

BLTP1 and BLTP2 have a N-terminal transmembrane helix that anchors the bridge (Kang et al., 2024a) to a prospective donor membrane, whereas the N-terminus of the group proteins formed by ATG2, VPS13 loosely anchor to their N-terminal membranes either by interacting with tethering proteins via peptide motifs or by weak interaction with membranes through their chorein domain (Levine, 2022; see Table 2). The C-terminus of the ATG2/VPS13 grouping is more highly specialised and provides a surface for interactions with adaptor proteins on the acceptor or target membrane. Interestingly, the recruiting motifs for BLTPs are often either small GTPases and/or phosphoinositide lipids (see Table 2), which suggest that recruitment may be dynamic and tied to signalling. In fact, in studies so far, very often the recruitment of BLTPs to specific junctions depends on the level of expression of their putative interaction partners. BLTP3 proteins are even less specialised at their N and C termini (having neither transmembrane helix nor specialised C terminal domains) and may be recruited by interactions with small GTPases(Hanna et al., 2025; Hanna et al., 2022; Gillingham et al., 2019; Wang J. et al., 2024).

In BLTP1-2, C-terminal specialisations are relatively simple: The C terminus is denoted by a single-helical segment, which has been demonstrated to interact with membrane phosphoinositide lipids (Wang et al., 2022; Neuman et al., 2022b), while peptide motifs in BLTP2 contact membrane adaptor proteins (Dai et al., 2025). In the ATG2/VPS13 grouping, this is more complicated: For ATG2A/B, the C-terminus sports an amphipathic helical bundle and an interface to interact with the WDR (WD40 repeat) family of proteins, such as WIPI4 (Chowdhury et al., 2018), which itself binds the phosphoinositide lipid PI3P. VPS13 family proteins are even further specialised with a cluster of well-conserved structures at the C terminus: a small globular domain [of varying fold in the different VPS13 family members, see Figure 1 (Levine, 2022; Dall'Armellina et al., 2023)], a 'collar' of Vps13 Adaptor-Binding (VAB) domain repeats forming a similar fold to WDR40 repeats at the end of the tube formed by the RBG repeats, a liprin-like amphipathic helical domain

TABLE 1 Known orthologues of BLTP proteins (alternative names for the same gene in brackets).

H. sapiens	*D. melanogaster*	*C. elegans*	*S. cerevisiae*	*D. discoideum*	*A. thaliana*
BLTP1 (KIAA1109)	Tweek	lpd-3	CSF1	DDB_G0289829	
BLTP2 (KIAA0100)	Hobbit	bltp-2	Fmp27 (HOB1), HOB2		SABRE, KINKY POLLEN
BLTP3A (UHRF1BP1) BLTP3B (SHIP164/ UHRF1BP1L)	CG34126	C44H4.4		DDB_G0279089	AT3G20720 (Q84R14)
ATG2A, ATG2B	Atg2	atg-2	ATG2	Atg2 (DDB_G0277419) DDB_G0282057	ATG2 (Wang et al., 2011)
VPS13A (ChAc) VPS13B, VPS13C VPS13D	Vps13, Vps13B, Vps13D	VPS-13A (T08g11) VPS-13D (C25H3.11) (Levine, 2022)	VPS13	VPS13A VPS13B VPS13C (TipC), VPS13D VPS13E VPS13F (Leiba et al., 2017)	AtVPS13S (Shrubby) AtVPS13M1 AtVPS13M2(Velayos-Baeza et al., 2004) AtVPS13X (Levine, 2022)

TABLE 2 Diseases associated with BLTPs, recruitment factors for N terminal and C terminal domains of BLTPs with specific subdomains if known.

Protein	Disease	N-terminal membrane (except chorein domain)	C-terminal membrane
BLTP1 (KIAA1109)	Alkuraya-Kucinskas Syndrome (Alazami et al., 2015; Gueneau et al., 2018) (MIM 617822)	Transmembrane helix (Kang et al., 2024a) spigot (C1orf43) via chorein and N terminal RBGs (Kang et al., 2024a) ER	Polybasic patch (expected to bind Phosphoinositide lipids) (Wang et al., 2022) Plasma membrane
BLTP2 (KIAA0100)		transmembrane helix (Neuman et al., 2022b) ER	Phosphoinositide lipids (PI, PIP, PIP2, PIP3) (Neuman et al., 2022b) PI4P (Dai et al., 2025) FAM102A/B *via* helical binding domain (Dai et al., 2025) Amphiphysin2 *via* RXP SH3 binding motif (Dai et al., 2025) Plasma membrane
BLTP3A (UHRF1BP1)	Systemic lupus erythematosus (Wen et al., 2020)	**rab7** *via* RBG2 (Hanna et al., 2025) late endosome/lysosome	**Rab45** (Hanna et al., 2022) Centrosome ? via RBG6 (Hanna et al., 2025) VAMP7-positive vesicles LC3, GABARAP-*via* LIR motif (Hanna et al., 2025) Stressed/damaged lysosome
BLTP3B (SHIP164/ UHRF1BP1L)	Parkinson's disease (Jansen et al., 2017)	**Rab5** (Gillingham et al., 2019) Early endosomes **RhoBTB3** (Wang et al., 2024) Golgi	syntaxin 6 (Otto et al., 2010) *via* LxxYY motif (Hanna et al., 2022) Early/recycling endosomes DyneinLL1/2 (Hanna et al., 2022) via C-terminal peptide **Rab45** (Hanna et al., 2022) Centrosome VPS26B (Wang et al., 2024) M6PR-positive endosome (not retromer)
ATG2A(BLTP4A) ATG2B (BLTP4B)	ATG2B: Familial susceptibility to myeloproliferative neoplasms (MIM: 616604) (Saliba et al., 2015)	**ATG9** (Wang et al., 2024) **TMEM41B** **VMP1** (Ghanbarpour et al., 2021) ER	Liprin-like domain (Kotani et al., 2018; Van Vliet et al., 2022) GABARAP/GABARAPL1/LC3A via LIR motif (Bozic et al., 2020) WIPI4 (Maeda et al., 2019; Chowdhury et al., 2018) via YFS motif (Zheng et al., 2017) **ATG9** (Wang et al., 2024; Van Vliet et al., 2022) Phosphoinositide lipids (PI3P) (Kaminska et al., 2016) Phagophore TOM40 via MAM localisation domain (MLD) (Tang et al., 2019) Mitochondria associated ER membrane/phagophore
VPS13A (BLTP5A)	Chorea-acanthocytosis (MIM: 200150) (Rampoldi et al., 2001)	VAPA/B via FFAT-motif (Yeshaw et al., 2019) ER	**XK** (Adlakha et al., 2022) via PH domain (Guillen-Samander et al., 2022) Plasma membrane ? via PH domain (Guillen-Samander et al., 2022) mitochondria SNX5 via VAB (Tornero-Ecija et al., 2023) **rab7** (Munoz-Braceras et al., 2019) late endosome/lysosome Lipid membranes via liprin-like domain/amphipathic helices (Kumar et al., 2018)

(Continued)

10.3389/fnins.2025.1534061

TABLE 2 (Continued)

Protein	Disease	N-terminal membrane (except chorein domain)	C-terminal membrane
VPS13B (BLTP5B)	Cohen syndrome (MIM: 216550) (Kolehmainen et al., 2003)	FAM177A1 (Ugur et al., 2024) via? Golgi	Sec23IP via VAB (Du et al., 2024) ER-exit site (ERES) Phosphoinositide lipids (PI4P) (Du et al., 2024) via PH (PI3P) (Koike and Jahn, 2019) via? **Rab14** (Pietra et al., 2013) endosomes Syntaxin 6 and syntaxin 13 together (Koike and Jahn, 2019) Transferrin receptor-positive early/recycling endosomes **rab6A/B/C** (Seifert et al., 2015) Golgi
VPS13C (BLTP5C)	Autosomal recessive early onset Parkinson's Disease 23 (Lesage et al., 2016; Jansen et al., 2017) (MIM: 616840) Dementia with Lewy bodies (Smolders et al., 2021) (MIM:127750)	VAPA/B via FFAT-motif ER	**pT73-rab10** (Schröder et al., 2024) lysosomes **rab7** via VAB (Hancock-Cerutti et al., 2022) late endosomes/lysosomes liprin-like domain/amphipathic helices (Kumar et al., 2018) phosphoinositide lipids
VPS13D (BLTP5D)	Autosomal recessive Spinocerebellar Ataxia 4 (Seong et al., 2018; Gauthier et al., 2018) (MIM: 607317)	? via N terminal region (Wang et al., 2021) mitochondria VAPB via pFFAT-motif (Guillen-Samander et al., 2021) ER	**Mitofusin 2** (Shen et al., 2021) **Miro1/2** via VAB (Guillen-Samander et al., 2021) Mitochondria/peroxisome liprin-like domain (Wang et al., 2021) TSG101 via VAB domain (Wang et al., 2021) lipid droplets K63-linked ubiquitin via UBA domain (Anding et al., 2018) p97/VCP via UBA and VAB domains (Du et al., 2021)
yeast VPS13		LIR motif ER	**MCP1** to VAB domain via PXXP motif (Adlakha et al., 2022; Bean et al., 2018; Gonzalez Montoro et al., 2018) mitochondria spo71 to VAB domain via PXXP motif (Bean et al., 2018; Park et al., 2013) prospore membrane ypt35 to VAB domain via PXXP motif (Bean et al., 2018) endosome/vacuole **Arf1** via PH domain (Kolakowski et al., 2021) Golgi phosphoinositide lipids (PI3P) (Rzepnikowska et al., 2017; De et al., 2017) [$PI(4,5)P_2$] (Kolakowski et al., 2021)

Bold underline, proteins with scramblase activity. **Bold italics**, small GTPases or dynamin-like GTPases. Interactors that have not been definitively associated with a direct physical interaction with the N or C terminus of BLTPs are omitted or indicated with a question mark. Red, organelle recruitment defined by the specified interactor(s). Please note that other organelle junctions sporting BLTPs have been found where the interaction that defines the recruitment is not known. LIR, LC3 interacting region.

10.3389/fnins.2025.1534061

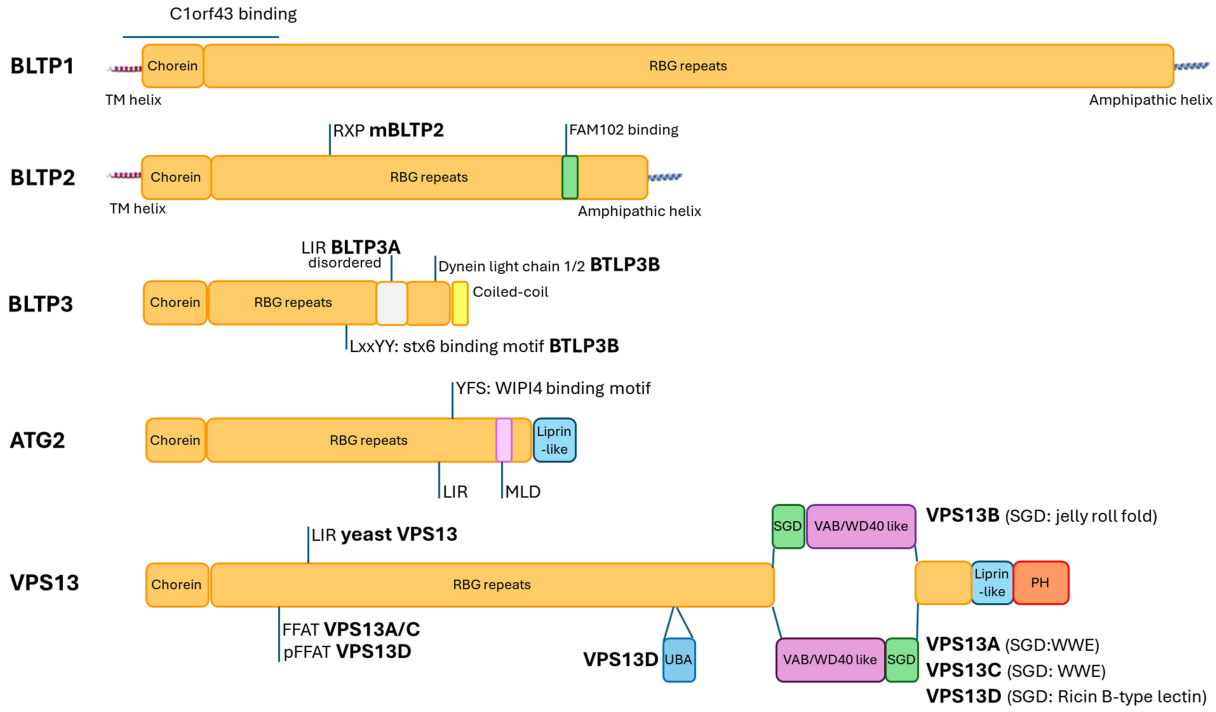

FIGURE 1
Cartoon of domain structure of BLTPs, with some specific interaction surfaces labelled. MLD: MAM localisation domain, UBA: ubiquitin-associated; SGD: small globular domain, VAB: VPS13 adaptor-binding domain, PH: pleckstrin homology domain, LIR: LC3 interacting motif; RXP: SH3 binding peptide motif; (p)FFAT: (phospho) Two phenylalanines in an acidic tract peptide motif.

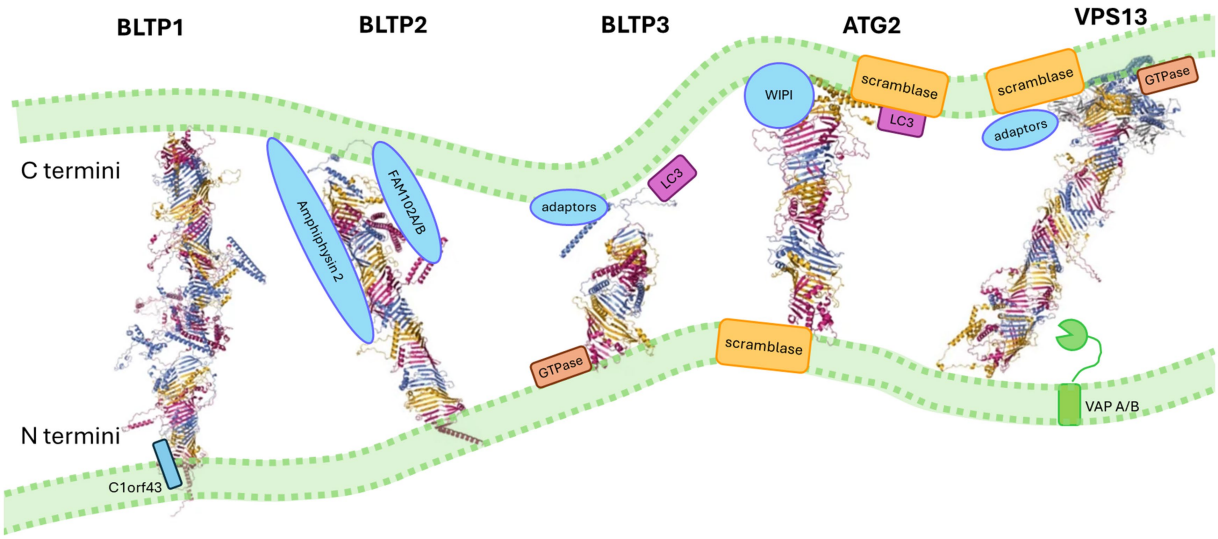

FIGURE 2
Representative structures of BLTPs. Models of generic BLTP family members taken from Braschi et al. (2022), where the authors coloured each RBG repeat in magenta, gold, and teal sequentially (https://creativecommons.org/licenses/by/4.0/). Proteins are aligned, so the N terminus interacts with the lower of the two generic membranes. When orthologues or paralogues bind interactors of a similar functional type, then the type of protein, rather than the specific interactor, is named.

which, models suggest, contacts and disturbs the target membrane outer leaflet (Dall'Armellina et al., 2023), and PH (pleckstrin homology) domains all decorating the C-terminal region. In VPS13 family proteins, the PH domain also interacts with phosphoinositide lipids (Rzepnikowska et al., 2017; De et al., 2017; John Peter et al., 2017).

In VPS13/ATG2 family proteins, this extra series of C-terminal domains appears to specify an interacting surface for proteins on the adaptor end of the bridge to recruit BLTPs to their target membrane, allowing dynamic refinement of the recruitment of bridge-like transporters to their target membranes. Ultimately, however, the C-terminal specialisations of these proteins are not completely

necessary for function, as loss of ATG2 in mammalian cells can be rescued by strong overexpression of the N-terminal portion of ATG2 alone (Valverde et al., 2019). This suggests that the minimum requirement is the ability to retrieve lipids from the donor membrane and some kind of channel to carry the solubilised lipid, which can, if necessary, randomly incorporate into its acceptor membrane.

A brief overview of BLTP functions

Functionally, BLTPs are known to play a crucial role in autophagy, particularly in facilitating the rapid expansion of the phagophore membrane through proteins such as the well-studied ATG2 proteins (recently reviewed here; Vargas Duarte and Reggiori, 2023; Choi et al., 2024) although other BLTPs, such as VPS13 family members (Anding et al., 2018; Munoz-Braceras et al., 2015; Lei et al., 2022), have been found to contribute to autophagy in a number of model systems, including yeast where VPS13 and ATG2 act redundantly(Dabrowski et al., 2023). Intriguingly, BLTP3A, while not recruited by autophagy (Hanna et al., 2025), has recently been implicated in a similar process: Conjugation of Atg8 to Single Membranes (CASM) reviewed here (Durgan and Florey, 2022), a non-canonical process where single membranes rather than phagophores recruit elements of the autophagy machinery, dependent on the activity of the lysosomal V-ATPase. The other family members are also responsible for large membrane reorganisations: BLTP1 is required for phagocytosis in macrophages (Jeng et al., 2019) and astrocytes (Kang et al., 2023).

Beyond autophagy, members of this family are implicated in numerous essential cellular processes, such as mitochondrial homeostasis (Jansen et al., 2017; Yeshaw et al., 2019; Munoz-Braceras et al., 2019; Lesage et al., 2016; Anding et al., 2018; Nagata et al., 2018; Pandey et al., 2024), cell polarity (Pietra et al., 2013), organelle sorting (Otto et al., 2010), cargo trafficking (Koike and Jahn, 2019; Seifert et al., 2015; Neuman and Bashirullah, 2018), formation of lipid droplets (Wang et al., 2022; Yeshaw et al., 2019; Kumar et al., 2018; Wang et al., 2021), synaptic vesicle endocytosis (Verstreken et al., 2009), phagocytosis (Kang et al., 2023), ciliogenesis(Valverde et al., 2019), coordination of signalling cascades on specific organelle membranes (Parolek and Burd, 2024; Khuong et al., 2010), regulation of organismal growth (Neuman and Bashirullah, 2018; Tokai et al., 2000), and the dynamic modulation of membrane properties (Khuong et al., 2010; Banerjee et al., 2024).

Frequently, BLPTs have been associated with inherited disorders (see Table 2), typically linked to recessively inherited disorders of the nervous system, such as the severe neurodevelopmental disorder, Alkuraya-Kučinskas syndrome (BLTP1), a commonly perinatal lethal disorder affecting multiple systems, particularly brain development, where surviving patients suffer seizures, cardiac and renal symptoms, and some degree of intellectual disability (Gueneau et al., 2018). There are four VPS13 family members in humans, each associated with a neurodevelopmental disorder: VPS13A mutations cause Choreoacanthocytosis, a progressive disorder in which patients develop chorea, or a Parkinson's disease-like dystonia without chorea (Monfrini et al., 2023), behavioural changes, and cognitive decline, marked by star-shaped red blood cells (acanthocytes) (Peikert et al., 1993); VPS13B is associated with Cohen syndrome, a disorder of developmental delay, intellectual disability, truncal obesity, progressive retinal dystrophy, and microcephaly; VPS13C is mutated in a young-adult onset form of Parkinson's disease, showing rapidly progressive degradation of dopaminergic neurons, with accompanying cognitive and motor decline, or in other cases, dementia with Lewy bodies (neurodegeneration characterised by parkinsonism, episodic changes in cognitive function, hallucination), while VPS13D is implicated in spinocerebellar ataxia, which manifests as developmental delay, and perinatal to adult-onset seizures and movement disorders such as spastic ataxia, spastic paraplegia, and chorea. BLTP3B was also found to be mutated in an early-onset cohort of Parkinson's disease patients, and its knockdown changed mitochondrial morphology (Jansen et al., 2017). Mutations in BLTP3A by contrast are found as a susceptibility locus for systemic lupus erythematosus (SLE), a debilitating autoimmune condition where episodes are often triggered by exposure to UV light. Consistent with the key roles BLTPs play in signalling, membrane homeostasis, and autophagy, mutations or low copy numbers in proteins of this family are also found in cancers (An et al., 2012; Furukawa et al., 2011; Yang et al., 2016; Kang et al., 2009), whereas dominant inheritance of a chromosomal duplication including ATG2B predisposes patients to myeloid malignancies, which may progress to leukemia (Saliba et al., 2015), BLTP3A is upregulated in lung adenocarcinoma (Dan et al., 2021), and BLTP2 is upregulated in several cancers (Song et al., 2006) including breast cancers where it is associated with increased invasiveness and cell metastasis (Banerjee et al., 2024; Zhong et al., 2018).

While this is a rapidly developing field, several recent reviews offer insight into the functional role of this protein family and their effects on membrane traffic and signalling properties in model systems (Levine, 2022; Dziurdzik and Conibear, 2021; Hanna et al., 2023; Vacca et al., 2024; Pandey et al., 2023; Melia and Reinisch, 2022). Taken together, BLTPs facilitate the transfer of lipids from donor membranes—most commonly, but not exclusively, the endoplasmic reticulum (ER)—to target organelles. The target of lipid transfer is dictated by the repertoire of organelle-specific interacting partners associated with each BLTP, which can dynamically vary depending on the availability of these adaptors. This suggests that BLTPs work by the formation of transient, rapidly dissociable membrane contacts, allowing for modulation of membrane composition and functional properties of target organelles on demand.

Open questions

Is lipid transport through RBG proteins directional?

While it is debated whether all members of the BLTP family mediate lipid transfer in one direction only, most of the bridge-like proteins themselves appear to span membrane contact sites in consistent directions, co-ordinated by interactions with adaptors that are specific to the N and C termini of these proteins. This is most clearly borne out in the interactions of the single VPS13 protein in yeast, where N-terminal ER-to-C-terminal organelle contacts are formed by competitive recruitment of the C-terminus to organelle-specific adaptors (Bean et al., 2018). Even there, the list of competing interactors is likely to be further extended, as yeast VPS13 is also detected at junctions between the yeast vacuole and mitochondria(Gonzalez Montoro et al., 2018), suggesting a different N-terminal adaptor, or a tripartite junction including ER. Nevertheless,

this suggests that the orientation of the BLTP at a given junction is important. Interestingly, one recent preprint (Hanna et al., 2025) suggested that some BLTPs may re-orient in response to signalling. In the scenario, it is assumed that the change in orientation determines whether the BLTP3A bridge forms between lysosomes and vesicles (at rest) or between the ER and lysosomes (under lysosomal damage conditions), via a rapid change in N and C terminal interacting partners. However, it is still unknown whether the direction (N-terminus to C-terminus) of lipid transfer changes. Previous *in vitro* experiments with the closely related BLTP3B/SHIP164 (Hanna et al., 2022) have demonstrated that recombinant BLTP3B protein is capable of dimerising in a head-to-tail orientation, but it is unclear whether this is a conformation found *in vivo*. If it were, lipids would translocate topologically 'backward' over one-half of the junction, and lipid transfer would not be an intrinsic property of the mechanism enabling lipid passage through the RBG hydrophobic groove.

While the example of BLTP3A is the most striking to date, it is apparent that the selection of membranes that the BLTPs transfer to and from is largely determined by the N and C terminal interacting proteins of these family, as the BLTPs do not display strong intrinsic preferences for target junctions in the absence of other factors recruiting them to membranes. As described in yeast, overexpression of proteins that can recruit VPS13 family proteins [the adaptor proteins mcp1 (John Peter et al., 2017), ypt35 (John Peter et al., 2017), and spo71 (Park et al., 2013)] compete (Adlakha et al., 2022; Bean et al., 2018) amongst each other to recruit the single yeast VPS13 protein to different ER-organelle membrane contact sites. This is somewhat distributed over VPS13 paralogues in other species, where each VPS13 has an evolutionarily distinct domain arrangement (Figure 2; Levine, 2022; Leterme et al., 2023). In humans, each of the four paralogues (VPS13A-D) have specific interactors which act together to recruit the family to target membranes (largely via specialised interactions to the VPS13 C-terminus, see Table 2), but even so, each human VPS13 is found at multiple organelle junctions.

Other proteins of the family appear to be less specialised, and it is unclear whether the distinction between the donor and acceptor ends of the protein (and therefore, the direction of lipid transport over these bridges), or the conditions for RBG proteins to be recruited to organelle junctions, is as highly regulated as it appears to be for the ATG2/VPS13 grouping when expressed at endogenous levels.

In some of these proteins, the selection of a 'donor' end of the protein may be fixed: BLTP1 has recently been identified with its N-terminal transmembrane helix in complex with two proteins (spigot/C1orf43, an ER-resident protein that cups the N-terminal chorein-like domain, and intake, a nematode-specific helical transmembrane protein which contacts both BLTP1(*C. elegans* LPD-3) and spigot) (Kang et al., 2024a), while BLTP2 sports its own N-terminal transmembrane helix. At the C-terminal, BLTP1 has a C-terminal amphiphilic helix and polybasic patch, which would be expected to interact with charged phosphoinositide lipid and perhaps dock to membranes (Wang et al., 2022), but would be far easier to dynamically dissolve and remodel (to perhaps select a new target membrane) than the interactions supported by the N-terminus. It is not clear whether the transport of its lipid cargo is in fact uni-directional (even if the orientation of the protein is fixed) as BLTP1 is suspected of being capable of transporting lipids between ER and plasma membrane bidirectionally (Toulmay et al., 2022; John Peter et al., 2022a) at its endogenous levels of expression.

Nevertheless, it would appear that at least some members of the BLTP family have specialisations that may favour unidirectional transport, particularly the VPS13/ATG2 grouping. In the case of VPS13 family proteins, donor/acceptor membranes are also largely determined by protein–protein interactions at the C-terminus of the protein (see Table 2). Interestingly, in at least some subcellular organelles, ATG2 and VPS13 proteins are partially redundant (Lei et al., 2022; Dabrowski et al., 2023), suggesting that despite refined mechanisms for targeting these proteins, which become relevant in human disease, the fundamental property of bulk lipid transfer is the most important facet of their function.

How selective are RBG transporters for specific cargo lipids?

Generally, evidence shows that the chorein domains of BLTPs can bind and solubilise the major membrane phospholipids [phosphatidylethanolamine (PE), phosphatidylcholine (PC), phosphatidic acid (PA), phosphatidylserine (PS), phosphatidylinositol (PI), and phosphatidylglycerol (PG)] and are a poor selector for cholesterol (reviewed here; Hamai and Drin, 2024). However, it does not appear that the chorein domains are particularly selective for their cargoes, which appear to be representative of the major glycerophospholipid classes present in donor membranes. Studies looking at the affinity or transport of lipids show that in recombinant systems, BLTPs can transport PE, PC, PA, and PS and to some extent PI (Kumar et al., 2018; Hancock-Cerutti et al., 2022; Valverde et al., 2019), as well as fluorescent nitrobenzoxadiazole (NBD)-labelled lipids. Deletion of Atg2 in *S. cerevisiae* stops R18 (octadecyl rhodamine B) transfer (Hirata et al., 2017). R-18 is a single chain C-18 lipid with a hydrophilic fluorescent 'headgroup', illustrating the lack of headgroup selectivity of BLTPs. In chimeric assays, the chorein domains of ATG2 and VPS13 can be swapped (Osawa et al., 2019) and still retain function.

As the research currently stands, selectivity for lipids is more likely to be driven by the recruitment of the complex to the appropriate junction, and regulation by the properties of the two membranes driving a transport gradient. Assays in reconstituted systems show that BLTP3B rapidly retrieves a packet of lipid from the donor liposomes and then remains stable if there is no acceptor liposome to receive transferred lipid, suggesting that donor lipid is moving down an internal gradient within the RBG tube (Hanna et al., 2022), which drives extraction from the donor.

X-ray crystallography resolved the *S. pombe* ATG2 chorein domain in complex with PE (Osawa et al., 2019), where the majority of the interactions were with the acyl chains of the lipid, with what appeared to be a relatively loose selectivity for acyl chain length and little interaction with the lipid headgroup except a weak interaction with the PE phosphoryl group stabilised by an arginine residue in the chorein domain (see Figure 3A). It is also possible that some lipids are incorporated into the flow of lipids into chorein domains as 'passengers' and are not necessarily selected for. Molecular dynamics (Wang Y. et al., 2024) models favour an entry mechanism of spontaneous absorption of PC by the hydrophobic chorein domain interior, when the acyl chains of the absorbed lipid have been exposed to the cytosol by membrane bending (e.g., a highly curved membrane modelled in this case by a 1,2-dioleoyl-sn-glycero-3-phosphocholine (DOPC) micelle). This process appears to involve a number of conformational steps in the chorein domain: First, one of the two

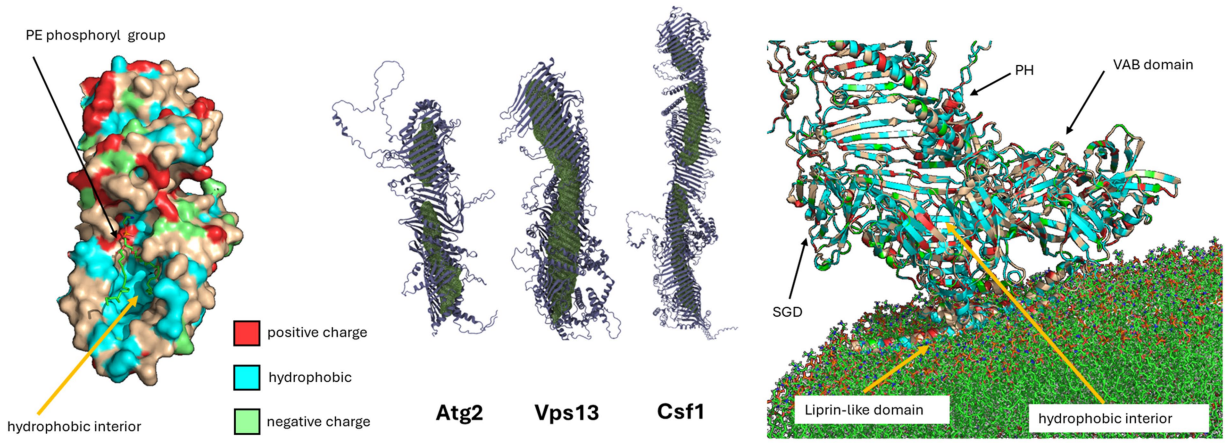

FIGURE 3
Lipid interaction with BLTPs. **(A)** X-ray crystallography of a single PE molecule with *S. pombe* ATG2 chorein domain (PDB:6A9J) showing acyl chain docking to the hydrophobic interior of the chorein domain, and phosphoryl group of PE close to a positive charge at the chorein domain mouth. **(B)** Computational model of lipid docking to the open ends of RBG repeats shows that there are discontinuous 'bottlenecks' where lipid is not docked in the interior of some RBGs. Image reproduced from Srinivasan et al. (2024), under the terms of the Creative Commons Attribution–NonCommercial–ShareAlike 4.0 International license. **(C)** Model of the C-terminal liprin-like domain of VPS13B interacting with model membranes [Modelarchive ma-xnr8z; (Dall'Armellina et al., 2023)], where the liprin-like domain docks on the target membrane, disturbs the cytosolic leaflet, and provides a continuous track to the hydrophobic interior of the RBG for lipid deposition on the target membrane.

DOPC acyl chains spontaneously inserts into the hydrophobic chorein domain cavity while the charged headgroup interacts with a charge at the 'mouth' of the chorein domain scoop; second, the charged headgroup interacts with other slightly deeper positively charged residues to flip the polar head of PC into the cavity; finally, the second acyl chain trails behind and the lipid is transferred onwards, dragging a new acyl chain from the next lipid to enter behind it, potentially generating a continuous stream of oriented lipid. It is speculated that the energy required to drive these conformational changes in the chorein domain, particularly that needed to untangle one acyl chain from its hydrophobic association with other lipids in the micelle, may be supplied by interacting proteins that lower this energy barrier.

Are lipids driven through BLTPs by gradients between donor and acceptor?

Current thinking suggests that BLTPs exploit membrane gradients to transfer bulk membrane phospholipids. Unless a gradient is built by the expenditure of energy (e.g., enzymatic activity), BLTPs would exploit passive gradients between membranes, as well as the properties of the transported lipids themselves. Some gradients are easily generated by local phenomena (e.g., placing the BLTP very close to a lipid synthase on the donor membrane (Lees and Reinisch, 2020) or a lipid hydrolase at the acceptor membrane, thus causing local depletion), or by deformation of the target membrane which may cause lipids to sort away from their site of arrival on a membrane. Liposome curvature has been shown to drive BLTP-mediated lipid transfer *in vitro* (Chowdhury et al., 2018), most likely because lipids are already partially exposed to the cytosol as the bending angle increases and thus are more easily solubilised by the chorein domain, and/or added more easily to the acceptor membrane as exposure of acyl chains on the bent target membrane favours the addition of further lipids.

The disturbance of acyl chains on the donor membrane is likely to facilitate lipid transfer. In models of the interaction of the liprin-like C terminal domain of VPS13 family proteins interacting with membranes, the liprin-like domain disturbs the cytosolic leaflet of the acceptor membrane bilayer, exposing the hydrophobic lipid chains to the 'incoming' lipid being donated by the BLTP, thus likely increasing the efficiency of their incorporation in the target membrane. Interestingly, several missense mutations of this liprin-like domain cause disease in human VPS13s, suggesting their relevance to the lipid transfer process (Dall'Armellina et al., 2023). Recent structural studies (Wang Y. et al., 2024) showed that in human ATG2A, this domain is extremely flexible with respect to its position relative to the RBG tube and assists in feeding lipids to the ATG9A scramblase in the target membrane.

Consistent with this mechanism being exploited by BLTPs *in vivo*, examination of subcellular organisation places lipid transfer via ATG2 to the very edge of the growing omegasome (Chowdhury et al., 2018), and BLTP2 is also found at the tips of tubular endosomes defined by Rab8 and Rab10 (Parolek and Burd, 2024), both where the curvature is highest.

Other properties, such as lipid packing, can also be sensed and/or rectified via BLTP-mediated transfer, suggesting that gradients of lipid composition or fluidity also drive BLTP function. This is illustrated in the case of the role of *C. elegans* lpd-3/BLTP1 countering the effect of cold stress on membrane fluidity (Wang et al., 2022), which is discussed below.

An important consideration is that the action of BLTPs is to drive bulk lipids to the cytosolic leaflet of a membrane bilayer, which then may or may not be redistributed by a scramblase. Eukaryotic membranes favour a less fluid, more tightly packed outer membrane leaflet, while the cytosolic face of the membrane bilayer (the target of

BLTP-mediated transfer) is more loosely packed, thus allowing spontaneous membrane deformation (Bogdanov, 2023), and consequent segregating and sorting of membrane subdomains, which may influence a number of properties of the acceptor membrane. While the ER, the most common source of donor lipid for BLTP-mediated transfer, is both enriched in lipid synthases and relatively symmetric across inner and outer membrane leaflets, the acceptor organelles are successively more and more cholesterol-enriched (Maxfield and van Meer, 2010) and asymmetric [the outer leaflet being more rigid and the cytosolic leaflets of most organelles and both leaflets of the ER harbouring more flexible unsaturated lipids (Dingjan and Futerman, 2021)]. Thus, it is conceivable that the deposition of lipids will allow significant changes to membrane signalling due to localised changes in membrane properties.

How the nature of the donor membrane composition may impact proteins such as BLTP1, which appears to transfer lipids via its N-terminal helix and partner transmembrane protein C1orf43 (Kang et al., 2024a) from the PS-rich luminal leaflet of the ER at to the similarly PS-enriched cytosolic leaflet of target membranes (Kobayashi and Menon, 2018), while most other ER-resident lipids are symmetrically distributed across bilayers, is yet to be explored. It is intriguing, however, that both BLTP1 and C1orf43 are required for phagocytosis of *L. pneumophila* (Jeng et al., 2019) by macrophages and for phagocytosis of neuronal debris (Kang et al., 2024a), suggesting that continuous access to the ER lumen is necessary for function. Similarly, yeast Csf1/BLTP1 immunoprecipitated the ER lumenal enzyme Mdc4 (Toulmay et al., 2022), which depletes PE for the synthesis of GPI anchors. This may suggest that local depletion of PE in the lumenal bilayer is relevant to BLTP1 function.

Can lipid transport through the RBG bridge be regulated?

Several models have been made of lipid interactions with members of the BLTP family, which all favour a continuous stream or bolus of lipid passing through the RBG portion of BLTPs (Li et al., 2020), following the hydrophobic track of residues down the centre of the RBG as predicted by mutagenesis studies (Valverde et al., 2019; Tan and Finkel, 2022). It is unclear whether, having entered the RBG 'tube', lipids are subject to any flow regulation as they pass from one side of the BLTP bridge to the other, but some indications exist that some kind of flow regulation or management may take place.

As lipids traverse the RBG repeats, modelling and cryo-electron microscopy find that BLTPs are suited to the co-ordinated deposition of multiple lipids at a time, which allows the lipids to orient and group themselves, thus minimising the energy needed to transfer lipids from one membrane to another. Recent cryo-electron microscopy studies (Kang et al., 2024a) and assays with NBD-PE in reconstituted systems (Hanna et al., 2022) show multiple lipids at a time are docked in the RBG groove.

Recent and elegant molecular dynamic (MD) simulations of lipid docking on open membrane-less models of the RBG portion of BLTPs (Srinivasan et al., 2024), shown in Figure 3B, show no intrinsic preference in terms of direction of entry for the open RBG repeats of ATG2 in MD simulations of free lipids in solution with BLTPs. Simulating sequential docking of multiple free lipids in yeast Atg2, Vps13, and Csf1/BLTP1, the authors show that these proteins can carry in the RBG repeat 'tube' at least 15, 49, and 53 phospholipids, respectively, where the charged lipid headgroup faces the solvent. Interestingly, this modelling also showed that the docked lipids were not equally distributed down the length of the RBG tube, instead finding bottlenecks in the hydrophobic track of Atg2 and Csf1/BLTP1 where lipids did not preferentially reside, which may provide an opportunity for transport down the length of the RBG tube to be regulated. These models, where only the open RBG tube is considered, would favour the bi-directional transport of lipids via BLTPs as the free lipids entered from both N and C terminal directions of the modelled open tubes. These bottlenecks in RBG repeats were also found in cryo-EM structures of ATG2A (Wang Y. et al., 2024), suggesting that the passage of lipids through BLTPs is not uninterrupted, and may require changes in conformation to allow passage of lipids. Several possible methods of regulation may exist that would modulate the diameter of the RBG tube during lipid transport, such as locally twisting or compressing RBG repeats, either by the many conserved flexible repeats and motifs that are scattered along the length of RBG proteins (Levine, 2022; Dall'Armellina et al., 2023) or by physical changes in the distance between membranes which may act as a kind of pump to drive lipids across the hydrophobic path.

Other models of BLTP family interaction with lipid in RBG bridges agree with a model of interrupted, and therefore regulatable, lipid transfer. A recent preprint (Kang et al., 2024a) showed that, in cryo-EM studies of *C. elegans* lpd-3/BLTP1 extracted with its native complex and cargo lipids, this protein was intimately twined via BLTP1's N-terminal transmembrane helix and its chorein domain with two ER transmembrane proteins (intake, a *C. elegans* specific gene, and C1orf43/spigot) which allowed a continuous hydrophobic path from the ER lumen to the interior of the BLTP1 RBG repeats, suggesting BLTP1 is continuously anchored to its donor membrane and in contact with transportable lipid. In this study, Kang et al. were able to reveal some very interesting features of the interaction of phospholipid with RBG repeats. First, they noted that the distribution of phospholipids along the RBGs resolved in their structure was not homogenous: The narrower ~25 Å RBG tubes at the N-terminus of BLTP1 harboured a single co-ordinated row of phospholipids, whereas the broader (~40 Å) RBG repeats towards the middle of the protein were associated with 2–5 rows of lipid within the RBG repeat. Most interestingly, while the hydrophobic tails of these lipids faced the hydrophobic interior, the phospholipid headgroup was oriented towards the water in the half-open RBG repeat, by the presence of alternating acid and basic residues, which coordinated the lipids in rows. The more ionisable residues per RBG repeat, the more rows of lipids could be co-ordinated, such that in the wider RBG repeats, lipids were packed at a similar density to one leaflet of a membrane bilayer. The authors speculate that this allows the interior of the RBG repeat to conduct oriented clusters of lipids as if they were small patches of a membrane leaflet. The continuous anchoring of BLTP1 with membrane integral proteins at its N-terminus, and the accommodation of more lipids at the centre of the bridge than at its beginning would likely drive a gradient of movement away from the donor membrane. Interestingly, this was also observed in ATG2A, where, except for a bottleneck at the N terminal region, the hydrophobic track broadened along RBGs until the last segment, which contacts the acceptor membrane. This segment was unresolved in these structures, suggesting an internally generated lipid transfer gradient from the N-terminal to the C-terminal of the BLTP (Wang Y. et al., 2024).

Unfortunately, it was not possible to solve the structure of the entire BLTP1 complex *ex vivo* at the resolution needed to identify docked lipids over the entire length of the membrane bridge, so the nature of the interaction of BLTP1 with the plasma membrane was not observed in this system. Computational models of BLTP1 structure favour a widening of RBG repeats from the N- to C-terminus, until reaching a narrow neck at the C-terminal region of the protein (Wang et al., 2022). However, BLTP1 (Toulmay et al., 2022; John Peter et al., 2022a) like SHIP164/BLTP3B (Hanna et al., 2022) is of the subgroup of BLTPs for which bidirectional lipid transport is suspected, and this correlates with very little specialisation of the C terminal acceptor end of the BLTP bridge.

There are arguments, however, that the more specialised members of the BLTP family (ATG2, VPS13) for which the evidence for unidirectional lipid transport is stronger, may have adopted features that make lipid transport favour the N-terminal to C-terminal direction. Our own study modelling interactions of the specialised N- and C-terminal domains of VPS13A-D with donor and acceptor membranes (Dall'Armellina et al., 2023) showed that the liprin-like helical bundle, which is found in ATG2/VPS13 proteins, allows a narrowing of the extended RBG repeats until a single helix with a hydrophobic face covers the last distance between the RBG tube and where the liprin-like domain disturbs the cytosolic face of the target membrane (Figure 3C). We speculate that these features reduce the ability of solubilised lipids to 'crawl' back up the RBG tube and thus impose a direction of transport, in addition to the liprin-like domain facilitating lipid admixture by disturbing the acceptor membrane cytosolic leaflet.

Based on our modelling on VPS13s, along with work from others since, we propose two models to regulate the passage of lipids through RBG bridges: (1) a spring-like action of compressing and expanding RBG repeats (which potentially may be regulated by interaction with the many conserved cytosolic loops and motifs down the length of the BLTP proteins), and (2) a transient interaction model, where VPS13 RBGs are rigid, and lipids fall down the gradient between donor and acceptor membranes. In this model, the N-terminal chorein domain is weakly associated with donor membranes via long, flexible tethers to proteins such as VAPA/B, allowing transient 'gulps' of donor lipids. This could well be similar in other BLTPs, as current evidence suggests that BLTPs are strongly associated with either their donor (BLTP1-2) or their acceptor (VPS13) membranes, but not both—allowing transient interactions with one side of the intraorganelle bridge to drive pulses of lipid down the RBG tube.

How fast are BLTPs?

The presence of BLTPs, despite their apparent lack of selectivity, also provides some advantages when dynamically manipulating membrane properties, as bulk transfer allows movement of lipids between organelle membranes on the scale of minutes (Wong et al., 2019; Reinisch and Prinz, 2021) thus allowing fast and presumably local response to changes in membranes: This is particularly seen by the action of VPS13C (Schröder et al., 2024; Wang X. et al., 2024) BLTP3A(Hanna et al., 2025) and ATG2 (Tan and Finkel, 2022) being recruited to damaged lysosomes for the process of lysosomal repair—a process that is accomplished on the scale of minutes and heavily involves a variety of other LTPs outside of the BLTP family.

In vitro studies using Förster resonance energy transfer (FRET)-based assays in liposomes have measured the transfer of a 2% mix of NBD-PE from donor liposomes at a surprisingly low rate of ~0.017 s-1 per molecule of the BLTP (Maeda et al., 2019). However, subsequent reanalysis of the composition of those liposomes, along with the fact that BLTPs unselectively transport phospholipids regardless of labelling, suggests that the maximal lipid flux per BLTP molecule in that same assay is 50 times higher, at 0.85 molecules s-1, (Hamai and Drin, 2024). This occurs even when there is not necessarily a very strong gradient between donor and acceptor liposomes, limiting the drive to traverse the BLTP. Assays where yeast Atg2-Atg18 are coupled with Atg9 scramblase show a doubling in the efficiency of *in vitro* NBD-PE transfer between liposomes (regardless if Atg9 was interacting with Atg2 on donor or acceptor liposomes), suggesting that transfer rates are dependent on whether both the inner and outer leaflets of membranes are accessible to lipids donated by BLTP complexes (Chumpen Ramirez et al., 2023).

In vivo measurements, however, put the lipid transfer rate much higher: ~200 lipids per second per molecule of Atg2 in yeast (Dabrowski et al., 2023). In all, this suggests that the rate at which lipids traverse the BLTP will be very much context-dependent, responding to local membrane geometry, membrane composition, and the role of BLTP-associated proteins in processing the lipids that are passing through.

What effect does BLTP-mediated lipid transport have on target membrane geometry?

Insights into the consequences of lipid transfer mediated by BLTPs have been gained through structure–function analyses and knockout studies across various organisms and cell types. Collectively, these findings suggest that the effects of BLTP-mediated lipid transfer depend on both the specific lipid being deposited and the manner in which the donated lipid is incorporated with the acceptor membrane. This process influences the geometry and biophysical properties of the target organelle, ultimately modulating cell signalling pathways and membrane sorting.

A key factor in determining how acceptor membranes are altered lies in the presence of accessory complex components associated with BLTPs. These proteins often function as part of larger macromolecular assemblies, interacting with accessory proteins such as Rabs and adaptor proteins or associating with membrane scramblases, which modulate the impact of the transferred lipid on the target membrane. The specific targeting and interaction partners at each BLTP-mediated intraorganellar contact appear to dictate the functional outcome of BLTP activity at a given membrane junction.

BLTPs are thought to deposit bulk membrane lipids onto their target membrane, but the context and method of deposition have different effects on the membrane properties of the target organelle. Experiments show BLTPs can drive membrane expansion in the case of VPS13/ATG2 proteins (Chowdhury et al., 2018; Da Costa et al., 2020) favouring models where these more specialised BLTPs do in fact drive unidirectional transport. Other members of the family such as BLTP1-2 have less specialisation at their C-termini but nevertheless drive changes in membrane properties such as membrane fluidity and consequent signalling.

One key distinction between the actions of BLTPs in their different cellular contexts is the presence or otherwise of associated scramblases as this imposes a geometry as to how the transported lipid

will be distributed on the acceptor membrane. These transmembrane proteins facilitate donated lipids accessing the lumenal leaflet of the membrane bilayer, which has the effect of equilibrating the donated lipid across both bilayers of the membrane, which allows expansion of acceptor membranes without much bending. This is best understood for the VPS13/ATG2 grouping of BLTPs. It was noted that VPS13A associates with the scramblase XK (Ryoden et al., 2022) and shares a common disease phenotype (Park and Neiman, 2020) where PS exposure and PC internalisation of the outer face of the plasma membrane are compromised. In yeast, VPS13 forms a complex with the yeast-specific MCP1 protein, which, despite no sequence conservation with XK, also has scramblase activity (Adlakha et al., 2022). This is also the case for the similar ATG2 proteins that interact with the lipid scramblases ATG9a, TMEM41B, and VMP1(Ghanbarpour et al., 2021; Maeda et al., 2020). Cryo-EM suggests that human ATG2A directly feeds lipid to the lateral pores found in a single ATG9 unit in a target membrane, funnelling transferred lipid to the central ATG9A scramblase pore formed by ATG9A trimers (Wang Y. et al., 2024), and thus to the equilibrated membrane bilayer.

In these cases, the equilibration of the inner and outer leaflets of the target organelle will also drive transfer gradients by spreading the donated lipid over both the inner and outer leaflets of the membrane bilayer, by helping to maintain a concentration gradient between the donor membrane and the acceptor membrane cytosolic leaflet. This method of lipid deposition is supported by the established role of scramblase-associated ATG2 in depositing lipids for phagophore formation (Maeda et al., 2019; Chowdhury et al., 2018; Valverde et al., 2019; Osawa et al., 2019). Interestingly, viral replication of tomato bushy stunt virus in yeast and plants requires both Atg2 and its associated scramblase Atg9 (Kang et al., 2024b) showing the importance of this mechanism to ATG2 function.

In proteins such as BLTP3B/SHIP164, which are not known thus far to form complexes with a scramblase, overexpression of the BLTP and a targeting protein (in this case its interactor, syntaxin 6) leads to excessive tubulation of endosomes, possibly driven by the asymmetric delivery of lipids to the outer leaflet of the acceptor membrane, which, if not equilibrated, would need to deform and bend to accommodate the excess lipid (Otto et al., 2010). This change in membrane geometry leads to changes in the trafficking of endosomal cargoes such as cation-independent mannose 6 phosphate receptor and transferrin receptor. This also appears to be the case for the VPS13 family of proteins when these proteins are not interacting with scramblase, where VPS13-mediated transport then favours membrane distortion: Yeast VPS13 directs lipid to lysosomes to accomplish ESCRT-mediated inward budding and membrane sorting to form ILVs (Suzuki et al., 2024) or VPS13B allows the formation of extended tubular ERGIC to accommodate the trafficking and secretion of long extracellular proteins such as procollagen (Du et al., 2024). Similarly, *Drosophila* BLTP1, apart from other roles in neurons, also has a role in astrocytes, where its depletion interferes with the formation of phagosomes for clearance of neuronal debris(Kang et al., 2024a; Kang et al., 2023).

Do BLTPs change the signalling properties of membranes?

Although BLTPs transport lipids that are abundant in most membranes, the donor and acceptor membranes connected by BLTP bridges exhibit distinct characteristics, such as the different phosphatidylinositol phosphates (PIPs) that define organelles, and varying levels of cholesterol, which does not appear to be transported as cargo. They also differ in lipid composition (e.g., PC/PE/PS ratio), lipid saturation levels, and the level of asymmetry between the cytosolic and lumenal/extracellular leaflets of the bilayer [reviewed here (Kobayashi and Menon, 2018; Van Meer et al., 2008)].

The rapid admixture of lipids from other organellar membranes, such as the relatively unsaturated lipids found in fluid ER, the site of synthesis for most of the lipids known to be transported via BLTPs, is likely to change the properties of both donor and acceptor membranes. These changes may be to the geometry (e.g., cone-shaped lipids such as PE favour membrane bending, and unsaturated lipids favour membrane flexibility), or the capacity of the membrane to form ordered domains for signalling [as, e.g., is found at ER-membrane contacts (King et al., 2020)]. This has been proposed for BLTP2, which drives lipids from the ER to the plasma membrane to donate lipids to macropinosomes and tubular endosomes as they fuse to the plasma membrane (Dai et al., 2025). The absence of BLTP2 in this context leads to the accumulation of vacuolar structures that are contiguous with the plasma membrane and open to extracellular space, showing the importance of lipid deposition and changed local membrane properties via these proteins to assist membrane traffic, membrane deformation, and consequent signalling.

Nevertheless, there is a degree of subtlety as to how each BLTP is able to change membrane properties. In systems where some level of functional redundancy might be anticipated between members of the BLTP family such as BLTP2 and BLTP1—which both mediate transfer between ER and the plasma membrane—certain functional roles are specialised. These roles may be influenced by specific protein interactions with these BLTPs, as well as by the physical context of their membrane junctions and the local curvature induced by lipid transfer. Both BLTP1 and BLTP2 have important roles in homeoviscous adaptation (HVA), that is, maintaining membrane sorting and signalling properties under cold stress (Ernst et al., 2016). This network of adaptations is large, contextually dependent, and involves many different potential lipid modifications, or selections for properties [e.g., acyl chain length or saturation (Ernst et al., 2016; Ballweg et al., 2020)]. *C. elegans* LPD-3/BLTP1 is responsible for mitigating membrane rigidification (such as cold stress), by depleting PC from the ER membrane and blocking compensatory upregulation FAT-7 fatty acid desaturase, which uses an alternate path to increase membrane fluidity (by generating unsaturated acyl chain on resident lipids). Interestingly, the BLTP1 function can be bypassed by the addition of unsaturated phospholipids (lecithins) to the plasma membrane (Wang et al., 2022; Pandey et al., 2023). In yeast, CSF1/BLTP1 mutations cause a cold-sensitive phenotype (Tokai et al., 2000), which manifests as a lack of adaptive response (generation of shorter acyl chain lipids and increased acyl chain unsaturation), which could be in part reverted by treatment with the unsaturated lipid oleic acid (John Peter et al., 2022b).

BLTP2 regulates membrane fluidity by increasing PE levels at PM, facilitating cancer growth (Banerjee et al., 2024). Its yeast orthologue, Fmp27, exhibits a cold-dependent growth phenotype, resolved by supplementation with propanolamine, a lipid similar to PE that cannot be converted to PC, suggesting a specific requirement for BLTP2-delivered PE at these sites. While wild-type yeast acclimatise to cold stress by raising the plasma membrane PE:PC ratio, yeast

lacking Fmp27/BLTP2 fail to increase plasma membrane PE (Banerjee et al., 2024). The authors also showed that a shift to cold temperature provoked a change in lipid unsaturation in both cell lines, which was abolished by the presence of abundant ethanolamine, a precursor to PE, indicating redundant pathways maintaining membrane fluidity in HVA (Banerjee et al., 2024).

PE is also a precursor of GPI anchors, and while mutation of yeast Fmp27/BLTP2 does not appreciably affect the synthesis of GPI anchors (Banerjee et al., 2024), yeast Csf1/BLTP1 mutants have disturbed GPI anchor biosynthesis (Toulmay et al., 2022). This highlights that although broadly similar, specificity is present between the effects of lipid transport by BLTPs and thus must be conveyed by either location or admixture of lipids.

However, the downstream consequences of altering membrane properties, even by manipulation of the highly abundant phospholipids that BLTPs are known to transfer, are considerable. Changing the balance of PE to PI, where PE is a curvature promotor and PI, because of hydrogen bonding between headgroups, favours uncurved membrane (Klose et al., 2012), induces membrane bending, lipid segregation, and consequent organisation of signalling complexes which affect minor membrane components and signalling lipids such as phosphoinositide lipids (PIPs). This is best illustrated in the downstream consequences of BLTP1 mutation in various model systems. In *C. elegans* and mouse fibroblasts, BLTP1 mutants show defects in the positioning and abundance of the low-abundance PIP lipid PI(3,4,5)P_3, as well as disorganised actin polymerisation (Wang et al., 2022; Khuong et al., 2010). In contrast, in *Drosophila melanogaster,* BLTP1 loss affects the plasma membrane positioning and abundance of PI(4,5)P_2, leading to defects in synaptic vesicle cycling (Verstreken et al., 2009; Khuong et al., 2010). It also appears that loss of this pathway triggers other strong signalling across membranes, leading to an insulin-dependent hyperactivation of mTOR signalling and consequent reduction in lifespan for LPD-3/BLTP1 mutants in *C. elegans*, which could be rescued by lecithin (Pandey et al., 2024), whereas insulin secretion is compromised in *Drosophila* Hobbit/BLTP2 mutants (Neuman and Bashirullah, 2018). A change in PIP signalling has also been observed in target membranes of cells depleted of VPS13 family proteins (Park et al., 2015), suggesting common effects of bulk phospholipid transfer by BLTPs on membrane signalling properties *via* PIP lipids.

It is unclear whether these effects on PIP lipid signalling are due to a direct defect in PIP lipid transfer *via* the RBG bridge, or the deficit in PIP lipids stems from downstream consequences of changes to membrane fluidity and therefore recruitment of specific PIP kinases and phosphatases, which preferentially segregate to lipid microdomains defined by acyl chain composition (Wang and Richards, 2012; Wenk et al., 2003).

Conclusion

Recent studies have identified several common characteristics of BLTPs: (1) a loose association with either donor or acceptor membranes; (2) the presence of internal gradients that promote lipid accumulation in regions with wider RBG repeats; (3) lipid transfer "bottlenecks," which may serve as regulatory points for lipid transfer; and (4) effects on PIP lipid signalling, likely secondary to the transfer of major lipid constituents such as phosphatidylcholine (PC) and phosphatidylethanolamine (PE). Whether bi-directional or unidirectional, the effects of lipid transfer appear to be driven by both the gradient of phospholipids between donor and acceptor membranes and association with other membrane proteins which drive lipids to equilibrate or not over associated membrane bilayers. The presence of these accessory complex members imposes specific membrane geometries and lipid sorting patterns, with significant implications for protein distribution and membrane signalling. Overall, the studies conducted so far suggest that from the simplest of principles (a scoop that can load lipids and a tube that can conduct it in co-ordinated patches), highly specific, context-dependent changes can be made to membrane function at all levels of membrane sorting and signalling, underpinning neuronal and organismal function. Our growing understanding of such an ancient, seemingly simple, group of lipid transfer proteins suggests that BLTP-mediated regulation of phospholipid gradients can orchestrate extensive and surprisingly sophisticated changes in cellular signalling and interactions with the extracellular environment.

Author contributions

LS: Writing – original draft, Writing – review & editing.

Funding

The author(s) declare that financial support was received for the research and/or publication of this article. Laura Swan acknowledges funding from the Wellcome Trust (ISSF 204822/Z/16/Z) and AFM Telethon, grant/award no. 22429.

Conflict of interest

The author declares that the research was conducted in the absence of any commercial or financial relationships that could be construed as a potential conflict of interest.

Generative AI statement

The author declares that no Gen AI was used in the creation of this manuscript.

Publisher's note

References

Adlakha, J., Hong, Z., Li, P., and Reinisch, K. M. (2022). Structural and biochemical insights into lipid transport by VPS13 proteins. *J. Cell Biol.* 221:2030. doi: 10.1083/jcb.202202030

Alazami, A. M., Patel, N., Shamseldin, H. E., Anazi, S., Al-Dosari, M. S., Alzahrani, F., et al. (2015). Accelerating novel candidate gene discovery in neurogenetic disorders via whole-exome sequencing of prescreened multiplex consanguineous families. *Cell Rep.* 10, 148–161. doi: 10.1016/j.celrep.2014.12.015

An, C. H., Kim, Y. R., Kim, H. S., Kim, S. S., Yoo, N. J., and Lee, S. H. (2012). Frameshift mutations of vacuolar protein sorting genes in gastric and colorectal cancers with microsatellite instability. *Hum. Pathol.* 43, 40–47. doi: 10.1016/j.humpath.2010.03.015

Anding, A. L., Wang, C., Chang, T. K., Sliter, D. A., Powers, C. M., Hofmann, K., et al. (2018). Vps13D encodes a ubiquitin-binding protein that is required for the regulation of mitochondrial size and clearance. *Curr. Biol.* 28, 287–295 e6. doi: 10.1016/j.cub.2017.11.064

Ballweg, S., Sezgin, E., Doktorova, M., Covino, R., Reinhard, J., Wunnicke, D., et al. (2020). Regulation of lipid saturation without sensing membrane fluidity. *Nat. Commun.* 11:756. doi: 10.1038/s41467-020-14528-1

Banerjee, S., Daetwyler, S., Bai, X., Michaud, M., Jouhet, J., Madhugiri, S., et al. (2024). The Vps13-like protein BLTP2 is pro-survival and regulates phosphatidylethanolamine levels in the plasma membrane to maintain its fluidity and function. *bioRxiv* 2024:8804. doi: 10.1101/2024.02.04.578804

Bean, B. D. M., Dziurdzik, S. K., Kolehmainen, K. L., Fowler, C. M. S., Kwong, W. K., Grad, L. I., et al. (2018). Competitive organelle-specific adaptors recruit Vps13 to membrane contact sites. *J. Cell Biol.* 217, 3593–3607. doi: 10.1083/jcb.201804111

Bogdanov, M. (2023). The power and challenge of lipid (a)symmetry across the membrane and cell. *Emerg. Top. Life Sci.* 7, 1–6. doi: 10.1042/ETLS20220088

Bozic, M., van den Bekerom, L., Milne, B. A., Goodman, N., Roberston, L., Prescott, A. R., et al. (2020). A conserved ATG2-GABARAP family interaction is critical for phagophore formation. *EMBO Rep.* 21:e48412. doi: 10.15252/embr.201948412

Braschi, B., Bruford, E. A., Cavanagh, A. T., Neuman, S. D., and Bashirullah, A. (2022). The bridge-like lipid transfer protein (BLTP) gene group: introducing new nomenclature based on structural homology indicating shared function. *Hum. Genomics* 16:66. doi: 10.1186/s40246-022-00439-3

Choi, J., Jang, H., Xuan, Z., and Park, D. (2024). Emerging roles of ATG9/ATG9A in autophagy: implications for cell and neurobiology. *Autophagy* 20, 2373–2387. doi: 10.1080/15548627.2024.2384349

Chowdhury, S., Otomo, C., Leitner, A., Ohashi, K., Aebersold, R., Lander, G. C., et al. (2018). Insights into autophagosome biogenesis from structural and biochemical analyses of the ATG2A-WIPI4 complex. *Proc. Natl. Acad. Sci. U. S. A.* 115, E9792–E9801. doi: 10.1073/pnas.1811874115

Chumpen Ramirez, S., Gomez-Sanchez, R., Verlhac, P., Hardenberg, R., Margheritis, E., Cosentino, K., et al. (2023). Atg9 interactions via its transmembrane domains are required for phagophore expansion during autophagy. *Autophagy* 19, 1459–1478. doi: 10.1080/15548627.2022.2136340

Da Costa, R., Bordessoules, M., Guilleman, M., Carmignac, V., Lhussiez, V., Courot, H., et al. (2020). Vps13b is required for acrosome biogenesis through functions in Golgi dynamic and membrane trafficking. *Cell. Mol. Life Sci.* 77, 511–529. doi: 10.1007/s00018-019-03192-4

Dabrowski, R., Tulli, S., and Graef, M. (2023). Parallel phospholipid transfer by Vps13 and Atg2 determines autophagosome biogenesis dynamics. *J. Cell Biol.* 222:1039. doi: 10.1083/jcb.202211039

Dai, A., Xu, P., Amos, C., Fujise, K., Wu, Y., Yang, H., et al. (2025). Multiple interactions mediate the localization of BLTP2 at ER-PM contacts to control plasma membrane dynamics. *bioRxiv* 2025:94. doi: 10.1101/2025.02.07.637094

Dall'Armellina, F., Stagi, M., and Swan, L. E. (2023). In silico modeling human VPS13 proteins associated with donor and target membranes suggests lipid transfer mechanisms. *Proteins* 91, 439–455. doi: 10.1002/prot.26446

Dan, W., Shi, L., Wang, L., Wu, D., Huang, X., and Zhong, Y. (2021). PP7080 expedites the proliferation and migration of lung adenocarcinoma cells via sponging miR-670-3p and regulating UHRF1BP1. *J. Gene Med.* 23:e3341. doi: 10.1002/jgm.3341

De, M., Oleskie, A. N., Ayyash, M., Dutta, S., Mancour, L., Abazeed, M. E., et al. (2017). The Vps13p-Cdc31p complex is directly required for TGN late endosome transport and TGN homotypic fusion. *J. Cell Biol.* 216, 425–439. doi: 10.1083/jcb.201606078

Dingjan, T., and Futerman, A. H. (2021). The fine-tuning of cell membrane lipid bilayers accentuates their compositional complexity. *BioEssays* 43:e2100021. doi: 10.1002/bies.202100021

Du, Y., Fan, X., Song, C., Chang, W., Xiong, J., Deng, L., et al. (2024). Sec23IP recruits VPS13B/COH1 to ER exit site-Golgi interface for tubular ERGIC formation. *J. Cell Biol.* 223:2083. doi: 10.1083/jcb.202402083

Du, Y., Wang, J., Xiong, J., Fang, N., and Ji, W. K. (2021). VPS13D interacts with VCP/p97 and negatively regulates endoplasmic reticulum-mitochondria interactions. *Mol. Biol. Cell* 32, 1474–1486. doi: 10.1091/mbc.E21-03-0097

Durgan, J., and Florey, O. (2022). Many roads lead to CASM: diverse stimuli of noncanonical autophagy share a unifying molecular mechanism. *Sci. Adv.* 8:eabo1274. doi: 10.1126/sciadv.abo1274

Dziurdzik, S. K., and Conibear, E. (2021). The Vps13 family of lipid transporters and its role at membrane contact sites. *Int. J. Mol. Sci.* 22:905. doi: 10.3390/ijms22062905

Ernst, R., Ejsing, C. S., and Antonny, B. (2016). Homeoviscous adaptation and the regulation of membrane lipids. *J. Mol. Biol.* 428, 4776–4791. doi: 10.1016/j.jmb.2016.08.013

Furukawa, T., Kuboki, Y., Tanji, E., Yoshida, S., Hatori, T., Yamamoto, M., et al. (2011). Whole-exome sequencing uncovers frequent GNAS mutations in intraductal papillary mucinous neoplasms of the pancreas. *Sci. Rep.* 1:161. doi: 10.1038/srep00161

Gauthier, J., Meijer, I. A., Lessel, D., Mencacci, N. E., Krainc, D., Hempel, M., et al. (2018). Recessive mutations in VPS13D cause childhood onset movement disorders. *Ann. Neurol.* 83, 1089–1095. doi: 10.1002/ana.25204

Ghanbarpour, A., Valverde, D. P., Melia, T. J., and Reinisch, K. M. (2021). A model for a partnership of lipid transfer proteins and scramblases in membrane expansion and organelle biogenesis. *Proc. Natl. Acad. Sci. U. S. A.* 118:e2101562118. doi: 10.1073/pnas.2101562118

Gillingham, A. K., Bertram, J., Begum, F., and Munro, S. (2019). In vivo identification of GTPase interactors by mitochondrial relocalization and proximity biotinylation. *eLife* 8:916. doi: 10.7554/eLife.45916

Gonzalez Montoro, A., Auffarth, K., Honscher, C., Bohnert, M., Becker, T., Warscheid, B., et al. (2018). Vps39 interacts with Tom40 to establish one of two functionally distinct vacuole-mitochondria contact sites. *Dev. Cell* 45, 621–636.e7. doi: 10.1016/j.devcel.2018.05.011

Gueneau, L., Fish, R. J., Shamseldin, H. E., Voisin, N., Mau-Them, F. T., and Preiksaitiene, E. G. (2018). KIAA1109 variants are associated with a severe disorder of brain development and arthrogryposis. *Am. J. Hum. Genet.* 102, 116–132. doi: 10.1016/j.ajhg.2017.12.002

Guillen-Samander, A., Leonzino, M., Hanna, M. G., Tang, N., Shen, H., and De Camilli, P. (2021). VPS13D bridges the ER to mitochondria and peroxisomes via Miro. *J. Cell Biol.* 220:10004. doi: 10.1083/jcb.202010004

Guillen-Samander, A., Wu, Y., Pineda, S. S., Garcia, F. J., Eisen, J. N., Leonzino, M., et al. (2022). A partnership between the lipid scramblase XK and the lipid transfer protein VPS13A at the plasma membrane. *Proc. Natl. Acad. Sci. U. S. A.* 119:e2205425119. doi: 10.1073/pnas.2205425119

Hamai, A., and Drin, G. (2024). Specificity of lipid transfer proteins: An in vitro story. *Biochimie* 227, 85–110. doi: 10.1016/j.biochi.2024.09.007

Hancock-Cerutti, W., Wu, Z., Xu, P., Yadavalli, N., Leonzino, M., Tharkeshwar, A. K., et al. (2022). ER-lysosome lipid transfer protein VPS13C/PARK23 prevents aberrant mtDNA-dependent STING signaling. *J. Cell Biol.* 221:46. doi: 10.1083/jcb.202106046

Hanna, M., Guillen-Samander, A., and De Camilli, P. (2023). RBG motif bridge-like lipid transport proteins: structure, functions, and open questions. *Annu. Rev. Cell Dev. Biol.* 39, 409–434. doi: 10.1146/annurev-cellbio-120420-014634

Hanna, M. G., Rodriguez Cruz, H. O., Fujise, K., Li, Z., Monetti, M., and De Camilli, P. (2025). Bridge-like lipid transfer protein 3A (BLTP3A) is associated with membranes of the late endocytic pathway and is an effector of CASM. *bioRxiv* 2024:5015. doi: 10.1101/2024.09.28.615015

Hanna, M. G., Suen, P. H., Wu, Y., Reinisch, K. M., and De Camilli, P. (2022). SHIP164 is a chorein motif lipid transfer protein that controls endosome-Golgi membrane traffic. *J. Cell Biol.* 221:1018. doi: 10.1083/jcb.202111018

Hirata, E., Ohya, Y., and Suzuki, K. (2017). Atg4 plays an important role in efficient expansion of autophagic isolation membranes by cleaving lipidated Atg8 in *Saccharomyces cerevisiae*. *PLoS One* 12:e0181047. doi: 10.1371/journal.pone.0181047

Jansen, I. E., Ye, H., Heetveld, S., Lechler, M. C., Michels, H., Seinstra, R. I., et al. (2017). Discovery and functional prioritization of Parkinson's disease candidate genes from large-scale whole exome sequencing. *Genome Biol.* 18:22. doi: 10.1186/s13059-017-1147-9

Jeng, E. E., Bhadkamkar, V., Ibe, N. U., Gause, H., Jiang, L., Chan, J., et al. (2019). Systematic identification of host cell regulators of *Legionella pneumophila* pathogenesis using a genome-wide CRISPR screen. *Cell Host Microbe* 26, 551–563.e6. doi: 10.1016/j.chom.2019.08.017

John Peter, A. T., Cheung, N. J., and Kornmann, B. (2022a). Csf1: a putative lipid transport protein required for Homeoviscous adaptation of the Lipidome. *Contact (Thousand Oaks)* 5:1974. doi: 10.1177/25152564221101974

John Peter, A. T., Herrmann, B., Antunes, D., Rapaport, D., Dimmer, K. S., and Kornmann, B. (2017). Vps13-Mcp1 interact at vacuole-mitochondria interfaces and bypass ER-mitochondria contact sites. *J. Cell Biol.* 216, 3219–3229. doi: 10.1083/jcb.201610055

John Peter, A. T., van Schie, S. N. S., Cheung, N. J., Michel, A. H., Peter, M., and Kornmann, B. (2022b). Rewiring phospholipid biosynthesis reveals resilience to membrane perturbations and uncovers regulators of lipid homeostasis. *EMBO J.* 41:e109998. doi: 10.15252/embj.2021109998

Kaminska, J., Rzepnikowska, W., Polak, A., Flis, K., Soczewka, P., Bala, K., et al. (2016). Phosphatidylinositol-3-phosphate regulates response of cells to proteotoxic stress. *Int. J. Biochem. Cell Biol.* 79, 494–504. doi: 10.1016/j.biocel.2016.08.007

Kang, Y., Jefferson, A., Sheehan, A., La Torre, R. D., Jay, T., Chiao, L., et al. (2023). Tweek-dependent formation of ER-PM contact sites enables astrocyte phagocytic function and remodeling of neurons. *bioRxiv* 2023:5932. doi: 10.1101/2023.11.06.565932

Kang, M. R., Kim, M. S., Oh, J. E., Kim, Y. R., Song, S. Y., Kim, S. S., et al. (2009). Frameshift mutations of autophagy-related genes ATG2B, ATG5, ATG9B and ATG12 in gastric and colorectal cancers with microsatellite instability. *J. Pathol.* 217, 702–706. doi: 10.1002/path.2509

Kang, Y., Lehmann, K. S., Vanegas, J., Long, H., Jefferson, A., Freeman, M., et al. (2024a). Structural basis of bulk lipid transfer by bridge-like lipid transfer protein LPD-3. *bioRxiv* 2024:600134. doi: 10.1101/2024.06.21.600134

Kang, Y., Pogany, J., and Nagy, P. D. (2024b). Proviral role of ATG2 autophagy related protein in tomato bushy stunt virus replication through bulk phospholipid transfer into the viral replication organelle. *Mol. Biol. Cell* 35:ar124. doi: 10.1091/mbc.E24-05-0236

Khuong, T. M., Habets, R. L., Slabbaert, J. R., and Verstreken, P. (2010). WASP is activated by phosphatidylinositol-4,5-bisphosphate to restrict synapse growth in a pathway parallel to bone morphogenetic protein signaling. *Proc. Natl. Acad. Sci. U. S. A.* 107, 17379–17384. doi: 10.1073/pnas.1001794107

King, C., Sengupta, P., Seo, A. Y., and Lippincott-Schwartz, J. (2020). ER membranes exhibit phase behavior at sites of organelle contact. *Proc. Natl. Acad. Sci. USA* 117, 7225–7235. doi: 10.1073/pnas.1910854117

Klose, C., Surma, M. A., Gerl, M. J., Meyenhofer, F., Shevchenko, A., and Simons, K. (2012). Flexibility of a eukaryotic Lipidome – insights from yeast Lipidomics. *PLoS One* 7:e35063. doi: 10.1371/journal.pone.0035063

Kobayashi, T., and Menon, A. K. (2018). Transbilayer lipid asymmetry. *Curr. Biol.* 28, R386–R391. doi: 10.1016/j.cub.2018.01.007

Koike, S., and Jahn, R. (2019). SNAREs define targeting specificity of trafficking vesicles by combinatorial interaction with tethering factors. *Nat. Commun.* 10:1608. doi: 10.1038/s41467-019-09617-9

Kolakowski, D., Rzepnikowska, W., Kaniak-Golik, A., Zoladek, T., and Kaminska, J. (2021). The GTPase Arf1 is a determinant of yeast Vps13 localization to the Golgi apparatus. *Int. J. Mol. Sci.* 22:274. doi: 10.3390/ijms222212274

Kolehmainen, J., Black, G. C., Saarinen, A., Chandler, K., Clayton-Smith, J., Traskelin, A. L., et al. (2003). Cohen syndrome is caused by mutations in a novel gene, COH1, encoding a transmembrane protein with a presumed role in vesicle-mediated sorting and intracellular protein transport. *Am. J. Hum. Genet.* 72, 1359–1369. doi: 10.1086/375454

Kotani, T., Kirisako, H., Koizumi, M., Ohsumi, Y., and Nakatogawa, H. (2018). The Atg2-Atg18 complex tethers pre-autophagosomal membranes to the endoplasmic reticulum for autophagosome formation. *Proc. Natl. Acad. Sci. U. S. A.* 115, 10363–10368. doi: 10.1073/pnas.1806727115

Kumar, N., Leonzino, M., Hancock-Cerutti, W., Horenkamp, F. A., Li, P., Lees, J. A., et al. (2018). VPS13A and VPS13C are lipid transport proteins differentially localized at ER contact sites. *J. Cell Biol.* 217, 3625–3639. doi: 10.1083/jcb.201807019

Lees, J. A., and Reinisch, K. M. (2020). Inter-organelle lipid transfer: a channel model for Vps13 and chorein-N motif proteins. *Curr. Opin. Cell Biol.* 65, 66–71. doi: 10.1016/j.ceb.2020.02.008

Lei, Y., Wen, X., and Klionsky, D. J. (2022). Vps13 is required for efficient autophagy in *Saccharomyces cerevisiae*. *Contact (Thousand Oaks)* 5:11363. doi: 10.1177/25152564221136388

Leiba, J., Sabra, A., Bodinier, R., Marchetti, A., Lima, W. C., Melotti, A., et al. (2017). Vps13F links bacterial recognition and intracellular killing in Dictyostelium. *Cell. Microbiol.* 19:e12722. doi: 10.1111/cmi.12722

Lesage, S., Drouet, V., Majounie, E., Deramecourt, V., Jacoupy, M., Nicolas, A., et al. (2016). Loss of VPS13C Function in Autosomal-Recessive Parkinsonism Causes Mitochondrial Dysfunction and Increases PINK1/Parkin-Dependent Mitophagy. *Am J Hum Genet* 98, 500–513. doi: 10.1016/j.ajhg.2016.01.014

Leterme, S., Bastien, O., Aiese Cigliano, R., Amato, A., and Michaud, M. (2023). Phylogenetic and structural analyses of VPS13 proteins in Archaeplastida reveal their complex evolutionary history in Viridiplantae. *Contact (Thousand Oaks)* 6:11976. doi: 10.1177/25152564231211976

Levine, T. P. (2019). Remote homology searches identify bacterial homologues of eukaryotic lipid transfer proteins, including Chorein-N domains in TamB and AsmA and Mdm31p. *BMC Mol. Cell Biol.* 20:43. doi: 10.1186/s12860-019-0226-z

Levine, T. P. (2022). Sequence analysis and structural predictions of lipid transfer bridges in the repeating Beta groove (RBG) superfamily reveal past and present domain variations affecting form, function and interactions of VPS13, ATG2, SHIP164, Hobbit and Tweek. *Contact (Thousand Oaks)* 5:11343. doi: 10.1177/25152564221134328

Li, P., Lees, J. A., Lusk, C. P., and Reinisch, K. M. (2020). Cryo-EM reconstruction of a VPS13 fragment reveals a long groove to channel lipids between membranes. *J. Cell Biol.* 219:161. doi: 10.1083/jcb.202001161

Maeda, S., Otomo, C., and Otomo, T. (2019). The autophagic membrane tether ATG2A transfers lipids between membranes. *eLife* 8:777. doi: 10.7554/eLife.45777

Maeda, S., Yamamoto, H., Kinch, L. N., Garza, C. M., Takahashi, S., Otomo, C., et al. (2020). Structure, lipid scrambling activity and role in autophagosome formation of ATG9A. *Nat. Struct. Mol. Biol.* 27, 1194–1201. doi: 10.1038/s41594-020-00520-2

Maxfield, F. R., and van Meer, G. (2010). Cholesterol, the central lipid of mammalian cells. *Curr. Opin. Cell Biol.* 22, 422–429. doi: 10.1016/j.ceb.2010.05.004

Melia, T. J., and Reinisch, K. M. (2022). A possible role for VPS13-family proteins in bulk lipid transfer, membrane expansion and organelle biogenesis. *J. Cell Sci.* 135:357. doi: 10.1242/jcs.259357

Monfrini, E., Di Fonzo, A., and Morgante, F. (2023). Chorea-Acanthocytosis presenting with parkinsonism-dystonia without chorea. *Mov. Disord. Clin. Pract.* 10, S32–S34. doi: 10.1002/mdc3.13771

Munoz-Braceras, S., Calvo, R., and Escalante, R. (2015). TipC and the chorea-acanthocytosis protein VPS13A regulate autophagy in Dictyostelium and human HeLa cells. *Autophagy* 11, 918–927. doi: 10.1080/15548627.2015.1034413

Munoz-Braceras, S., Tornero-Ecija, A. R., Vincent, O., and Escalante, R. (2019). VPS13A is closely associated with mitochondria and is required for efficient lysosomal degradation. *Dis. Model. Mech.* 12:681. doi: 10.1242/dmm.036681

Nagata, O., Nakamura, M., Sakimoto, H., Urata, Y., Sasaki, N., Shiokawa, N., et al. (2018). Mouse model of chorea-acanthocytosis exhibits male infertility caused by impaired sperm motility as a result of ultrastructural morphological abnormalities in the mitochondrial sheath in the sperm midpiece. *Biochem. Biophys. Res. Commun.* 503, 915–920. doi: 10.1016/j.bbrc.2018.06.096

Neuman, S. D., and Bashirullah, A. (2018). Hobbit regulates intracellular trafficking to drive insulin-dependent growth during Drosophila development. *Development* 145:356. doi: 10.1242/dev.161356

Neuman, S. D., Jorgensen, J. R., Cavanagh, A. T., Smyth, J. T., Selegue, J. E., Emr, S. D., et al. (2022b). The hob proteins are novel and conserved lipid-binding proteins at ER-PM contact sites. *J. Cell Sci.* 135:86. doi: 10.1242/jcs.259086

Neuman, S. D., Levine, T. P., and Bashirullah, A. (2022a). A novel superfamily of bridge-like lipid transfer proteins. *Trends Cell Biol.* 32, 962–974. doi: 10.1016/j.tcb.2022.03.011

Osawa, T., Kotani, T., Kawaoka, T., Hirata, E., Suzuki, K., Nakatogawa, H., et al. (2019). Atg2 mediates direct lipid transfer between membranes for autophagosome formation. *Nat. Struct. Mol. Biol.* 26, 281–288. doi: 10.1038/s41594-019-0203-4

Otto, G. P., Razi, M., Morvan, J., Stenner, F., and Tooze, S. A. (2010). A novel syntaxin 6-interacting protein, SHIP164, regulates syntaxin 6-dependent sorting from early endosomes. *Traffic* 11, 688–705. doi: 10.1111/j.1600-0854.2010.01049.x

Pandey, T., Wang, B., Wang, C., Zu, J., Deng, H., and Shen, K. (2024). LPD-3 as a megaprotein brake for aging and insulin-mTOR signaling in *C. elegans*. *Cell Rep.* 43:113899. doi: 10.1016/j.celrep.2024.113899

Pandey, T., Zhang, J., Wang, B., and Ma, D. K. (2023). Bridge-like lipid transfer proteins (BLTPs) in *C. elegans*: from genetics to structures and functions. *Contact (Thousand Oaks)* 6:6489. doi: 10.1177/25152564231186489

Park, J. S., Halegoua, S., Kishida, S., and Neiman, A. M. (2015). A conserved function in phosphatidylinositol metabolism for mammalian Vps13 family proteins. *PLoS One* 10:e0124836. doi: 10.1371/journal.pone.0124836

Park, J. S., and Neiman, A. M. (2020). XK is a partner for VPS13A: a molecular link between chorea-Acanthocytosis and McLeod syndrome. *Mol. Biol. Cell* 31, 2425–2436. doi: 10.1091/mbc.E19-08-0439-T

Park, J. S., Okumura, Y., Tachikawa, H., and Neiman, A. M. (2013). SPO71 encodes a developmental stage-specific partner for Vps13 in *Saccharomyces cerevisiae*. *Eukaryot. Cell* 12, 1530–1537. doi: 10.1128/EC.00239-13

Parolek, J., and Burd, C. G. (2024). Bridge-like lipid transfer protein family member 2 suppresses ciliogenesis. *Mol. Biol. Cell* 35:br11. doi: 10.1091/mbc.E24-02-0065

Peikert, K., Dobson-Stone, C., Rampoldi, L., Miltenberger-Miltenyi, G., Neiman, A., De Camilli, P., et al. (1993). "VPS13A disease" in GeneReviews®. eds. M. P. Adam, J. Feldman, G. M. Mirzaa, R. A. Pagon, S. E. Wallace and A. Amemiya (Seattle, WA: University of Washington).

Pietra, S., Gustavsson, A., Kiefer, C., Kalmbach, L., Horstedt, P., Ikeda, Y., et al. (2013). Arabidopsis SABRE and CLASP interact to stabilize cell division plane orientation and planar polarity. *Nat. Commun.* 4:2779. doi: 10.1038/ncomms3779

Rampoldi, L., Dobson-Stone, C., Rubio, J. P., Danek, A., Chalmers, R. M., Wood, N. W., et al. (2001). A conserved sorting-associated protein is mutant in chorea-acanthocytosis. *Nat. Genet.* 28, 119–120. doi: 10.1038/88821

Reinisch, K. M., and Prinz, W. A. (2021). Mechanisms of nonvesicular lipid transport. *J. Cell Biol.* 220:2058. doi: 10.1083/jcb.202012058

Ryoden, Y., Segawa, K., and Nagata, S. (2022). Requirement of Xk and Vps13a for the P2X7-mediated phospholipid scrambling and cell lysis in mouse T cells. *Proc. Natl. Acad. Sci. USA* 119:6119. doi: 10.1073/pnas.2119286119

Rzepnikowska, W., Flis, K., Kaminska, J., Grynberg, M., Urbanek, A., Ayscough, K. R., et al. (2017). Amino acid substitution equivalent to human chorea-acanthocytosis I2771R in yeast Vps13 protein affects its binding to phosphatidylinositol 3-phosphate. *Hum. Mol. Genet.* 26, 1497–1510. doi: 10.1093/hmg/ddx054

Saliba, J., Saint-Martin, C., Di Stefano, A., Lenglet, G., Marty, C., Keren, B., et al. (2015). Germline duplication of ATG2B and GSKIP predisposes to familial myeloid malignancies. *Nat. Genet.* 47, 1131–1140. doi: 10.1038/ng.3380

Schröder, L. F., Peng, W., Gao, G., Wong, Y. C., Schwake, M., and Krainc, D. (2024). VPS13C regulates phospho-Rab10-mediated lysosomal function in human dopaminergic neurons. *J. Cell Biol.* 223:4042. doi: 10.1083/jcb.202304042

Seifert, W., Kuhnisch, J., Maritzen, T., Lommatzsch, S., Hennies, H. C., Bachmann, S., et al. (2015). Cohen syndrome-associated protein COH1 physically and functionally interacts with the small GTPase RAB6 at the Golgi complex and directs neurite outgrowth. *J. Biol. Chem.* 290, 3349–3358. doi: 10.1074/jbc.M114.608174

Seong, E., Insolera, R., Dulovic, M., Kamsteeg, E. J., Trinh, J., Bruggemann, N., et al. (2018). Mutations in VPS13D lead to a new recessive ataxia with spasticity and mitochondrial defects. *Ann. Neurol.* 83, 1075–1088. doi: 10.1002/ana.25220

Shen, J. L., Fortier, T. M., Zhao, Y. G., Wang, R., Burmeister, M., and Baehrecke, E. H. (2021). Vmp1, Vps13D, and Marf/Mfn2 function in a conserved pathway to regulate mitochondria and ER contact in development and disease. *Curr. Biol.* 31, 3028–3039.e7. doi: 10.1016/j.cub.2021.04.062

Smolders, S., Philtjens, S., Crosiers, D., Sieben, A., Hens, E., Heeman, B., et al. (2021). Contribution of rare homozygous and compound heterozygous VPS13C missense mutations to dementia with Lewy bodies and Parkinson's disease. *Acta Neuropathol. Commun.* 9:25. doi: 10.1186/s40478-021-01121-w

Song, J., Yang, W., Shih Ie, M., Zhang, Z., and Bai, J. (2006). Identification of BCOX1, a novel gene overexpressed in breast cancer. *Biochim. Biophys. Acta* 1760, 62–69. doi: 10.1016/j.bbagen.2005.09.017

Srinivasan, S., Alvarez, D., John Peter, A. T., and Vanni, S. (2024). Unbiased MD simulations identify lipid binding sites in lipid transfer proteins. *J. Cell Biol.* 223:55. doi: 10.1083/jcb.202312055

Suzuki, S. W., West, M., Zhang, Y., Fan, J. S., Roberts, R. T., Odorizzi, G., et al. (2024). A role for Vps13-mediated lipid transfer at the ER-endosome contact site in ESCRT-mediated sorting. *J. Cell Biol.* 223:7094. doi: 10.1083/jcb.202307094

Tan, J. X., and Finkel, T. (2022). A phosphoinositide signalling pathway mediates rapid lysosomal repair. *Nature* 609, 815–821. doi: 10.1038/s41586-022-05164-4

Tang, Z., Takahashi, Y., He, H., Hattori, T., Chen, C., Liang, X., et al. (2019). TOM40 targets Atg2 to mitochondria-associated ER membranes for Phagophore expansion. *Cell Rep.* 28, 1744–1757 e5. doi: 10.1016/j.celrep.2019.07.036

Tokai, M., Kawasaki, H., Kikuchi, Y., and Ouchi, K. (2000). Cloning and characterization of the CSF1 gene of *Saccharomyces cerevisiae*, which is required for nutrient uptake at low temperature. *J. Bacteriol.* 182, 2865–2868. doi: 10.1128/JB.182.10.2865-2868.2000

Tornero-Ecija, A., Zapata-Del-Bano, A., Anton-Esteban, L., Vincent, O., and Escalante, R. (2023). The association of lipid transfer protein VPS13A with endosomes is mediated by sorting nexin SNX5. *Life Sci. Alliance* 6:e202201852. doi: 10.26508/lsa.202201852

Toulmay, A., Whittle, F. B., Yang, J., Bai, X., Diarra, J., Banerjee, S., et al. (2022). Vps13-like proteins provide phosphatidylethanolamine for GPI anchor synthesis in the ER. *J. Cell Biol.* 221:1095. doi: 10.1083/jcb.202111095

Ugur, B., Hancock-Cerutti, W., Leonzino, M., and De Camilli, P. (2020). Role of VPS13, a protein with similarity to ATG2, in physiology and disease. *Curr. Opin. Genet. Dev.* 65, 61–68. doi: 10.1016/j.gde.2020.05.027

Ugur, B., Schueder, F., Shin, J., Hanna, M. G., Wu, Y., Leonzino, M., et al. (2024). VPS13B is localized at the interface between Golgi cisternae and is a functional partner of FAM177A1. *J. Cell Biol.* 223:189. doi: 10.1083/jcb.202311189

Vacca, F., Yalcin, B., and Ansar, M. (2024). Exploring the pathological mechanisms underlying Cohen syndrome. *Front. Neurosci.* 18:1431400. doi: 10.3389/fnins.2024.1431400

Valverde, D. P., Yu, S., Boggavarapu, V., Kumar, N., Lees, J. A., Walz, T., et al. (2019). ATG2 transports lipids to promote autophagosome biogenesis. *J. Cell Biol.* 218, 1787–1798. doi: 10.1083/jcb.201811139

Van Meer, G., Voelker, D. R., and Feigenson, G. W. (2008). Membrane lipids: where they are and how they behave. *Nat. Rev. Mol. Cell Biol.* 9, 112–124. doi: 10.1038/nrm2330

Van Vliet, A. R., Chiduza, G. N., Maslen, S. L., Pye, V. E., Joshi, D., De Tito, S., et al. (2022). ATG9A and ATG2A form a heteromeric complex essential for autophagosome formation. *Mol. Cell* 82, 4324–4339.e8. doi: 10.1016/j.molcel.2022.10.017

Vargas Duarte, P., and Reggiori, F. (2023). The organization and function of the Phagophore-ER membrane contact sites. *Contact (Thousand Oaks)* 6:3898. doi: 10.1177/25152564231183898

Velayos-Baeza, A., Vettori, A., Copley, R. R., Dobson-Stone, C., and Monaco, A. P. (2004). Analysis of the human VPS13 gene family. *Genomics* 84, 536–549. doi: 10.1016/j.ygeno.2004.04.012

Verstreken, P., Ohyama, T., Haueter, C., Habets, R. L., Lin, Y. Q., Swan, L. E., et al. (2009). Tweek, an evolutionarily conserved protein, is required for synaptic vesicle recycling. *Neuron* 63, 203–215. doi: 10.1016/j.neuron.2009.06.017

Wang, Y., Dahmane, S., Ti, R., Mai, X., Zhu, L., Carlson, L. A., et al. (2024). Structural basis for lipid transfer by the ATG2A-ATG9A complex. *Nat. Struct. Mol. Biol.* 32, 35–47. doi: 10.1038/s41594-024-01376-6

Wang, J., Fang, N., Xiong, J., Du, Y., Cao, Y., and Ji, W. K. (2021). An ESCRT-dependent step in fatty acid transfer from lipid droplets to mitochondria through VPS13D-TSG101 interactions. *Nat. Commun.* 12:1252. doi: 10.1038/s41467-021-21525-5

Wang, Y., Nishimura, M. T., Zhao, T., and Tang, D. (2011). ATG2, an autophagy-related protein, negatively affects powdery mildew resistance and mildew-induced cell death in Arabidopsis. *Plant J.* 68, 74–87. doi: 10.1111/j.1365-313X.2011.04669.x

Wang, J., and Richards, D. A. (2012). Segregation of PIP2 and PIP3 into distinct nanoscale regions within the plasma membrane. *Biol. Open* 1, 857–862. doi: 10.1242/bio.20122071

Wang, C., Wang, B., Pandey, T., Long, Y., Zhang, J., Oh, F., et al. (2022). A conserved megaprotein-based molecular bridge critical for lipid trafficking and cold resilience. *Nat. Commun.* 13:6805. doi: 10.1038/s41467-022-34450-y

Wang, J., Xiong, J., Zhang, S., Li, D., Chu, Q., Chang, W., et al. (2024). Biogenesis of Rab14-positive endosome buds at Golgi-endosome contacts by the RhoBTB3-SHIP164-Vps26B complex. *Cell Discov.* 10:38. doi: 10.1038/s41421-024-00651-6

Wang, X., Xu, P., Bentley-DeSousa, A., Hancock-Cerutti, W., Cai, S., Johnson, B. T., et al. (2024). Lysosome damage triggers acute formation of ER to lysosomes membrane tethers mediated by the bridge-like lipid transport protein VPS13C. *bioRxiv* 2024:8070. doi: 10.1101/2024.06.08.598070

Wen, L., Liu, L., Shen, X., Li, H., Zhu, Z., Huang, H., et al. (2020). The association of the UHRF1BP1 gene with systemic lupus erythematosus was replicated in a Han Chinese population from mainland China. *Ann. Hum. Genet.* 84, 221–228. doi: 10.1111/ahg.12362

Wenk, M. R., Lucast, L., Di Paolo, G., Romanelli, A. J., Suchy, S. F., Nussbaum, R. L., et al. (2003). Phosphoinositide profiling in complex lipid mixtures using electrospray ionization mass spectrometry. *Nat. Biotechnol.* 21, 813–817. doi: 10.1038/nbt837

Wong, L. H., Gatta, A. T., and Levine, T. P. (2019). Lipid transfer proteins: the lipid commute via shuttles, bridges and tubes. *Nat. Rev. Mol. Cell Biol.* 20, 85–101. doi: 10.1038/s41580-018-0071-5

Yang, Y., Zhang, Y., Qu, X., Xia, J., Li, D., Li, X., et al. (2016). Identification of differentially expressed genes in the development of osteosarcoma using RNA-seq. *Oncotarget* 7, 87194–87205. doi: 10.18632/oncotarget.13554

Yeshaw, W. M., van der Zwaag, M., Pinto, F., Lahaye, L. L., Faber, A. I., Gomez-Sanchez, R., et al. (2019). Human VPS13A is associated with multiple organelles and influences mitochondrial morphology and lipid droplet motility. *eLife* 8:561. doi: 10.7554/eLife.43561

Zheng, J. X., Li, Y., Ding, Y. H., Liu, J. J., Zhang, M. J., Dong, M. Q., et al. (2017). Architecture of the ATG2B-WDR45 complex and an aromatic Y/HF motif crucial for complex formation. *Autophagy* 13, 1870–1883. doi: 10.1080/15548627.2017.1359381

Zhong, Z., Pannu, V., Rosenow, M., Stark, A., and Spetzler, D. (2018). KIAA0100 modulates Cancer cell aggression behavior of MDA-MB-231 through microtubule and heat shock proteins. *Cancers (Basel)* 10:180. doi: 10.3390/cancers10060180

‘Glossary

ATG2 - Autophagy-related 2

BLTP - Bridge-like lipid transporter

CASM - Conjugation of Atg8 to single membranes

ChAc - Chorea-acanthocytosis

ER - Endoplasmic reticulum

ERGIC - ER-Golgi intermediate compartment

ESCRT - Endosomal sorting complex required for transport

FFAT - Two phenylalanines in an acidic tract

GTPase - Guanosine triphosphatase

ILV - Intraluminal vesicle

LC3 - Microtubule-associated proteins 1A/1B light chain 3

LIR - LC3-interacting region

MLD - Mitochondrial-associated membrane localisation domain

mTOR - Mechanistic target of rapamycin

NBD - Nitrobenzoxadiazole (fluorescent lipid label)

PA - Phosphatidic acid

PC - Phosphatidylcholine

PE - Phosphatidylethanolamine

PG - Phosphatidylglycerol

PH - Pleckstrin homology

PI - Phosphatidylinositol

PM - Plasma membrane

PS - Phosphatidylserine

RBG - Repeating beta groove

RNA - Ribonucleic acid

RXP - Arginine-X-Proline motif

SH3 - Src homology 3

SNARE - Soluble NSF attachment protein receptor

TSG101 - Tumour susceptibility gene 101

UHRF1BP1 - Ubiquitin-like with PHD and RING finger domains 1 binding protein 1

UHRF1BP1L - UHRF1BP1-like protein

VAB - VPS13 adaptor-binding domain

VAMP7 - Vesicle-associated membrane protein 7

VAPA/B - Vesicle-associated membrane protein-associated protein A/B

VMP1 - Vacuole membrane protein 1

VPS13 - Vacuolar protein sorting 13

WD40 - Tryptophan (W) aspartate (D) motif of 40 amino acids

WIPI - WD repeat domain phosphoinositide-interacting protein

WWE - Trp Trp Glu motif domain

XK - Kell blood group precursor

Frontiers in Neuroscience

Provides a holistic understanding of brain function from genes to behavior

Part of the most cited neuroscience journal series which explores the brain - from the new eras of causation and anatomical neurosciences to neuroeconomics and neuroenergetics.

Discover the latest Research Topics

See more →

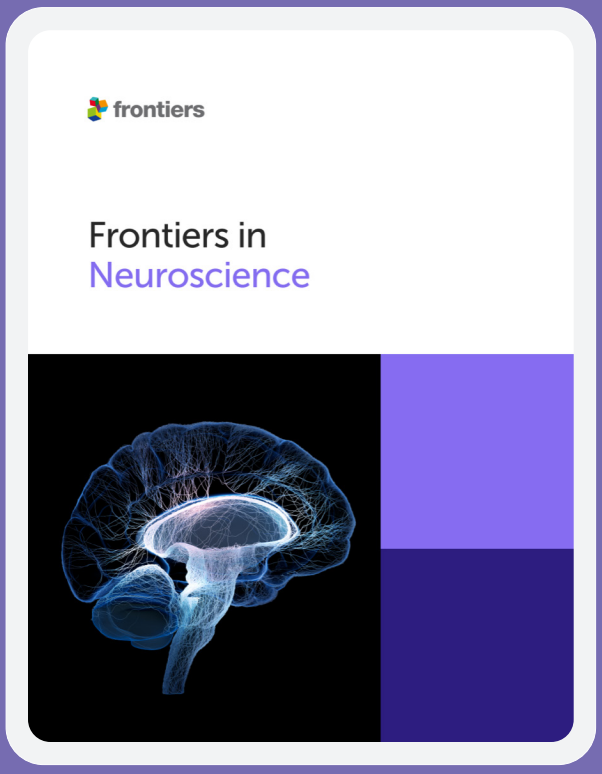

Frontiers

Avenue du Tribunal-Fédéral 34
1005 Lausanne, Switzerland
frontiersin.org

Contact us

+41 (0)21 510 17 00
frontiersin.org/about/contact